Universidade de Aveiro Departamento de Química
2017

Matheus Mendonça Pereira

Sistemas aquosos bifásicos constituídos por líquidos iónicos para concentração e purificação de biomarcadores tumorais

Ionic-liquid-based aqueous biphasic systems as concentration and purification platforms of cancer biomarkers

Universidade de Aveiro Departamento de Química
2017

Matheus Mendonça Pereira

Sistemas aquosos bifásicos constituídos por líquidos iónicos para concentração e purificação de biomarcadores tumorais

Ionic-liquid-based aqueous biphasic systems as concentration and purification platforms of cancer biomarkers

Tese apresentada à Universidade de Aveiro para cumprimento dos requisitos necessários à obtenção do grau de Doutor em Engenharia Química, realizada sob a orientação científica da Doutora Mara Guadalupe Freire Martins, Investigadora Coordenadora do Departamento de Química, CICECO, da Universidade de Aveiro, e coorientação do Professor Doutor João Manuel da Costa e Araújo Pereira Coutinho, Professor Catedrático do Departamento de Química, CICECO, da Universidade de Aveiro.

Apoio financeiro do POCTI no âmbito do III Quadro Comunitário de Apoio.

Apoio financeiro da Coordenação de Aperfeiçoamento de Pessoal de Nível Superior-CAPES (2740-13-3). Parte da investigação que conduziu aos resultados aqui apresentados foi financiada pelo Conselho Europeu de Investigação ao abrigo do Sétimo Programa-Quadro da União Europeia (FP7/2007-2013)/ERC No. 337753.

o júri

presidente	Professor Doutor Vítor António Ferreira da Costa, Professor Catedrático da Universidade de Aveiro
vogais	Doutora Mara Guadalupe Freire Martins, Investigadora Coordenadora da Universidade de Aveiro (orientadora)
	Doutora Ana Catarina Almeida Sousa, Investigadora, CNRS LabEx DRIIHM, CNRS - INEE - ECCOREV (Unité FR3098), OHMi Estarreja-OHM Bassin Minier de Provence, França
	Doutor Álvaro Silva Lima, Professor Titular da Universidade Tiradentes, Brasil
	Doutor Aminou Mohamadou, Professor Associado da Université de Reims Champagne-Ardenne, França
	Doutora Fani Pereira de Sousa, Professora Auxiliar da Universidade da Beira Interior

agradecimentos

Não poderia deixar de relatar meus sinceros agradecimentos a todos aqueles que de alguma forma contribuíram para a elaboração dessa tese.
Agradeço em primeiro lugar aos meus grandes ídolos meu pai e minha mãe.
À minha mãe pelo amor dedicado, pelas vibrações nos momentos importantes e pelo colo quando necessário. Por ter me ensinado desde sempre a ter bom senso nas minhas decisões e por tê-las apoiado incondicionalmente.
Ao meu pai pelo seu incentivo contínuo à minha carreira, pelo orgulho declarado e pelo exemplo de busca ao crescimento profissional e pessoal.
À minha irmã Camilla que além de ser a única que ri realmente das minhas piadas, sempre torce por mim com muito orgulho.
Ao Ivan, pela companhia, dedicação e incentivos constantes durante toda minha trajetória. Pelo carinho e olhar especial nos momentos difíceis e pelo sorriso e brilho no olhar nas minhas vitórias.
A todos amigos e colegas do Path. Agradeço a todos pela ajuda e pelo alto astral de todos os dias. Valeu a força, galera!
Ao Profº João pelos ensinamentos, pela experiência transmitida e pelas dicas sempre essenciais. Agradeço também pela oportunidade de fazer parte da família Path.
Á Drª Mara, pela paciência de sentar e discutir ponto a ponto cada resultado, o que foi indispensável para o andamento do trabalho. Pelas preocupações, pela confiança e pela oportunidade.
Agradeço o apoio financeiro da CAPES, pela bolsa de Doutorado Pleno no Exterior.

palavras-chave

Cancro, biomarcadores tumorais, extração, concentração, sistemas aquosos bifásicos, líquidos iónicos.

resumo

O cancro é mundialmente uma das principais causas de morte, com cerca de 14 milhões de novos casos diagnosticados por ano. Neste sentido, o desenvolvimento de métodos de diagnóstico mais eficientes em estágio inicial da doença é crucial para auxiliar o tratamento e aumentar a taxa de sobrevida dos pacientes, além de diminuir as despesas associadas aos tratamentos avançados. O antígeno específico da próstata (PSA) e a lactato desidrogenase (LDH) são proteínas comumente encontradas nos fluidos humanos (urina e soro) e têm sido alvo de atenção como biomarcadores do cancro e na monitorização do seu tratamento. No entanto, devido à sua baixa concentração e à complexidade das matrizes biológicas com uma grande quantidade de outros metabólitos presentes (proteínas, DNA, RNA), é geralmente aplicado um ou mais passos de pré-tratamento de amostras. Neste trabalho, foram estudadas técnicas alternativas de pré-tratamento baseadas em sistemas aquosos bifásicos (SAB) constituídos por líquidos iónicos (LIs) para extrair, concentrar e purificar proteínas que podem ser usadas como biomarcadores de cancro, como a PSA e LDH. Para este fim, foram realizados vários trabalhos preliminares para identificar os componentes e condições de formação mais promissores para criar SAB que possam ser utilizados para a extração de proteínas. Estes trabalhos contemplam a utilização de SAB para a extração de aminoácidos e proteínas modelo, assim como a utilização de SAB em matrizes mais complexas. Finalmente, os SAB foram aplicados para a extração e concentração de biomarcadores tumorais, nomeadamente PSA e LDH. Em suma, com este trabalho verificou-se que a versatilidade dos LIs permite adaptar a capacidade de extração e concentração, seletividade, e/ou precipitação induzida de biomarcadores de cancro a partir de fluidos humanos. Os sistemas aqui desenvolvidos são uma alternativa viável e eficiente para o pré-tratamento de amostras biológicas (soro e urina), contribuindo assim para o desenvolvimento de métodos de diagnóstico de cancro precoces.

keywords

Cancer, tumor biomarkers, extraction, concentration, aqueous biphasic systems, ionic liquids.

abstract

Cancer is worldwide a major cause of death, with *ca.* 14 million new diagnosed cases each year. Therefore, the search for more efficient early-stage diagnosis methods is crucial aiming at increasing the treatment rate and survival of patients, as well as to decrease the expenses associated to advanced treatment. Prostate specific antigen (PSA) and lactate dehydrogenase (LDH) are proteins commonly found in human fluids (urine and serum), and have been considered as cancer biomarkers and in the monitoring of cancer treatment. However, due to their low concentration and the complexity of biological matrices with a large amount of other metabolites present (proteins, DNA, RNA), the pretreatment of samples for their concentration and purification is usually applied. In this work, alternative pretreatment techniques based on aqueous biphasic systems (ABS) composed of ionic liquids (ILs) have been studied to extract, concentrate and purify proteins that can be used as cancer biomarkers, such as PSA and LDH. To this end, several preliminary works were performed to identify the most promising phase-forming components and conditions to create ABS that could be used for the extraction of proteins. These works comprise studies on the extraction of amino acids and model proteins in ABS, followed by investigations on their use with more complex matrices. Finally, ABS were investigated for the extraction and concentration of tumor biomarkers, namely PSA and LDH. In summary, the versatility of ILs allows the tailoring of the ABS extraction and concentration capacity, selectivity, and/or induced precipitation of cancer biomarkers from human fluids. The systems here developed are a viable and efficient alternative for the pretreatment of biological samples (serum and urine), thus contributing to the development of early-stage methods of cancer diagnosis.

CONTENTS

LIST OF TABLES

LIST OF FIGURES

NOTATION

List of symbols

$\mathrm{p}K_a$	acid dissociation constant
$[x]$	concentration of component x
$[x]_y$	concentration of component x in the phase y
R^2	correlation coefficient
$EE_A\%$	extraction efficiency percentage of component A
$DE_A\%$	depletion efficiency percentage of component A
$RY_A\%$	recovery efficiency percentage of component A
ΔG_{hyd}	Gibbs energy of ion hydration
K_{ow}	octanol-water partition coefficient
K_i	partition coefficient of component i
α	ratio between the weight of the salting-out specie rich phase and the total weight of the mixture **or** hydrogen bond acidity **or** degree of dissociation

List of abbreviations

ABS	aqueous biphasic systems
ADT	autodocktools
AFP	alpha-fetoprotein
amaCr	α-methylacyl coenzyme a racemase
AZGP1	zinc-alpha 2-glycoprotein
BSA	bovine serum albumin
BPH	benign prostatic hyperplasia
CCC	counter-current chromatography
CEA	carcinoembryonic antigen
CgA	chromogranin A
CHES	*N*-cyclohexyl-2-aminoethanesulfonic acid
COL1A1	Collagen, type I, alpha 1
CPC	centrifugal partition chromatography
CRPC	castration-resistant prostate cancer
CTC	circulating tumor cells counts
DRE	dithiothreitol
DTT	digital rectal examination
ECM	extracellular matrix
ESA	equine serum albumin
ELISA	enzyme-linked immunosorbent assay
FDA	Food and Drug Administration
fPSA	free PSA
FTIR	fourier transform infrared spectroscopy
GBs	Good's buffers
GCA	glycocholic acid
Golm1	golgi membrane protein 1
HCC	hepatocelular carcinoma
HEPES	4-(2-hydroxyethyl)-1-piperazineethanesulfonic acid
HIF-1	hypoxia inducible factor 1
HPLC	high performance liquid chromatography
HSA	human serum albumin
HSCCC	high-speed counter-current chromatography
IARC	International Agency for Research on Cancer
IgG	immunoglobulin G
IL	ionic liquid
IL-6	interleukin 6
KLK-4	kallikrein-4
LC	liquid chromatography
LFA	lateral flow immunoassay
LDH	lactate dehydrogenase
LSA	leporine serum albumin
Mcm5	minichromosome maintenance 5 protein
MES	2-(*N*-morpholino)ethanesulfonic acid
MRJPs	Major Royal Jelly Proteins
NMR	nuclear magnetic resonance
NCDs	non-communicable diseases
OVA	ovalbumin
*p*LDH	lactate dehydrogenase of Plasmodium
PAP	Prostatic acid phosphatase
PCa	Prostate cancer
PCR	polymerase chain reaction
PEG	polyethyleneglycol
pI	isoelectric point
PSA	prostate-specific antigen
SDS-PAGE	sodium dodecyl sulphate polyacrylamide gel electrophoresis
SE-HPLC	size-exclusion HPLC
SEMG1	semenogelin 1
SEMG2	semenogelin 2
SERS	surface enhanced Raman spectroscopy
SPE	solid-phase extraction
SPR	surface plasmon resonance
Src-3	steroid Receptor Co-Activator-3
SVE	extracellular vesicles
TES	*N*-tris(hydroxymethyl)methyl-2-aminoethanesulfonic acid
TL	tie-line
TLL	tie-line length
tPSA	total PSA
Tricine	*N*-tris(hydroxymethyl) methylglycine
Trp	tryptophan
TRUS	transrectal ultrasound
Tyr	tyrosin
UV-Vis	ultraviolet-visible

List of ionic liquids

$[P_{4444}]Br$	Tetrabutylphosphonium bromide
$[P_{4444}]Cl$	Tetrabutylphosphonium chloride
$[P_{i(444)1}][TOS]$	Triisobutylmethylphosphonium tosylate
$[P_{4441}][MeSO_4]$	Tributylmethylphosphonium methylsulphate
$[Bu_3PC_2]Br$	Tri(n-butyl)[2-ethoxy-2-oxoethyl]phosphonium bromide
$[Bu_3PC_4]Br$	Tri(n-butyl)[2-butoxy-2-oxoethyl]phosphonium bromide
$[N_{4444}]Cl$	Tetrabutylammonium chloride
$[MepyrNC_2]Br$	N-(1-methylpyrrolidyl-2-ethoxy-2-oxoethyl)ammonium bromide
$[Et_3NC_2]Br$	Triethyl[2-ethoxy-2-oxoethyl]ammonium bromide
$[Pr_3NC_2]Br$	Tri(n-propyl)[2-ethoxy-2-oxoethyl]ammonium bromide
$[Bu_3NC_2]Br$	Tri(n-butyl)[2-ethoxy-2-oxoethyl]ammonium bromide
$[MePyrNC_4][Br]$	N-(1-methylpyrrolidyl-2-butoxy-2-oxoethyl)ammonium bromide
$[Et_3NC_4]Br$	Tri(n-ethyl)[2-butoxy-2-oxoethyl]ammonium bromide
$[Pr_3NC_4]Br$	Tri(n-propyl)[2-butoxy-2-oxoethyl]ammonium bromide
$[Bu_3NC_4]Br$	Tri(n-butyl)[2-butoxy-2-oxoethyl]ammonium bromide
$[Pr_3NC_4][Sac])$	Tri(n-propyl)[2-butoxy-2-oxoethyl]ammonium saccharinate
$[Pr_3NC_4][Lac])$	Tri(n-propyl)[2-butoxy-2-oxoethyl]ammonium lactate
$[Pr_3NC_4][Pyr])$	Tri(n-propyl)[2-butoxy-2-oxoethyl]ammonium pyruvate
$[Pr_3NC_4][Dca]$	Tri(n-propyl)[2-butoxy-2-oxoethyl]ammonium dicyanamide
$[Pr_3NC_4][Sal]$	Tri(n-propyl)[2-butoxy-2-oxoethyl]ammonium salicylate
$[Pr_3NC_2][Sal]$	Tri(n-ethyl)[2-butoxy-2-oxoethyl]ammonium salicylate
$[P_{4444}][MES]$	Tetrabutylphosphonium 2-(N-morpholino)ethanesulfonate
$[P_{4444}][TES]$	Tetrabutylphosphonium 2-[[1,3-dihydroxy-2-(hydroxymethyl)propan-2-yl]amino]ethanesulfonate
$[P_{4444}][CHES]$	Tetrabutylphosphonium 2-(cyxlohexylamino)ethanesulfonate
$[P_{4444}][HEPES]$	Tetrabutylphosphonium 2-[4-(2-hydroxyethyl)piperazin-1-yl]ethanesulfonate
$[P_{4444}][Tricine]$	Tetrabutylphosphonium N-2(2-Hydroxy-1,1-bis(hydroxymethyl)ethyl)glycine.

1. INTRODUCTION

1.1. Cancer update overview

Cancer is a major cause of death worldwide, with *ca*. 14 million new cases diagnosed each year[1]. According to the International Agency for Research on Cancer (IARC), in 2012, 32.6 million people lived with cancer and 8.2 million people died with this disease. The future trends disclose an even worst scenario, with over 20 million new cancer cases expected in 2025[2]. Generally, the cancer incidence (excluding non-melanoma skin cancer) is higher for male individuals (205 *per* 100,000) compared to females (165 *per* 100,000)[2].

In Portugal, the cancer incidence in 2012 was of 246.2 *per* 100,000 individuals,[2] being the prostate, breast, colorectal, bladder and lung the types of cancer with higher incidence rates[2]. In Brazil, the cancer incidence in 2012 was 205.5 *per* 100,000 individuals,[2] and the most prevalent cancers were prostate, breast and colorectal. According to the Brazilian National Cancer institute, 600,000 news cases were estimated to occur in 2016[3]. Although the cancer incidence is lower in Brazil, the cancer mortality is higher in this country (103.7 deaths *per* 100,000 individuals in Brazil *versus* 99.0 deaths per 100,000 individuals in Portugal). This relative higher mortality in Brazil is probably associated with differences in the implementation of early stage diagnosis programs between the two countries. In fact, cost-effective techniques for early stage diagnosis are extremely important in order to reduce the mortality and improve the prognosis associated with the most prevalent cancer types. Generally, the higher mortality rates are registered in countries where early stage diagnosis programs are not implemented. The worst scenario is found in low and middle income countries that register approximately 70% of cancer deaths[4]. Prostate, colorectal, breast and lung cancer cases in Latin America, Africa and South-West Asia are between 2 to 5 times higher than in developed countries. Because several cancers have a high chance of cure if diagnosed early and treated adequately, it is possible to reduce the cancer burden through early detection.

Currently, the most common techniques used in early stage diagnosis are based on immunoassays which demand extensive sample processing and highly sophisticated/expensive technical equipment. Thus, the development of low-cost and effective early-stage diagnosis and point of care prognosis methods are of great importance, particularly in developing countries. The development of cost-effective diagnosis techniques will allow to implement global and intensive public actions so that mortality rates associated with cancer might be reduced. This is particularly relevant because cancer constitutes one of the most important non-communicable diseases (NCDs), that it is expected to rise in the future due to the population ageing and the increased

exposure to cancer triggers, such as physical, chemical and biological carcinogens.

Most cancers are the result of a combination of genetic predisposition, lifestyle factors (sedentary lifestyle, unhealthy diet and drugs consumption) and exposure to environmental agents (e.g. chemical, physical and biological carcinogens)[1]. In his initial research in 1953, Nordling *et al.*[5] proposed that the cancer progression in organisms occurs by successive mutations and developed the multi-mutation theory of cancer. However, this initial hypothesis has been updated. Advances in DNA amplification and sequencing allowed to better understand some of the complex mechanisms of cancer cells and the dynamic changes in the genome[6]. The change of a normal cell into a neoplasic state involves the acquisition of several capabilities/traits that enables them to become tumorogenic and ultimately malignant. These distinctive and complementary capabilities that enables tumor growth and metastatic dissemination were compiled and conceptualized by Hanahan & Weinberg[6,7] into the hallmarks of cancer. Figure 1.1. depicts the malignant cell development hallmarks that lead to cancer development[6].

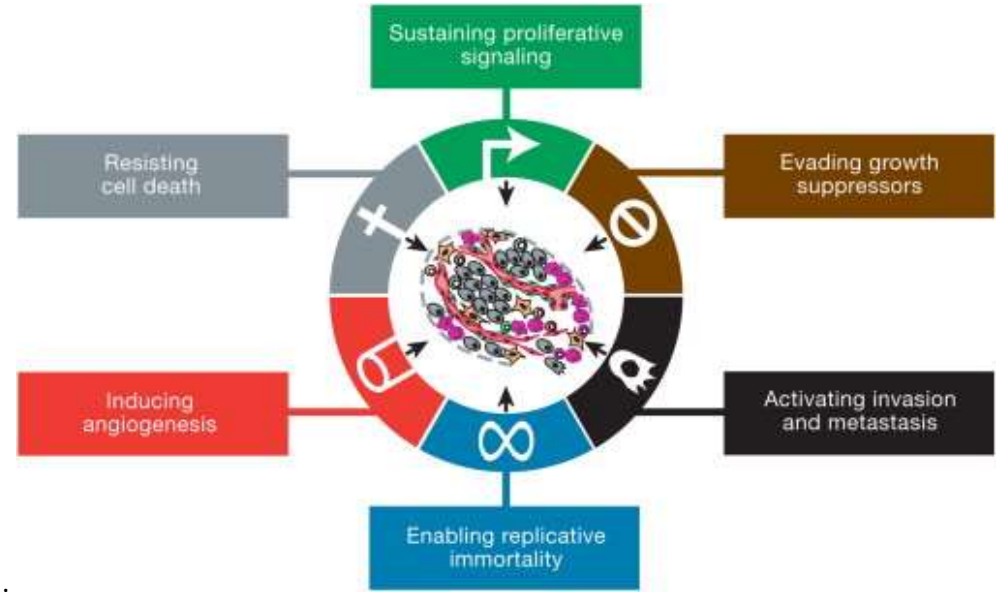

Figure 1.1. Illustration of cancer hallmarks according to Hanahan & Weinberg[6].

The hallmarks of cancer are constituted by six biological capabilities that emerge during the complex development of human tumors[6]. These hallmarks include sustaining proliferative signaling, evading growth suppressors, resisting cell death, enabling replicative immortality, inducing angiogenesis, and activating invasion and metastasis[6]. The cancer cells fundamental ability is to maintain chronic proliferation. In normal tissues, the production and release of growth-promoting signals (basic instructions that cells receive in their growth and-division cycle)

are controlled naturally[6]. In cancer cells, these signals are deregulated and start to be self-sufficient; therefore, cancers cells can regulate their progression through the cell cycle as well as growth. This hallmark of sustaining proliferative signaling is complemented by the ability to evade growth suppressors. In fact, cancer cells are able to regulate the cell proliferation by inactivating tumor suppressor genes[6]. The most common tumor suppressor genes encode RB (retinoblastoma-associated) and TP53 proteins. They regulate the biological function that covers the control of cell proliferation and senescence programs[6].

The hallmark of resisting to cell death is based on the ability of cancer cells to overcome apoptosis [8–10]. In cancer treatments, the apoptotic program of cancer cells is activated by several physiologic stresses, including the DNA damage that can be associated with hyperproliferation. Nevertheless, cancer cells developed a variety of strategies to limit or to circumvent apoptosis, which is commonly considered as a barrier to cancer[8,9].

Another hallmark is the enabling of replicative mortality. Normal cells are limited to a number of successive cell growth-and-division cycles. In contrast, cancer cells possess an unlimited replicative potential (enabling replicative immortality) that promotes the growth of macroscopic tumors[6]. There are two major barriers to cell proliferation: senescence and crisis. Repeated cell growth-and-division cycles lead to a natural induction to a nonproliferative state (senescence). Then, the cells that successful pass through the first phase, enter into a crisis phase, that leads to the death of the majority of cells. The cancer cells replicative behavior (cell growth-and-division cycles) is blocked in one of these barriers[6].

The induction of angiogenesis constitutes another important cancer hallmark. Since cancer tumors demand nutrients and oxygen to growth, and they release metabolic products and carbon dioxide[11], they require blood vessels. The tumor angiogenesis process occurs by the development of vasculature through the creation of new or the spread of vessels. In tumor progression, the angiogenesis starts and remains continuously, in order to sustain the growth of neoplastic cells[12]. The angiogenesis is regulated by signaling proteins which act as stimulator or inhibitor on cell surface receptors[5].

The sixth hallmark is characterized by the active invasion and metastasis mechanisms, in which cancer cells promote morphological modifications which allow their attachment to other cells and to the extracellular matrix (ECM)[5]. The invasion and metastasis process was already characterized in a sequence entitled: "invasion-metastasis cascade"[13,14]. The process starts with successive biological changes in cells, allowing the invasion by cancer cells into blood and

lymphatic vessels, and finish with growth of micro metastatic lesions on macroscopic tumors (metastasis).

The progress achieved in the last decade in cancer research allowed to identify novel potential hallmarks, namely the reprogramming of energy metabolism and evading immune destruction[6]. Genomic instability and mutability confer cancer cells the ability to modify or reprogram their cellular metabolism[6]. The succession of alterations in the genomes of neoplastic cells to promote mutant genotype confers a strategy to find subclones that can spread easily in the local tissue environment[6]. The role of the immune system in the resistance or eradication of cancer cells[6] is currently considered an important aspect of the development of tumors. The immune system constantly tracks and eliminate cancer cells; however, at some point, solid tumors display the ability to avoid the immune system detection[6]. Thus, the tumor immunity ability plays an expressive role in tumor formation and progression in humans[6].

These six hallmarks, together with the two emerging ones, provide a solid foundation to understand the biology of cancer and thus can be applied to develop new approaches to detect and treat cancer[6]. The correct identification of cancer stages alongside with early stage diagnosis are critical aspects that, if properly addressed, may increase the patient life-span and treatment efficacy[15]. Traditionally, cancer screening is based on the morphologic assessment of relevant cells collected through biopsy, however for many cancer types, including prostate, lung and ovary, this approach is not adequate to detect cancer in preliminary stages[15]. Recently, the increasing knowledge of the biology of cancer allowed to develop alternative possibilities to identify cancer at earlier stages. The connection between cancer tumors and blood vessels, for example, is responsible for the exchange of biomolecules between the tumors and the blood stream. Thus, the metabolic products associated with malignant cells can be found in human fluids. These biomolecules, which are usually expressed abnormally in the presence of cancer, may then be used as cancer biomarkers[15].

According to the National Cancer Institute, cancer biomarkers are molecules with biological activity or expression that are present in human fluids (saliva[16,17], urine[18–20], tears[21,22] and serum[23–25]), being their levels indicative of a pathologic condition[26]. Advances in genomics, proteomics and molecular biology allowed to identify several biomarkers that are now used as tools for early cancer detection[27], for the evaluation of disease progression and response to treatment, disease relapse, and more recently for point of care diagnosis. Cancer biomarkers can also be applied to distinguish benign from malignant tumors, or one type of malignancy from another.[28] Biochemical cancer biomarkers include DNA[29–31], mRNA[32,33], enzymes[34,35], proteins[36,37] and other

metabolites[38,39].

In the last decades, the importance of biomarkers in cancer detection research increased significantly[40]. A wide range of cancer biomarkers are currently used in clinical practice, and are approved by the Food and Drug Administration (FDA)[41]. Table 1.1. describes some of the cancer biomarkers used for diagnosis, stage definition, evaluation of response to treatment and prognosis of cancer.

Table 1.1. Examples of cancer biomarkers identified by the National Cancer Institute[42].

Tumorous biomarker	Biological fluids	Cancer type	[REF]
Alpha-Fetoprotein (AFP)	Blood	Hepatocelular carcinoma (HCC)	43
CA15-3/CA27.29	Blood	Breast	44
CA19-9	Blood	Pancreas and gallbladder	45,46
CA-125	Blood	Ovaries	47
Calcitonin	Blood	Medullary thyroid	48
Carcinoembryonic antigen (CEA)	Blood	Colorectal and breast	49,50
Chromogranin A (CgA)	Blood	Neuroendocrine tumors	51
Collagen, type I, alpha 1 (COL1A1)	Urine	Prostate	52
Cytokeratin fragments	Blood	Lung	53
EGFR	Blood	Prostate	54
Epidermal growth factor-containing fibulin-like extracellular matrix protein 1 (EFEMP1)	Blood and urine	Prostate	55
Exosomes	Urine	Prostate	56
HER2	Blood	Prostate	54
Lactate dehydrogenase (LDH)	Blood	Germ cell tumors	57,58
MMP-9	Urine	Prostate	59
miRNA (miR-222-3p*miR-24-3p/miR-30c-5p)	Urine	Prostate	60
Oncosomes (CD9 and STEAP)	Blood	Prostate	61
Prostate-specific antigen (PSA)	Blood and urine	Prostate	62
Prostatic acid phosphatase (PAP)	Blood	Prostate	63
Zinc-alpha 2-glycoprotein (AZGP1)	Blood	Prostate	64

1.2. Prostate cancer

Prostate cancer (PCa) is the second most common type of cancer in men, representing 17% of the cancer-related diseases in males[65]. It is the fifth leading cause of cancer death worldwide with the highest mortality rates found in the Caribbean and Southern and Middle Africa[65]. Ethnicity and age are amongst the major risk factors with 97% of prostate cancer cases occurring in men over 50 years old[65]. Considering that life expectancy is increasing in developed countries, an increase in PCa cases is therefore expected. The costs associated with the treatment of prostate cancer are high; in Europe alone, the total economic costs associated with the treatment of PCa exceeded €8.43 billion up to 2013[66]. In order to decrease the burden associated with the increasing incidence of PCa, effective diagnosis and treatment monitoring is of utmost importance. Prostate cancer diagnosis is usually performed through digital rectal examination (DRE), transrectal ultrasound (TRUS) guided biopsy, and measurement of PCa biomarkers in blood. DRE is the most common procedure. However, DRE has poor reliability, particularly in small tumors that have not reached the prostatic capsule and therefore will not be identified[67]. Transrectal ultrasound guided biopsy is an invasive technique that allows the classical identification of cancer cells through biopsy. However, it has several and serious side effects, like febrile urinary tract infection (UTI), urosepsis, bleeding and hematuria. In addition, this procedure is also connected to 15%-20% of false negative results[68]. In addition to DRE and TRUS, several biomarkers have been identified and can be used in prostate cancer diagnosis (Table 1.2.). The prostate-specific antigen (PSA) blood test is still the most used diagnosis method due to its strong correlation with PCa[69].

In recent years, due to the increase in the available treatments, the monitoring of treatment efficacy, disease relapse and prognosis are gaining importance. For that, new biomarkers have been studied and implemented in the clinical practice. These biomarkers allow to identify patients with a poor prognosis so that novel treatments can be initiated earlier[70]. In the past few years, several studies suggested that serum LDH levels in patients with solid tumors, including prostate cancer, are correlated with an adverse prognosis[70]. Therefore, the concomitant evaluation of both PSA and LDH in the same patient will allow to achieve better PCa diagnosis and prognosis, so that the most effective treatment may be selected at earlier stages.

Table 1.2. Examples of PCa biomarkers.

Tumorous biomarker	Biological fluids	[REF]
8-hydroxydeoxyguanosine	Urine	[71]
α-methylacyl coenzyme a racemase (amaCr)	Urine	[72,73]
annexin a3	Urine	[74]
Collagen, type I, alpha 1 (COL1A1)	Urine	[52]
E-cadherin	Blood	[75–77]
EGFR	Blood	[54]
Epidermal growth factor-containing fibulin-like extracellular matrix protein 1 (EFEMP1)	Blood and urine	[55]
Exosomes	Urine	[56]
Golgi membrane protein 1 (Golm1)	Urine	[78]
GSTP1.	Urine	[79–81]
HER2	Blood	[54]
Interleukin 6 (IL-6) and Interleukin 6 Receptor (IL-6R)	Blood	[82,83]
Kallikrein-4 (KLK-4)	Blood	[84]
Minichromosome maintenance 5 protein (Mcm5)	Blood	[85]
MMP-9	Urine	[59]
miRNA (miR-222-3p*miR-24-3p/miR-30c-5p)	Urine	[60]
Oncosomes (CD9 and STEAP)	Blood	[61]
PCA3	Blood and Urine	[86–88]
Prostate-specific antigen (PSA)	Blood and urine	[62]
Prostatic acid phosphatase (PAP)	Blood	[63]
Steroid Receptor Co-Activator-3 (Src-3)	Blood	[89,90]
TMPRSS2–ETS	Urine	[91–93]
Zinc-alpha 2-glycoprotein (AZGP1)	Blood	[64]

1.2.1. Prostate-specific antigen (PSA)

Prostate-specific antigen (PSA) is a serine protease (human kallikrein gene family) (Figure 1.2.) with 33 KDa and an isoelectric point (pI) of 6.5 – 8[94,95], produced and secreted in prostatic epithelium glands. In 1988, the physiological function of PSA was revealed as a liquefying agent of seminal fluids, and this concept is the most commonly accepted until today[96]. PSA liquefies the seminal clot produced after ejaculation, facilitating the spermatozoa transport along the female

reproductive tract. The dissolution of the gel proteins from the seminal fluid (cleavage of semenogelin 1 and 2 (SEMG1, SEMG2), fibronectin, laminin and gelatin) occurs due to the chymotrypsin like endoproteolytic PSA activity[96,97]. In normal prostatic conditions, only a small portion of PSA escapes the prostatic gland and enters the circulatory system. The PSA diffuses into the circulatory system in its free form, where it interacts with protease inhibitors (primarily alpha1-antichymotrypsin, ACT) and forms a complex that can detected as a 80-90 KDa protein complex[98]. This complexed form manifests little or no catalytic activity in blood[99]. Increased levels of PSA in blood are believed to be a consequence of the disruption in the prostate architecture, including the basement membrane disordering, the loss of basal cell layer, alterations in the duct lumen architecture and epithelial cell polarity. Prostate tumors are characterized by such disruptions and thus by enabling the passage of PSA into circulation, elevating the basal PSA levels.

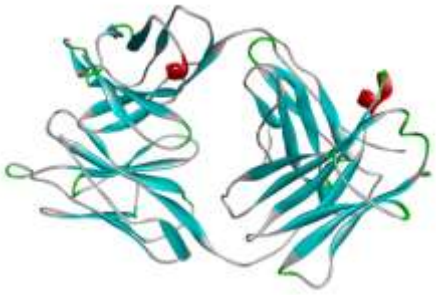

Figure 1.2. Structure of Prostate-specific antigen (PSA) (PDB: 2zch).

The quantification of total PSA (tPSA) and free PSA (fPSA) in human fluids has a significant role in the clinical management of PCa patients[100]. In 1979, Wang et al.[101] reported the purification of PSA from prostate tissue. The authors showed that PSA was present in normal and benign hyperplastic prostate, as well as in malignant prostatic tissue and was undetected in any other human tissues[101]. After this study, PSA emerged as a potential prostate cancer biomarker. Catalona and co-workers[102] latter proposed the serum PSA measurement as a first-line screening test for prostate cancer. Mostly based in Catalona[102] seminal work, in 1994, the FDA approved PSA as a biomarker to be evaluated in screening methods to identify prostate cancer.

A PSA value of > 4.0 $ng.mL^{-1}$ has been defined in the literature[103] as abnormal and it is frequently used as a cut-off, although for younger men a cut-off level of < 2.5 $ng.mL^{-1}$ was recently proposed. For values between 4.0 and 10.0 $ng.mL^{-1}$, the grey zone, there exists a 22% to 27% likelihood of cancer, whereas values above 10 $ng.mL^{-1}$ yield up to a 67% chance of prostate

cancer[104]. Because PSA levels increase steadily with age, some urologists advocate the use of age-related "normal" PSA cut-offs[105], rather than using the limit of > 4 ng.mL^{-1} as universal. Oesterling et al.[106] and Luboldt et al.[107] concluded that the upper limit of the PSA cutoff, achieving 95% of specificity, would increase with age. Therefore, to maintain the equitable 95% specificity or an equivalent 5% false-positive rate across different ages, the PSA cutoff for recommending biopsy must necessarily increase with age. PSA test as a screening method for PCa is recommended to male individuals above 50 years old; however, in African American man the age decreases to 40 years old, since ethnicity is a relevant factor for PCa incidence[108].

PSA is present in different biological fluids including blood, urine and semen. Hence, the quantification of PSA in any of these fluids could be used to identify PCa. The quantification of PSA levels in urine was firstly studied by Graves and co-workers[109] in 1985. Since then, other authors reported the PSA quantification in urine[110–112]. In fact, urine PSA levels showed to be advantageous compared to serum PSA, being considered a non-invasive alternative for the early detection of PCa cancer. Although the exact mechanism by which urinary PSA levels are altered in PCa patients is not fully understood, some authors suggest that the disturbance of prostate architecture and the neovascularization alters the secretion of prostatic secretions (including PSA) in the prostatic urethra[113]. These changes lead to a decrease of PSA excretion through urine and to a consequent increase in PSA levels in the bloodstream. Thus, in prostate cancer patients the levels of PSA in blood are higher and the levels in urine are lower than the ones found in healthy patients[113]. The threshold value for PSA in urine was set at 150 ng.mL^{-1}. This cutoff value for urinary PSA displays a sensitivity of 92.5%[113] and it is recommended that patients with PSA levels <150 ng.mL^{-1} in urine should perform a prostatic biopsy[113]. Despite the many advantages of urine PSA testing, this technique is not yet used in the clinical practice, probably due to the lack of validated and cost-effective detection and quantification methods.

1.2.2. Lactate dehydrogenase (LDH)

Lactate dehydrogenase (LDH), EC1.1.1.27 (Figure 1.3), is a NAD+-dependent enzyme (oxidoreductases family), with a molecular weight between 115 and 154 kDa[114]. LDH is responsible for the anaerobic conversion of pyruvate to lactate in the last step of lactic fermentation[115]. The oxidation reaction occurs in the LDH active site that presents hydrophilic and charged amino acids residues, such as glutamate, glutamine, aspartate, arginine and histidine[116]. LDH is usually present in the liver, cardiac muscle, kidneys, skeletal muscle and erythrocytes. It is composed of four polypeptide chains, each one encoded by a separated gene (M and H)[115], resulting in five

combinations of polypeptide subunits and five molecular isoforms of LDH (M_4, MH_3, M_2H_2, M_3H and $H_{4)}$, found in different quantities depending on the originating tissue[117 118].

As previously mentioned, one of the hallmarks of cancer is the reprogramming of energy metabolism and neo-angiogenesis. Cancer cells energetic demands led these cells to produce high levels of pyruvate and lactate[119]. Several authors suggested that LDH ensures both an efficient anaerobic/glycolytic metabolism and a reduced dependence on oxygen under hypoxic conditions in tumor cells[115]. The relation between LDH levels and hypoxia is mediated by a tumor-driven angiogenesis pathway through the abnormal activation of the hypoxia inducible factor 1 (HIF-1)[115]. The biological activity of this hypoxia inducible factor is modulated by HIF-1α. This factor, in turn, upregulates several genes responsible for glycolytic energy metabolism, angiogenesis, erythropoiesis and cell survival. Because tumor hypoxia is enough to alter the gene expression of this factor, it will downregulate several other genes that encode for vascular endothelial growth factor, as an indirect marker of tumor hypoxia, neo-angiogenesis and worse prognosis, and therefore it is an useful cancer biomarker, particularly for prognosis evaluation[115].

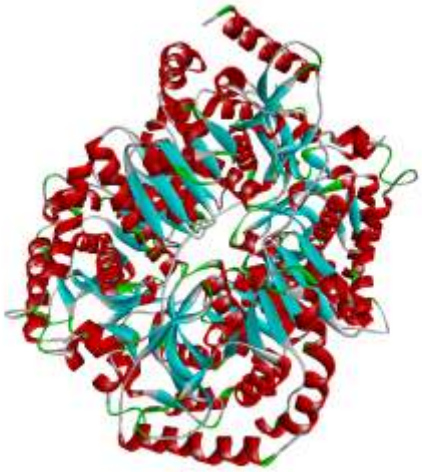

Figure 1.3. Structure of Lactate dehydrogenase (LDH) (PDB: 1i10).

LDH was already approved by the American Society of Clinical Oncology as a biomarker of germ cell tumors[120]. More recently, the LDH role in melanoma, lung cancer, prostate cancer, osteosarcoma and kidney cell carcinoma[121–124] was highlighted in clinical trials. The normal levels of LDH in serum range between 100 and 300 U/L, and individuals with LDH levels (>225 U/L) have survival rates significantly reduced[125]. Individuals that display high levels of LDH (> 300 U/L) showed an average survival of 7 months, against the 12 months for patients with regular LDH levels[125]. The cutoff value corresponding to a high LDH is generally set at 250 U/L[70], and LDH values have already been incorporated in prognostic scores for different types of cancer[126].

However, the clinical significance of LDH levels in biological fluids is still under discussion[127]. Nishikawa et al.[128] proposed that urine LDH isoenzymes levels might be a useful tool to evaluate urinary tract malignancy, especially in early stages. Notwithstanding, LDH-5 levels in body fluids can change with bacterial infections, particularly in urine [127].

LDH isoenzymes are expressed in different levels in individuals that present PCa or benign prostatic hyperplasia (BPH)[129]. High LDH-5 levels and low LDH-1 levels occur in PCa cases, while in BPH cases the opposite behavior is observed[130]. In PCa early stage patients, LDH levels are barely abnormal. However, LDH levels display an added-value for assessment of prognosis, therapeutic efficacy and evaluation of symptoms[131]. LDH levels already shown to be an efficient prognostic indicator for PCa and breast cancer in patients with bone metastasis[131,132]. Moreover, LDH-5 overexpression is sensitive to highly proliferating prostate carcinomas and can be useful to monitor the radiotherapy evolution[133]. LDH levels associated to circulating tumor cells counts (CTC) is an effective biomarker for castration-resistant prostate cancer (CRPC)[134], and also an effective tool for discrimination between high-risk and low-risk patients with CRPC[135]. The results of two recent systematic reviews and meta-analysis[70,124] further strengthened the usefulness of LDH as a prognosis biomarker in metastatic carcinomas. LDH levels quantified before treatment are considered as a simple and cost-effective prognostic factor that also has the potential to be a predictive biomarker that can be used to guide therapeutic decisions[70].

1.3. Cancer biomarkers detection methods

Cancer biomarkers are of high relevance for early cancer detection. However, these biomarkers are usually present at low levels and present in complex matrices such as human fluids. Therefore, the major challenges in cancer detection through the identification/quantification of biomarkers are to avoid the interferences of other contaminant molecules and to concentrate cancer biomarkers up to levels above the equipment detection limits.

Several techniques have been applied for cancer biomarkers detection and quantification[136], such as polymerase chain reaction (PCR)[137,138], enzyme-linked immunosorbent assay (ELISA)[139,140], electrophoresis[141,142], surface plasmon resonance (SPR)[143,144], surface enhanced Raman spectroscopy (SERS)[145–147], microcantilivers[148,149], and colorimetric[150,151], electrochemical[152,153] and fluorescence assays[154,155]. The choice of these methods are obviously dependent on the type of biomarker to be quantified. For protein biomarkers, for example, the methods most commonly used include ELISA, and electrochemical, electrical and optical detection methods [139,140]. More

recently, the identification and quantification of proteins as cancer biomarkers by mass spectrometry has also been applied[136]. In general, the quantification of protein biomarkers exhibits several difficulties associated with their intrinsic nature. Those difficulties include for example their sensitivity to changes in temperature, pH and ionic strength, their incapacity to replicate themselves contrarily to what happens with nucleic acid biomarkers that are easily "amplified", and their concomitant occurrence with other proteins and biomolecules in biological fluids and tissues[136]. Such difficulties are, for some biomarkers and types of cancer, translated into a lack of accuracy, sensitivity and specificity of diagnostic methods.

The identification and quantification of PSA is the most widely used assay to detect prostate cancer at earlier stages. Amongst the various identification and quantification techniques available for PSA, ELISA[151,156], fluorescence microscopy[157], surface plasmon resonance technology[158], immunochromatography[159,160], lateral flow immunoassay[161], and immunochemiluminescence are the most employed. In the clinical practice, immunoassays are generally preferred and are approved by the FDA[162]. Even though some of these techniques have an adequate detection limit, most of them display significant drawbacks. ELISA is a powerful technique for antigen quantification, but requires highly skilled technical operators, laborious treatment steps, high cost specific antibodies, signal amplification using biochemical reactions, and specific and expensive equipment, and is thus time-consuming and expensive[156,163–165]. On the other hand, fluorescence and electrochemistry-based methods require the labelling of the target analyte for signal amplification. Furthermore, prolonged exposure of fluorescence dyes to excitation light source causes the photobleaching and quenching of signals that may lead to underestimated results[136].

Over the recent years, several authors have reported new PSA detection technologies using DNA microarrays and protein microarrays[166] with promising results in terms of detection limits; however, such sophisticated technologies are far from being commercially available. Mass spectrometric methods with or without antibodies[167] have also been proposed; yet, they require highly sophisticated and expensive equipment that is generally not available in clinical laboratories.

Non-invasive methods for the PSA quantification in urine have been additionally developed[113]. However, the urine samples polishing is not an easy task. Several methods of extraction and pre-concentration of urine samples, such as dialysis and lyophilization[168,169], filtration[170], precipitation[171] and SPE[172] have been proposed. The major drawback in urine proteomic analysis is the fact that protein losses are high, not allowing accurate quantifications[173],

thus requiring the development of a simple and efficient method to extract and concentrate PSA from human urine.

LDH detection in biological samples is commonly performed using spectrophotometric assays[174]. This method is based on the LDH ability to catalyze lactates to pyruvates. During this reaction, NAD+ is reduced to NADH, which can be monitored at 340 nm. LDH also can be quantified by liquid chromatographic (LC)[175,176] and electrochemical methods[177]. All of the aforementioned methods present however clinical diagnostic limitations (low accuracy, sensitivity and specificity) and some (particularly LC-based methods) are of high cost requiring expensive analytical equipment[136].

Generally, the quantification of LDH occurs in human serum, plasma and blood. Due to the high amount of protein in these biological fluids, a correct sample preparation is the most crucial step in the biomarkers quantification[178]. Serum is a human fluid that contains more than 10,000 proteins[179]. The abundance of albumin in serum (35–50 mg/mL) is the most critical challenge in proteomic quantification[180]. High levels of proteins in serum promotes interferences with the identification and quantification of lower abundance proteins (lower than ng/mL in serum), such as cancer biomarkers[180].

In general, all cancer biomarkers quantification methods in human fluids (serum, plasma, whole blood and urine) require samples' pre-treatment in order to eliminate the high amount of other non-target proteins and metabolites to allow an accurate diagnosis. In this context, aqueous biphasic systems (ABS) can be seen as viable methods of extraction, concentration and purification of selected cancer biomarkers from human fluids, with significant advantages over conventional methods. The use of ABS to separate the target proteins from matrix interferences, such as other proteins and metabolites, will contribute to avoid false positives or negatives, one important limitation of the commercially available methods.

1.4. Aqueous biphasic systems

Aqueous biphasic systems (ABS) are used in liquid-liquid extraction methods that received a large attention for being mainly composed of water, promoting thus a biocompatible environment for bioactive molecules[181]. ABS are also considered environmental-friendly technologies since the use of volatile and hazardous organic solvents is avoided. They are usually constituted by two polymers, a polymer and a salt or two salts, that above a given concentration undergo separation into two coexisting phases[182].

Polymer-based ABS were demonstrated to be a promising technique for the extraction and

concentration of several biomolecules from human fluids, such as lactate dehydrogenase of *Plasmodium* (pLDH)[183], DNA[184], extracellular vesicles (SVE)[185,186] and alkaline phosphatase[187]. Furthermore, polymer-polymer and polymer-salt ABS were already applied in human disease monitoring and diagnosis including bone diseases[187] and cancer[185,186]. Raymond *et al.*[187] demonstrated that a system constituted by polyethylene glycol + dextran is capable to separate selectively alkaline phosphatase from its isoforms, valuable in the detection of bone diseases. The authors reported that the difference of the partition behavior of the alkaline phosphatase isoforms is based on the type of surfactants applied and specific anchoring interactions, which benefit the selective separation. In the cancer detection field, the system composed of polyethylene glycol + dextran was used to isolate extracellular vesicles from human serum[185,186]. These were isolated in one-step with purities between 70-75%. However, to increase their purity, a combined process with centrifugation and ABS allowed the removal of proteins from human serum increasing the purity of the extracellular vesicles up to 95%[185]. The behavior of PSA partition in presence of other human proteins (human serum albumin, human transferrin, and human gamma-globulin) was evaluated in ABS constituted by dextran-ficoll[157], where low PSA partition coefficients were obtained (around 1.5). The authors reported that the PSA partition to the dextran-rich phase decreases in the presence of other proteins. Electrostatic forces induced by protein-protein interactions lead to the formation of PSA-protein complex which induce changes in the partition of PSA[157]. The effect was more pronounced in presence of high levels of proteins, showing that the PSA accurate quantification in human fluids is only possible by samples' pre-treatment and by the removal of contaminant proteins.

Despite being widely exploited, conventional polymer-based ABS present some limitations in their phases polarities and a high viscosity, making difficult the phase separation and to tailor these systems selectivity. On the other hand, less traditional ABS composed of organic solvents + salts, ionic liquids (ILs) + salts and surfactants + salts present a higher polarity difference between the two phases, representing thus a more efficient and selective alternative to common polymer-based ABS. These alternative ABS were applied to detect malaria[183], cancer[184] and endocrine disruptors[188] in human fluids. In an attempt to produce an apparatus for malaria detection, lateral flow immunoassay (LFA) combined to surfactant-based ABS was established[183]. The authors developed a diagnostic strip paper that in contact with the ABS detects lactate dehydrogenase from Plasmodium (*p*LDH). In this work, ABS allowed to concentrate *p*LDH around 10 times and significantly decreased the time of diagnosis to around 8h[183]. The concentration of biomarkers using ABS constituted by surfactants + salts was also addressed by Mashayekhi et *al.*[184] to improve

early cancer detection. DNA fragments were extracted mainly to the ABS top phase (salt-rich phase) and under the best conditions an increase of 9-fold of the DNA concentration was achieved.

Recently IL-based ABS have been extensively investigated[182]. ILs are molten salts constituted by a large organic cation and an inorganic/organic anion with melting temperatures below 100 °C[189]. Due to their ionic composition, most ILs present unique characteristics, such as negligible volatility at room temperature, non-flammability, high thermal and chemical stabilities, and a strong solvation capability for a wide range of compounds[190,189]. Some common chemical structures of ILs are displayed in Figure 1.4.

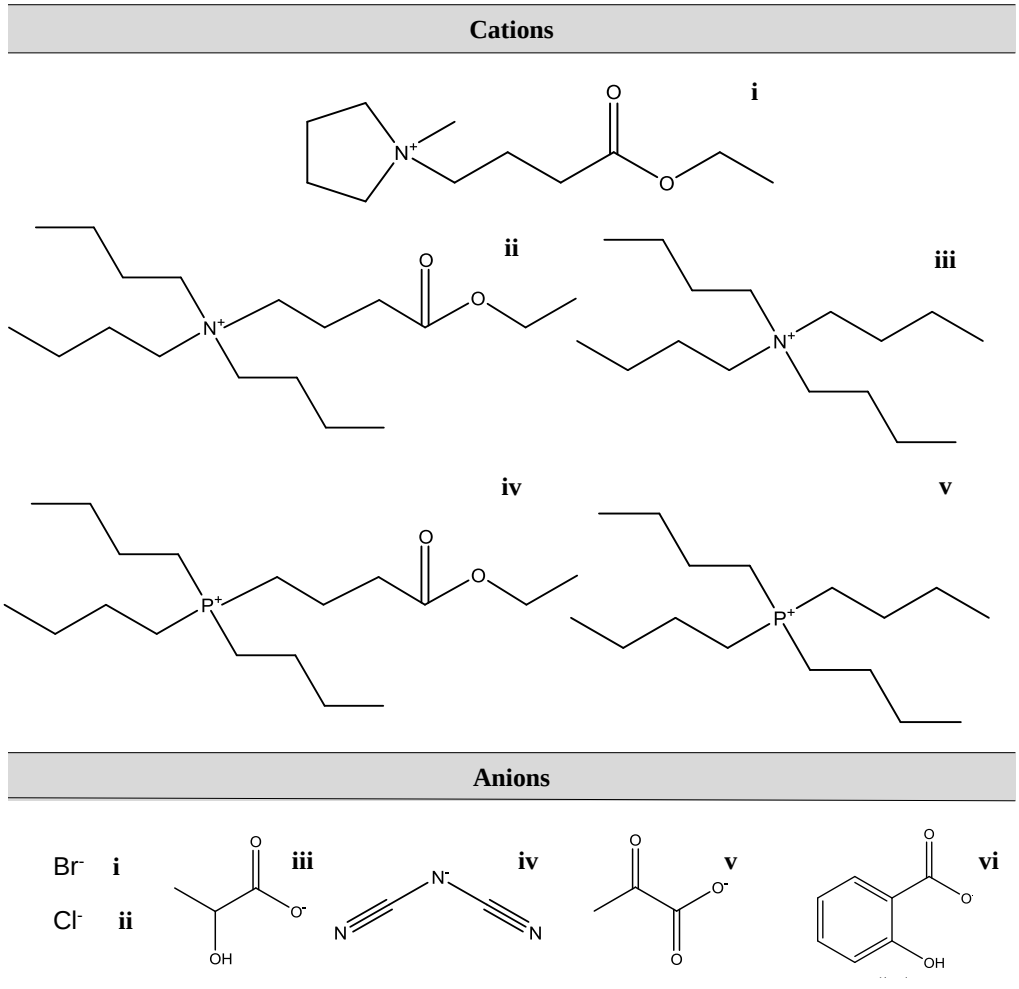

Figure 1.4. Chemical structures of ILs. Cations: (i) N-(1-methylpyrrolidyl-4-butoxy-4-oxoethyl)ammonium, (ii) tri(n-butyl)[4-butoxy-4-oxoethyl]ammonium, (iii) tetrabutylammonium, (iv) tri(*n*-butyl)[4-butoxy-4-oxoethyl] phosphonium, (v) Tetrabutylphosphonium. Anions: (i) bromide, (ii) chloride, (iii) lactate, (iv) dicyanamide, (v) pyruvate, (vi) salicylate.

One of the most important advantages of ILs is the fact that their physicochemical properties

can be tailored by manipulating the chemical structure of their ions, and thus it is possible to synthesize ILs for a specific application. Due to this characteristic, the ILs solubility, solvation ability, biodegradability and toxicological features can be tailored for a given purpose. Their tailoring ability is extensible to IL-based ABS[191], supporting the large interest devoted to this type of systems in the past years. IL-based ABS have been used in the separation of enzymes, proteins, amino acids, antibiotics, among many other solutes[182,192,193]. Albeit these studies can be used as guidelines for the application of IL-based ABS in the extraction of proteins, in most of these works, imidazolium-based ILs and inorganic salts were used as phase-forming components[182,193]. Regarding proteins, these IL-based ABS have been applied in the extraction of alcohol dehydrogenases[194], *aloe* proteins[195], azocasein[196], BSA[192,197–201], *Cordyceps sinensis* proteins[202], cytochrome c[203–205], hemoglobin[198,199,206], *Horseradish* peroxidase[207], immunoglobulin Y and G[208], lipases[209–213], myoglobin[192,214], papain[200,215], pepsin[192], rubisco[216], transferrin[197] and Y-globulins[203]. Yet, to the best of our knowledge, works on the use of IL-based ABS and cancer biomarkers have not yet been reported. Most of the works in literature with IL-based ABS and proteins were carried out with imidazolium-based ILs[193]. Aiming at finding more biocompatible alternatives, the ABS studied in this thesis for the extraction of amino acids, proteins and cancer biomarkers are formed by ammonium- or phosphonium-based ILs. These tetraalkyl-based compounds also are less expensive and thermally more stable than the equivalent imidazolium counterparts[217].

1.5. Scope and objectives

Cancer is a global epidemic with more than 14 million new cases diagnosed each year and with an estimated annual economic cost of approximately €1 trilion[1]. Thus, investments in cancer early-stage diagnosis methods are critically required to decrease mortality, to increase the patient's lifespan and to decrease the associated economic and social burden of this disease. In the last decades, advances in scientific and medical research resulted in the ability to develop novel strategies to prevent and detect several diseases, including cancer. Nevertheless, the development of early detection methods for cancer is still at an initial stage, and a wide range of problems need to be solved until low-cost yet efficient methods become available worldwide. The quantification of cancer biomarkers in human fluids is a key method for cancer early-stage detection. The levels of prostate-specific antigen (PSA) and lactate dehydrogenase (LDH) in human fluids have been used as relevant diagnosis and prognosis biomarkers of prostate cancer. However, due to their low levels in human fluids and complexity of biological matrices, expensive and time-consuming methods are necessary to purify and concentrate these cancer biomarkers before their

quantification. Based on this need, this thesis focus on the development of novel strategies for the pretreatment of human samples envisaging early-stage cancer detection according to the following steps:

I) SCREENING of cost-effective ABS platforms for the separation and purification of amino acids and proteins to better understand the complexity and conditions required to deal with protein-based cancer biomarkers;

II) DEVELOPMENT of IL-based ABS as effective tools of concentration and purification of cancer biomarkers from human fluids aiming their easier and more accurate detection/quantification.

In order to visualize the thesis scope and structure, an illustrative representation of its layout is displayed in Figure 1.5.

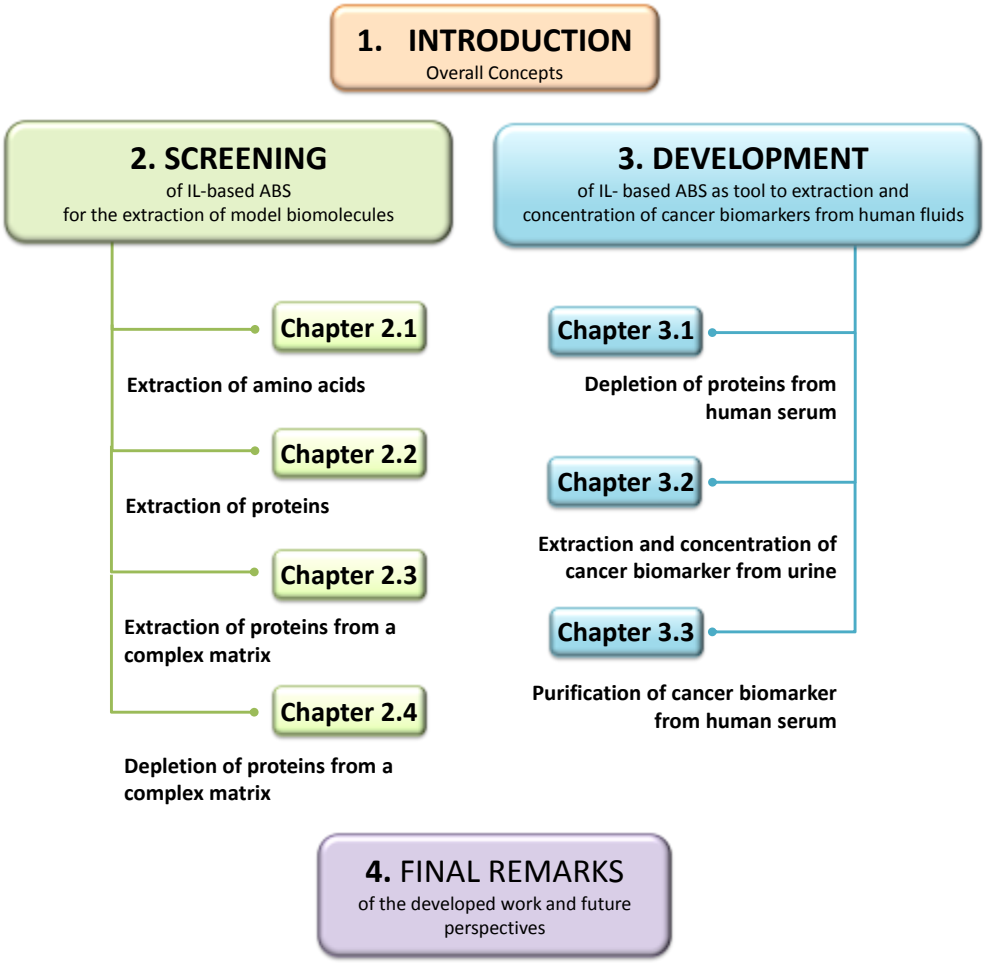

Figure 1.5. Present thesis layout.

In order to better understand the partition behavior of cancer biomarkers in IL-based ABS, and since these biomarkers are proteins, ABS composed of glycine-betaine-based ILs and Na_2SO_4 were initially studied (**Chapter 2.1**). Further to the ILs synthesis and characterization, the ABS

phase diagrams were determined and their ability to extract biomolecules was evaluated with two amino acids, namely tyrosine and tryptophan. The results obtained indicate that the amino acids preferentially partition to the IL-rich phase with remarkable extraction efficiencies. The acquired knowledge with the amino acids behavior in ABS represents a relevant basis to understand the interactions of more complex structures, such as proteins. In the following Chapter (**Chapter 2.2**), novel ABS composed of phosphonium- and ammonium-based ILs and a citrate-based salt were developed and used for the extraction of the protein Bovine Serum Albumin (BSA). These ILs, being more hydrophobic than the well-studied imidazolium-based, allow the use of lower amounts of phase-forming components to create ABS. Moreover, these ILs tend to be less toxic and more biodegradable than their imidazolium counterparts. It is shown that the extraction efficiencies of BSA to the IL-rich phase are of 100%, maintained up to high protein concentrations (at least up to 10 $g.L^{-1}$). The recovery of the BSA from the IL-rich phase by dialysis was also demonstrated in addition to the IL recyclability and reusability. The protein stability in the IL-rich phase also was confirmed. In the following chapter, **Chapter 2.3**, the ability of ABS composed of polyethylene glycols of different molecular weights (PEG 400, 600 and 1000 $g.mol^{-1}$) and a citrate-based salt to selectively extract ovalbumin (OVA) from complex protein mixtures (directly from egg white) was investigated. These ABS do not require the use of ILs and make use of a more biocompatible and biodegradable salt. In almost all ABS it was observed a preferential partition of ovalbumin to the polymer-rich phase, with extraction efficiencies higher than 90%. The best ABS were then applied to the purification of ovalbumin from egg white allowing to gather novel knowledge on the behavior of several proteins and on dealing with complex matrices. Successful results were obtained since pure OVA was isolated and recovered from the complex matrix. In **Chapter 2.4** the recovery of Major Royal Jelly Proteins (MRJPs) from honey (biological complex mixture) was investigated using ABS composed of phosphonium-based ILs and carbohydrates. In all systems, MRJPs almost completely precipitate at the ABS interface. The obtained recovery yield of MRJPs range between 83.8 and 97.3%, with MRJP1 obtained with a purity level ranging from 80% to 90%. This work demonstrates the use of ABS as depletion methods, relevant as pretreatment strategies of biological samples.

All the works developed in **Chapter 2** provide new knowledge towards the understanding of the behavior of amino acids and proteins in IL-ABS, i.e. which conditions favor their selective extraction or precipitation. This type of knowledge is relevant to identify the most promising ABS to be used in the concentration and purification of cancer biomarkers. Amino acids were investigated since they correspond to the structural units of proteins. OVA and BSA were chosen

as model proteins because they correspond to albumins extensively studied in a wide variety of fields, and have a similar amino acids sequence with HSA, the most abundant protein in human serum. The last work, carried out with honey and MRJPs, was performed to address the use of ABS in highly complex matrices.

Based on the previous knowledge and on the requirement of finding more biocompatible IL-based ABS for the pretreatment of human fluids, **Chapter 3.1** addresses the synthesis of glycine-betaine-based-ILs and their study as phase-forming components of ABS for the depletion of Human Serum Albumin (HSA) and Immunoglobulin G (IgG) from human serum. The obtained results reveal that most of the systems investigated allow the complete depletion of HSA and IgG from serum to the ABS interphase, in a single-step. The depletion of these highly abundant proteins allow the identification of low abundance proteins in serum, such as transferrin. In **Chapter 3.2**, IL-based ABS were applied to extract and concentrate cancer biomarkers, namely PSA, present in human urine. The complete extraction of PSA to the IL-rich phase was achieved, with its simultaneous concentration up to 250-fold in the IL-rich phase. Finally, in **Chapter 3.3**, the selectivity of the investigated IL-based ABS for LDH in presence of contaminant proteins typically found in human serum was ascertained. The IL-based ABS developed allowed the one-step extraction of LDH from human serum, while leading to the precipitation of the remaining proteins present in serum, representing thus a depletion method.

The final section of this thesis (**Chapter 4**) provides a global view of the developed work, with some final remarks and future perspectives.

1.6. References

1. Cancer. WHO (2015). World Health Organization (2015) Cancer. Accessed on February 3, 2017; Available from: http://www.who.int/mediacentre/factsheets/fs297/en/.

2. Ferlay, J., Soerjomataram, I., Dikshit, R., Eser, S., Mathers, C., Rebelo, M., Parkin, D.M., Forman, D., Bray, F.. Int J Cancer. 2015;136(5):359-386.

3. Instituto Nacional de Cancer José Alencar Gomes da Silva. INCA - Instituto Nacional de Câncer - Estimativa 2016.; 2016.

4. Forouzanfar, M.H., Afshin, A., Alexander, L.T., Biryukov, S., Brauer, M., Cercy, K., Charlson, F.J., Cohen, A.J., Dandona, L., Estep, K., Ferrari, A.J., Frostad, J.J., Fullman, N., Godwin, W.W., Griswold M, Hay SI, Kyu HH, Larson, H.J., Lim, S.S., Liu, P.Y., Lopez, A.D., Lozano, R., Marczak, L., Mokdad, A.H., Moradi-Lakeh, M., Naghavi, M., Reitsma, M.B., Roth, G.A., Sur, P.J., Vos, T., Wagner, J.A., Wang, H., Zhao, Y., Zhou, M., Barber, R.M., Bell, B., Blore, J.D., Casey, D.C., Coates, M.M., Cooperrider, K., Cornaby, L., Dicker, D., Erskine, H.E., Fleming, T., Foreman, K., Gakidou, E., Haagsma, J.A., Johnson, C.O., Kemmer, L., Ku, T., Leung, J., Masiye, F., Millear, A., Mirarefin, M., Misganaw, A., Mullany, E., Mumford, J.E., Ng, M., Olsen, H., Rao, P., Reinig, N., Roman, Y., Sandar, L., Santomauro, D.F., Slepak, E.L., Sorensen, R.J.D., Thomas, B.A., Vollset, S.E., Whiteford, H.A., Zipkin, B., Murray, C.J.L., Mock, C.N., Anderson, B.O., Futran, N.D., Anderson, H.R., Bhutta, Z.A., Nisar, M.I., Akseer, N., Krueger, H., Gotay, C.C., Kissoon, N., Kopec, J.A., Pourmalek, F., Burnett, R., Abajobir, A.A., Knibbs, L,D., Veerman, J.L., Lalloo, R., Scott, J.G., Alam, N.K.M., Gouda, H.N., Guo, Y., McGrath, J.J., Charlson, F.J., Erskine, H.E., Jeemon, P., Dandona, R., Goenka, S. Lancet. 2016;388(10053):1659-1724.

5. Exploring cancer proliferative signaling pathways. Acessed on September 29, 2015; Available from: http//www.thermofisher.com/content/dam/LifeTech/global/promotions/global/images/aai-2015/aai.
6. Hanahan, D., Weinberg, R.A. Cell. 2011;144(5):646-674.
7. Hanahan, D., Weinberg, R.A. Cell. 2000;100(1):57-70.
8. Adams, J.M., Cory, S. Natl Inst Heath. 2007;26(9):1324-1337.
9. Lowe, S.W., Cepero, E., Evan, G. Nature. 2004;432(7015):307-315.
10. Evan, G., Littlewood. T. Science (80-). 1998;281(5381):1317-1322.
11. Kumar, V., Abbas, A. AJ. Robbins Basic Pathology. 9th editio. Elsevier Saunders; 2013.
12. Hanahan, D., Folkman, J. Cell. 1996;86(3):353-364.
13. Talmadge, J.E., Fidler, I.J. Cancer Res. 2010;70(14):5649-5669.
14. Fidler, I.J. Nat Rev Cancer. 2003;3(6):453-458.
15. Feng, Q., Yu, M., Kiviat, N.B..Crit Rev Clin Lab Sci. 2006;43(5-6):497-560.
16. Sun, Y., Xia, Z., Shang, Z., Sun, K., Niu, X., Qian, L., Fan, L.. Nat Publ Gr. 2016;(April):1-11.
17. Xiao, H., Zhang, Y., Kim, Y., Kim, S., Kim, J.J., Kim, K.M., Yoshizawa, J., Fan, L-Y., Cao, C-X., Wong, D.T.W. Sci Rep. 2016;6(October 2015):22165.
18. Zhang, H., Cao, J., Li, L., Liu, Y., Zhao, H., Li, N., Li, B., Zhang, A., Huang, H., Chen, S., Dong, M., Yu, L., Zhang, J., Chen, L... Sci Rep. 2015;5:1-13.
19. Hessels, D., Schalken, J. A.. Asian J Androl. 2013;15(3):333-339.
20. Sapre, N., Macintyre, G., Clarkson, M., Naeem, H., Cmero, M., Kowalczyk, A., Anderson, P.D., Costello, A.J., Corcoran, N.M., Hovens, C.M. Br J Cancer. 2016;114(4):454-462.
21. Lebrecht, A., Boehm, D., Schmidt, M., Koelbl, H., Schwirz, R.L., Grus, F.H.. Cancer Genomics and Proteomics. 2009;6(3):177-182.
22. Lebrecht, A., Boehm, D., Schmidt, M., Koelbl, H., Grus, F.H.. Cancer Genomics and Proteomics. 2009;6(2):75-84.
23. Zhang, Y., Zhang, D., Wang, F., Xu, D., Guo, Y., Cui, W... Sci Rep. 2015;5(August):17942.
24. Taylor, D.D., Gercel-Taylor, C.. Gynecol Oncol. 2008;110(1):13-21.
25. Resnick, K.E., Alder, H., Hagan, J.P., Richardson, D.L., Croce, C.M., Cohn, D.E.. Gynecol Oncol. 2009;112(1):55-59.
26. National Cancer Institute at the National Institutes of Health. Accessed November 1, 2015; Available from http//www.cancer.gov/publications/dictionaries/cancer-terms?CdrID=45618. 2012.
27. Ludwig, J.A., Weinstein, J.N. B. Nat Rev Cancer. 2005;5(11):845-856.
28. Mayeux, R.. NeuroRx. 2004;1(2):182-188.
29. DeVos, T., Tetzner, R., Model, F., Weiss, G., Schuster, M., Distler, J., Steiger, K.V., Grützmann, R., Pilarsky, C., Habermann, J.K., Fleshner, P.R., Oubre, B.M., Day, R., Sledziewski, A.Z., Lofton-Day, C.. Clin Chem. 2009;55(7):1337-1346.
30. Dawson, S-J., Tsui, D.W.Y., Murtaza, M., Biggs, H., Rueda, O.M., Chin, S-F., Dunning, M.J., Gale, D., Forshew, T., Mahler-Araujo, B., Rajan, S., Humphray, S., Becq, J,, Halsall. D., Wallis, M., Bentley, D., Caldas, C., Rosenfeld, N.. N Engl J Med. 2013;368(13):1199-1209.
31. Brock, M.V., Hooker, C.M., Ota-Machida, E., Han, Y., Guo, M., Ames, S., Glockner, S., Piantadosi, S., Gabrielson, E., Pridham, G., Pelosky, K., Belinsky, S.A., Yang, S.C., Baylin, S.B., Herman, J.G.. N Engl J Med. 2008;358(11):1118-1128.
32. Chen, X., Ba, Y., Ma, L., Cai, X., Yin, Y., Wang, K., Guo, J., Zhang, Y., Chen, J., Guo, X., Li, Q., Li, X., Wang, W., Zhang, Y., Wang, J., Jiang, X., Xiang ,Y., Xu, C., Zheng, P., Zhang, J., Li, R., Zhang, H., Shang, X., Gong, T., Ning, G., Wang, J., Zen, K., Zhang, J., Zhang, C-Y.. Cell Res. 2008;18(10):997-1006.
33. Mitchell, P.S., Parkin, R.K., Kroh, E.M., Fritz, B.R., Wyman, S.K., Pogosova-Agadjanyan, E.L., Peterson, A., Noteboom, J., O'Briant, K.C., Allen, A., Lin, D.W., Urban, N., Drescher, C.W., Knudsen, B.S., Stirewalt, D.L., Gentleman, R., Vessella, R.L., Nelson, P.S., Martin, D.B., Tewari, M.. Proc Natl Acad Sci U S A. 2008;105(30):10513-10518.
34. Shpitzer, T., Hamzany, Y., Bahar, G., Feinmesser, R., Savulescu, D., Borovoi, I., Gavish, M., Nagler, R.M.. Br J Cancer. 2009;101(7):1194-1198.
35. Agrawal, A.. J Clin Diagnostic Res. 2016:6-8.
36. Verma, M., Wright, G.L., Hanash, S.M., Gopal-Srivastava, R., Srivastava, S.. Ann N Y Acad Sci. 2001;945:103-115.
37. Ankerst, D.P., Gelfond, J., Goros, M., Herrera, J., Strobl, A., Thompson, I.M., Hernandez, J., Leach, R.J.. J Urol. 2016.
38. Tessem, M.B., Swanson, M.G., Keshari, K.R., Albers, M.J., Joun, D., Tabatabai, Z.L., Simko, J.P., Shinohara, K., Nelson, S.J., Vigneron, D.B., Gribbestad, I.S., Kurhanewicz, J.. Magn Reson Med. 2008;60(3):510-516.
39. Cameron, S.J.S, Lewis, K.E., Beckmann, M., Allison, G.G., Ghosal, R., Lewis, P.D., Mur, L.A.J.. Lung Cancer. 2016;94:88-95.
40. Ward, J.B., Henderson, R.E.. Environ Health Perspect. 1996;104(5):895-900.
41. Füzéry, A.K., Levin, J., Chan, M.M., Chan, D.W.. Clin Proteomics. 2013;10(1):13.
42. National Cancer Institute. Accessed on August 17, 2017; Available from: https://www.nih.gov/about-nih/what-we-do/nih-almanac/national-cancer-institute-nci.
43. Houessinon, A., Gicquel, A., Bochereau, F., Louandre, C., Nyga, R., Godin, C., Degonville, J., Fournier, E., Saidak, Z., Drullion, C., Barbare, J-C., Chauffert, B., François, C., Pluquet, O., Galmiche, A.. Cancer Lett. 2016;370(2):242-249.
44. Gion, M., Mione, R., Leon, A.E., Dittadi, R.. Clin Chem. 1999;45(5):630-637.
45. Ballehaninna, U.K., Chamberlain, R.S.. Indian J Surg Oncol. 2011;2(2):88-100.

46. Rana, S., Dutta, U., Kochhar, R., Rana, S.V., Gupta, R., Pal, R., Jain, K., Srinivasan, R., Nagi, B., Nain, C.K., Singh, K.. J Gastrointest Cancer. 2012;43(2):267-271.
47. Jacobs, I., Oram, D., Fairbanks, J., Turner, J., Frost, C., Grudzinskas, Jg... BJOG An Int J Obstet Gynaecol. 1990;97(10):922-929.
48. Elisei, R., Bottici, V., Luchetti, F., Di Coscio, G., Romei, C., Grasso, L., Miccoli, P., Iacconi, P., Basolo, F., Pinchera, A., Pacini, F.. J Clin Endocrinol Metab. 2004;89(1):163-168.
49. Su, B-B., Shi, H., Wan, J.. World J Gastroenterol. 2012;18(17):2121-2126.
50. Guadagni, F., Ferroni, P., Carlini, S., Mariotti, S., Spila, A., Aloe, S., Alessandro, R., Carone, M.D., Cicchetti, A., Ricciotti, A., Venturo, I., Perri, P., Di Filippo, F., Cognetti, F., Botti, C., Roselli, M.. Clin Cancer Res. 2001;7(8):2357-2362.
51. Gut, P., Czarnywojtek, A., Fischbach, J., Bączyk, M., Ziemnicka, K., Wrotkowska, E., Gryczyńska, M., Ruchała, M.. Arch Med Sci. 2016;12(1):1-9.
52. Jedinak, A., Vuichoud, C., El-Hayek, A., Kaplan, K., Savage, J., Prophet, S., Feldman, A.S., Camphausen, K.A., Loughlin, K.R., Moses, M.A.. Cancer Res. 2017;77(13):711.
53. Bastawisy, A. El., Azzouny, M. El., Mohammed, G., Allah, A.A., Behiry, E.. Cancer Med Sci. 2014;8:394. 54. Day, K.C., Hiles, G.L., Kozminsky, M., Dawsey, S.J., Paul, A., Broses, L.J., Shah, R., Kunja, L.P., Hall, C., Palanisamy, N., Daignault-Newton, S., El-Sawy, L., Wilson, S.J., Chou, A., Ignatoski, K.W., Keller, E., Thomas, D., Nagrath, S., Morgan, T., Day, M.L.. Cancer Res. 2017;77(1):74-85.
55. Shen, H., Zhang, L., Zhou, J., Chen, Z., Yang, G., Liao, Y., Zhu, M.. Med Sci Monit. 2017;23:216-222.
56. Skotland, T., Ekroos, K., Kauhanen, D., Simolin, H., Seierstad, T., Berge, V., Sandvig, K., Llorente, A.. Eur J Cancer. 2017;70:122-132.
57. Yu, S-L., Xu, L-T., Qi, Q., Geng, Y-W., Chen, H., Meng, Z-Q., Wang, P., Chen, Z. Sci Rep. 2017;7:45194.
58. Lippert, M.C., Javadpour, N.. Cancer. 1981;48(10):2274-2278.
59. Kawahara, R., Ortega, F., Rosa-Fernandes, L., Guimaraes, V., Leite, K., Nahas, W., Srougi, M., Larsen, M., Palmisano, G.. J Urol. 2017;197(4):1166-1167.
60. Fredsøe, J., Rasmussen, A.K.I., Thomsen, A.R., Mouritzen, P., Høyer, S., Borre, M., Ørntoft, T.F., Sørensen, K.D.. Eur Urol Focus. 2017.
61. Deng, F., Kim, Y., Poon, A., Liao, T., Leong. H.. J Urol. 2017;197(4):e1266.
62. Ferrer-Batallé, M., Llop, E., Ramírez, M., Aleixandre, R.N., Saez, M., Comet, J., de Llorens, R,. Peracaula, R.. Int J Mol Sci. 2017;18(4):845.
63. Ercole, C.J., Lange, P.H., Mathisen, M., Chiou, R.K., Reddy, P.K., Vessella, R.L.. J Urol. 1987;138(5):1181-1184.
64. Zhang, A.Y., Grogan, J.S., Mahon, L.K., Rasiah, K., Sved, P., Eisinger, D.R., Boulas, J., Vasilaris, A., Henshall. S.M., Stricker, P.D., Kench, J.G., Horvath, L.G.. Ann Oncol. 2017;28(8):1903-1909.
65. Torre, L.A., Bray, F., Siegel, R.L, Ferlay, J., Lortet-tieulent, J., Jemal, A. CA a cancer J Clin. 2015;65(2):87-108.
66. Luengo-Fernandez, R., Leal, J., Gray, A., Sullivan, R.. Lancet Oncol. 2017;14(12):1165-1174.
67. Hoffman, R.M.. N Engl J Med. 2011;365(21):2013-2019.
68. Lundström, K-J., Drevin, L., Carlsson, S., Garmo, H., Loeb, S., Stattin, P., Bill-Axelson, A.. J Urol. 2014; (4):1116-22.
69. Stephan, C., Ralla, B., Jung, K.. Biochim Biophys Acta - Rev Cancer. 2014;1846(1):99-112.
70. Zhang, J., Yao, Y-H., Li, B-G., Yang, Q., Zhang, P-Y., Wang, H-T.. Sci Rep. 2015;5:9800.
71. Chiou, C-C., Chang, P-Y., Chan, E-C., Wu, T-L., Tsao, K-C., Wu, J.T.. Clin Chim Acta. 2003;334(1):87-94.
72. Ouyang, B., Bracken, B., Burke, B., Chung, E., Liang, J., Ho, S-M.. J Urol. 2009;181(6):2508-2514.
73. Rogers, C., Yan, G., Zha, S., Gonzalgo, M.l., Isaacs, W.B., Luo, J., Marzo, A., Nelson, W., Pavlovich, C... J Urol. 2004;172(4):1501-1503.
74. Schostak, M., Schwall, G.P., Poznanović, S., Groebe, K., Müller, M., Messinger, D., Miller, K., Krause, H., Pelzer, A., Horninger, W., Klocker, H., Hennenlotter, J., Feyerabend, S., Stenzl, A., Schrattenholz, A.. J Urol. 2009;181(1):343-353.
75. Kuefer, R., Hofer, M.D., Zorn, C.S.M., Engel, O., Volkmer, B.G., Juarez-Brito, M.A., Eggel, M., Gschwend, J.E., Rubin, M.A., Day, M.L... Br J Cancer. 2005;92(11):2018-2023.
76. Tomita, K., van Bokhoven, A., van Leenders, G.J.L.H., Ruijter, E.T.G., Jansen, C.F.J., Bussemakers, M.J.G, Schalken, J.A.. Cancer Res. 2000;60(13):3650-3654.
77. Mao, Q., Zheng, X., Yang, K., Qin, J., Bai, Y., Jia, X., Li, Y., Xie, L.. Cancer Invest. 2010;28(10):1013-1018.
78. Varambally, S., Laxman, B., Mehra, R., Cao, Q., Dhanasekaran, S.M., Tomlins, S.A., Granger, J., Vellaichamy, A., Sreekumar, A., Yu, J., Gu, W., Shen, R., Ghosh, D., Wright, L.M., Kladney, R.D., Kuefer, R., Rubin, M.A., Fimmel, C.J., Chinnaiyan, A.M.. Neoplasia. 2008;10(11):1285—1294.
79. Hoque, M.O., Topaloglu, O., Begum, S., Henrique, R., Rosenbaum, E., van Criekinge, W., Westra, W.H., Sidransky, D.. J Clin Oncol. 2005;23(27):6569-6575.
80. Payne, S.R., Serth, J., Schostak, M., Kamradt, J., Strauss, A., Thelen, P., Model, F., Day, J.K., Liebenberg, V., Morotti, A., Yamamura, S., Lograsso, J., Sledziewski, A., Semjonow, A.. Prostate. 2009;69(12):1257-1269.
81. Rouprêt, M., Hupertan, V., Yates, D.R., Catto, J.W.F., Rehman, I., Meuth, M., Ricci, S., Lacave, R., Cancel-Tassin, G., De La Taille, A., Rozet, F., Cathelineau, X., Vallancien, G., Hamdy, F.C., Cussenot, O.. Clin Cancer Res. 2007;13(6):1720-1725.
82. Culig, Z., Puhr, M.. Mol Cell Endocrinol. 2012;360(1):52-58.
83. Santer, F.R., Malinowska, K., Culig, Z., Cavarretta, I,T.. Endocr Relat Cancer. 2010;17(1):241-253.

84. Seiz, L., Matthias, K., Susanne, F., Peter, G., Apostolos, G., Manfred, S., Arndt, L., Viktor, M.. Biol Chem. 2010;391:391.
85. Dudderidge, T.J., Kelly, J.D., Wollenschlaeger, A., Okoturo, O., Prevost, T., Robson, W., Leung, H.Y., Williams, G.H., Stoeber, K.. Br J Cancer. 2010;103(5):701-707.
86. Bussemakers, M.J.G., van Bokhoven, A., Verhaegh, G.W., Smit, F.P., Karthaus, H.F.M., Schalken, J.A., Debruyne, F.M.J., Ru, N., Isaacs, W.B.. Cancer Res. 1999;59(23):5975-5979.
87. de Kok, J.B., Verhaegh, G.W., Roelofs, R.W., Hessels, D., Kiemeney, L.A., Aalders, T.W., Swinkels, D.W., Schalken, J.A.. Cancer Res. 2002;62(9):2695 LP-2698.
88. Hessels, D., Schalken, J.A.. Nat Rev Urol. 2009;6(5):255-261.
89. Zhou, H-J., Yan, J., Luo, W., Ayala, G., Lin, S-H., Erdem, H., Ittmann, M., Tsai, S.Y., Tsai, M-J.. Cancer Res. 2005;65(17):7976-7983.
90. Fizazi, K.. Ann Oncol. 2007;18(11):1765-1773.
91. Tomlins, S.A., Rhodes, D.R., Perner, S., Dhanasekaran, S.M., Mehra, R., Sun, X-W., Varambally, S., Cao, X., Tchinda, J., Kuefer, R., Lee, C., Montie, J.E., Shah, R.B., Pienta, K.J., Rubin, M.A., Chinnaiyan, A.M.. Science (80). 2005;310(5748):644-648.
92. Laxman, B., Tomlins, S.A., Mehra, R., Morris, D.S., Wang, L., Helgeson, B.E., Shah, R.B., Rubinb, M.A., Wei, J.T., Chinnaiyan, A.M.. Neoplasia. 2006;8(10):885-888.
93. Hessels, D., Smit, F.P., Verhaegh, G.W., Witjes, J.A., Cornel, E.B., Schalken, J.A.. Clin Cancer Res. 2007;13(17):5103-5108.
94. Hernández, J., Thompson, I.M.. Cancer. 2004;101(5):894-904.
95. Kumar, V., Hassan, M.I., Singh, A.K., Dey, S., Singh, T.P., Yadav, S.. Clin Chim Acta. 2009;403(1-2):17-22.
96. Lilja, H., Oldbring, J., Rannevik, G., Laurell, C.B.. J Clin Invest. 1987;80(2):281-285.
97. Lilja, H.. J Clin Invest. 1985;76(5):1899-1903.
98. Lilja, H., Christensson, A., Dahlén, U., Matikainen, M.T., Nilsson, O., Pettersson, K., Lövgren, T.. Clin Chem. 1991;37(9):1618-1625.
99. Lilja, H., Ulmert, D., Vickers, A.J.. Nat Rev Cancer. 2008;8(4):268-278.
100. Shariat, S.F., Canto, E.I., Kattan, M.W., Slawin, K.M.. Rev Urol. 2004;6(2):58-72.
101. Wang, M. C., Valenzuela, L. A., Murphy, G. P., and Chu TM.. Invest Urol. 1979;17(2):159-163.
102. Catalona, W.J., Smith, D.S., Ratliff, T.L., Dodds, K.M., Coplen, D.E., Yuan, J.J.J., Petros, J.A., Andriole, G.L.. N Engl J Med. 1991;324(17):1156-1161.
103. Heidenreich, A., Bellmunt, J., Bolla, M., Joniau, S., Mason, M., Matveev, V., Mottet, N., Schmid, H-P., van der Kwast, T., Wiegel, T., Zattoni, F.. Eur Urol. 2011;59(1):61-71.
104. Gretzer, M.B., Partin, A.W.. Eur Urol Suppl. 2002;1(6):21-27.
105. Reed, A., Ankerst, D.P., Pollock, B.H., Thompson, I.M., Parekh, D.J.. J Urol. 2007;178(5):1929-1932.
106. Oesterling, J.E., Jacobsen, S.J., Chute, C.G., Guess, H.A., Girman, C.J., Panser, L.A., Lieber, M.M.... JAMA. 1993;270(7):860-864.
107. Luboldt, H.J., Schindler, J.F., Rübben, H.. EAU-EBU Updat Ser. 2007;5(1):38-48.
108. España, F., Martínez, M., Royo, M., Vera, C.D., Estellés, A., Aznar, J., Jiménez-Cruz, J.F.. Eur Urol 1997;32:268–72..
109. Graves, H.C., Sensabaugh, G.F., Blake, E.T... N Engl J Med. 1985;312(6):338-343..
110. Irani, J., Levillain, P., Goujon, J-M., Bon, D., Dore, B., Aubert, J.. J Urol. 1997;157(4):1301-1303.
111. Pannek, J., Rittenhouse, H.G., Evans, C.L., Finlay, J.A., Bruzek, D.J., Cox, J.L., Chan, D.W., Subong, E.N.P., Partin, A.W. . Urology. 1997;50(5):715-721
112. Malavaud, B., Salama, G., Miédougé, M., Vincent, C., Rischmann, P., Sarramon, J-P., Serre, G.. Prostate. 1998;34(1):23-28.
113. Bolduc, S., Lacombe, L., Naud, A., Grégoire, M., Fradet, Y., Tremblay, R.R.. Can Urol Assoc J. 2007;1(4):377-381.
114. Jaenicke, R., Knof, S.. Eur J Biochem. 1968;4(2):157-163.
115. Scartozzi, M., Faloppi, L., Bianconi, M., Giampieri, R., Maccaroni, E., Bittoni, A., Del Prete, M., Loretelli, C., Belvederesi, L., Baroni, G.S., Cascinu, S.. PLoS One. 2012;7(3):1-5.
116. Adams, M.J., Buehner, M., Chandrasekhar, K., Ford, G.C., Hackert, M.L., Rossmann, M.G., Smiley, I.E., Allison, W.S., Everse, J., Kaplan, N.O., Taylor, S.S.. Proc Natl Acad Sci U S A. 1973;70(7):1968-1972.
117. Markert, C.L.. Science (80). 1963;140(3573):1329-1330.
118. Brinster, R.L.. Nature. 1967;214(5094):1246–1247.
119. Warburg, O.. Science (80). 1956;123(3191):309-314.
120. Gilligan, T.D., Seidenfeld, J., Basch, E.M., Einhorn, L.H., Fancher, T., Smith, D.C., Stephenson, J., Vaughn, D.J., Cosby, R., Hayes, D.F.. J Clin Oncol. 2010;28(20):3388-3404.
121. Ziaian, B., Saberi, A., Ghayyoumi, M.A., Safaei, A., Ghaderi, A., Mojtahedi, Z.. Asian Pacific J Cancer Prev. 2014;15(4):1617-1620.
122. Chen. J., Sun, M-X., Hua, Y-Q., Cai, Z-D.. J Cancer Res Clin Oncol. 2014;140(7):1205-10
123. Girgis, H., Masui, O., White, N.M., Scorilas, A., Rotondo, F., Seivwright, A., Gabril, M., Filter, E.R., Girgis, A.H., Bjarnason, G., Jewett, M.A., Evans, A., Al-Haddad, S., Siu, K.M., Yousef, G.M.. Mol Cancer. 2014;13(1):101.

124. Petrelli, F., Cabiddu, M., Coinu, A., Borgonovo, K., Ghilardi, M., Lonati, V., Barni, S.. Acta Oncol (Madr). 2015;54(7):961-970.
125. Hermes, A., Gatzemeier, U., Waschki, B., Reck, M.. Respir Med. 2010;104(12):1937-1942.
126. International Prognostic Factors Study Group, Lorch, A., Beyer, J., Bascoul-Mollevi, C., Kramar, A., Einhorn, L.H., Necchi, A., Massard, C., De Giorgi, U., Fléchon, A., Margolin, K.A., Lotz, J.P., Germa Lluch. J.R., Powles, T., Kollmannsberger, C.K.. J Clin Oncol. 2010;28(33):4906-4911.
127. Augoff, K., Hryniewicz-Jankowska, A., Tabola, R.. Cancer Lett. 2015;358(1):1-7.
128. Nishikawa, A., Tanaka, T., Takeuchi, T., Fujihiro, S., Mori, H.. Br J Cancer. 1991;63(5):819-821.
129. Flocks, R.H., Schmidt, J.D.. J Surg Oncol. 1972;4(2):161-167.
130. Prout, G.R., Macalalag, E.V., Denis, L.J., Preston, L.W.. J Urol. 1965;94(4):451-461.
131. Naruse, K., Yamada, Y., Aoki, S., Taki, T., Nakamura, K., Tomiume, M., Zennami, K., Katsuda, R., Sai, S., Nishio, Y., Inoue, Y., Noguchi, H., Honda N. Hinyokika Kiyo. 2007;53(5):287-92.
132. Brown, J.E., Cook, R.J., Lipton, A., Coleman, R.E.. Clin Cancer Res. 2012;18(22):6348-6355.
133. Koukourakis, M.I., Giatromanolaki, A., Panteliadou, M., Pouliliou, S.E., Chondrou, P.S., Mavropoulou, S., Sivridis, E. Br J Cancer. 2014;110(9):2217-2223.
134. Scher, H.I., Heller, G., Molina, A., Attard, G., Danila, D.C., Jia, X., Peng, W., Sandhu, S.K., Olmos, D., Riisnaes, R., McCormack, R., Burzykowski, T., Kheoh, T., Fleisher, M., Buyse, M., de Bono, J.S.. J Clin Oncol. 2015;33(12):1348-1355.
135. Sidaway, P.. Nat Rev Urol. 2015;12(5):241.
136. Wu, L., Qu, X.. Chem Soc Rev. 2015:2963-2997.
137. Dehbid,M., Aleyasin, S. A., Vaziri, H. . J Mol Biomark Diagn. 2016;1(s8).
138. Ma, J., Li, N., Lin, Y., Gupta, C., Jiang, F. r. Biomark Cancer. 2016;8:1-7.
139. Tan, G., Liu, Q., Tang, X., Kang, T., Li, Y., Lu, J., Zhao, X., Tang, F.. BMC Cancer. 2016;16(1):241.
140. Zangar, R.C., Daly, D.S., White, A.M.. Expert Rev Proteomics. 2006;3(1):37-44.
141. Garcia-Schwarz, G., Santiago, J.G.. Angew Chemie Int Ed. 2013;52(44):11534-11537.
142. Lee, H., Park, J-E., Nam, J-M. Nature Comm. 2014;5:3367.
143. Law, W.C., Yong, K.T., Baev, A., Prasad, P.N.. ACS Nano. 2011;5(6):4858-4864.
144. Krishnan, S., Mani, V., Wasalathanthri, D., Kumar, C.V., Rusling, J.F.. Angew Chemie Int Ed. 2011;50(5):1175-1178.
145. Samanta, A., Maiti, K.K., Soh, K.S., Liao, X., Vendrell, M., Dinish, U.S., Yun, S.W., Bhuvaneswari, R., Kim, H., Rautela, S., Chung, J., Olivo, M., Chang, Y-T.. Angew Chemie Int Ed. 2011;50(27):6089-6092.
146. Panikkanvalappil, S.R., Mackey, M.A., El-Sayed, M.A.. J Am Chem Soc. 2013;135(12):4815-4821.
147. Li, M., Cushing, S.K., Zhang, J., Suri, S., Evans, R., Petros, W.P., Gibson, L.F., Ma, D., Liu, Y., Wu, N.. ACS Nano. 2013;7(6):4967-4976.
148. Wu, G., Datar, R.H., Hansen, K.M., Thundat, T., Cote, R.J., Majumdar, A.. Nat Biotechnol. 2001;19(September):856-860.
149. Loo, L., Capobianco, J.A., Wu, W., Gao, X., Shih, W.Y., Shih, W.H., Pourrezaei, K., Robinson, M.K., Adams, G.P.. Anal Chem. 2011;83(9):3392-3397.
150. Liang, L., Ge, S., Li, L., Liu, F., Yu, J.. Anal Chim Acta. 2015;862:70-76.
151. Adel Ahmed, H., Azzazy, H.M.E.. Biosens Bioelectron. 2013;49:478-484.
152. Wu, Y., Xue, P., Hui, K.M., Kang, Y.. Biosens Bioelectron. 2014;52:180-187.
153. Wang, P., Ge, L., Yan, M., Song, X., Ge, S., Yu, J.. Biosens Bioelectron. 2012;32(1):238-243.
154. Hu, M., Yan, J., He, Y., Lu, H., Weng, L., Song, S., Fan, C., Wang, L.. ACS Nano. 2010;4(1):488-494.
155. Hoffman, J.M., Stayton, P.S., Hoffman, A.S., Lai, J.J.. Bioconjug Chem. 2015;26(1):29-38.
156. Oh, S.W., Kim, Y.M., Kim, H.J., Kim, S.J., Cho, J-S., Choi, E.Y.. Clin Chim Acta. 2009;406(1-2):18-22.
157. Taylor, P., Fedotoff, O., Mikheeva, L.M., Chait, A., Uversky, V.N., Boris. Y.. J Biomol Struct Dyn. 2012;29(5):1051-1064.
158. Kumar, V., Hassan, M.I., Singh, A.K., Dey, S., Singh, T.P., Yadav, S.. Clin Chim Acta. 2009;403(1-2):17-22.
159. Li, X., Li, W., Yang, Q., Gong, X., Guo, W., Dong, C., Liu, J., Xuan, L., Chang, J.. ACS Appl Mater Interfaces. 2014;6(9):6406-6414.
160. Oberpenning, F., Hetzel, S., Weining, C., Brandt, B., De Angelis, G., Heinecke, A., Lein, M., Fornara, P., Schmid, H-P., Hertle, L., Semjonow, A. . Eur Urol. 2017;43(5):478-484.
161. Miano, R., Mele, G.O., Germani, S., Bove, P., Sansalone, S., Pugliese, P.F., Micali, F.. Prostate Cancer Prostatic Dis. 2005;8:219-223.
162. De Angelis, G., Rittenhouse, H.G., Mikolajczyk, S.D., Blair Shamel, L., Semjonow, A.. Rev Urol. 2007;9(3):113-123.
163. Kalyvas, M., Zammit, S., Chem, C.. Clin Chem. 1996;42(5):675-684.
164. Peter, J., Unverzagt, C., Lenz, H., Hoesel, W.. Anal Biochem. 1999;273(1):98-104.
165. Poon, C., Chan, H., Li, H.. Sensors Actuators B Chem. 2014;190:737-744.
166. Sonawane, M.D., Nimse, S.B., Song, K-S., Kim, T.. RSC Adv. 2016;6(9):7599-7609.
167. Shi, T., Fillmore, T.L., Sun, X., Zhao, R., Schepmoes, A.A., Hossain, M., Xie, F., Wu, S., Kim, J-S., Jones, N., Moore, R.J., Pasa-Tolić, L., Kagan, J., Rodland, K.D., Liu, T., Tang, K., Camp, D.G., Smith, R.D., Qian, W-J.. Proc Natl Acad Sci U S A. 2012;109(38):15395-15400.
168. Anderson, N.G., Anderson, N.L., Tollaksen, S.L., Hahn, H., Giere, F., Edwards, J.. Anal Biochem. 1979;95(1):48-61.

169. Rasmussen, H.H., Orntoft, T.F., Wolf, H., Celis, J.E.. J Urol. 1996;155(6):2113-2119.
170. Tantipaiboonwong, P., Sinchaikul, S., Sriyam, S., Phutrakul, S., Chen, S.T.. Proteomics. 2005;5(4):1140-1149.
171. Thongboonkerd, V., McLeish, K.R., Arthur, J.M., Klein, J.B.. Kidney Int. 2002;62(4):1461-1469.
172. Álvarez Sánchez, B., Capote, F.P., Jiménez, J.R., Luque de Castro, M.D.. J Chromatogr A. 2008;1207(1-2):46-54.
173. Khan, A., Packer, N.H.. J Proteome Res. 2006;5(10):2824-2838.
174. Schumann, G., Bonora, R., Ceriotti, F., Clerc-Renaud, P., Ferrero, C.A., Férard, G., Franck, P.F., Gella, F.J., Hoelzel, W., Jørgensen, P.J., Kanno, T., Kessne, A., Klauker, R., Kristiansen, N., Lessinger, J.M., Linsinger, T.P., Misaki, H., Panteghini, M., Pauwels, J., Schimmel, H.G., Vialle, A., Weidemann, G., Siekmann, L.. Clin Chem Lab Med . 2002;40:643.
175. Scheijen, J.L.J.M., Hanssen, N.M.J., Van De Waarenburg, M.P.H., Jonkers, D.M.A.E., Stehouwer, C.D.A., Schalkwijk, C.G. L. Exp Diabetes Res. 2012;2012.
176. Nandakumar, M.P., Nandakumar, R., Mattiasson, B.. Biotechnol Lett. 2000;22(18):1453-1457.
177. Nesakumar, N., Thandavan, K., Sethuraman, S., Krishnan, U.M., Rayappan, J.B.B.. J Colloid Interface Sci. 2014;414:90-96.
178. Ahmed, F.E.. J Sep Sci. 2009;32(5-6):771-798.
179. Anderson, N.L., Anderson, N.G.. Mol Cell Proteomics. 2002;1(11):845-867.
180. Chandramouli, K., Qian, P-Y.. Hum Genomics Proteomics. 2009;2009:22.
181. Albertsson, P.A. Partition of cell particles and macromolecules: separation and purification of biomolecules, cell organelles, membranes, and cells in aqueous polymer two-phase systems and their use in biochemical analysis and biotechnology. Wiley. 1986;3rd edn:371.
182. Freire, M.G, Cláudio, A.F.M., Araújo, J.M.M., Coutinho, J. A. P., Marrucho, I.M., Canongia Lopes, J.N., Rebelo, L.P.N.. Chem Soc Rev. 2012;41(14):4966-4995.
183. Pereira, D.Y., Chiu, R.Y.T., Zhang, S.C.L., Wu, B.M., Kamei, D.T.. Anal Chim Acta. 2015;882:83-89.
184. Mashayekhi, F., Meyer, A.S., Shiigi, S.A., Nguyen, V., Kamei, D.T.. Biotechnol Bioeng. 2009;102(6):1613-1623.
185. Kim, J., Shin, H., Kim, J., Kim, J., Park, J.. PLoS One. 2015;10(6):1-16.
186. Shin, H., Han, C., Labuz, J.M., Kim, J., Kim, J., Cho, S., Gho, Y.S., Takayama, S., Park, J.. Sci Rep. 2015;5:1-11.
187. Raymond, F.D., Moss, D.W., Fisher, D.. Clin Chim Acta. 1994;227(1-2):111-120.
188. Passos, H., Sousa, A.C., Pastorinho, M.R., Nogueira, A.J., Rebelo, L.P.N., Coutinho, J.A.P., Freire, M.G.. Anal Methods. 2012;4(9):2664-2667.
189. Seddon, K.R.. Nat Mater. 2003;2(6):363-365.
190. Crowhurst, L., Mawdsley, P.R., Perez-Arlandis, J.M., Salter, P. A., Welton, T.. Phys Chem Chem Phys. 2003;5(13):2790-2794.
191. Pereira, J.F.B, Rebelo, L.P.N., Rogers, R.D., Coutinho, J. A. P., Freire, M.G.. Phys Chem Chem Phys. 2013;15(45):19580-19583.
192. Dreyer, S., Salim, P., Kragl, U.. Biochem Eng J. 2009;46(2):176-185.
193. Ventura, S.P.M., e Silva, F.A., Quental, M.V., Mondal, D., Freire, M.G., Coutinho, J.A.P.. Chem Rev. 2017;117(10):6984-7052.
194. Dreyer, S., Kragl, U.. Biotechnol Bioeng. 2008;99(6):1416-1424.
195. Tan, Z., Li, F., Xu, X., Xing, J.. Desalination. 2012;286:389-393.
196. Passos, H., Luís, A., Coutinho, J.A.P., Freire, M.G.. Sci Rep. 2016;6:20276.
197. Du, Z., Yu, Y-L., Wang, J-H.. Chemistry. 2007;13(7):2130-2137.
198. Pei, Y., Li, L., Li, Z., Wu, C., Wang, J.. Sep Sci Technol. 2012;47(2):277-283.
199. Ding, X., Wang, Y., Zeng, Q., Chen, J., Huang, Y., Xu, K.. Anal Chim Acta. 2014;815:22-32.
200. Li, Z., Liu, X., Pei, Y., Wang, J., He, M.. Green Chem. 2012;14(10):2941-2950.
201. Bezold, F., Goll, J., Minceva, M.. J Chromatogr A. 2015;1388:126-132.
202. Yan, J.K., Ma, H.L., Pei, J.J., Wang, Z.B., Wu, J-Y... Sep Purif Technol. 2014;135:278-284.
203. Pei, Y., Wang, J., Wu, K., Xuan, X., Lu, X.. Sep Purif Technol. 2009;64(3):288-295.
204. Lu, Y., Lu, W., Wang, W., Guo, Q., Yang, Y.. Talanta. 2011;85(3):1621-1626.
205. Wu, C., Wang, J., Li, Z., Jing, J., Wang, H.. J Chromatogr A. 2013;1305:1-6.
206. Lin, X., Wang, Y., Zeng, Q., Ding, X., Chen, J.. Analyst. 2013;138(21):6445-6453.
207. Cao, Q., Quan, L., He, C., Li, N., Li, K., Liu, F.. Talanta. 2008;77(1):160-165.
208. Taha, M., Almeida, M.R., e Silva, F.A., Domingues, P., Ventura, S.P.M., Coutinho, J.A.P., Freire, M.G.. Chem - A Eur J. 2015;21(12):4781-4788.
209. Souza, R.L., Lima, R.A., Coutinho, J.A.P., Soares, C.M.F., Lima, Á.S.. Sep Purif Technol. 2015;155:118-126.
210. Ventura, S.P.M., de Barros, R.L.F., Barbosa, J.M. de P., Soares, C.M.F., Lima, A.S., Coutinho, J.A.P.. Green Chem. 2012;14(3):734-740.
211. Lee, S.Y., Vicente, F.A., e Silva, F.A., Sintra, T.E., Taha, M., Khoiroh, I., Coutinho, J.A.P., Show, P.L., Ventura, S.P.M.. ACS Sustain Chem Eng. 2015;3(12):3420-3428.
212. Deive, F.J., Rodríguez, A., Rebelo, L.P.N., Marrucho, I.M.. Sep Purif Technol. 2012;97:205-210.
213. Ventura, S.P.M., Sousa, S.G., Freire, M.G., Serafim, L.S., Lima, Á.S., Coutinho, J. A.P.. J Chromatogr B Anal Technol Biomed Life Sci. 2011;879(26):2679-2687.
214. Sheikhian, L., Akhond, M., Absalan, G., Goltz, D.M.. Sep Sci Technol. 2013;48(15):2372-2380.

215. Bai, Z., Chao, Y., Zhang, M., Han, C., Zhu, W., Chang, Y., Li, H., Sun, Y.. J Chem. 2013;2013:1-6.
216. Desai, R.K., Streefland, M., Wijffels, R.H., Eppink, M.. Green Chem. 2014;16(5):2670.
217. Plechkova, N.V., Seddon, K.R.. Chem Soc Rev. 2008;37(1):123-150.

2. Screening of aqueous biphasic systems as alternative extraction and purification Platforms for proteins

2.1. Extraction of amino acids using aqueous biphasic systems formed by glycine-betaine ionic liquid analogues

This chapter is based on an unpublished work with the following authors involved:

Matheus M. Pereira, Joana Gomes, João A. P. Coutinho, Aminou Mohamadou and Mara G. Freire

2.1.1. Abstract

Given the biotechnology advances observed in recent years in terms of upstream, the development of effective and biocompatible downstream processes becomes mandatory to decrease the costs of biotechnological products. Although a large interest has been devoted to ionic-liquid-based aqueous biphasic systems (IL-based ABS) as tailored separation platforms, imidazolium-based ILs have been the preferred choice as phase-forming agents. To overcome the toxicity and biodegradability issues associated to imidazolium-based ILs, in this work, ABS composed of IL analogues of glycine-betaine (AGB-ILs) were investigated. Six AGB-ILs were synthesized, characterized in terms of ecotoxicity, and applied towards the development of novel bio-based ABS. Then, the respective ABS ternary phase diagrams, as well as the tie-lines and tie-line lengths, were determined at 25°C. Finally, their performance as extraction platforms was evaluated with two amino acids (L-tryptophan and L-tyrosine). In all studied systems, amino acids migrate preferentially to the IL-rich phase, with maximum extraction efficiencies of 97% and 100% for L- tyrosine and L-Tryptophan, respectively, achieved in a single-step. In summary, this work demonstrates that novel bio-based ABS composed of AGB-ILs are improved platforms for the extraction of biomolecules, and thus can be envisaged as promising separation strategies for other value-added compounds of biotechnological interest.

2.1.2. Introduction

Advances in biotechnology have enhanced the production of a wide variety of value-added biocompounds[1]. Nevertheless, the major drawback is still their recovery and purification from the original complex media by cost-effective techniques, while keeping their biological activity. Therefore, the development of more benign and effective separation techniques has been a hot topic of research in the past few years[2].

Aqueous biphasic systems (ABS) fit within the liquid-liquid extraction/purification techniques. These are formed by two compounds (two salts, two polymers or a polymer and a salt), that when dissolved above given concentrations in aqueous media result in the formation of two immiscible

Contributions: M.G.F., J.A.P.C. and A.M. conceived and directed this work. M.M.P. and J.G. acquired the experimental data. M.M.P., A.M., J.A.P.C. and M.G.F interpreted the experimental data. The manuscript was mainly written by M.M.P. and M.G.F. with significant contributions from the remaining authors.

aqueous liquid phases, each enriched in one of the phase-forming components[3,4]. Due to the large amount of water in their composition, ABS could be seen as more biocompatible extraction platforms when compared to liquid-liquid extraction systems employing volatile organic compounds. Although widely studied in the past decades[2,5], conventional polymer-based ABS have coexisting phases of high viscosity turning the phases separation step difficult to occur in a short time and without energetic/centrifugation inputs. Furthermore, the coexisting phases in these more conventional polymer-based ABS display a restricted polarity difference, which hampers enhanced extraction efficiencies and high selectivity to be achieved in a single-step[6]. In fact, several attempts can be found in the literature to improve the performance of polymer-based ABS, either by introducing additives or by the functionalization of polymers. However, after the introduction of ionic-liquid-based ABS by Gutowski *et al.*[7], a shift in the ABS research field was noticed. These systems have shown remarkable extraction efficiencies and high selectivity's, observed for a wide variety of biocompounds and matrices[5].

Ionic liquids (ILs) are salts, with melting temperatures below 100°C[8]. Due to their ionic nature, most ILs present notable properties, such as a negligible volatility at atmospheric conditions, non-flammability, high thermal and chemical stabilities, and a strong solvation ability for a wide range of compounds[8,9]. Besides these features, they have been labelled as "designer solvents" due to the ability of combining a large number of ions with significantly different chemical structures, allowing the design of improved ILs for particular applications. This characteristic is also reflected in IL-based ABS[5], and is one of the main reasons behind the outstanding performance of these more recent systems over the conventional polymer-based ones. IL-based ABS have been successfully applied in the separation of antioxidants[10], alkaloids[11,12], amino acids[13], proteins/enzymes[14,15,16], among others. The largest fraction of IL-based ABS investigated hitherto are based on imidazolium-based ILs and inorganic salts as phase-forming components[5]. However, imidazolium-based ILs display high toxicity and may compromise the biological activity of several molecules, thus motivating the research on more benign ILs to be applied in ABS. Although some reports have appeared in the past few years with this issue in mind, these studies were mainly carried out with cholinium-based ILs, either combined with salts or with polymers to create ABS[17–23]. However, nowadays, there are other ILs derived from natural sources that could be explored in the creation of ABS. Among these, analogues of glycine-betaine-(AGB)[24] can be seen as a promising alternative. These organic osmolytes accumulate in a variety of plant species in response to environmental stress[25,26]. Both compounds have positive effects on enzyme and membrane integrity along with adaptative roles in mediating osmotic adjustment in

plants growing under stress conditions. Hydrophobic ILs based on AGB have been applied in the extraction of pesticides[27] and metal ions[28–30]. However, based on their natural-derived source, and if coupled with anions that turn them miscible with water, these ILs can be used in the creation of more biocompatible ABS aiming at the separation and recovery of biologically active compounds. Taking into account this possibility and advantages connected to AGB-ILs, this work is focused on the development of more biocompatible IL-based ABS and on the evaluation of their performance to extract amino acids. To this end, six AGB-ILs have been synthesized, and their ability to create ABS with Na_2SO_4 addressed. The respective ternary phase diagrams were determined at 25°C to infer the mixture compositions required to form two-phase system, followed by the evaluation of their performance to extract amino acids. Their ecotoxicity towards the marine bacterium *Vibrio fischeri* will also be discussed.

2.1.3. Experimental procedures

Materials. The AGB-ILs were synthesized by us according to previously reported protocols[24]. The ILs triethyl[2-ethoxy-2-oxoethyl]ammonium bromide ($[Et_3NC_2]Br$), tri(n-propyl)[2-ethoxy-2-oxoethyl]ammonium bromide, ($[Pr_3NC_2]Br$), tri(n-butyl)[2-ethoxy-2-oxoethyl]ammonium bromide ($[Bu_3NC_2]Br$), tri(n-butyl)[2-ethoxy-2-oxoethyl]phosphonium bromide ($[Bu_3PC_2]Br$), and n-(1-methylpyrrolidyl-2-ethoxy-2-oxoethyl)ammonium bromide ($[MepyrNC_2]Br$) were synthesized by the reaction of ethyl 2-bromoacetate and triethylamine, tri(*n*-propyl)-amine, tri(*n*-butyl)amine, tri(n-butyl)phosphine or n-methylpyrrolidine, respectively. The synthesis pathway for the AGB-based ILs is depicted in Appendix A. Tri(n-butyl)[2-butoxy-2-oxoethyl]phosphonium bromide ($[Bu_3PC_4]Br$) was synthesized in this work for the first time by the reaction of tri(n-butyl)phosphine (83.8 mL, 65.2 g, 0.35 mol) in ethyl acetate (150 mL) and 4-bromobutyric acid ethyl ester (29.6 mL, 37.5 g, 0.22 mol) in 50 mL of ethyl acetate. The mixture was refluxed under constant stirring for 2 days at 40°C, and then stirred at room temperature for one day. The brownish oil produced was recovered and washed three times with ethyl acetate (250 mL) and kept at 60 °C. The white product obtained with a yield of 85%, which crystallized after 48 h, was washed with ethyl acetate (250 mL) and diethyl ether (250 mL) and then dried in vacuum. After this procedure, the purity of each IL was further checked by ^1H nuclear magnetic resonance (NMR) (*cf.* Appendix A). The purity of the synthesized ILs is > 98%. All ILs synthesized in this study were solid at room temperature. The chemical structures of the ILs synthesized are depicted in Figure 2.1.1.

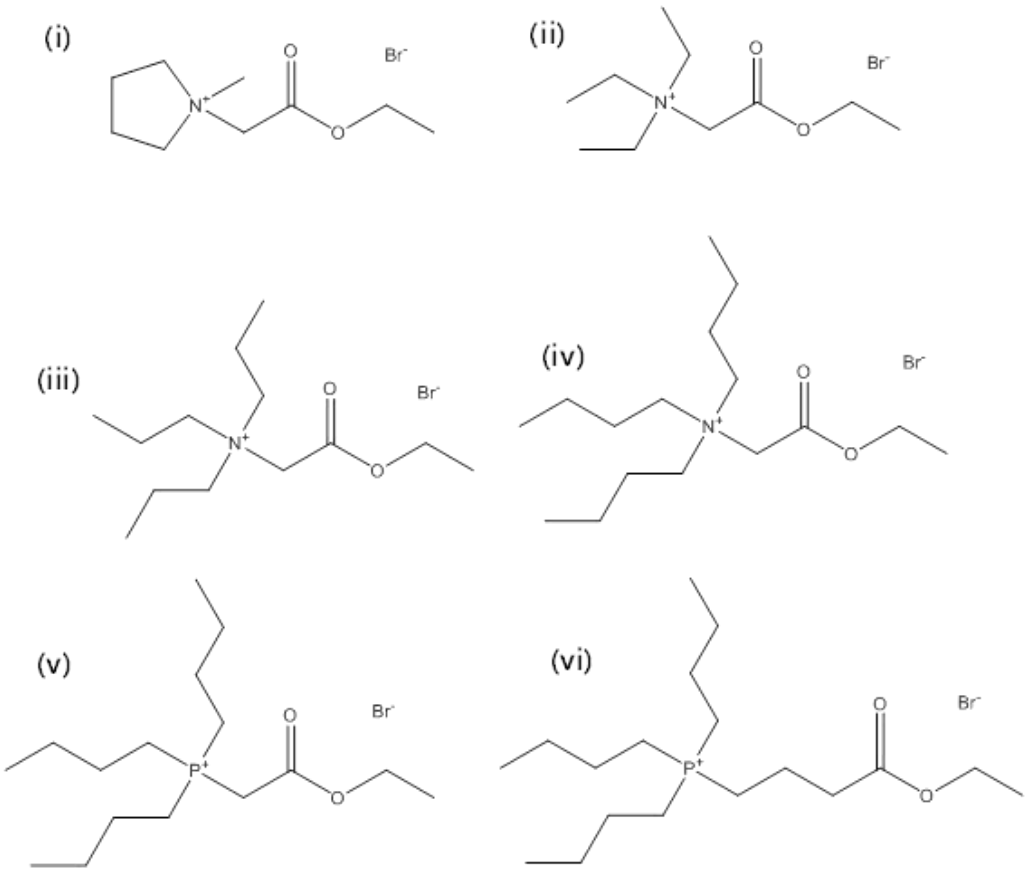

Figure 2.1.1. Chemical structure of the synthesized ILs: (i) [MepyrNC$_2$]Br; (ii) [Et$_3$NC$_2$]Br; (iii) [Pr$_3$NC$_2$]Br; (iv) [Bu$_3$NC$_2$]Br; (v) [Bu$_3$PC$_2$]Br; and (vi) [Bu$_3$PC$_4$]Br.

All tertiary amines and the 2-bromoacetic acid ethyl ester were acquired from Sigma-Aldrich. $NaSO_4$ (anhydrous, 100 wt% pure) was from Prolabo. L-Tryptophan (purity > 99.0 wt%) and L-tyrosine (purity 99.0 wt%) were acquired from Sigma–Aldrich and Fluka, respectively.

Microtox® toxicity tests. The Microtox® test was used to evaluate the ecotoxicity of the ILs synthesized towards the marine bacterium *Vibrio fischeri*, through the determination of its luminescence inhibition in presence of aqueous solutions of ILs. The bacterium was exposed to a series of aqueous diluted solutions of each IL, ranging from 0 to 81.9 wt%, being 100% the concentration of the stock solution. After 5, 15 and 30 min of exposure of the bacterium to each IL aqueous solutions, the light output of the bacterium was assessed and compared with the light output of the blank control (an aqueous solution without the presence of any AGB-ILs), enabling the calculation of the EC_{50} values at 5, 15 and 30 min through the Microtox® Omni™ Software version[31].

Phase diagrams and tie-lines. Aqueous solutions of each synthesized IL ([MepyrNC$_2$]Br, [Et$_3$NC$_2$]Br, [Pr$_3$NC$_2$]Br, [Bu$_3$NC$_2$]Br, [Bu$_3$PC$_2$]Br, [Bu$_3$PC$_4$]Br), at concentrations between 50 and 70 wt%, and aqueous solutions of Na_2SO_4 at 17 wt%, were initially prepared and used for the determination of the binodal curves. The phase diagrams were determined through the cloud point titration method at 25°C and atmospheric pressure. Further details are given elsewhere[32]. The system compositions were determined by the weight quantification of all components added within $\pm$ 10^{-4} g. The tie-lines (TLs) were determined by a gravimetric method proposed by Merchuk[33]. Different mixture points at the biphasic region (total weight of 3 g) were prepared in small glass ampoules (*ca.* 5 mL), vigorously stirred, centrifuged for 10 min and allowed to reach equilibrium by the separation of the phases for at least 10 min at 25°C. After separation of the two phases, both the top and bottom phases were weighted. Each individual TL was determined by application of the lever-arm rule to the relationship between the top phase composition and the overall system composition. The experimental binodal curves were correlated using Equation (2.1.1):

$$[IL] = Aexp[(B[salt]^{0.5}) - (C[salt]^3)] \quad (2.1.1)$$

where $[IL]$ and $[salt]$ are the IL and the salt weight fraction percentages, respectively, and A, B, and C are constants obtained by the regression of the experimental data (see Appendix A).

The determination of the TLs was accomplished through the solution of the following system of four equations (Equations (2.1.2) to (2.1.5)) aiming at determining four unknown values ($[IL]_{\mathrm{IL}}$, $[IL]_{\mathrm{salt}}$, $[salt]_{\mathrm{IL}}$ and $[salt]_{\mathrm{salt}}$):

$$[IL]_{salt} = Aexp\left[\left(B[salt]_{IL}^{0.5}\right) - (C[salt]_{IL}^{3})\right] \quad (2.1.2)$$

$$[IL]_{salt} = Aexp\left[\left(B[salt]_{salt}^{0.5}\right) - \left(C[salt]_{salt}^{3}\right)\right] \quad (2.1.3)$$

$$[IL]_{IL} = \frac{[IL]_M}{\alpha} - \frac{1-\alpha}{\alpha}[IL]_{salt} \quad (2.1.4)$$

$$[salt]_{IL} = \frac{[salt]_M}{\alpha} - \frac{1-\alpha}{\alpha}[salt]_{salt} \quad (2.1.5)$$

where the subscripts "IL", "salt" and "M" represent the top and the bottom phases and the mixture composition, respectively. The parameter α is the ratio between the weight of the top

phase and the weight of the overall mixture. For the calculation of each tie-line length (TLL), Equation (2.1.6) was employed:

$$TLL = \sqrt{([salt]_{IL} - [salt]_{salt})^2 + ([IL]_{IL} - [IL]_{salt})^2} \quad (2.1.6)$$

pH measurements. The pH of the IL- and Na_2SO_4-rich aqueous phases was measured at 25°C using a Mettler Toledo S47 SevenMulti™ dual meter pH/conductivity equipment within ±0.02. The calibration of the pH meter was carried out with two buffers (pH values of 4.00 and 7.00, acquired from Metrohm).

Extraction of amino acids. The ternary mixtures compositions used in the partitioning experiments were chosen based on the phase diagrams determined in this work, *i.e.* at compositions which lead to the formation of two phase systems. Aqueous solutions of amino acids were prepared at a concentration of 0.83 $g.L^{-1}$ for L-tryptophan and 0.44 $g.L^{-1}$ for L-Tyrosine, and used as the aqueous solution in each ABS preparation. Each mixture was vigorously stirred, centrifuged for 10 min, and left to equilibrate for more 10 min at 25°C to reach the amino acids complete partitioning between the coexisting phases. After, a careful separation of the phases was performed and the amount of each amino acid in each phase was quantified by UV-spectroscopy, using a BioTeck Synergy HT microplate reader, at a wavelength of 280 nm, and using calibration curves previously established (*cf.* Appendix A). At least three independent ABS were prepared and 3 samples of each phase quantified. The percentage extraction efficiency of L-tryptophan ($\boldsymbol{EE_{TRY}}\%$) and L-tyrosine ($\boldsymbol{EE_{TYR}}\%$), is the percentage ratio between the amount of each amino acid in the IL-rich phase to that in the total mixture, defined according to Equation (2.1.7):

$$EE_{\mathrm{AA}}\% = \frac{w_{AA}^{IL}}{w_{AA}^{IL} + w_{AA}^{Salt}} \times 100 \quad (2.1.7)$$

where w_{AA}^{IL} and w_{AA}^{Salt} are the total weight of amino acids in the IL-rich and in the salt-rich aqueous phases, respectively. In all systems the top phase corresponds to the IL-rich phase whereas the bottom phase is mainly constituted by the Na_2SO_4 salt and water.

2.1.4. Results and discussion

Ecotoxicity of AGB-ILs. The evaluation of the AGB-ILs toxicity was determined by exposing the marine bacterium *Vibrio fischeri* to several aqueous solutions of each IL, at different concentrations, for which the EC_{50} values were determined after 5, 15 and 30 min of exposure.

The EC_{50} data at 30 min are presented in Table 2.1.1. The corresponding EC_{50} values for 5 and 15 min are presented in the Appendix A. According to the EC_{50} values at 30 min (maximum exposure time), the toxicity of the synthesized AGB-ILs increases according to the rank: $[Et_3NC_2]Br$ < $[Bu_3PC_2]Br$ < $[MepyrNC_2]Br$ ≈ $[Pr_3NC_2]Br$ < $[Bu_3NC_2]Br$ < $[Bu_3PC_4]Br$. All ILs investigated share the common bromide anion; however, they comprise cations with different central atoms (N *vs.* P), with different alkyl side chains length, and with cyclic *vs*. non-cyclic cationic structures. The results obtained reveal that an increase in the alkyl side chain length increases the IL ecotoxic nature (as observed by the ranks: $[Et_3NC_2]Br$ < $[Pr_3NC_2]Br$ < $[Bu_3NC_2]Br$ and $[Bu_3PC_2]Br$ < $[Bu_3PC_4]Br$). Longer aliphatic moieties strongly interact with (or better penetrate) the phospholipid bilayer of membranes cells, as reflected by the stronger inhibition of the bacterium luminescence. ILs with longer alkyl side chains are more ecotoxic, in good agreement with the literature[34,35]. Taking into account the cation central atom, the EC_{50} values decrease considerably from $[Bu_3PC_2]Br$ (2141.9 mg. L^{-1}) to $[Bu_3NC_2]Br$ (340.0 mg.L^{-1}), meaning that the phosphonium-based IL is less toxic than its ammonium-based counterpart. This trend is the opposite to what has been found in the literature, for which the EC_{50} values are higher in ammonium-based ILs compared to their phosphonium counterparts[36]. This result indicates that the presence of an alkoxy group may change the ILs ecotoxicity. Since the $[MepyrNC_2]Br$ presents a cyclic cation structure, it is expected to be more toxic than the linear-based counterparts[36–39]. In fact, this IL is more toxic than $[Et_3NC_2]Br$, in spite of having a lower total number of carbons in the aliphatic chains connected to the N central atom.

Table 2.1.1. EC_{50} values (mg.dm^{-3}) with the respective 95% confidence limits (within brackets) of AGB-ILs after 30 minutes of exposure of the marine bacterium *Vibrio fischeri*.

AGB-IL	EC_{50} (mg·dm^{-3}) at 30 min	(lower limit; upper limit)
$[Bu_3PC_4]Br$	191.3	182.07; 200.57
$[Bu_3PC_2]Br$	2141.9	1519.93; 2763.84
$[Bu_3NC_2]Br$	340.0	299.20; 380.83
$[Pr_3NC_2]Br$	1589.8	673.78; 2505.87
$[Et_3NC_2]Br$	4634.8	3823.66; 5502.15
$[MepyrNC_2]Br$	1590.0	1165.35; 2014.71

Phase diagrams and tie-lines. Novel ternary phase diagrams for several ILs ($[MepyrNC_2]Br$, $[Et_3NC_2]Br$, $[Pr_3NC_2]Br$, $[Bu_3NC_2]Br$, $[Bu_3PC_2]Br$, $[Bu_3PC_4]Br$) + Na_2SO_4 + water were determined at 25°C and atmospheric pressure. The respective phase diagrams are displayed in Figure 2.1.2. In all

ABS, the top phase corresponds to the IL-rich phase while the bottom phase is mainly constituted by Na_2SO_4 and water.

In all phase diagrams shown in Figure 2.1.2, the monophasic and the biphasic areas are localized below and above the solubility curves, respectively. AGB-ILs with phase diagrams with a larger area above the solubility curve present a higher ability to form two phases, *i.e.* require a lower amount of salt to create two-phase systems. Overall, the ability of AGB-ILs to form ABS at 25°C follows the rank: $[Bu_3PC_4]Br$ > $[Bu_3PC_2]Br$ > $[Bu_3NC_2]Br$ > $[Pr_3NC_2]Br$ > $[Et_3NC_2]Br$ > $[MepyrNC_2]Br$. It was previously shown that tetraalkylammonium- and tetraalkylphosphonium-based ILs present a higher ability to create ABS with a given salt, *i.e.* require a lower amount of salt or IL to undergo liquid-liquid demixing, than imidazolium-based ILs[40]. This trend was also observed in this work with AGB-ILs (*cf.* the Appendix A). This feature is a major advantage since lower amounts of IL or salt are required to create ABS, meaning that a higher amount of water will be present, an advantage when envisioning their use as separation techniques of biologically active compounds.

In Figures 2.1.2a and 2.1.2b are represented the phases diagrams for the systems composed of $[Bu_3PC_2]Br$ and $[Bu_3PC_4]Br$, and of $[Bu_3NC_2]Br$, $[Pr_3NC_2]Br$, $[Et_3NC_2]Br$ and $[MepyrNC_2]Br$, allowing to address the effect of the IL cation alkyl chain length on the ABS formation ability. In general, ILs with longer alkyl side chains are more hydrophobic and more easily salted-out by the salt from aqueous media. Accordingly, $[Bu_3PC_2]Br$ requires a larger amount of Na_2SO_4 to form ABS than $[Bu_3PC_4]Br$. In the same line, the longer the alkyl side chain in the $[Et_3\text{-}Bu_3NC_2]Br$ series of ILs, the lower the amount of salt or IL required to form two-phase systems. These trends are in accordance with the literature[41], in which an increase in the IL cation alkyl side chain leads to a higher ability to create ABS. Finally, $[MepyrNC_2]Br$ is the IL with the lowest ability to create ABS. Although this IL comprises a cyclic ring contrarily to the remaining ILs, it presents a higher affinity for water due to the lower number of methylene groups in its structure, and thus requires higher amounts of salt to be salted-out from aqueous media.

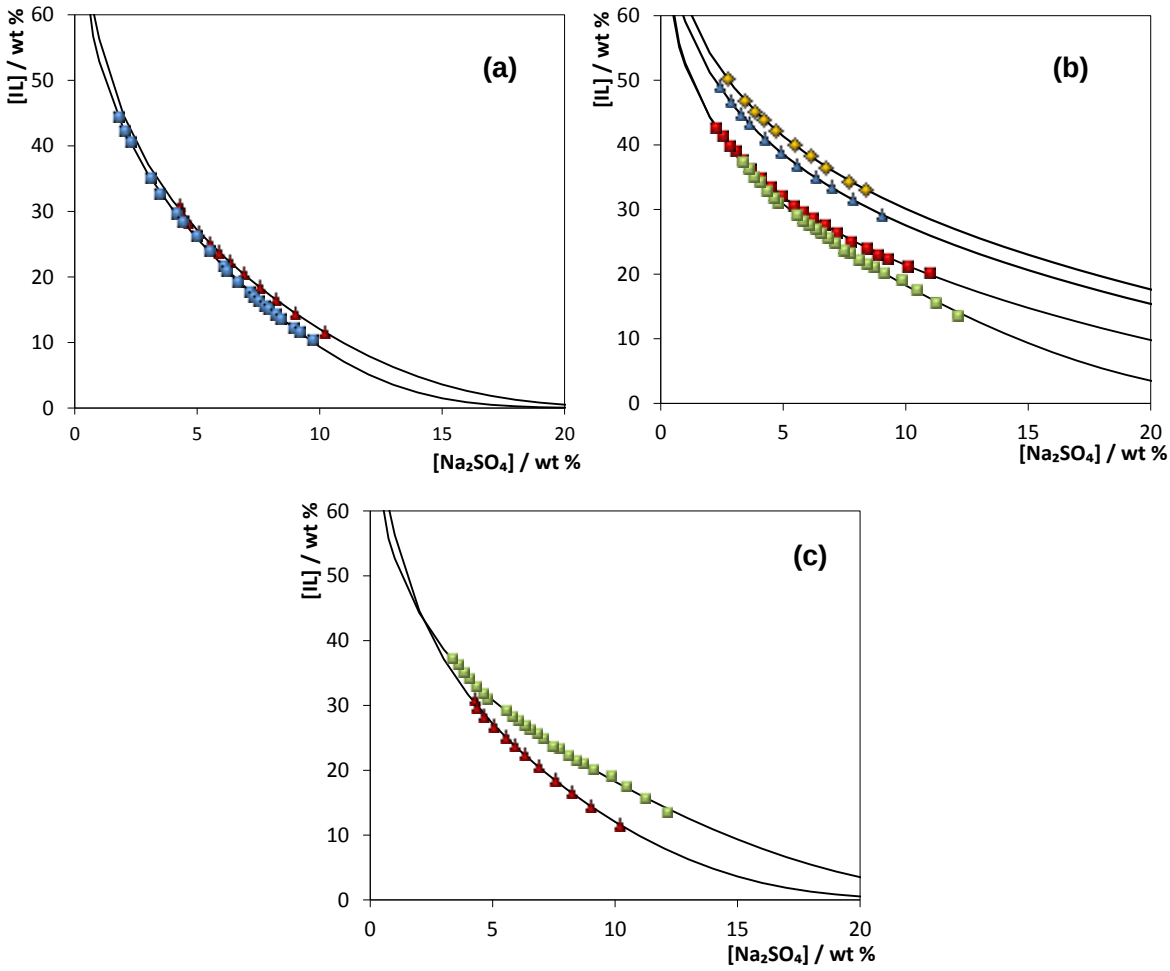

Figure 2.1.2. Phase diagrams for the systems composed of IL + Na_2SO_4 + H_2O at 25 °C: **(a)** $[Bu_3PC_2]Br$ (▲); $[Bu_3PC_4]Br$ (●); **(b)** $[MepyrNC_2]Br$ (◆); $[Et_3NC_2]Br$ (▲); $[Pr_3NC_2]Br$ (●); $[Bu_3NC_2]Br$ (■); **(c)** $[Bu_3PC_2]Br$ (▲); $[Bu_3NC_2]Br$ (■).

The phase diagrams for the systems constituted by $[Bu_3PC_4]Br$ and $[Bu_3NC_4]Br$ are depicted in Figure 2.1.2c. Although with a similar cation chemical structure, $[Bu_3PC_4]Br$ presents a better phase separation in presence of aqueous solutions of Na_2SO_4. The higher ability of phosphonium-based ILs to create ABS when compared with their ammonium-based counterparts was already demonstrated with other salts[40,42,43]. In general, phosphonium-based ILs are more hydrophobic than ammonium-based ones as a result of the cation central atom charge distribution[44].

All experimental data corresponding to the binodal curves were fitted using Equation (2.1.1), as presented in Figure 2.1.2. The regression parameters estimated by least-squares regression, standard deviations (σ), and correlation coefficients (R^2) are displayed in Table 2.1.2. Equation (2.1.1) adequately describes the experimental binodal curves, confirmed by the good correlation coefficients obtained.

Table 2.1.2. Correlation parameters of Equation 2.1.1 used to describe the experimental binodal data at 25°C.

IL	$A \pm \sigma$	$B \pm \sigma$	$10^5 (C \pm \sigma)$	R^2
IL + Na_2SO_4 + water				
$[Bu_3PC_4]Br$	88.82 ± 0.97	-0.518 ± 0.007	61.38 ± 1.89	0.9997
$[Bu_3PC_2]Br$	98.20 ± 7.33	-0.556 ± 0.036	34.09 ± 5.29	0.9984
$[Bu_3NC_2]Br$	80.07 ± 1.74	-0.418 ± 0.011	15.71 ± 1.38	0.9986
$[Pr_3NC_2]Br$	77.60 ± 0.73	-0.395 ± 0.005	3.75 ± 0.91	0.9995
$[Et_3NC_2]Br$	83.40 ± 0.59	-0.345 ± 0.004	1.86 ± 0.941	0.9998
$[MepyrNC_2]Br$	82.24 ± 1.33	-0.328 ± 0.008	1.50 ± 1.97	0.9994

The experimental TLs determined for each ABS, along with their respective length (TLL), as well as the compositions of each phase for the mixtures corresponding to the extraction studies, are reported in Table 2.1.3. The graphical representation of the TLs for all the systems investigated is presented in Appendix A**.**

Table 2.1.3. Experimental TLs and TLLs of the ABS composed of IL + Na_2SO_4+ H_2O at 25°C.

Weight fraction composition / (wt %)							
IL + Na_2SO_4+ water							
IL	$[IL]_{IL}$	$[salt]_{IL}$	$[IL]_M$	$[salt]_M$	$[IL]_{salt}$	$[salt]_{salt}$	**TLL**
$[Bu_3PC_4]Br$	67.80	0.27	39.78	7.45	0.31	17.79	69.73
	62.54	0.46	23.33	9.92	1.35	15.23	62.95
$[Bu_3PC_2]Br$	62.77	0.64	39.98	7.43	0.81	19.08	64.65
	65.39	0.53	37.28	10.20	0.10	22.99	69.03
$[Bu_3NC_2]Br$	43.84	2.06	24.75	9.96	5.52	17.91	41.46
	52.28	0.86	29.79	9.85	4.16	19.25	53.38
	55.03	0.80	40.39	7.47	0.69	25.58	59.72
	61.71	0.38	38.27	10.78	0.32	27.61	67.15
$[Pr_3NC_2]Br$	51.44	1.08	40.00	7.65	4.03	28.31	54.67
	57.31	0.58	41.09	10.13	2.037	33.12	64.13
$[Et_3NC_2]Br$	41.09	4.20	36.71	6.60	15.25	20.14	30.36
	44.97	3.20	38.19	7.38	12.57	23.19	38.07
$[MepyrNC_2]Br$	43.94	4.20	39.16	7.54	12.03	26.50	38.92
	46.10	3.63	37.32	9.82	10.30	28.86	43.80

Extraction of amino acids. The extraction efficiency of the investigated systems for two amino acids, namely L-tryptophan and L-tyrosine, was determined at a common mixture composition (≈40 wt% of IL, ≈7.5 wt% of Na_2SO_4 and ≈52.5 wt% of an aqueous solution containing L-tryptophan or L-tyrosine) in order to address the potential of the investigated systems to act as separation platforms. The results obtained at 25°C are displayed in Figure 2.1.3. The chemical structures of the two amino acids are also provided as an inset. In all systems, L-tryptophan and L-tyrosine preferentially migrate to the most hydrophobic phase, *i.e.* the IL-rich phase, with extraction efficiencies higher than 70%, and up to 100%, achieved in a single-step. In general, higher extraction efficiencies are obtained for L-tryptophan. Furthermore, the extraction efficiency of the studied ABS for L-tryptophan (to the IL-rich phase) follows the rank: $[Bu_3NC_2]Br$ > $[MepyrNC_2]Br$ ≈ $[Et_3NC_2]Br$ ≈ $[Pr_3NC_2]Br$ > $[Bu_3PC_2]Br$ > $[Bu_3PC_4]Br$, while the behavior observed for L-tyrosine is according to: $[MepyrNC_2]Br$ ≈ $[Et_3NC_2]Br$ > $[Pr_3NC_2]Br$ > $[Bu_3NC_2]Br$ > $[Bu_3PC_2]Br$ > $[Bu_3PC_4]Br$. With the exception of the IL $[Bu_3NC_2]Br$, the ILs rank in terms of extraction performance is similar for both amino acids. The trend on the extraction efficiencies closely depends on the IL hydrophobicity; the higher the IL hydrophobicity, as discussed according to their phase diagrams, the lower the extraction efficiencies.

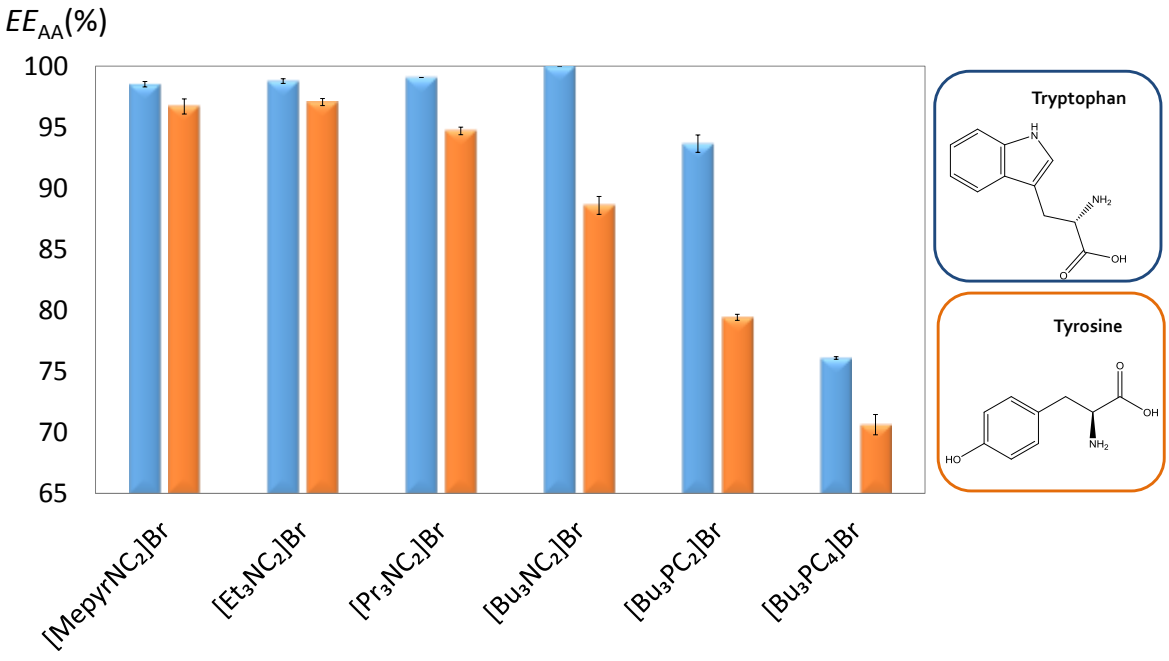

Figure 2.1.3. Extraction efficiency (*EE*%) of tryptophan (blue bars) and tyrosine (orange bars) in ABS composed of 40 wt% of IL + 7.5 wt% of Na_2SO_4 at 25°C.

In general, the amino acids partition in IL-based ABS is ruled by different driving forces, including the ability of ILs to establish specific interactions with amino acids and the salting-out

strength of the salt used to create ABS. In IL-based ABS constituted by imidazolium-based ILs, it was already reported that electrostatic, π···π and H-bonding interactions play a pivotal role[32,41,45,46]. Nevertheless, salting-out effects appear to be dominant, especially when employing high-charge density salts, *e.g.* $K_3C_6H_5O_7$ or K_3PO_4 [32,41,45,46]. In the same line, the amino acids (L-tryptophan, L-phenylalanine, L-tyrosine, L-leucine, and L-valine) partitioning in pH-controlled IL-based ABS (constituted by $[C_4mim]Br$ and $K_3C_6H_5O_7/C_6H_8O_7$) allowed to conclude that hydrophobic interactions are the main driving force; however, electrostatic interactions and salting-out effects have also a strong contribution[46].

Depending on the system pH, different chemical species of amino acids are predominantly present due to their functional groups ionization/protonation (-COOH and $-NH_2$ groups). According to the pH measurements of the IL- and Na_2SO_4- rich phase, which range between 3.1 and 6.2, as shown in the Appendix A, both amino acids (L-tryptophan and L-tyrosine) are predominately positively charged in the investigated ABS (protonation constants of L-tryptophan: pKa = 2.38; 9.39); and of L-tyrosine: pKa = 2.20; 9.11; 10.7)[47]. Even so, they partition to the phase with a lower ionic strength further supporting the influence of the salting-out effect exerted by the salt.

In summary, the systems investigated display a good performance to extract amino acids from aqueous media, with the additional advantage of using lower amounts of salt in the ABS composition (compared to previously published data)[48] and through the use of more environmentally-friendly and biocompatible ILs.

2.1.5. Conclusions

In order to develop more benign and biocompatible ABS, in this work, a series of AGB-ILs (based on glycine-betaine analogues) were synthesized, characterized in terms of ecotoxicity, applied in the creation of novel ABS, and used to extract amino acids, namely L-tryptophan and L-tyrosine. The systems investigated demonstrated to be remarkable separation routes, with maximum extraction efficiencies for L-tryptophan and L-tyrosine of 100% and 97%, respectively, achieved in a single-step. Besides the low ecotoxicity of AGB-ILs, the extraction efficiencies are considerably higher than those reported with conventional polymer-based ABS. Thus, the systems here investigated improve the biocompatibility and sustainability of ABS and still act as remarkable extraction platforms. According to the reported results, the application of these novel ABS could be extended to other added-value compounds.

2.1.6. References

1. Rito-Palomares, M.. J Chromatogr B Anal Technol Biomed Life Sci. 2004;807(1):3-11.

2. Ventura, S.P.M., e Silva, F.A., Quental, M. V., Mondal, D., Freire, M.G., Coutinho, J.A.P.. Chem Rev. 2017;117(10):6984-7052.
3. Albertsson, P.A.. Nature. 1958;182(4637):709-711.
4. Asenjo, J., Andrews, B.. J Chromatogr A. 2011;1218(49):8826-8835.
5. Freire, M.G., Cláudio, A.F.M., Araújo, J.M.M., Coutinho, J.A.P., Marrucho, I.M., Canongia Lopes, J.N., Rebelo, L.P.N.. Chem Soc Rev. 2012;41(14):4966-4995.
6. Pereira, J,F.B., Rebelo, L.P.N., Rogers, R.D., Coutinho, J.A.P, Freire, M.G.. Phys Chem Chem Phys. 2013;15(45):19580-19583.
7. Gutowski, K.E., Broker, G., Willauer, H.D., Huddleston, J.G., Swatloski, R.P., Holbrey, J.D., Rogers, R.D.. J Am Chem Soc. 2003;125(22):6632-6633.
8. Seddon, K.R.. Nat Mater. 2003;2(6):363-365.
9. Crowhurst, L., Mawdsley, P.R., Perez-Arlandis, J.M., Salter, P, Welton, T.. Phys Chem Chem Phys. 2003;5(13):2790-2794.
10. Santos, J.H., e Silva, F.A,. Ventura, S.P.M,. Coutinho, J.A.P., de Souza, R.L., Soares, C.M.F., Lima ÁS.. Biotechnol Prog. 2015;31(1):70-77.
11. Freire, M.G., Neves, C.M.S.S., Marrucho, I.M., Canongia Lopes, J.N., Rebelo, L.P.N,. Coutinho, J.A.P.. Green Chem. 2010;12(10):1715-1718.
12. Freire, M.G., Teles, A.R.R., Canongia Lopes, J.N, Rebelo, L.P.N., Marrucho, I.M., Coutinho, J.A. P.. Sep Sci Technol. 2012;47(2):284-291.
13. Zafarani-Moattar, M.T., Hamzehzadeh, S., Nasiri, S.. Biotechnol Prog. 2011;28(1):146-156.
14. Ventura, S.P.M., de Barros, R.L.F., Barbosa, J.M. de P., Soares, C.M.F., Lima, A.S., Coutinho, J.A.P.. Green Chem. 2012;14(3):734-740.
15. Ventura, S.P.M., Sousa, S.G., Freire, M.G., Serafim, L.S., Lima, Á.S., Coutinho, J.A.P.. J Chromatogr B Anal Technol Biomed Life Sci. 2011;879(26):2679-2687.
16. Passos ,H., Luís, A., Coutinho, J.A.P., Freire, M.G.. Sci Rep. 2016;6:20276.
17. Mourão, T., Tomé, L.C., Florindo, C., Rebelo, L.P.N., Marrucho, I.M.. ACS Sustain Chem Eng. 2014;2(10):2426-2434.
18. Li, Z., Liu, X., Pei, Y., Wang, J., He, M.. Green Chem. 2012;14(10):2941.
19. Shahriari, S., Tomé, L.C., Araújo, J.M.M., Rebelo, L.P.N., Coutinho, J.A.P, Marrucho, I.M., Freire, M.G.. RSC Adv. 2013;3(6):1835.
20. Pereira, J.F.B., Kurnia, K,A., Cojocaru, O.A., Gurau, G., Rebelo, L.P.N., Rogers, R.D., Freire, M.G., Coutinho, J.A.P.. Phys Chem Chem Phys. 2014;16(12):5723-5731.
21. Wu, C., Wang, J., Li, Z., Jing, J., Wang, H.. J Chromatogr A. 2013;1305:1-6.
22. Wu,C., Wang, J., Wang, H., Pei, Y., Li, Z.. J Chromatogr A. 2011;1218(48):8587-8593.
23. Quental, M.V., Caban, M., Pereira, M.M., Stepnowski, P., Coutinho, J.A.P., Freire, M.G.. Biotechnol J. 2015;10(9):1457-1466.
24. Messadi, A., Mohamadou, A., Boudesocque, S., Dupont, L., Fricoteaux, P., Nguyen-Van-Nhien, A., Courty, M.. J Mol Liq. 2013;184:68-72.
25. Sakamoto,, A., Murata, N.. Plant, Cell Environ. 2002;25(2):163-171.
26. Ashraf, M., Foolad, M.R.. Environ Exp Bot. 2007;59(2):206-216.
27. De Gaetano, Y., Hubert, J., Mohamadou, A., Boudesocque, S., Plantier-Royon, R., Renault, J.H., Dupont, L.. Chem Eng J. 2016;285:596-604.
28. Messadi, A., Mohamadou, A., Boudesocque, S., Dupont, L., Guillon, E.. Sep Purif Technol. 2013;107:172-178.
29. Zhou, Y., Boudesocque, S., Mohamadou, A., Dupont, L.. Sep Sci Technol. 2015;50(1):38-44.
30. Boudesocque, S., Mohamadou, A., Dupont, L.. New J Chem. 2014;38(11):5573-5581.
31. A. Environmental, Carlbad CA, USA, 1998.
32. Passos, H., Ferreira, A.R., Cláudio, A.F.M., Coutinho, J.A.P., Freire, M.G.. Biochem Eng J. 2012;67:68-76.
33. Merchuk, J.C., Andrews, B.A., Asenjo, J.A.. J Chromatogr B Biomed Sci Appl. 1998;711(1-2):285-293.
34. Ventura, S.P.M., Gonçalves, A.M.M., Sintra, T., Pereira, J.L., Gonçalves, F., Coutinho, J.A.P.. Ecotoxicology. 2013;22(1):1-12.
35. Stolte, S., Matzke, M., Arning, J., Boschen, A., Pitner, W-R., Welz-Biermann, U., Jastorff, B., Ranke, J.. Green Chem. 2007;9(11):1170-1179.
36. Couling, D.J., Bernot, R.J., Docherty, K.M., Dixon, J.K., Maginn, E.J.. Green Chem. 2006;8(1):82-90.
37. Bernot, R.J., Kennedy, E.E., Lamberti, G.A.. Environ Toxicol Chem. 2005;24(7):21.
38. Pretti, C., Chiappe, C., Baldetti, I., Brunini, S., Monni, G., Intorre, L.. Ecotoxicol Environ Saf. 2009;72(4):1170-1176.
39. Wang, X., Ohlin, C.A., Lu, Q., Fei, Z., Hu, J., Dyson, P.J.. Green Chem. 2007;9(11):1191-1197.
40. Louros, C.L.S., Cláudio, A.F.M., Neves, C.M.S.S., Freire, M.G, Marrucho, I.M, Jérôme, P., Coutinho, J.A.P.. Int J Mol Sci. 2010;11(4):1777-1791.
41. Neves, C.M.S.S., Ventura, S.P.M., Freire, M.G., Marrucho, I.M., Coutinho, J.A.P.. J Phys Chem B. 2009;113(15):5194-5199.
42. Pereira, M.M., Pedro, S.N., Quental, M.V., Lima, Á.S., Coutinho, J.A.P., Freire, M.G.. J Biotechnol. 2015;206:17-25.
43. Sintra, T.E., Cruz, R., Ventura, S.P.M., Coutinho, J.A.P.. J Chem Thermodyn. 2014;77:206-213.

44. Carvalho, P.J., Ventura, S.P.M., Batista, M.L.S., Schröder, B., Gonçalves, F., Esperança, J., Mutelet, F., Coutinho, J.A. .P.. J Chem Phys. 2014;140(6):64505.
45. Ventura, S.P.M., Neves, C.M.S.S., Freire, M.G., Marrucho, I.M., Oliveira, J., Coutinho, J.A.P.. J Phys Chem B. 2009;113(27):9304-9310.
46. Zafarani-Moattar, M.T., Hamzehzadeh, S.. Biotechnol Prog. 2011;27(4):986-997.
47. Wang, J., Pei, Y., Zhao, Y., Hu, Z.. Green Chem. 2005;7(4):196-202.
48. Almeida, M.R.,Passos, H., Pereira, M.M., Lima, A.S., Coutinho, J.A.P. Freire, M.G.. Sep Sci Technol. 2014;128:1-10.

2.2. Enhanced extraction of bovine serum albumin with aqueous biphasic systems of phosphonium- and ammonium-based ionic liquids

This chapter is based on the published manuscript

Matheus M. Pereira, Sónia N. Pedro, Maria V. Quental, Álvaro S. Lima, João A. P. Coutinho and Mara G. Freire

Journal of Biotechnology. 206 (2015) 17-25.

2.2.1. Abstract

Novel aqueous biphasic systems (ABS) composed of phosphonium- or ammonium-based ionic liquids (ILs), combined with a buffered aqueous solution of potassium citrate/citric acid (pH=7.0), were investigated for the extraction of proteins. For that purpose, the phase diagrams, tie-lines and tie-line lengths were determined at 25°C, and the performance of these ABS for the extraction of bovine serum albumin (BSA) was then evaluated. The obtained results reveal that, with the exception of the more hydrophobic ILs, most of the systems investigated allow the complete extraction of BSA to the IL-rich phase in a single-step. These remarkable extraction efficiencies are far superior to those afforded by more conventional extraction systems previously reported. The composition of the biphasic systems, i.e. the amount of phase-forming components, was also investigated aiming at reducing the overall costs of the process without losing efficiency on the protein extraction. It is shown that the extraction efficiencies of BSA are maintained at 100% up to high protein concentrations (at least up to 10 $g.L^{-1}$). The recovery of the BSA from the IL-rich phase by dialysis is also shown in addition to the demonstration of the IL recyclability and reusability, at least for 3 times. In the sequential three-step extractions (BSA recovery/IL reusability), the extraction efficiencies of BSA for the IL-rich phase were maintained at 100%. For the improved ABS, the preservation of the protein native conformation was confirmed by Size Exclusion High-Performance Liquid Chromatography (used also as the quantification method) and by Fourier Transform Infra-Red spectroscopy. According to the results herein reported, ABS composed of phosphonium- or ammonium-based ILs and a biodegradable organic salt represent an alternative and remarkable platform for the extraction of BSA and may be extended to other proteins of interest.

2.2.2. Introduction

Proteins are biomolecules formed by a sequence of amino acids and which perform a wide array of functions within living organisms[1]. However, the proteins specific functions are

Contributions: M.G.F., J.A.P.C. and A.S.L. conceived and directed this work. M.M.P., S.N.P. and M.V.Q. acquired the experimental data. M.M.P., A.S.L., J.A.P.C. and M.G.F interpreted the experimental data. The manuscript was mainly written by M.M.P. and M.G.F. with significant contributions from the remaining authors.

dependent on the stability of their native structure[2]. Most proteins have low structural stability and may be denatured in presence of some chemical compounds, namely polymers, salts or organic solvents[3–6], high temperature and pressure conditions[7,8] or through pH changes[9]. Therefore, when foreseeing the extraction and/or purification of proteins, those parameters must be addressed aiming at maintaining the proteins structure - a major challenge in the biotechnology field.

Serum albumins are the major soluble protein constituents in body fluids and have many relevant physiological functions. Amongst several valuable characteristics, one of the most important relays on their function as carriers of various compounds within the circulatory system[10]. BSA (bovine serum albumin), a protein with some common features to other serum albumins, such as ESA (equine serum albumin), LSA (leporine serum albumin) and HSA (human serum albumin)[11], has been extensively studied as a model protein in a wide variety of fields. Some examples include studies on the interaction of serum albumins with chlorophylls[12] and with ionic surfactants[13] due to the particular similarity (in 76% of the amino acid sequence) between BSA and HSA[14,15]. For these investigations, pure proteins are required. The extraction and purification of BSA was already investigated using various methodologies, such as reversed micelle approaches[16–18], ultrafiltration[19] or tangential flow filtration[20], precipitation[21,22] and by liquid-liquid approaches[23,24].

Amongst the several extraction and purification methods commonly applied to proteins, the use of aqueous biphasic systems (ABS) received a remarkable attention since they are mainly composed of water and thus are of high biocompatibility - favorable environment for the purification of biologically active biomolecules[25,26]. ABS fit within the liquid-liquid extraction/purification techniques and are environmentally-friendly since the use of volatile and hazardous organic solvents is avoided. ABS are typically composed of non-volatile pairs dissolved in aqueous media, such as two polymers, a polymer and a salt or two salts, which above given concentrations undergo liquid-liquid demixing. The selective partitioning of a target molecule, e.g. a protein, depends upon its affinity for each aqueous-rich phase, as well as on other parameters, such as pH, temperature and system composition. ABS have gained relevant attention since several early-stage processing steps, namely clarification, concentration and purification can be carried out in a single-stage. Moreover, the application of ABS at a large-scale has already been demonstrated[26]. Typical polymer-based ABS display, however, a high viscosity, which hinders the mass transfer and also lead to a slower phase separation. In the past decade, ionic-liquid-based ABS were proposed by Gutowski *et al.*[27] as alternatives to polymer-based systems. Ionic liquids

(ILs) belong to the molten salts group (with melting temperatures below 100°C) and are usually constituted by a large organic cation and an inorganic/organic anion. Due to their ionic character, most ILs present a negligible volatility at atmospheric conditions, non-flammability, high thermal and chemical stabilities, and a strong solvation capability for a large variety of compounds[28,29]. Nevertheless, one of the most important features of ILs arises from their tailoring ability resulting from cation-anion combinations – a property that is further extended to IL-based ABS[30]. Due to the large amount of water and non-volatile nature of ILs, the respective ABS also appear as viable media for biocompatible extractions. IL-based ABS have been used in the separation of enzymes, proteins, amino acids and antibiotics[31,32]. Albeit these studies can be used as guidelines for the application of IL-based ABS in the extraction of proteins, in most of these works, imidazolium-based ILs and inorganic salts were used as phase-forming components[32]. In particular, these IL-based ABS have been applied in the extraction of bovine serum albumin, lysozyme, trypsin, myoglobin, peroxidase, cytochrome c, globulins, hemoglobin and ovalbumin[32–36]. Mainly ILs with anions with a strong alkaline or acidic character were investigated, and phosphate buffered solutions were employed to maintain the pH of the aqueous medium while avoiding the denaturation of proteins[34,37,38]. Nonetheless, phosphate ions can bind to metal ions, such as calcium, zinc or magnesium, which are essential to maintain the integrity of some proteins/enzymes[39]. These high-charge density phosphate-based salts can be adequately substituted by more biocompatible and biodegradable organic salts, such as citrate-based salts that combined with citric acid afford a wide buffered pH region. On the other hand, few studies have considered phosphonium- and ammonium-based ILs as phase-forming constituents of ABS for the extraction of proteins[38,40,41]. Kragl and co-workers[42] studied ABS constituted by Ammoeng 110 to purify two alcohol dehydrogenases. The authors[42] concluded that this IL stabilizes the enzymes and increases the solubility of hydrophobic species. More recently, Desai *et al.*[43] studied ABS formed by an ammonium- or phosphonium-based IL and a phosphate-buffered solution to extract rubisco – a vegetable protein. These tetraalkyl-based compounds are less expensive and thermally more stable than the equivalent imidazolium-based counterparts, are available on a multi-ton scale, and have already been used in industrial processes[44]. Still, to decrease the cost of IL-based processes, studies on the recovery and reusability of ILs are of outstanding importance when envisaging their scale-up and industrial implementation. For instance, imidazolium-based ILs employed in the extraction of gallic acid by ABS were recovered and reused by back-extraction approaches[45].

This work aims at investigating the extraction capacity of ABS formed by phosphonium- and ammonium-based ILs and a citrate-based salt for BSA, and to further evaluate the protein stability in the IL-rich phase, as well as the protein recovery and recyclability/reusability of ILs.

2.2.3. Experimental procedures

Materials. The ABS studied in this work are composed of a buffer aqueous solution constituted by potassium citrate, $K_3C_6H_5O_7 \cdot H_2O$, ≥ 99 wt% pure from Sigma–Aldrich, and citric acid, $C_6H_8O_7 \cdot H2O$, 100 wt% pure from Fisher Scientific. The ionic liquids studied were the following: tetrabutylammonium chloride ($[N_{4444}]Cl$), > 97% pure, tetrabutylphosphonium bromide ($[P_{4444}]Br$), > 96% pure, tetrabutylphosphonium chloride ($[P_{4444}]Cl$), > 95% pure, tri(isobutyl)methylphosphonium tosylate ($[P_{i(444)1}][Tos]$), > 95% pure, and tri(butyl)methylphosphonium methylsulfate ($[P_{4441}][MeSO_4]$), > 99% pure. All phosphonium-based ILs were generously offered by Cytec Ind., while the ammonium-based compound was acquired from Sigma-Aldrich. The chemical structures of the ILs studied are depicted in Figure 2.2.1. Bovine Serum Albumin (BSA), fraction V, pH 7.0, fat acid free, was purchased from Acros.

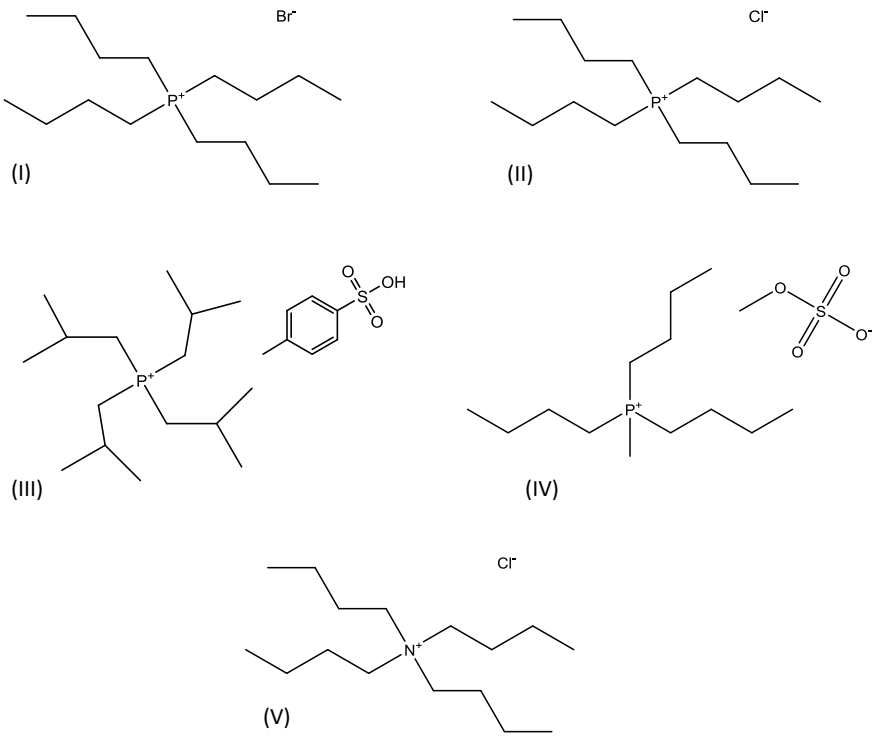

Figure 2.2.1. Chemical structure of the studied ILs: $[P_{4444}]Br$ (I); $[P_{4444}]Cl$ (II); $[P_{i(444)1}][Tos]$ (III); $[P_{4441}][MeSO_4]$ (IV); and $[N_{4444}]Cl$ (V).

Phase diagrams and tie-lines. Aqueous solutions of each IL ([P_{4444}]Br, [P_{4444}]Cl, [$P_{i(444)1}$][Tos], [$_{P4441}$][$MeSO_4$] and [N_{4444}]Cl) at *circa* 90 wt% and aqueous solutions of the mixture $K_3C_6H_5O_7/C_6H_8O_7$ (as a buffer solution at pH = 7.0, mole ratio of ≈ 15:1) at ≈ 50 wt% were prepared and used for the determination of the binodal curves. The phase diagrams were determined through the cloud point titration method[46] at 25°C and atmospheric pressure. The system compositions were determined by the weight quantification of all components added within $\pm 10^{-4}$ g. The tie-lines (TLs) were determined by a gravimetric method originally proposed by Merchuk *et al.* [47]. Different mixture points at the biphasic region were prepared in small glass ampoules (*ca.* 5 mL) especially designed for the purpose, vigorously stirred and allowed to reach equilibrium by the separation of the phases for at least 10 min at 25°C. After separation of the two phases, both the top and bottom phases were weighted. Each individual TL was determined by application of the lever-arm rule to the relationship between the top weight phase composition and the overall system composition. The experimental binodal curves were correlated using Equation (2.1.1):

$$[IL] = Aexp[(B[salt]^{0.5}) - (C[salt]^3)] \quad (2.2.1)$$

where $[IL]$ and $[salt]$ are the IL and the salt weight fraction percentages, respectively, and A, B, and C are constants obtained by the regression of the experimental data (see Appendix B).

The determination of the TLs was accomplished through the solution of the following system of four equations (Equations (2.1.2) to (2.1.5)) aiming at determining four unknown values ($[IL]_{\mathrm{IL}}$, $[IL]_{\mathrm{salt}}$, $[salt]_{\mathrm{IL}}$ and $[salt]_{\mathrm{salt}}$):

$$[IL]_{salt} = Aexp\left[\left(B[salt]_{IL}^{0.5}\right) - (C[salt]_{IL}^{3})\right] \quad (2.2.2)$$

$$[IL]_{salt} = Aexp\left[\left(B[salt]_{salt}^{0.5}\right) - \left(C[salt]_{salt}^{3}\right)\right] \quad (2.2.3)$$

$$[IL]_{IL} = \frac{[IL]_M}{\alpha} - \frac{1-\alpha}{\alpha}[IL]_{salt} \quad (2.2.4)$$

$$[salt]_{IL} = \frac{[salt]_M}{\alpha} - \frac{1-\alpha}{\alpha}[salt]_{salt} \quad (2.2.5)$$

where the subscripts "IL", "salt" and "M" represent the top and the bottom phases and the mixture composition, respectively. The parameter α is the ratio between the weight of the top phase and the weight of the overall mixture. For the calculation of each tie-line length (TLL), Equation (2.1.6) was employed:

$$TLL = \sqrt{([salt]_{IL} - [salt]_{salt})^2 + ([IL]_{IL} - [IL]_{salt})^2} \quad (2.2.6)$$

Extraction of bovine serum albumin (BSA). The ternary mixtures compositions used in the partitioning experiments were chosen based on the phase diagrams determined in this work for each IL-salt-water system. Different mixture compositions were studied to evaluate the effect of the concentration of the phase-forming components through the extraction of BSA. BSA at concentrations of *circa* 0.5, 1.0, 5.0 and 10.0 g.L^{-1} were also used as the aqueous solution. Each mixture was vigorously stirred, centrifuged for 10 min, and left to equilibrate for 10 min at 25°C to reach the BSA complete partitioning between the coexisting phases. After, a careful separation of the phases was performed and the amount of BSA in each phase was quantified by SE-HPLC (Size Exclusion High-Performance Liquid Chromatography). Each phase was diluted at a 1:10 (v:v) ratio in a phosphate buffer solution before injection. A Chromaster HPLC (VWR, Hitachi) coupled to an UV detector was used. SE-HPLC was performed with an analytical column (25 cm x 2 mm i.d., 25 µm), Lichrospher 100 RP-18, from Merck. A 100 mM phosphate buffer in MiliQ water (mobile phase) was run isocratically with a flow rate of 1 mL·min^{-1}. The temperature of the column and auto-sampler was kept constant at 25°C. The injection volume was of 25 µL. The wavelength was set at 280 nm whereas the retention time of BSA was found to be *circa* 16 min within an analysis time of 40 min. The quantification of BSA in each phase was carried out by an external standard calibration method (R^2=0.9997) - *cf*. Appendix B with the established calibration curve and associated standard deviations. The limit of detection of BSA was found to be 0.011 g.L^{-1}. At least three independent ABS were prepared and 3 samples of each phase were quantified. The percentage extraction efficiency of BSA, $\boldsymbol{EE_{BSA}}\%$, is the percentage ratio between the amount of protein in the IL-rich aqueous phase to that in the total mixture, and is defined according to Equation (2.2.7):

$$EE_{\mathrm{BSA}}\% = \frac{w_{BSA}^{IL}}{w_{BSA}^{IL} + w_{BSA}^{Salt}} \times 100 \quad (2.2.7)$$

where w_{BSA}^{IL} and w_{BSA}^{Salt} are the total weight of protein in the IL-rich and in the salt-rich aqueous phases, respectively. In all systems the top phase corresponds to the IL-rich phase whereas the bottom phase is mainly constituted by the citrate-based salt and water.

Recovery of bovine serum albumin (BSA) from the IL-rich phase and reusability of the ILs. In order to guarantee the recovery of BSA after the extraction to the IL-rich phase and the ILs recyclability, a three-step recovery/extraction process was here attempted. In this approach, the

system composed of 30 wt% [$P_{i(444)1}$][Tos] + 30 wt% of $K_3C_6H_5O_7/C_6H_8O_7$ + 40 wt% of an aqueous solution of BSA at 0.5 $g.L^{-1}$ was chosen. After the initial extraction of BSA as described before, which occurs for the IL-rich phase, the protein was recovered by dialysis. The IL-rich phase containing BSA was dialyzed against 100 mL of ultra-pure water, for 12h at room temperature and under moderate agitation, using a dialysis tubing cellulose membrane (average flat width 10 mm (0.4 in.), molecular weight cut-off = 14,000) from Sigma. The dialysate solution containing BSA was recovered, and the aqueous phase containing the IL was dried under vacuum at 60°C up to a constant weight, and then reused to form a new ABS with $K_3C_6H_5O_7/C_6H_8O_7$ and an aqueous solution of BSA at 0.5 $g.L^{-1}$ in order to perform a subsequent extraction of the protein. This step was repeated one more time to ascertain on the recyclability and reusability of the IL employed and its efficiency when employed as a phase-forming component of a given ABS for the extraction of proteins.

Fourier transform infrared spectroscopy (FT-IR). FT-IR spectra were recorded using a Perkin Elmer Spectrum Bx spectrophotometer with a resolution of 4 cm^{-1}. Several aqueous solutions containing BSA (1.0 $g.L^{-1}$) and ILs at different concentrations were used to perform the FT-IR analysis. The spectra were obtained in the wavelength range from 1700 to 1500 cm^{-1}.

2.2.4. Results and discussion

Phase diagrams and tie-lines. Novel phase diagrams for the various systems consisting of IL + water + $K_3C_6H_5O_7/C_6H_8O_7$ buffer (pH = 7.0) at 25°C and atmospheric pressure were determined in this work. The respective phase diagrams are depicted in Figure 2.2.2 and Figure 2.2.3. The corresponding data are provided in Appendix B. All the calculations considering the weight fraction of the phase-forming components were carried out discounting the complexed water in the commercial citrate-based salt.

Figure2.2.2 depicts the phase diagrams for the systems constituted by phosphonium-based ILs and allows the evaluation of the ILs ability to form ABS. In all phase diagrams, the two-phase region is positioned above the solubility curve while the monophasic region is localized below. Diagrams with the largest area above the binodal curve have therefore a higher ability to form two phases, *i.e.* the IL is more easily salted-out by the salt. Therefore, the capacity of phosphonium-based ILs to form ABS (or ILs more easily salted-out) follows the order: [P_{4444}]Br > [P_{4441}][$MeSO_4$] > [P_{4444}]Cl > [$P_{i(444)1}$][Tos]. Since not all the cations and anions are common there is a balanced effect of both ions to be hydrated and to form ABS. Nevertheless, the results obtained here are in close agreement with the trend previously described in the literature for ABS

composed of phosphonium-based ILs + K_3PO_4 + water[48]. In general, phosphonium-based ILs have a higher ability to undergo phase separation in ABS when compared with their imidazolium-based counterparts[48] – a major advantage when considering the amount of phase-forming compounds required to form liquid-liquid systems.

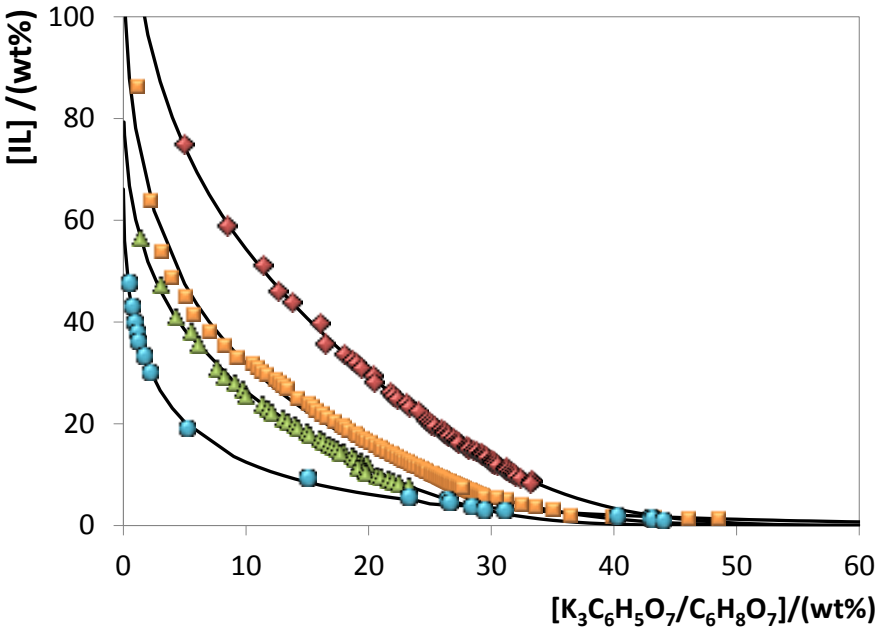

Figure 2.2.2. Phase diagrams for the systems composed of IL + $K_3C_6H_5O_7/C_6H_8O_7$ + H_2O at 25°C and pH 7.0: $[P_{4444}]Br$ (●); $[P_{4441}][MeSO_4]$ (▲); $[P_{4444}]Cl$ (■); $[P_{i(444)1}][Tos]$ (◆); and adjusted binodal data through Equation 2.2.1 (—).

Since several ILs with different lengths at the cation alkyl chains were investigated, a direct comparison can only be made between $[P_{4444}]Br$ and $[P_{4444}]Cl$, whereas the first is more able to undergo a phase separation. The Cl^- anion presents a higher aptitude to be hydrated or to form hydration complexes, and thus more salt is required to induce the salting-out when compared with bromide-based ILs[49]. Bromide has a weaker ability to hydrogen-bond with water or to form hydration complexes, and less salt is required for phase separation in ABS. In addition, when comparing the performance of $[P_{4441}][MeSO_4]$ and $[P_{i(444)1}][Tos]$, the [Tos]-based IL requires a higher amount of salt to undergo liquid-liquid demixing.

The phase diagrams for the systems composed of $[N_{4444}]Cl$ and $[P_{4444}]Cl$ are presented in Figure 2.2.3. Although similar, the $[P_{4444}]$-based IL presents a slightly higher ability to form ABS. The higher hydrophobicity of phosphonium-based ILs (when compared to the ammonium-based counterparts) was shown by Carvalho *et al.* [50] and is reflected in the phase behavior of ternary systems composed of similar ILs, water and other salts[46]. It is well-accepted that the water-IL

miscibility derives essentially from hydrogen-bonding interactions mainly occurring with the anion[51]. Nevertheless, the anion is similar in both cases, and the small deviations in the phase diagram are a result of the charge distribution at the central atom of the IL cation. Even so, both tetrabutyl-based cations are known for their high capacity to form ABS mainly due to the presence of heteroatoms surrounded by four alkyl chains and no aromatic character, and therefore with a low affinity for water.

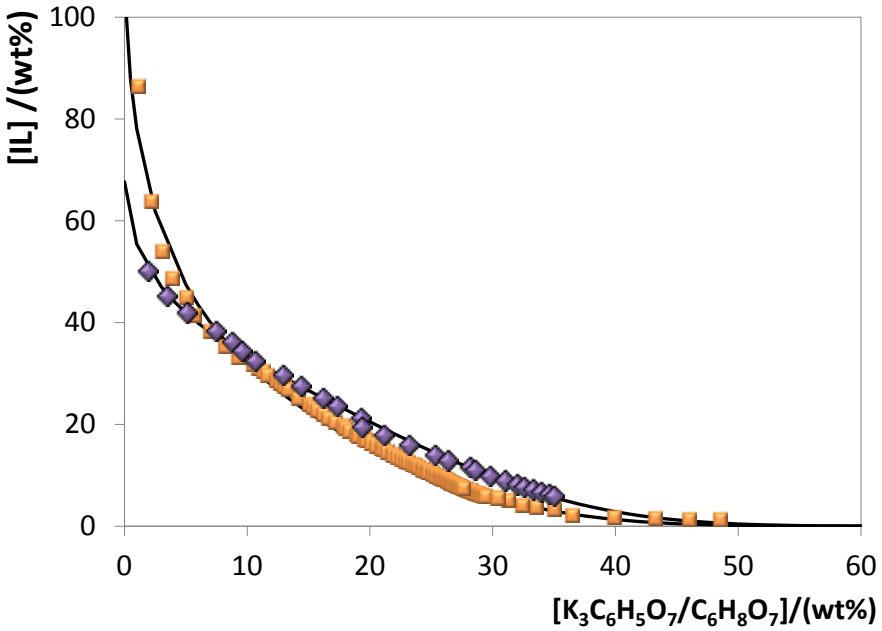

Figure 2.2.3. Phase diagrams for the systems composed of IL + $K_3C_6H_5O_7/C_6H_8O_7$ + H_2O at 25°C and pH 7.0: $[P_{4444}]Cl$ (■);$[N_{4444}]Cl$ (◆); and adjusted binodal data through Equation (2.2.1) (—).

Table 2.2.1. Correlation parameters of Equation (2.2.1) used to describe the experimental binodal data at 25°C.

IL	$A \pm \sigma$	$B \pm \sigma$	$10^5 (C \pm \sigma)$	R^2
IL + $K_3C_6H_5O_7/C_6H_8O_7$ + water				
$[P_{4444}]Br$	66.13 ± 0.98	-0.527 ± 0.013	0.21 ± 0.24	0.9988
$[P_{4444}]Cl$	116.40 ± 2.65	-0.399 ± 0.009	3.05 ± 0.20	0.9849
$[N_{4444}]Cl$	69.16 ± 1.22	-0.222 ± 0.007	2.78 ± 0.12	0.9978
$[P_{i(444)1}][Tos]$	149.90 ± 2.39	-0.318 ± 0.006	2.83 ± 0.10	0.9953
$[P_{4441}][MeSO_4]$	85.89 ± 1.30	-0.356 ± 0.007	5.40 ± 0.29	0.9971

The experimental data corresponding to the binodal curves were fitted using Equation (2.2.1) as shown in Figure 2.2.2 and Figure 2.2.3. The regression parameters estimated by least-squares regression, standard deviations (σ) and correlation coefficients (R^2) are displayed in Table 2.2.1.

Equation (2.2.1) adequately describes the experimental binodal curves as confirmed by the good correlation coefficients obtained.

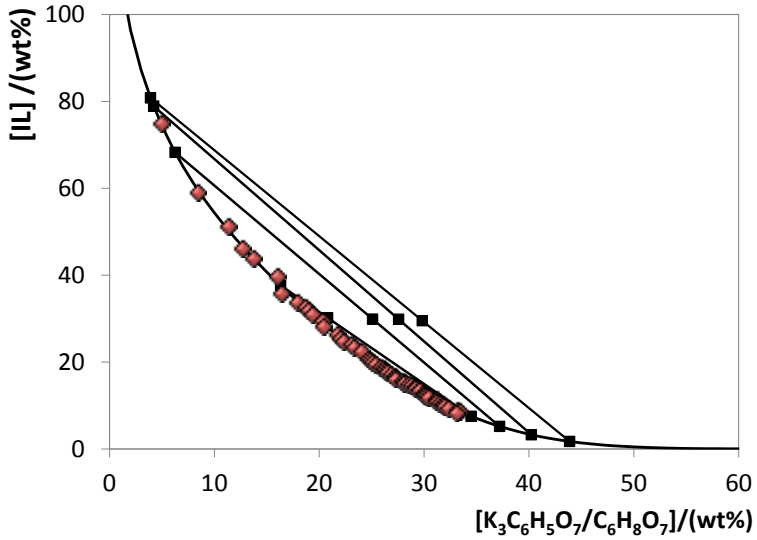

Figure 2.2.4. Phase diagrams for the systems composed of $[P_{i(444)1}][Tos]$+ $K_3C_6H_5O_7/C_6H_8O_7$ + H_2O at 25°C and pH 7.0: binodal curve data (◆); TL data (■); and adjusted binodal data through Equation (2.2.1) (—).

Table 2.2.2. Experimental TLs and TLLs of the ABS composed of IL + $K_3C_6H_5O_7/C_6H_8O_7$ + H_2O at 25°C.

Weight fraction composition / (wt %)							
IL + $K_3C_6H_5O_7/C_6H_8O_7$ + water							
IL	**$[IL]_{IL}$**	**$[salt]_{IL}$**	**$[IL]_M$**	**$[salt]_M$**	**$[IL]_{salt}$**	**$[salt]_{salt}$**	**TLL**
$[P_{4444}]Br$	58.75	0.05	29.17	29.38	0.02	58.30	82.72
	52.02	0.21	19.99	20.30	1.74	31.75	59.35
$[P_{4444}]Cl$	80.98	0.83	28.82	29.10	0.56	44.43	91.48
	75.06	1.20	27.08	27.09	1.08	41.11	84.05
$[N_{4444}]Cl$	60.80	0.34	30.25	30.68	0.02	60.71	85.67
	58.51	0.57	24.21	24.68	3.05	39.56	67.79
$[P_{i(444)1}][Tos]$	80.78	3.90	29.51	29.83	1.74	43.87	85.57
	78.90	4.21	29.86	27.57	3.28	40.23	83.76
	68.25	6.25	29.89	25.09	5.20	37.20	70.23
	37.62	16.32	30.19	20.80	7.52	34.48	35.15
$[P_{4441}][MeSO_4]$	58.35	1.18	29.10	28.93	$3.38E^{-04}$	56.55	80.44
	41.87	4.03	19.61	19.88	1.72	32.62	49.29

The experimental TLs in each ABS, along with their respective length, and at the compositions for which the extraction studies of BSA were conducted, are reported in Table 2.2.2. An example of the TLs obtained for the $[P_{i(444)1}][Tos]$-based system is depicted in Figure 2.2.4. The graphical representation of the TLs for the remaining systems are presented in Appendix B.

Extraction of bovine serum albumin (BSA). The extraction efficiencies of BSA in each IL-based ABS, and which allow the evaluation of the IL for such a purpose, were determined for a common mixture composition (30 wt% of IL, 30 wt% of $K_3C_6H_5O_7/C_6H_8O_7$ and 40 wt% of an aqueous solution containing BSA at 0.5 $g.L^{-1}$). The results obtained are reported in Table 2.2.3. In all systems, the top phase corresponds to the IL-rich phase while the bottom phase is majorly composed of the citrate-based salt and water.

Table 2.2.3. Extraction efficiency of BSA (EE_{BSA}%) at 25°C and pH 7.0 in the ABS composed of ILs and $K_3C_6H_5O_7/C_6H_8O_7$.

IL	Weight fraction composition / (wt %)		EE_{BSA}%
	IL	Salt	
$[P_{4444}]Br$	29.98 ± 0.11	30.01 ± 0.93	-
$[P_{4444}]Cl$	30.40 ± 0.80	30.48 ± 0.38	100
$[N_{4444}]Cl$	31.30 ± 0.73	30.97 ± 1.30	100
$[P_{i(444)1}][Tos]$	29.92 ± 0.27	30.39 ± 0.32	100
$[P_{4441}][MeSO_4]$	31.30 ± 0.72	30.97 ± 1.30	100

With the exception of the ABS composed of $[P_{4444}]Br$, for which a complete precipitation of the protein was observed (no protein was detected at the coexisting phases as determined by SE-HPLC), all the other ABS are able to completely extract BSA to the IL-rich phase – with extraction efficiencies of 100% attained in a single-step. For these systems, the SE-HPLC chromatograms used for the BSA quantification confirm the presence of BSA only at the IL-rich phase, as well as the absence of BSA aggregates or the protein fragmentation – Figure 2.2.5. Moreover, for these systems, no losses of protein by precipitation where observed.

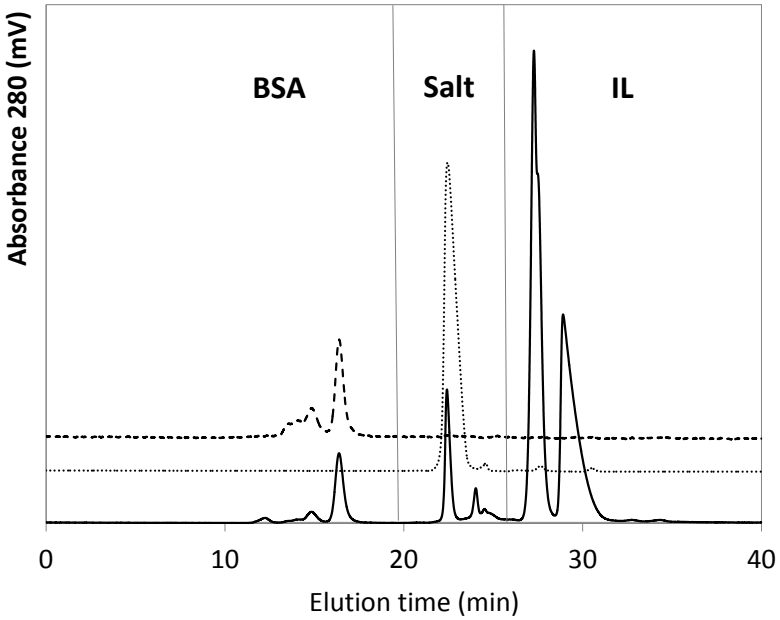

Figure 2.2.5. Size exclusion chromatography results of a BSA standard solution (---); BSA in the salt rich-phase (····); and BSA in the IL rich-phase (—) corresponding to the ABS composed of $[P_{i(444)1}][Tos]$ (20 wt%) + $K_3C_6H_5O_7/C_6H_8O_7$ (30 wt%).

$[P_{4444}]Br$ is the most hydrophobic IL investigated (from the ILs trend shown in Figure 2.2.2) and leads to the complete precipitation and/or denaturation of BSA, being therefore not adequate for this type of extractions. When comparing the TL data presented in Table 2.2.2**.** for the similar mixture composition, it can be inferred that neither the IL content or water content at the IL-rich phase seem to be responsible for the protein precipitation. The composition of water in the $[P_{4444}]Br$-rich phase is around 40 wt% and similar to that found in the $[P_{4441}][MeSO_4]$-rich phase. Therefore, these data indicate that the changes in the protein structure may result from specific interactions occurring between the protein and the IL. Hydrophobic interactions responsible for proteins precipitation have been reported with polymers (PEG and PPG), organic solvents (acetone, ethanol, methanol and dimethyl sulfoxide) and salts[52–54]. For instance, the precipitation of rubisco was also observed with the molecular weight increase of the polymers used as phase-forming components of ABS, and that was related with a decrease in the free volume available as well as with the hydrophobicity increase in such a phase[43].

In general, and with the exception of the $[P_{4444}]Br$-based ABS, BSA still preferentially partitions to the most hydrophobic phase, *i.e.*, the IL-rich phase. This trend is similar to that observed in ABS formed by polyethylene glycol (PEG) and potassium citrate, where BSA preferentially partitions for the more hydrophobic PEG-rich phase[18]. Lu *et al.*[18] also reported that either an increase on the salt or polymer concentration, *i.e.* increase of the TLL, leads to a

preferential partitioning of BSA to the polymer-rich phase. This behavior was explained based on the salting-out effect afforded by an increased concentration of salt in the system, leading thus to a preferential exclusion of the protein to the opposite phase[18]. The isoelectric point of BSA is 4.7[55]. Hence, BSA is negatively charged at pH 7 and in all the studied ABS. Based on the overall results shown in Table 2.2.3., the partitioning of BSA to the IL-rich phase seems to be driven by a combined effect of favorable dispersive interactions, salting-out effect exerted by the citrate-based salt, and electrostatic interactions between the positively charged IL cations and the negatively charged amino acid residues at the surface of the protein.

Overall, the extraction efficiencies achieved in this work are significantly higher than those observed in polymer-based ABS previously reported[56–58]. Saravanan *et al.*[58] studied PEG4000-magnesium sulfate ABS to purify BSA with a maximum yield of 82.68%. In ABS composed of PEG and sodium citrate, Perumalsamy and Batcha[59] reported extraction efficiencies lower than 50%. Thus, IL-based ABS seem to be more effective in the extraction of proteins from aqueous media than polymer-based systems. Lin *et al.*[60] compared the effects of eight imidazolium-based ILs and identified the optimal conditions for the extraction of four proteins. Under the optimum conditions, the average recovery of BSA was 90.5%. Ding *et al.*[61] also investigated the use of a series of functionalized alkylguanidinium ILs as phase-forming components of ABS, while applying single factor experiments to optimize the extraction performance, with a maximum extraction efficiency of BSA of 97%. Even in dye-affinity systems (containing the Reactive Red-120 dye) and after the optimization of the pH of the aqueous phase, temperature, and composition of the ABS, the maximum extraction efficiencies achieved of BSA for the IL-rich phase are below 100%[62]. Therefore, remarkable extraction efficiencies of BSA were obtained in this work with ABS composed of more stable and less expensive phosphonium- or ammonium-based ILs and a biodegradable organic salt. The ABS studied in this work seem to have an enhanced potential for the extraction of proteins, and their application to the purification and concentration of added-value proteins is a main topic of further work at our laboratory.

Influence of the IL, salt and bovine serum albumin (BSA) concentrations. Aiming at reducing the amount of salt and IL required to form ABS, while keeping the complete extraction ability for BSA, a series of ABS containing variable concentrations of $[P_{i(444)1}][Tos]$ (20-30 wt%) and salt (20-30 wt%) was prepared. $[P_{i(444)1}][Tos]$ was selected since it is the only IL that is liquid at room temperature (from the set of ILs investigated) and therefore easier to handle and to prepare the target mixture compositions. The results obtained for the IL concentration effect are depicted in Table 2.2.4. In all systems, the complete extraction of BSA was attained. Therefore, the

concentration of IL can be decreased down to 20 wt% without losing the ABS complete extraction performance.

Table 2.2.4. Effect of the IL, salt and protein concentration in the extraction efficiencies of BSA (EE_{BSA}%) for the system composed of [$P_{i(444)1}$][Tos] (from 20 to 30 wt%) + $K_3C_6H_5O_7/C_6H_8O_7$ (from 20 to 30 wt%) at 25°C and pH 7.0.

[BSA] / (g.L^{-1})	Weight fraction composition / (wt %)		EE_{BSA}%
	IL	Salt	
0.5	30.22 ± 0.21	25.74 ± 0.04	100
	31.56 ± 0.93	20.77 ± 0.03	100
	26.22 ± 0.36	30.48 ± 0.36	100
1.0	20.41 ± 0.37	30.64 ± 0.09	100
	20.13 ± 0.07	30.41 ± 0.12	100
5.0	20.21 ± 0.06	30.32 ± 0.17	100
10.0	20.43 ± 0.15	30.47 ± 0.38	100

The effect of the salt concentration through the extraction efficiency of BSA is also shown in Table 2.2.4.. All compositions allow the complete extraction of BSA, in a single-step, and without precipitation and/or denaturation of the protein. The variation of the salt amount has been reported to drive the migration of proteins to the top phase due to a decrease in the difference of the electrostatic potential between the coexisting phases in PEG-salt systems[63]. Even so, in IL-salt-based ABS, the extraction efficiencies are kept at 100% within the salt concentration range evaluated. In fact, the mixture compositions (20 wt% of salt + 30 wt% of IL) and (30 wt% of salt + 20 wt% of IL) are very close to the binodal curve and correspond to minimum concentrations required to form ABS with [$P_{i(444)1}$][Tos].

The results presented in Table 2.2.4. show the extraction efficiencies of BSA, in a given ABS and composition, as a function of the protein concentration at the aqueous phase. It is shown that the investigated [$P_{i(444)1}$][Tos]-based ABS can be used to completely extract BSA from aqueous solutions with a concentration up to 10 g·L^{-1} (without the saturation of the IL-rich phase and with no precipitation and/or denaturation effects observed).

Recovery of bovine serum albumin (BSA) from the IL-rich phase and reusability of the ILs. To guarantee the development of a sustainable and low-cost extraction procedure, we additionally evaluated the recovery of BSA from the IL-rich phase and further use of the IL to create a new ABS and to conduct subsequent extractions with new aqueous solutions containing BSA. In this step,

the ABS composed of 30 wt% of [$P_{i(444)1}$][Tos], 30 wt% of $K_3C_6H_5O_7/C_6H_8O_7$ and 40 wt% of an aqueous solution containing BSA at 0.5 $g.L^{-1}$ was investigated. After the first extraction, the top phase was separated, and the BSA recovered by dialysis. After the separation of BSA, the IL-rich phase was dried under vacuum at 60°C. Then, the non-volatile components at the IL-rich phase, namely the IL and salt, were used to create a new ABS by the addition of a fresh aqueous solution containing BSA at 0.5 $g.L^{-1}$, as well as more citrate-based salt to achieve the initial mixture composition. After the formation of the ABS and the conditions mentioned before for achieving the equilibrium, the phases were separated and the amount of BSA in each phase was again quantified. This overall procedure was repeated one more time. In all experiments of BSA recovery/IL reusability, the complete extraction of BSA (extraction efficiency of 100%) to the IL rich-phase was verified, meaning that ILs can be reused in ABS without a decrease on the systems extraction efficiency. However, it should be highlighted that unless cyclic, closed, and more complex systems are used, inevitable losses of IL will occur by the simple transference of the fluid into different vials. Moreover, and from the TLs data shown in Table 2.2.2, there is also the loss of 1.74 wt% of [$P_{i(444)1}$][Tos] *per* extraction, which corresponds to the IL present in the salt-rich phase. For the three consecutive extractions investigated, a total loss of 9.96 wt% of [$P_{i(444)1}$][Tos] occurs.

Bovine serum albumin (BSA) stability in ionic liquid solutions. Proteins are complex macromolecules which retain their structural and functional stability in their native environment; yet, small variations in their environment, such as temperature, pressure, pH and presence of some solutes can alter their native structure. Most works reported in the literature focused on the extraction ability of IL-based ABS for proteins[64–66], and few studies[41,60,67] have investigated the protein stability after being extracted into the IL-rich phase. However, if proteins are being extracted to a given phase, the protein stability is a prerequisite that cannot be discarded. The SE-HPLC chromatograms used for the BSA quantification, with one example being displayed in Fig.2.2.5, allow to endorse that there is no significant fragmentation or formation of aggregates of BSA under the studied conditions. In addition, the native structure of BSA at the IL-rich phase, in the systems investigated, was always confirmed by the size-exclusion chromatograms. The absence of BSA at the salt-rich phase also confirms the complete extraction of the protein for the IL-rich phase in the studied systems. Recently, Desai *et al.*[43] demonstrated that other proteins, such as IgG and Rubisco, due to their higher molecular weight, tend to cluster into aggregates in presence of phosphonium-based ILs. Baker and Heller[68] also reported the aggregation of HSA in an aqueous solution with 50 wt% of an imidazolium-based IL. However, BSA remained stable in all

the IL-based ABS tested (with exception of the $[P_{4444}]$Br-based system) supporting the viability of these systems to deal with the extraction/purification of proteins.

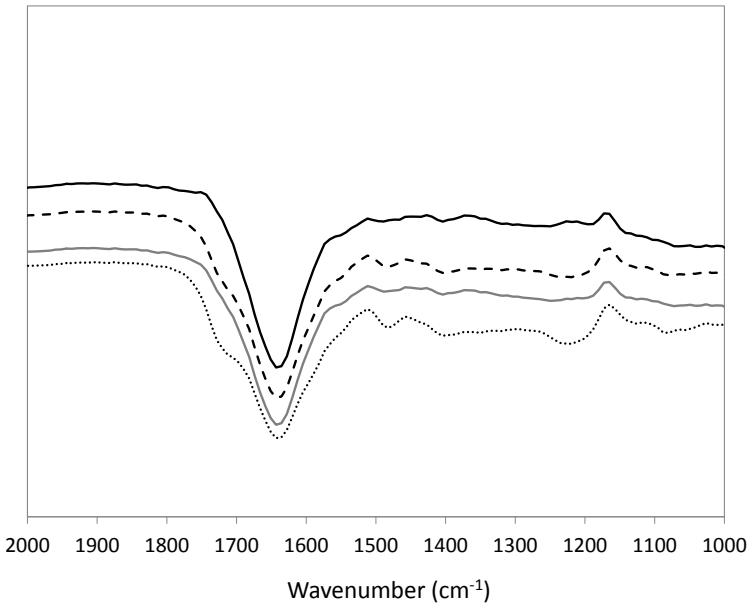

Figure 2.2.6. FT-IR spectra of a BSA standard solution (0.5 $g.L^{-1}$) (—); BSA in a 12.5 wt% $[P_{i(444)1}]$[Tos] aqueous solution (-----); BSA in a 25 wt% $[P_{i(444)1}]$[Tos] aqueous solution (—); and BSA in a 50 wt% $[P_{i(444)1}]$[Tos] aqueous solution (·····).

FT-IR spectra provides information for identifying the structure of proteins based on energy absorption bands of specific functional groups or chemical bonds. The most widely used absorption bands as structure probes for proteins are the amide I vibrations[69], which fall between 1690 and 1600 cm^{-1}. Fig. 2.2.5. depicts the FT-IR spectra of BSA in a buffered aqueous solution and BSA in an aqueous solution of $[P_{i(444)1}]$[Tos] at different concentrations (up to 50 wt%). These results corroborate that there are no significant changes of the protein absorbance peaks suggesting that the protein may maintain its spatial structure in aqueous solutions of $[P_{i(444)1}]$[Tos].

2.2.5. Conclusions

In this work, the ability of less studied classes of IL-based ABS, composed of phosphonium- or ammonium-based ILs, was evaluated in what concerns their performance for the extraction of proteins, namely BSA. For that purpose, the respective phase diagrams, tie-lines and tie-line lengths were also ascertained. For almost all the studied systems, and at all the conditions analyzed, BSA preferentially migrates to the IL-rich phase, with the exception of the more hydrophobic IL investigated ($[P_{4444}]$Br) that induced the precipitation of the protein. However, the remaining phosphonium- and ammonium-based ABS were able to completely extract BSA top the

IL-rich phase. Remarkable extraction efficiencies of 100% were obtained in a single-step, without evidence of protein denaturation in concentrations up to 10 $g.L^{-1}$ of BSA. Moreover, the recovery of the protein by dialysis and the IL reusability were also investigated in three-step consecutive extractions, and where it was demonstrated that IL-based ABS can be adequately reused without losses on their extraction performance. ABS composed of phosphonium- or ammonium-based ILs and a biodegradable organic salt are improved systems for the extraction of BSA when compared with the more traditional polymer-based or other IL-based ABS. Furthermore, tetralkylphosphonium- and tetralkylammonium-based ILs are less expensive, and thermally and chemically more stable, than the widely studied imidazolium-based counterparts. According to the reported results, these new ABS can be foreseen as alternative and cost-effective platforms for the separation and purification of other proteins of interest.

2.2.6. References

1. Zhao, H.. Biotechnol Bioeng. 2007;98(2):313-317.
2. Roberts, C.J.. Biotechnol Bioeng. 2007;98(5):927-938.
3. Wallqvist, A., Covell, D.G., Thirumalai, D. J. Am. Chem. Soc.. 1998;7863(14):427-428.
4. Jiang, W., Schwendeman, S.P.. Biotechnol Bioeng. 2000;70(5):507-517.
5. Li, S., Schöneich, C., Borchardt, R.T.. Biotechnol Bioeng. 1995;48(5):490-500.
6. Raja, S., Murty, V.R., Thivaharan, V., Rajasekar, V., Ramesh, V.. Sci Technol. 2012;1(1):7-16.
7. Fang, N.Y., Lee, J., Yin, S.J., Wang,W., Wang, Z.J., Yang, J.M., Qian, G.Y., Si, Y.X., Park, Y.D.. Process Biochem. 2014;49(6):936-947.
8. Vasilchuk, D., Pandharipande, P.P., Suladze, S., Sanchez-Ruiz, J.M., Makhatadze, G.I..J Phys Chem B. 2014;118(23):6117-6122.
9. Dissanayake, M., Ramchandran, L., Piyadasa, C., Vasiljevic, T.. Int Dairy J. 2013;28(2):56-61.
10. Mandeville, J.S., Tajmir-Riahi, H.A. C. Biomacromolecules. 2010;11(2):465-472.
11. Bujacz, A.. Acta Crystallogr D Biol Crystallogr. 2012;68(Pt 10):1278-1289.
12. Gorza. F.D.S., Pedro, G.C., Trescher, T.F., da Silva, R.J., Silva, J.R., de Souza, N.C.. Biomed Res Int. 2014;2014:872701.
13. Gelamo, E.L., Tabak, M.. Spectrochim Acta Part A Mol Biomol Spectrosc. 2000;56(11):2255-2271.
14. Gelamo, E.L., Silva, C.H.T.P., Imasato, H., Tabak, M. I. Biochim Biophys Acta - Protein Struct Mol Enzymol. 2002;1594(1):84-99.
15. Huang, B.X., Kim, H.Y., Dass, C.. J Am Soc Mass Spectrom. 2004;15(8):1237-1247.
16. Hebbar, H.U., Raghavarao, K.S.M.S.. Process Biochem. 2007;42(12):1602-1608.
17. Hayes, D.G., Marchio, C.. Biotechnol Bioeng. 1998;59(5):557-566.
18. Lu, Y.M., Yang, Y.Z., Zhao, X.D., Xia, C.B.. Food Bioprod Process. 2010;88(1):40-46.
19. Corbatón-Báguena, M.J., Álvarez-Blanco, S., Vincent-Vela, M.C.. Sep Purif Technol. 2014;125:1-10.
20. van Reis, R., Gadam, S., Frautschy, L.N., Orlando, S., Goodrich, E.M., Saksena, S., Kuriyel, R., Simpson, C.M., Pearl, S., Zydney, A.L.. Biotechnol Bioeng. 1997;56(1):71-82.
21. Lee, V.E., Schulman, J.M., Stiefel, E.I., Lee, C.C.. J Inorg Biochem. 2007;101(11-12):1707-1718.
22. Ling, Y.Q, Nie, H.L, Brandford-White, C., Williams, G.R., Zhu, L.M.. Colloids Surf B Biointerfaces. 2012;94:281-287.
23. Puthirasigamany, M., Hamm, I., van Winssen, F.A., Nikbin, N., Kreis, P., Gorak, A., Zeiner, T.. Food Bioprod Process. 2014;92(2):152-160.
24. Johansson, H.O., Persson, J., Tjerneld, F.. Biotechnol Bioeng. 1999;66(4):247-257.
25. Albertsson, P.A.. Nature. 1958;182(4637):709-711.
26. Asenjo, J.A., Andrews, B.A.. J Chromatogr A. 2011;1218(49):8826-8835.
27. Gutowski, K.E., Broker, G.A., Willauer, H.D., Huddleston, J.G., Swatloski, R.P., Holbrey, J.D., Rogers, R.D.. J Am Chem Soc. 2003;125(22):6632-6633.
28. Crowhurst, L., Mawdsley, P.R., Perez-Arlandis, J.M., Salter, P.A., Welton, T.. Phys Chem Chem Phys. 2003;5(13):2790-2794.
29. Seddon, K.R.. Nat Mater. 2003;2(6):363-365.
30. Pereira, J.F.B., Rebelo, L.P.N., Rogers, R.D., Coutinho, J.A.P., Freire, M.G.. Phys Chem Chem Phys. 2013;15(45):19580-19583.

31. Dreyer, S., Kragl, U.. Biotechnol Bioeng. 2008;99(6):1416-1424.
32. Freire, M.G., Cláudio, A.F.M., Araújo, J.M.M., Coutinho, J.A.P, Marrucho, I.M., Canongia Lopes, J.N., Rebelo, L.P.N.. Chem Soc Rev. 2012;41(14):4966-4995.
33. Pei, Y., Wang, J., Wu, K., Xuan, X., Lu, X.. Sep Purif Technol. 2009;64(3):288-295.
34. Selvakumar, P., Ling, T.C., Walker, S., Lyddiatt, A.. Sep Purif Technol. 2012;90:182-188.
35. Yan, J.K., Ma, H.L., Pei, J.J., Wang, Z.B., Wu, J.Y. F. Sep Purif Technol. 2014;135:278-284.
36. Zeng, Q., Wang, Y., Li, N., Huang, X., Ding, X., Lin, X., Huang, S., Liu, X.. Talanta. 2013;116:409-416.
37. Alvarez-Guerra, E., Irabien, A.. Sep Purif Technol. 2012;98:432-440.
38. Ito, Y., Kohno, Y., Nakamura, N., Ohno, H.. Int J Mol Sci. 2013;14(9):18350-18361.
39. Good, N.E., Winget, G.D., Winter, W., Connolly, T.N., Izawa, S., Singh, R.M.M.. Biochemistry. 1966;5(2):467-477.
40. Chen, J., Wang, Y., Zeng, Q., Ding, X., Huang, Y.. Anal Methods. 2014;6(12):4067-4076.
41. Taha, M., e Silva, F.A., Quental, M.V., Ventura, S.P.M., Freire, M.G., Coutinho, J.A.P.. Green Chem. 2014;16(6):3149.
42. Dreyer, S., Salim, P., Kragl, U.. Biochem Eng J. 2009;46(2):176-185.
43. Desai, R.K., Streefland, M., Wijffels, R.H., Eppink, M.H.M.. Green Chem. 2014;16(5):2670-2679.
44. Plechkova, N.V, Seddon, K.R.. Chem Soc Rev. 2008;37(1):123-150.
45. Cláudio, A.F.M., Marques, C.F.C., Boal-Palheiros, I., Freire, M.G., Coutinho, J.A.P.. Green Chem. 2014;16(1):259.
46. Passos, H, Ferreira, A.R., Cláudio, A.F.M, Coutinho, J.A.P, Freire, M,G.. Biochem Eng J. 2012;67:68-76.
47. Merchuk, J.C., Andrews, B.A., Asenjo, J.A.. J Chromatogr B Biomed Sci Appl. 1998;711(1-2):285-293.
48. Louros, C.L.S., Cláudio, A.F.M., Neves, C.M.S.S., Freire, M.G., Marrucho, I.M., Jérôme, P., Coutinho, J.A.P.. Int J Mol Sci. 2010;11(4):1777-1791.
49. Cláudio, A.F.M., Swift, L., Hallett, J.P., Welton, T., Coutinho, J.A. P, Freire, M.G.. Phys Chem Chem Phys. 2014;16(14):6593-6601.
50. Carvalho, P.J., Ventura, S.P.M., Batista, M.L.S., Schröder, B., Gonçalves, F., Esperança, J., Mutelet, F., Coutinho, J.A.P.. J Chem Phys. 2014;140(6):64505.
51. Freire, M.G., Neves, C.M.S.S., Carvalho, P.J., Gardas, R.L., Fernandes, A.M., Marrucho, I.M., Santos, L.M.N.B.F., Coutinho, J.A.P.. J Phys Chem B. 2007;111(45):13082-13089.
52. Arakawa, T., Kita, Y., Timasheff, S.N.. Biophys Chem. 2007;131(1-3):62-70.
53. Kumar, V., Sharma, V.K., Kalonia, D.S.. Int J Pharm. 2009;366(1-2):38-43.
54. Tscheliessnig, A., Satzer, P., Hammerschmidt, N., Schulz, H., Helk, B., Jungbauer, A.. J Biotechnol. 2014;188C:17-28.
55. Yan, J., Du, Y., Chen, F., Yuan, H., Hu, F. Mol Pharm. 2013;10(7):2568-77.
56. Johansson, H.O., Ishii, M., Minaguti, M., Feitosa, E., Penna, T.C.V., Pessoa, A.. Sep Purif Technol. 2008;62(1):166-174.
57. Porto, T.S., Medeiros e Silva, G.M., Porto, C.S., Cavalcanti, M.T.H., Neto, B.B., Lima-Filho, J.L., Converti, A., Porto, A.L.F., Pessoa, A.. Chem Eng Process Process Intensif. 2008;47(4):716-721.
58. Saravanan, S., Rao, J.R., Nair, B.U., Ramasami, T. Process Biochem. 2008;43(9):905-911.
59. Perumalsamy, M., Batcha, M.I.. Process Biochem. 2011;46(2):494-497.
60. Lin, X., Wang, Y., Zeng, Q., Ding, X., Chen, J.. Analyst. 2013;138(21):6445-6453.
61. Ding, X., Wang, Y., Zeng, Q., Chen, J., Huang, Y., Xu, K.. Anal Chim Acta. 2014;815:22-32.
62. Sheikhian, L., Akhond, M., Absalan, G., Goltz, D.M.. Sep Sci Technol. 2013;48(15):2372-2380.
63. Nascimento, K.S., Rosa, P.A.J., Nascimento, K.S., Cavada, B.S., Azevedo, A.M., Aires-Barros, M,R.. Sep Purif Technol. 2010;75(1):48-54.
64. Kohno, Y., Saita, S., Murata, K., Nakamura, N., Ohno, H.. Polym Chem. 2011;2(4):862.
65. Shu, Y., Chen, X.W., Wang, J.H.. Talanta. 2010;81(1-2):637-642.
66. Tzeng, Y.P., Shen, C.W., Yu, T.. J Chromatogr A. 2008;1193(1-2):1-6.
67. Huang, S., Wang, Y., Zhou, Y., Li, L., Zeng, Q., Ding, X.. Anal Methods. 2013;5(13):3395-3402.
68. Baker, G.A., Heller, W,T.. Chem Eng J. 2009;147(1):6-12.
69. Barth, A.. Biochim Biophys Acta. 2007;1767(9):1073-1101.

2.3. Single-Step Purification of Ovalbumin from Egg White Using Aqueous Biphasic Systems

This chapter is based on the published manuscript

Matheus M. Pereira, Rafaela A. P. Cruz, Mafalda R. Almeida, Álvaro S. Lima, João A. P. Coutinho and Mara G. Freire

Process Biochemistry. 51(2016) 781-791.

2.3.1. Abstract

The ability of aqueous biphasic systems (ABS) composed of polyethylene glycols of different molecular weights (PEG 400, 600 and 1000 $g.mol^{-1}$) and buffered aqueous solutions of potassium citrate/citric acid (pH = 5.0 - 8.0) to selectively extract ovalbumin from egg white was here investigated. Phase diagrams, tie-lines and tie-line lengths were determined at 25°C and the partitioning of ovalbumin in these systems was then evaluated. Aiming at optimizing the selective extraction of ovalbumin in the studied ABS, factors such as pH, PEG molecular weight and amount of the phase-forming components were initially investigated with pure commercial ovalbumin. In almost all ABS, it was observed a preferential partitioning of ovalbumin to the polymer-rich phase, with extraction efficiencies higher than 90%. The best ABS were then applied in the purification of ovalbumin from real egg white samples. In order to ascertain on the ovalbumin purity and yield, sodium dodecyl sulphate polyacrylamide gel electrophoresis (SDS-PAGE) and size exclusion high performance liquid chromatography (SE-HPLC) analyses were conducted, confirming that the isolation/purification of ovalbumin from egg white was completely achieved in a single-step with a recovery yield of 65%. The results obtained show that polymer-salt-based ABS allow the selective extraction of ovalbumin from egg white with a simpler approach and better performance than previously reported. Finally, it is shown that ovalbumin can be completely recovered from the PEG-rich phase by an induced precipitation using an inexpensive and sustainable separation platform which can be easily applied on an industrial scale.

2.3.2. Introduction

Egg white is an aqueous-rich medium mainly composed of proteins, *circa* 10-12%, such as ovalbumin, ovotransferrin, lysozyme and ovomucin[1]. In addition to their nutritional importance, egg white proteins display multiple functional properties, such as foaming, emulsification and heat-setting. As a result, egg white plays a major role in the food industry[2]. Furthermore, new applications involving egg white proteins are increasingly being found due to their antimicrobial

Contributions: M.G.F., J.A.P.C. and A.S.L. conceived and directed this work. M.M.P., R.A.P.C. and M.R.A. acquired the experimental data. M.M.P., A.S.L., J.A.P.C. and M.G.F interpreted the experimental data. The manuscript was mainly written by M.M.P. and M.G.F. with significant contributions from the remaining authors.

and antioxidant properties[3], which have contributed for the production of health- and pharmaceutical-related products. Ovalbumin is the main protein of egg white, being responsible for most of its functional properties, and represents about 54% of the total protein content[4]. Ovalbumin is a glycoprotein consisting of 385 amino acids (45 kDa) with an isoelectric point of 4.5[5]. Because of the remarkable applications involving egg white proteins of high purity level[6–9], the development of novel cost-effective purification techniques is in great demand.

Ovalbumin was one of the first proteins isolated from egg white[10]. For that purpose, Hopkins[10] developed a method using high amounts of ammonium sulfate for ovalbumin precipitation. Nevertheless, the high amount of salt used can lead to the proteins irreversible unfolding. Nowadays, proteins from egg white are typically separated by electrophoresis, ion-exchange chromatography, size exclusion liquid chromatography, ultrafiltration, adsorption, among others[11–18]. However, some of these methods, currently employed, are multi-stage and with high equipment and operating costs. In the context of the development of alternative processes for the purification of proteins, a large interest has been devoted to aqueous biphasic systems (ABS) in the past decades[13]. ABS are a liquid-liquid extraction/purification technique which provides a highly biocompatible media since they are mainly composed of water[19]. Nevertheless, the extraction and purification of proteins from a complex matrix, such as egg white, is a difficult task due to some similarities between the proteins present in the raw material.

Most works in the literature have been focused on the evaluation of the extraction and recovery ability of ABS employing commercial and pure egg white proteins. For instance, Saravan *et al.*[20] studied the partitioning behavior of ovalbumin in poly(ethyleneglycol) (PEG)–poly(acrylic acid) ABS, achieving an extraction yield of 87.4%. Nerli *et al.*[21] investigated the thermodynamic forces involved in the partitioning of ovalbumin in various aqueous two-phase polymer systems (constituted by PEGs of different molecular weights and dextran). The authors[21] demonstrated that the ovalbumin transfer to the top phase is exothermic, which suggests electrostatic interactions between the hydroxyl groups of PEG and the hydrophilic side chain of the protein. Dallora *et al.*[22] investigated the partition coefficients of trypsin and lysozyme, and demonstrated that they can range between 1.0 and 2.4 for trypsin and from 2.3 to 9.0 for lysozyme, depending on the polymer chain size and on the tie-line length. The analysis of the separation factor, defined as the ratio of partition coefficients of two proteins, shows that high degrees of separation could be achieved[22]. In addition to these studies employing pure proteins, Coen *et al.*[23] investigated the purification of egg white proteins using ammonium-sulfate precipitation and found some difficulties in the separation of lysozyme and ovalbumin. The extraction of lysozyme from egg

white was also attempted using an ABS composed of PEG 600 and a sulfate-based salt at 25°C and pH = 10[24]. The authors reported an extraction of 70% of lysozyme from egg white with no loss in the enzymatic activity. Yang and co-workers[25] demonstrated the application of PEG 4000/potassium citrate ABS to extract lysozyme from egg white. Diederich *et al.*[26] showed the selective separation of avidin from the remaining proteins from egg white using an ABS composed of PEG 600 + potassium phosphate + 3 wt% NaCl, with a purity level higher than 60% and recovery yields > 90% (for avidin). In an attempt to reach higher purification levels, multi-stage ABS separations, by means of liquid-liquid chromatography, have been also investigated. Shibusawa *et al.*[27,28] fractionated chicken egg white proteins by high-speed counter-current chromatography (HSCCC) using an ABS composed of PEG 1000 and potassium phosphate salts at different pH values. After the optimization of several operational conditions, the authors[27,28] demonstrated to be able to purify the proteins present in the crude sample solution prepared from fresh egg white using CCC. Zhi *et al.*[29] also employed ABS coupled to HSCCC aiming at purifying the major protein components in hen egg white, including ovaltransferrin, ovalbumin and lysozyme. Ovalbumin was successfully purified (up to 95%) from the hen egg white sample with a PEG 1000 + potassium phosphate ABS[29]. Other approaches have been described for the purification of egg white proteins, namely by the use of ion exchange columns followed by precipitations steps[30,31]. It should be however highlighted that most works reporting higher purification levels of egg white proteins comprise several stages of equilibrium and require specialized equipment, such as those using HSCCC[27–29].

This work is focused on the development of an one-step extraction/purification process of ovalbumin from egg white using ABS constituted by polyethylene glycol of different molecular weights (PEG 400, PEG 600 and PEG 1000) and a citrate-buffered medium (pH = 5, 6, 7 and 8 according to different $K_3C_6H_5O_7$:$C_6H_8O_7$ mole fraction ratios). Initially, the phase diagrams of each ternary system, *i.e.* the description of the binodal curves which separate the monophasic from the biphasic regimes, were determined at 25°C. The respective tie-lines and tie-line lengths were also determined. These biphasic systems were then optimized regarding their extraction performance for commercial ovalbumin and finally employed to separate ovalbumin from egg white.

2.3.3. Experimental procedures

Materials. The ABS studied in this work are composed of a buffer aqueous solution constituted by potassium citrate monohydrate, $K_3C_6H_5O_7{\cdot}H_2O$, ≥ 99 wt% pure from Sigma–Aldrich, and citric acid monohydrate, $C_6H_8O_7{\cdot}H_2O$, 100 wt% pure from Fisher Scientific. Polyethylene glycol of different molecular weights, namely 400 g.mol^{-1} (PEG 400), 600 g.mol^{-1} (PEG 600), and 1000

g.mol^{-1} (PEG 1000), and ovalbumin from hen egg white, were acquired from Fluka. All compounds were used as received. Fresh eggs were bought in a local supermarket.

Phase diagrams and tie-lines. Aqueous solutions of polyethylene glycol (PEG 400, PEG 600 and PEG 1000) at 90 wt% and aqueous solutions of the buffer $K_3C_6H_5O_7/C_6H_8O_7$ (pH = 5, 6, 7 and 8 according to different $K_3C_6H_5O_7$:$C_6H_8O_7$ mole fraction ratios) at ≈ 50 wt% were prepared and used for the determination of the binodal curves. The phase diagrams were determined through the cloud point titration method[32,33] at 25°C and atmospheric pressure. The system compositions were determined by the weight quantification of all components added within $\pm 10^{-4}$ g. The tie-lines (TLs) were determined by a gravimetric method originally proposed by Merchuk *et al.*[34]. A mixture point in the biphasic region of the phase diagram was prepared using small ampules (*ca*. 10 mL) especially designed for the purpose, vigorously stirred, and allowed to reach equilibrium by the separation of the phases for at least 12 h at (25 ± 1)°C. After separation of the two phases, both the top and bottom phases were weighted. Each individual TL was determined by application of the lever-arm rule to the relationship between the top phase weight and the overall system composition. The experimental binodal curves were correlated using Equation (2.3.1):

$$[PEG] = Aexp[(B[salt]^{0.5}) - (C[salt]^3)] \quad (2.3.1)$$

where $[PEG]$ and $[salt]$ are the polymer and the salt weight fraction percentages, respectively, and A, B, and C are constants obtained by the regression of the experimental data (see Appendix C).

The determination of the TLs was accomplished through the solution of the following system of four equations (Equations (2.3.2) to (2.3.5)) aiming at determining four unknown values ($[PEG]_{\mathrm{PEG}}$, $[PEG]_{\mathrm{salt}}$, $[salt]_{\mathrm{PEG}}$ and $[salt]_{\mathrm{salt}}$):

$$[PEG]_{salt} = Aexp\left[\left(B[salt]_{PEG}^{0.5}\right) - \left(C[salt]_{PEG}^{3}\right)\right] \quad (2.3.2)$$

$$[PEG]_{salt} = Aexp\left[\left(B[salt]_{salt}^{0.5}\right) - \left(C[salt]_{salt}^{3}\right)\right] \quad (2.3.3)$$

$$[PEG]_{PEG} = \frac{[PEG]_M}{\alpha} - \frac{1-\alpha}{\alpha}[PEG]_{salt} \quad (2.3.4)$$

$$[salt]_{PEG} = \frac{[salt]_M}{\alpha} - \frac{1-\alpha}{\alpha}[salt]_{salt} \quad (2.3.5)$$

where the subscripts "PEG", "salt" and "M" represent the polymer (top) and the salt (bottom) rich phases and the mixture composition, respectively. The parameter α is the ratio between the weight of the top phase and the weight of the total mixture. The tie-line lengths (TLLs) were determined according Equation (2.3.6):

$$TLL = \sqrt{([salt]_{PEG} - [salt]_{salt})^2 + ([PEG]_{PEG} - [PEG]_{salt})^2} \quad (2.3.6)$$

Partitioning of commercial ovalbumin in PEG-salt ABS. Fixed mixture compositions in several ABS were selected and used to evaluate their performance for the extraction of ovalbumin. Initial optimization tests were carried out with pure commercial ovalbumin. Then, the best ABS was employed in the separation of ovalbumin from egg white. Commercial ovalbumin was diluted in water at a concentration of *circa* 0.5 $g.L^{-1}$ while egg white was diluted in water at 1:10 (v:v). These aqueous solutions were then used in the formation of each ABS (plus PEG and $K_3C_6H_5O_7/C_6H_8O_7$) at given concentrations. Each mixture was vigorously stirred and left to equilibrate for 12 h at (25 ± 1)°C. Finally, the two liquid phases were separated and weighted followed by the determination of the concentration of ovalbumin in each phase. The protein amount was quantified through UV-spectroscopy, using a SHIMADZU UV-1700, Pharma-Spec Spectrometer, at a wavelength of 280 nm, and using a calibration curve previously established. The partition coefficient of ovalbumin, K_{Ova}, was determined according to Equation (2.3.7)**:**

$$K_{\mathrm{OVA}}\% = \frac{[Ova]_{PEG}}{[Ova]_{salt}} \quad (2.3.7)$$

where $[Ova]_{PEG}$ and $[Ova]_{salt}$ are the concentration of protein in the PEG-rich and in the salt-rich aqueous phases, respectively.

The percentage extraction efficiencies of ovalbumin, $\boldsymbol{EE_{Ova}}\%$, are defined as the percentage ratio between the amount (total weight) of ovalbumin in the PEG-rich aqueous phase and that in the total mixture, according to Equation (2.3.8)**:**

$$EE_{\mathrm{Ova}}\% = \frac{w_{Ova}^{PEG}}{w_{Ova}^{PEG} + w_{Ova}^{Salt}} \boldsymbol{x}100 \quad (2.3.8)$$

where w_{Ova}^{PEG} and w_{Ova}^{Salt} are the total weight of protein in the PEG-rich and in the salt-rich aqueous phases, respectively. Control or “blank” solutions at the same mixture compositions used in the extraction/separation studies (with no protein added) were always used to reduce possible interferences of the phase-forming components through the ovalbumin quantification.

Partitioning of ovalbumin directly extracted from egg white in PEG-salt ABS. After the initial optimization tests carried out with commercial ovalbumin, a fixed mixture composition (25 wt% of PEG + 25 wt% of $K_3C_6H_5O_7/C_6H_8O_7$ (pH 7) + 50 wt% of an aqueous solution containing egg white at 1:10 (v:v)) was used to evaluate the performance of the studied ABS for the extraction and further purification of ovalbumin from egg white. Each mixture was vigorously stirred and left to equilibrate for 12 h at (25 ± 1)°C. The two liquid phases were separated and weighted followed by the determination of the concentration of ovalbumin and total proteins in each phase. The total protein amount was quantified through UV-spectroscopy, using a SHIMADZU UV-1700, Pharma-Spec Spectrometer, at a wavelength of 280 nm, and using a calibration curve previously established. The quantification of ovalbumin, purification efficiency and identification of all proteins in each phase were carried out by SDS-PAGE and SE-HPLC. At least three independent ABS were prepared and 3 samples of each phase were quantified.

The percentage recovery yield of ovalbumin, $\boldsymbol{RY_{Ova}}\%$, is the percentage ratio between the amount of protein in the PEG-rich aqueous phase to that in the initial egg white solution, and is defined according to Equation (2.3.9)**:**

$$RY_{\mathrm{Ova}}\% = \frac{w_{Ova}^{PEG}}{w_{Ova}^{Egg\ white}}\ \boldsymbol{x}100 \qquad (2.3.9)$$

where $w_{Ova}^{Egg\ white}$ and w_{Ova}^{PEG} are the total weight of ovalbumin in the egg white solution and in the PEG-rich phase, respectively.

The purification efficiency was calculated dividing the HPLC peak area corresponding to ovalbumin by the total area of the peaks corresponding to all proteins in the PEG-rich phase (taking into account all the dilution factors applied to each solution) according to Equation (2.3.10):

$$Purity_{\mathrm{Ova}}\% = \frac{A_{Ova}^{PEG}}{A_{Total\ proteins}^{PEG}}\ \boldsymbol{x}100 \qquad (2.3.10)$$

where A_{Ova}^{PEG} and $A_{Total\ Proteins}^{PEG}$ are the peak areas corresponding to ovalbumin and the total area of the peaks corresponding to all proteins present in the PEG-rich phase, respectively.

Recovery of ovalbumin from the PEG-rich phase. After the optimization of the extraction/purification conditions using ABS, the isolation of ovalbumin from the PEG-rich phase was carried out. For this purpose the following ABS was used as a proof of concept: 25 wt% of PEG

400 + 25 wt% of $K_3C_6H_5O_7/C_6H_8O_7$ (pH = 7) + 50 wt% of an aqueous solution containing egg white at 1:10 (v:v). The PEG-rich phase containing ovalbumin from egg white was separated and further centrifuged at (4.0 ± 0.5)°C during 20 min at 5000 rpm. This procedure was adapted from the literature [35] and allows the precipitation of proteins as a result of their low solubility in PEG aqueous solutions at low temperatures. The pellet obtained was then resuspended in a phosphate buffer solution (50 mM and pH 7.4). This solution containing ovalbumin was further evaluated by FT-IR and SE-HPLC. After the induced precipitation step, the PEG-rich phase was also analyzed by SE-HPLC in order to ensure that all proteins were precipitated.

Sodium dodecyl sulphate polyacrylamide gel electrophoresis (SDS-PAGE). Taking into account the UV-spectroscopy quantification of the total amount of proteins in each phase, all samples were diluted so that the amount of total protein in each gel lane in the SDS-PAGE was *circa* 0.5 µg. Samples of the aqueous phases of each ABS containing ovalbumin were diluted at 2:1 (v:v) in a dissociation buffer consisting of 2.5 mL of 0.5 M Tris-HCl pH 6.8, 4.0 mL of 10 % (w/v) SDS solution, 2.0 mL of glycerol, 2.0 mg of bromophenol blue and 310 mg of dithiothreitol (DTT). This overall solution was heated at 95°C for 5 min to denature the proteins by reducing disulfide linkages, and thus overcoming some forms of the tertiary protein folding and breaking up the quaternary protein structure. Electrophoresis was run on polyacrylamide gels (stacking: 4 % and resolving: 20 %) with a running buffer constituted by 250 mM Tris-HCl, 1.92 M glycine, and 1 % SDS. The proteins were stained with Coomassie Brilliant Blue G-250 0.1 % (w/v), methanol 50 % (v/v), acetic acid 7 % (v/v) and water 42.9 % (v/v). All gels were placed in an orbital shaker at a moderate speed during 2-3 h at room temperature. The gels were further distained in a solution containing acetic acid at 7 % (v/v), methanol at 20 % (v/v) and water at 73 % (v/v) in an orbital shaker at a moderate speed during 3-4 h at room temperature. SDS-PAGE Molecular Weight Standards, namely marker molecular weight full-range from VWR, were used as protein standards. All gels were analyzed using the Image Lab 3.0 (BIO-RAD) analysis tool.

Size Exclusion High-Performance Liquid Chromatography (SE-HPLC). A mixture composed of 25 wt% of PEG 400 + 25 wt% of $K_3C_6H_5O_7/C_6H_8O_7$ (pH = 7) + 50 wt% of an aqueous solution containing egg white at 1:10 (v:v) was studied to evaluate the yield and purity of ovalbumin. After 12h at 25°C to attain the equilibrium, a careful separation of the phases was performed and the amount of ovalbumin and remaining proteins in each phase was quantified by SE-HPLC (Size Exclusion High-Performance Liquid Chromatography). The phases were diluted at a 1:10 (v:v) ratio in a phosphate buffer saline solution before injection. A Chromaster HPLC (VWR, Hitachi) coupled

to a DAD detector was used. SE-HPLC was performed with an analytical column (25 cm × 2 mm i.d., 25 μm), Lichrospher 100 RP-18, from Merck. A 100 mM phosphate buffer in MiliQ water (mobile phase) was run isocratically with a flow rate of 1 mL·min^{-1}. The temperature of the column and auto-sampler was kept constant at 25°C. The injection volume was of 25 μL. The wavelength was set at 280 nm whereas the retention time of ovalbumin was found to be *circa* 18 min within an analysis time of 30 min. The quantification of ovalbumin in each phase was carried out by an external standard calibration method in the range of 0.01 to 1.0 g.L^{-1} of protein.

Fourier transform infrared spectroscopy (FT-IR). FT-IR spectra were recorded using a Perkin Elmer Spectrum Bx spectrophotometer with a resolution of 4 cm^{-1}. Several aqueous solutions containing ovalbumin at a fixed concentration (1.0 g.L^{-1}) and PEGs at different concentrations were used to perform the FT-IR analysis. The spectra were obtained in the wavelength range from 1800 to 1400 cm^{-1}.

2.3.4. Results and discussion

Phase diagrams and tie-lines. All phase diagrams (PEG + water + $K_3C_6H_5O_7/C_6H_8O_7$) were determined at 25°C and at atmospheric pressure. The binodal curves depicted in Figure 2.3.1. illustrate the impact of pH (pH = 5, 6, 7 and 8) on the behavior of PEG-400-based phase diagrams. The effect of the molecular weight of the polymer (PEG 400, PEG 600 and PEG 1000) is shown in Figure 2.3.2. The detailed experimental weight fraction data are reported in Appendix C. In all studied ABS, the top phase corresponds to the PEG-rich aqueous phase while the bottom phase is mainly composed of the $K_3C_6H_5O_7/C_6H_8O_7$ aqueous buffer. In all calculations, the water amount in the original salt was considered in the total amount of water.

Figure 2.3.1 shows the binodal curves for ABS composed of PEG 400 at different pH values achieved by the use of different $K_3C_6H_5O_7/C_6H_8O_7$ mole fractions. In general, the higher the pH of the aqueous solution the larger is the biphasic region, *i.e.* lower amounts of salt are required to form an ABS at a given concentration of PEG. In ABS composed of polymers and salts, the latter tends to be preferentially hydrated (Gibbs free energy of hydration of $C_6H_5O_7^{3-}$ ($\Delta_{hyd}G$) = −2765 kJ.mol^{-1})[36], and to induce the salting-out of the more hydrophobic substance (PEG). Therefore, the variations on the binodal curves observed with the pH values are a direct consequence of the $K_3C_6H_5O_7/C_6H_8O_7$ ratio and further speciation and relative abundance of the trivalent, divalent and monovalent citrate anions. Larger amounts of the trivalent citrate anion ($C_6H_5O_7^{3-}$) exist at higher pH values, a stronger salting-out species when compared with $C_6H_6O_7^{2-}$ and $C_6H_7O_7^{-}$ (according to

the Hofmeister series[37]), and thus, lower amounts of the phase-forming components are required to undergo liquid-liquid demixing.

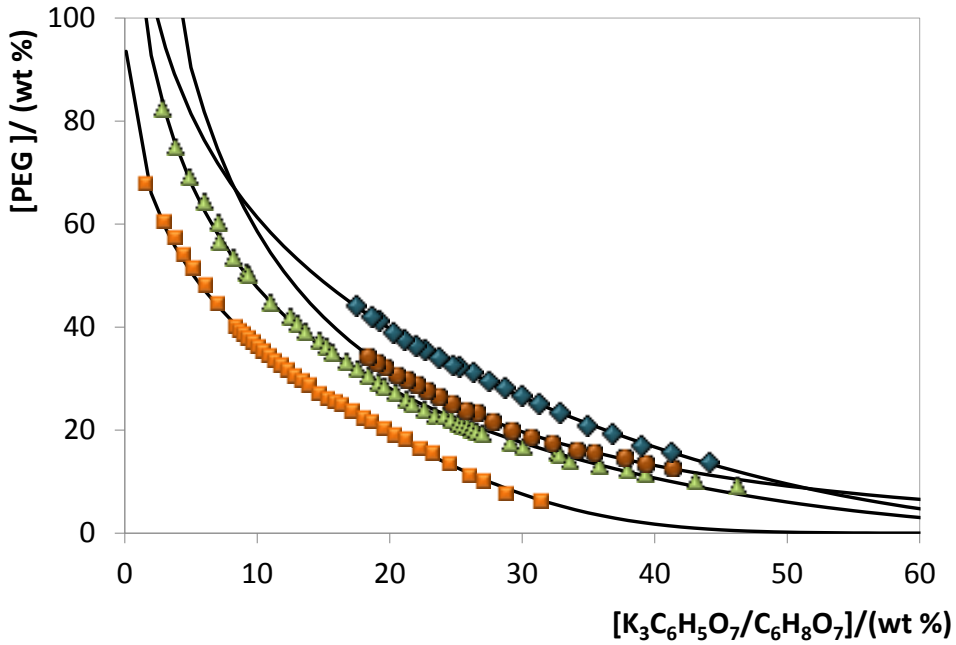

Figure 2.3.1. Phase diagrams for the systems composed of PEG 400 + $K_3C_6H_5O_7/C_6H_8O_7$ + H_2O at 25°C: pH 5 (◆); pH 6 (●); pH 7 (▲); pH 8 (■). Adjusted binodal data using Equation (2.3.1) (—).

Figure 2.3.2 depicts the phase diagrams for ABS formed by PEGs of different molecular weights and the citrate-based salt at a fixed pH value (pH = 7). PEG-based ABS reveal different abilities for phase separation induced by the length of their polymeric chains. The capacity for forming ABS according to the polymer molecular weight follows the order: PEG 1000 > PEG 600 > PEG 400. This effect was also observed with polymer/ionic liquid, polymer/salt and polymer/polymer combinations[38–40]. The increase of the polymer molecular weight leads to an increased hydrophobicity of these molecules, reducing their affinity for water. Therefore, the formation of ABS by a salting-out phenomenon induced by the citrate-based salt is more favorable for polymers of higher molecular weight.

The experimental data corresponding to the binodal curves were fitted using Equation (2.3.1). The regression parameters estimated by least-squares regression, standard deviations (σ) and correlation coefficients (R^2) are displayed in Table 2.3.1. Equation (2.3.1) is able to correlate the experimental binodal curves with high accuracy, as shown by the correlation coefficients obtained (R^2 > 0.9961).

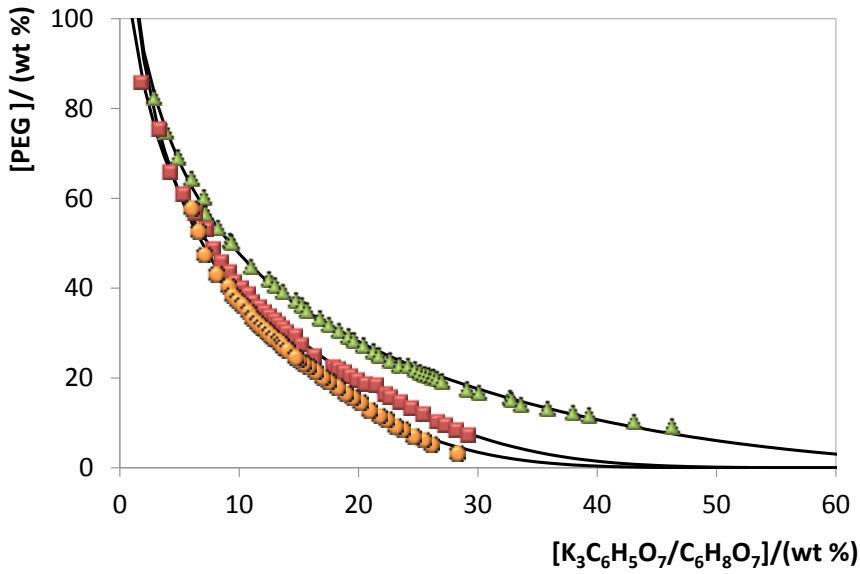

Figure 2.3.2. Phase diagrams for the systems composed of PEG + $K_3C_6H_5O_7/C_6H_8O_7$ + H_2O at 25°C and pH 7.0: PEG 400 (▲); PEG 600 (■); PEG 1000 (●). Adjusted binodal data using Equation (2.3.1) (—).

Table 2.3.1. Correlation parameters used to describe the experimental binodal data by Equation (2.3.1)**.**

PEG	pH	$A \pm \sigma$	$B \pm \sigma$	$10^5 (C \pm \sigma)$	R^2
PEG + $K_3C_6H_5O_7/C_6H_8O_7$ + water					
400	5.0	160.0 ± 7.4	-0.302 ± 0.010	0.54 ± 0.04	0.9998
	6.0	257.8 ± 6.0	-0.469 ± 0.018	0.01 ± 0.07	0.9991
	7.0	158.3 ± 2.0	-0.378 ± 0.045	0.47 ± 0.06	0.9980
	8.0	103.4 ± 1.3	-0.317 ± 0.005	3.23 ± 0.16	0.9979
PEG + $K_3C_6H_5O_7/C_6H_8O_7$ + water					
600	7.0	149.8 ± 2.4	-0.398 ± 0.006	3.3 ± 0.19	0.9975
1000	7.0	179.4 ± 8.4	-0.480 ± 0.016	4.8 ± 0.41	0.9961

The experimental TLs in each ABS, along with their respective length, and at the compositions for which the extraction studies of ovalbumin were determined are reported in Table 2.3.3. An example of the TLs obtained is depicted in Figure 2.3.3.

Table 2.3.2. Experimental TLs and TLLs of the ABS composed of IL + $K_3C_6H_5O_7/C_6H_8O_7$ + H_2O at 25°C.

Weight fraction composition / (wt %)							
PEG 400 + $K_3C_6H_5O_7/C_6H_8O_7$ + water							
pH	**$[PEG]_{PEG}$**	**$[salt]_{PEG}$**	**$[PEG]_M$**	**$[salt]_M$**	**$[PEG]_{salt}$**	**$[salt]_{salt}$**	**TLL**
5.0	41.56	18.86	30.01	29.99	9.93	49.38	43.96
	54.60	12.43	35.00	29.99	6.70	55.36	64.33
6.0	42.57	14.74	29.96	25.02	14.54	37.87	37.87
	45.94	13.52	29.99	29.85	8.60	51.76	53.45
7.0	38.35	13.82	29.72	19.92	21.39	25.80	20.76
	45.44	10.79	29.75	25.20	8.13	45.03	50.63
	49.27	9.46	29.98	29.97	3.50	58.13	66.80
	36.00	15.02	25.28	24.75	13.50	35.45	30.38
	48.82	9.61	25.22	34.66	3.03	60.09	68.15
	67.33	5.10	40.08	30.01	2.09	64.73	88.38
8.0	53.36	4.32	25.06	24.99	1.09	42.50	64.72
	64.69	2.19	30.13	29.84	0.06	53.90	82.77
PEG + $K_3C_6H_5O_7/C_6H_8O_7$ + water at pH 7.0							
PEG	**$[PEG]_{PEG}$**	**$[salt]_{PEG}$**	**$[PEG]_M$**	**$[salt]_M$**	**$[PEG]_{salt}$**	**$[salt]_{salt}$**	**TLL**
600	73.68	3.16	30.17	25.92	1.19	41.08	81.81
	74.70	3.04	30.13	30.33	0.21	48.66	87.35
	63.64	4.57	29.98	19.99	6.19	30.88	63.18
	60.27	5.15	25.01	25.02	2.14	37.89	66.71
	86.69	1.87	35.05	24.96	1.47	39.96	93.34
1000	57.95	5.45	29.95	25.09	0.05	46.04	70.70
	59.43	5.21	29.94	30.03	0.00	55.16	77.63
	46.49	7.64	29.97	20.06	0.04	46.87	60.80
	58.47	5.37	35.05	25.03	0.00	54.44	76.33
	41.72	8.79	25.04	25.00	0.01	49.29	58.13

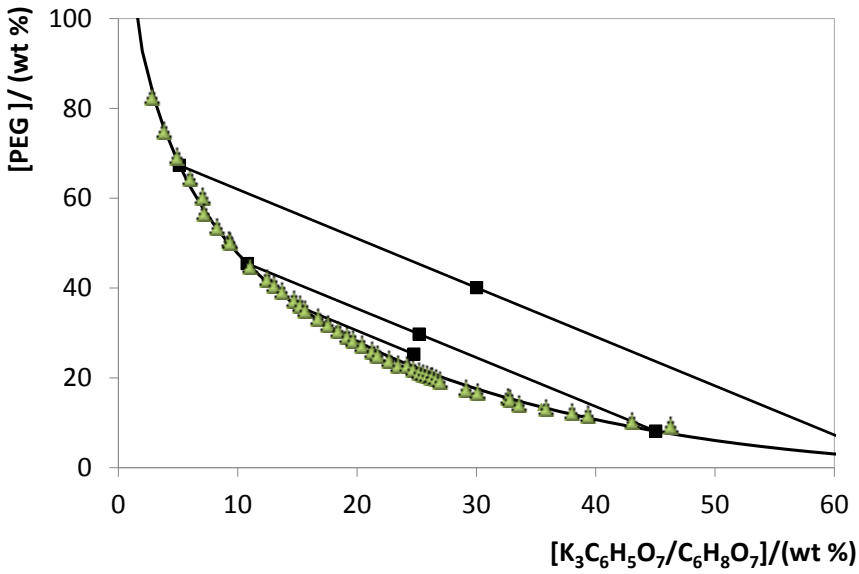

Figure 2.3.3. Phase diagram for the system composed of PEG 400 + $K_3C_6H_5O_7/C_6H_8O_7$ + H_2O at 25°C and pH 7.0: binodal curve data (▲); TL data (●); adjusted binodal data using Equation (2.3.1) (—).

Extraction of bovine serum albumin (BSA). Figure 2.3.4. shows the partitioning of commercial ovalbumin, expressed both in partition coefficient and in extraction efficiency, in an ABS composed of PEG 400 and $C_6H_5K_3O_7/C_6H_8O_7$ at different pH values. All these experiments were carried out at a common mixture composition (30 wt% of PEG 400 + 30 wt% of $C_6H_5K_3O_7/C_6H_8O_7$). For all investigated systems, ovalbumin preferentially migrates to the top phase (PEG-rich phase) with $K_{Ova} > 1$. The partition coefficients range between 12.67 and 54.74 and the extraction efficiencies between 94.8 and 97.7%. Amongst the pH values investigated, the higher partition coefficients and extraction efficiencies were obtained with the buffered systems at pH 7 and 8. Given that the isoelectric point of ovalbumin is 4.5[5], in all systems evaluated the protein is negatively charged. In PEG–salt ABS it has been reported that proteins prefer the top or the bottom phase depending on the nature of the phase forming-components and their concentration[41,42]. At pH 7.0, ovalbumin is negatively charged and still prefers the phase of lower ionic strength (polymer-rich) in all systems evaluated. Based on the overall results, the salting-out effect exerted by the salt plays an important role since the higher extraction efficiencies for the polymer-rich phase were obtained at higher pH values – those in which the amount of the strongest salting-out species ($C_6H_5O_7^{3-}$) is higher.

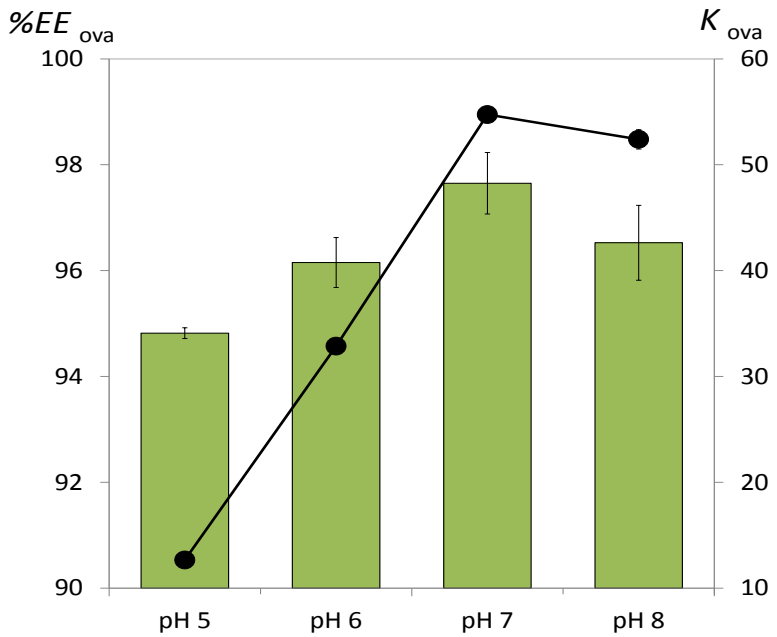

Figure 2.3.4. Influence of the pH in the extraction efficiency (EE_{Ova}%, bars) and partition coefficient (K_{Ova}, symbols) of ovalbumin in ABS composed of 30 wt% of PEG 400 + 30 wt% of $K_3C_6H_5O_7/C_6H_8O_7$ ABS at 25°C and different pH values.

Given that the best results were obtained at pH 7-8 (which further imply a lower loss of the target protein for the opposite phase and higher recovery yields), further mixtures at pH 7 for various concentrations of PEG 400, 600 and 1000 (from 20 to 30 wt%) and $K_3C_6H_5O_7/C_6H_8O_7$ (from 25 to 35 wt%) were investigated and their impact on the protein partition evaluated. Figure 2.3.5 depicts the effect of the salt concentration. Interestingly, depending on the PEG employed, opposite trends are observed. An increase in the salt content leads to an increase in the partition coefficients and extraction efficiencies of ovalbumin for the polymer-rich phase in systems composed of PEG 1000, while the opposite effect is observed with PEG 400. With ABS constituted by PEG 600 there are no major differences on the partition coefficients and extraction efficiencies as a function of the salt concentration. Therefore, there is a combined effect of the forces acting on the protein migration in ABS composed of polymers of different molecular weight. For ABS composed of PEG of higher molecular weight, an increase in the salt content supports the salting-out of the protein (exerted by the citrate-based salt) favoring thus its migration to the polymer-rich phase. The volume exclusion effects derived from the high molecular weight polymers do not seem to play a significant role, whereas higher amounts of salt seem to exert a large effect on the protein preferential migration. On the other hand, for more hydrophilic polymers, *i.e.* those of lower molecular weight, an increase in the salt content is not favorable for the proteins migration for the phase of lower ionic strength. According to the TLs data given in Table 2.3.2, the amount

of PEG 1000 in the salt-rich phase is almost negligible, supporting the salting-out mechanism exerted by the citrate-based salt and favorable protein-PEG hydrophobic interactions, while for PEG 400 an increase in the salt content leads to a decrease of the PEG amount at the salt-rich phase, with its concomitant increase at the polymer-rich phase, which seems to be not favorable for the preferential protein partitioning. Nevertheless, for an ABS constituted by 30 wt% of salt and 30 wt% of polymer there are no major differences in the partition coefficients and extraction efficiencies afforded by PEGs of different molecular weight. Even so, in all the evaluated situations, ovalbumin preferentially migrates to the most hydrophobic-(PEG)-rich phase confirming that protein-polymer interactions and salting-out effects play a significant role.

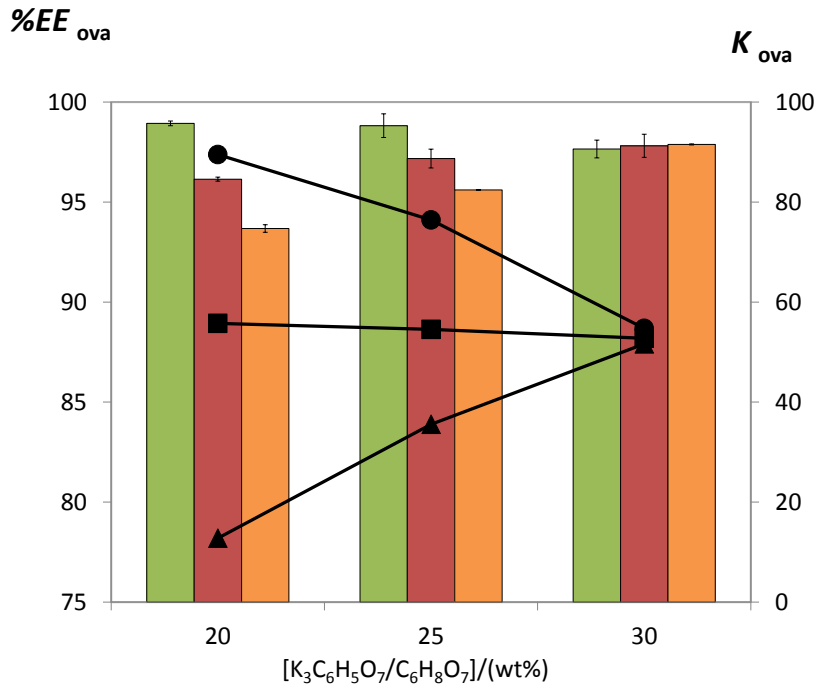

Figure 2.3.5. Extraction efficiency (EE_{Ova}%, bars) and partition coefficient (K_{Ova}, symbols) of ovalbumin in ABS composed of 30 wt% of PEG 400 (green bars and ●), PEG 600 (red bars and ■) and PEG 1000 (orange bars and ▲) and different concentrations of $K_3C_6H_5O_7/C_6H_8O_7$ at 25°C and pH = 7.0.

Figure 2.3.6 shows the effect of the PEG concentration on the ovalbumin partitioning process. The ABS investigated are composed of 25 wt% of $K_3C_6H_5O_7/C_6H_8O_7$ and PEG concentrations ranging from 25 to 35 wt%. At all concentrations, the partition coefficients decrease in the following order: PEG 400 > PEG 600 > PEG 1000 (based ABS). For PEG 600 and 1000, an increase in the PEG concentration leads to a decrease on both partition coefficients and extraction efficiencies of ovalbumin to the polymer-rich phase. At higher concentrations of PEG, ovalbumin starts to lose its affinity for the polymer-rich phase that is predominately less rich in

water (*cf.* Table 2.3.2. with the TLs data). This effect is less notorious in systems composed of PEG 400 (the most hydrophilic polymer investigated), and therefore no major differences are observed amongst the partition coefficients and extraction efficiencies of ovalbumin at different concentrations of PEG 400.

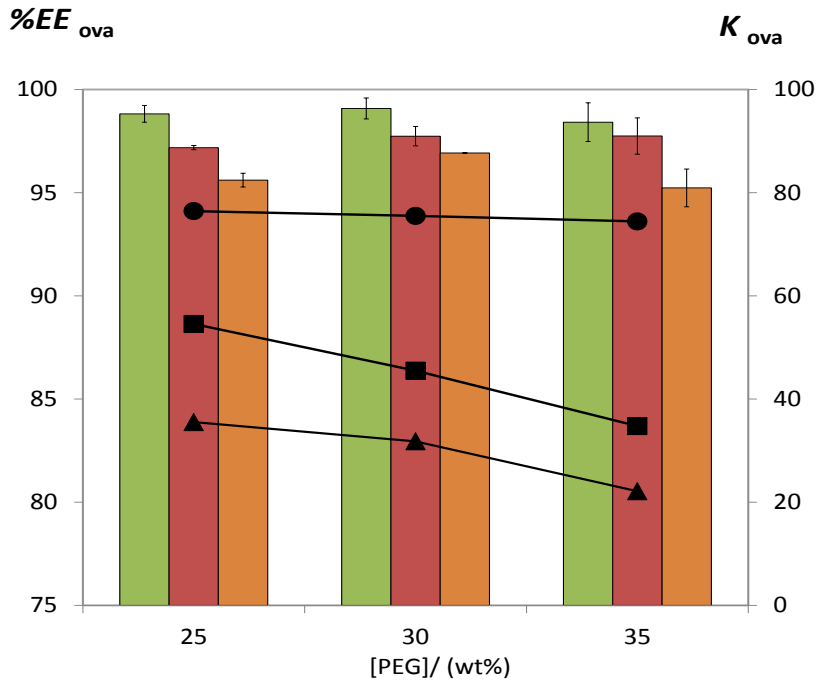

Figure 2.3.6. Extraction efficiency (EE_{Ova}%, bars) and partition coefficient (K_{Ova}, symbols) of ovalbumin in ABS composed of 25 wt% of $K_3C_6H_5O_7/C_6H_8O_7$ and different concentration of PEG 400 (green bars and ●), PEG 600 (red bars and ■) and PEG 1000 (orange bars and ▲) at 25°C and pH = 7.0.

Extraction/separation of ovalbumin directly from egg white. After optimizing the extraction/separation process with commercial ovalbumin, the ABS with better performance were then applied to extract and separate ovalbumin from a real matrix, egg white. A constant mixture composition (25 wt% of PEG + 25 wt% of $K_3C_6H_5O_7/C_6H_8O_7$ (pH 7) + 50 wt% of an aqueous solution containing egg white at 1:10 (v:v)) was used and the effect of the molecular weight of PEG was evaluated. In all these experiments the pH was maintained at 7, since according to the previous optimization experiments carried out with commercial ovalbumin a lower loss of the target protein for the opposite phase was observed, which imply higher recovery yields at pH 7. Several mixtures at pH 7 for various concentrations of PEG 400, 600 and 1000 (from 20 to 30 wt%) and $K_3C_6H_5O_7/C_6H_8O_7$ (from 25 to 35 wt%) were investigated and their impact on the protein partition evaluated. The total amount of proteins in egg white, partition coefficients and extraction

efficiency are provided in Appendix C. Figure 2.3.7 depicts the partition coefficient and extraction efficiency values obtained for the total proteins extracted from egg white.

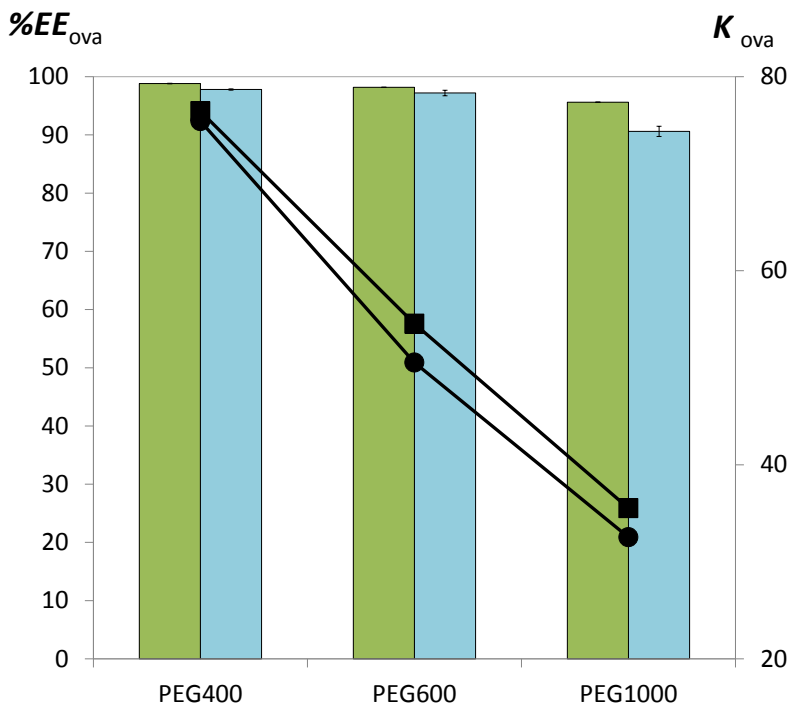

Figure 2.3.7. Extraction efficiency (EE_{Ova}%, bars) and partition coefficient (K_{Ova}, symbols) of commercial ovalbumin (green bars and ■) and proteins from egg white dissolved in water (1:10, v:v) (blue bars and ●) in ABS composed of 25 wt% of PEG + 25 wt% $K_3C_6H_5O_7/C_6H_8O_7$ at 25°C and pH = 7.0.

Although the partition coefficients and extraction efficiencies of commercial ovalbumin and the total protein extracted from egg white are similar, a large amount of precipitated proteins at the interface was observed when working with the water soluble fraction of proteins from egg white. Based on the UV spectroscopy quantification there are no guarantees that the protein extracted to the PEG-rich phase is preferentially ovalbumin. Therefore, all the coexisting phases and the precipitated proteins at the interface (after the respective recovery and re-suspension in a phosphate buffer solution) were analyzed by SDS-PAGE. It is visible from Figure 2.3.8 that only ovalbumin is present in the PEG-rich phase, whereas the contaminant proteins were precipitated at the interface. The precipitated proteins were identified according to molecular weight markers and are estimated to be ovotransferrin, ovoinhibitor, ovomucin and a smaller fraction of ovalbumin. Moreover, from the SE-HPLC chromatograms used for the proteins quantification, shown in Figure 2.3.9, it can be concluded that only ovalbumin is present at the PEG-rich phase since no other peaks were identified (meaning that pure ovalbumin was obtained in the one-step

ABS process). These SE-HPLC chromatograms also indicate that there is no significant ovalbumin aggregation or fragmentation under the studied conditions since no other peaks were identified. Thus, and although polymers such as PEG are used in the precipitation and aggregation of proteins[43], the amount of water in the PEG-rich phase, as well as its low molecular weight, is favorable for maintaining a protein-friendly environment for ovalbumin. Previously, it was showed that chicken egg white lysozyme tends to cluster into aggregates in presence of PEG 1000 after incubation at 90°C for 30 min[44,45]. At high temperatures, and due to the lower critical solution temperature behavior of PEG-water systems, there is a decrease on the hydration shell of the proteins[44,45]. In this work, the extractions were carried out at a low temperature, 25°C, and using polymers of low molecular weight (from 400 to 1000 $g.mol^{-1}$).

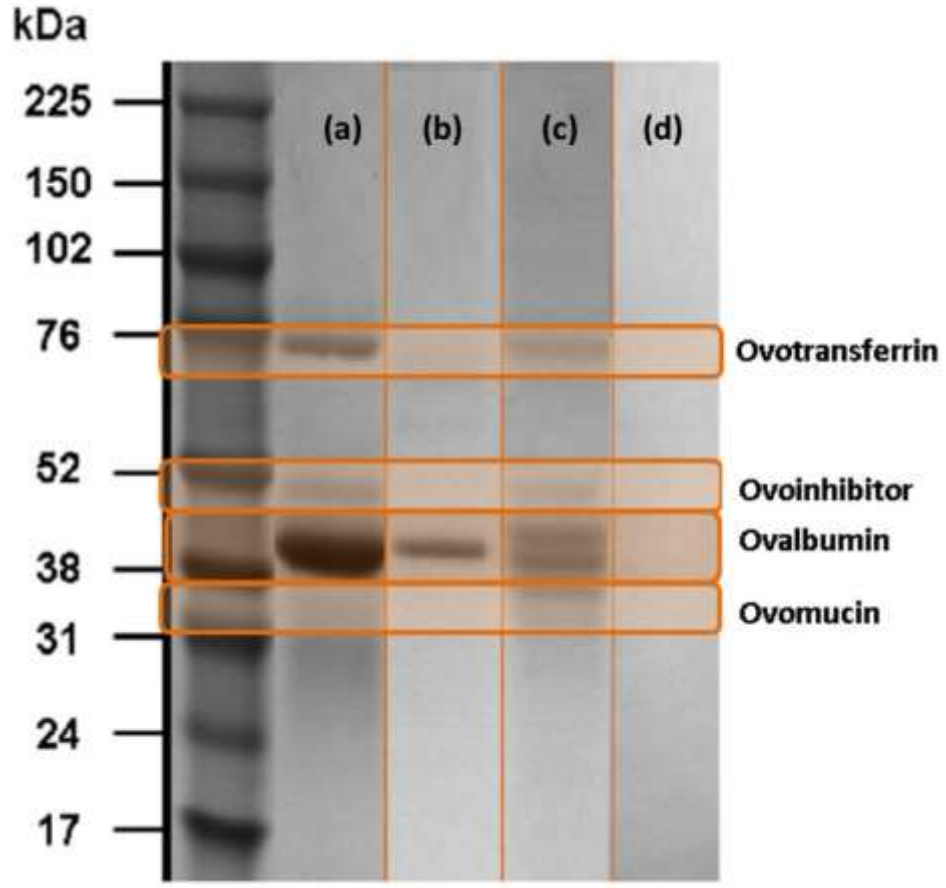

Figure 2.3.8. SDS-PAGE of the (a) egg white in water (1:10 (v:v, egg white:buffer)), and (b) PEG–rich phase, (c) precipitated proteins re-dissolved in a buffer solution and (d) salt-rich phase of the ABS composed of 25 wt% of PEG 400 + 25 wt% of $K_3C_6H_5O_7/C_6H_8O_7$ + 50 wt% of an egg white aqueous solution (1:10, v:v).

According to the quantification of ovalbumin in the coexisting phases of the system composed of 25 wt% of PEG 400 + 25 wt% of $K_3C_6H_5O_7/C_6H_8O_7$ (pH 7) + 50 wt% of an aqueous solution containing egg white at 1:10 (v:v)) carried out by SE-HPLC, (32.6 ± 0.2)% of ovalbumin precipitates at the interface, whereas the remaining ovalbumin from egg white (64.8 ± 2.5)% is extracted and remains stable in the PEG-based ABS. Despite this loss in ovalbumin, no other proteins were detected by SE-HPLC at the PEG-rich phase, in agreement with the results obtained by SDS-PAGE. These results confirm that PEG-based ABS can be used for the extraction and purification of ovalbumin from egg white, with a recovery yield of 65%, supporting thus their viability for the extraction/purification of proteins from complex matrices. Moreover, it is shown that a simple and easily scalable single-step process can be used to purify ovalbumin from egg white without using sophisticated equipment, such as CCC or centrifugal partition chromatography (CPC), as previously attempted [27–29].

Figure 2.3.10 displays the FT-IR spectra of ovalbumin in water and in several aqueous solutions of PEG 400 at different concentrations (up to 50 wt%) in equilibrium for 12h. FT-IR spectroscopy provides information about the secondary structure of proteins based on energy absorption bands of their functional groups or chemical bonds. Most analyses are between 1690-1600 cm^{-1} (in the spectra range) for the specific investigation of the protein structure which corresponds to the vibration of the amide I group[46]. The results obtained show that aqueous solutions of PEG 400 do not change the absorbance peaks of amide I suggesting that the protein maintains its spatial structure in the PEG-rich phase.

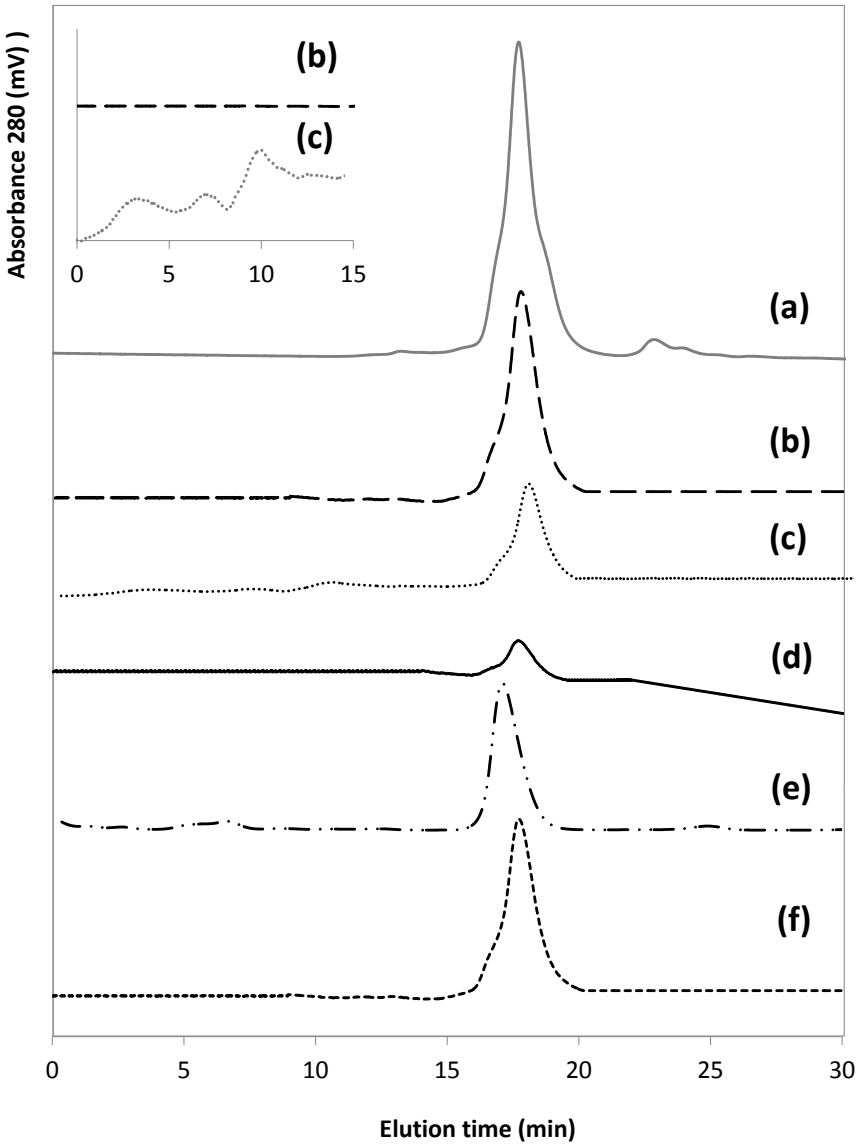

Figure 2.3.9. Size exclusion chromatograms of (a) egg white in water (1:10, v:v, egg white:buffer), (b) PEG–rich phase, (c) precipitated proteins re-dissolved in a buffer solution, (d) salt-rich phase of the ABS composed of 25 wt% of PEG 400 + 25 wt% of $K_3C_6H_5O_7/C_6H_8O_7$ + 50 wt% of an egg white aqueous solution (1:10, v:v), (e) commercial ovalbumin; and (f) recovered ovalbumin after the purification and precipitation steps.

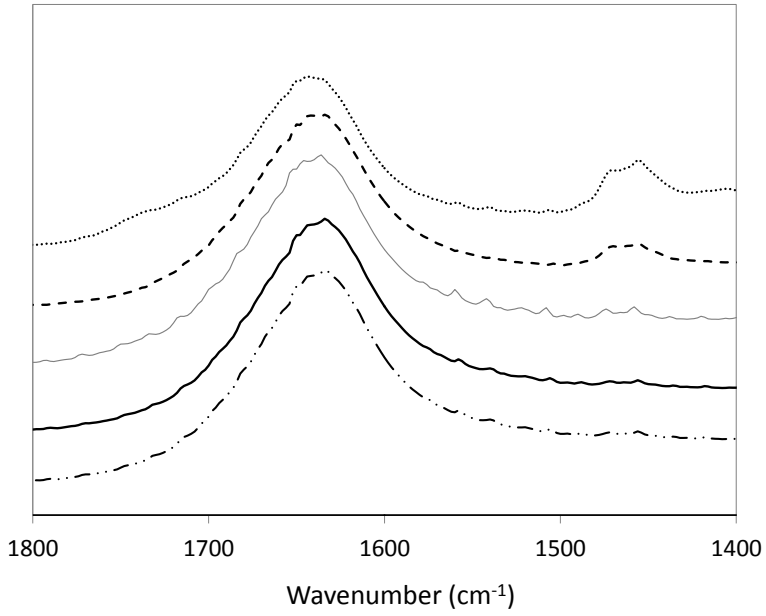

Figure 2.3.10. FT-IR spectra of a standard aqueous solution containing ovalbumin (1 g.L^{-1}) (—); ovalbumin in a 12.5 wt% PEG 400 aqueous solution (—); ovalbumin in a 25 wt% PEG 400 aqueous solution (-----); ovalbumin in a 50 wt% PEG 400 aqueous solution (··—···—··); and precipitated ovalbumin re-suspended in a buffer solution.

Recovery of ovalbumin from the PEG-rich phase. After the purification step, the ovalbumin recovery from the PEG-rich phase was achieved by an induced precipitation step, and separated by centrifugation at 4°C. This procedure was adapted from literature[35] and is based on the low solubility of proteins in polymers aqueous solutions at low temperatures. The pellet obtained was then resuspended in a phosphate buffer solution (50 mM and pH 7.4). This "new" aqueous solution rich in ovalbumin was further evaluated by FT-IR and SE-HPLC. The PEG-rich phase was also analyzed by SE-HPLC confirming the complete precipitation of ovalbumin. According to the FT-IR results, shown in Figure 2.3.10, there are no changes in the absorbance peaks of amide I suggesting that the recovered protein maintained its structure. Moreover, from the SE-HPLC results, depicted in Figure 2.3.9, the recovered protein does not present the formation of aggregates or even complexation (monomers and dimers). A comparison between the chromatograms of commercial ovalbumin and the extracted, purified and isolated ovalbumin from egg yolk achieved in this work is also provided in Figure 2.3.9. In summary, the obtained results confirm the viability of using the proposed ABS for the extraction of ovalbumin from egg white and a following precipitation step for its recovery from the PEG-rich phase. This "cleaning" step also allows the reuse of the coexisting phases of ABS for further purification stages.

Since ABS separations do not require a solid support matrix, adsorptive loss and denaturation of proteins are minimized, as previously confirmed by the stability studies of the recovered protein. According to the identification and quantification of ovalbumin and remaining proteins (by SDS-PAGE and SE-HPLC) in the coexisting phases of the optimized system, only ovalbumin is present at the PEG-rich phase while the remaining and contaminant proteins present in egg white precipitate at the interface. If only ovalbumin is identified at the PEG-rich phase it thus confirms the selective nature of the studied systems for albumin and their ability to act as purification routes, with a recovery yield of (64.8 ± 2.5)% of the total ovalbumin present in egg white.

Only three works[27–29] were found in the literature with values of ovalbumin purity similar to those found in this work, obtained from egg white. Shibusawa *et al.*[27,28] separated the proteins present in chicken egg white by counter-current chromatography (CCC) and high-speed counter-current chromatography (HSCCC) using ABS composed of 16 wt% of PEG 1000 and 12.5% wt% of K_2HPO_4. The authors[27,28] separated ovotransferrin, ovalbumin, ovomucin and lysozyme by collecting different fractions at different times of elution and by applying reverse modes when required. Zhi *et al.*[29] successfully purified ovalbumin from hen egg white using an ABS formed by 16 wt% of PEG 1000 and 17 wt% of K_3PO_4 at pH 9.2 with HSCCC, using the PEG-rich phase as the stationary phase. CCC is essentially a form of liquid-liquid partition chromatography. Amongst other chromatographic methods, this method does not require the use of a solid support as the stationary phase; instead, one of the ABS phases acts as the stationary phase by being retained in the column by gravity or centrifugal force. In CPC (centrifugal partition chromatography) and CCC it is necessary first to equilibrate the ABS in a separatory funnel and then to separate the two phases for further use as mobile and stationary phases. Also, individual partition coefficients (in separated experiments) need to be determined first for each protein to optimize the chromatographic conditions. In this context, and according to our results, the major novelty of our work consists on the development of a simpler, cheaper and less time-consuming method that does not require the use of chromatographic equipment. In fact, in our work, only one stage of equilibrium is required to successfully separate ovalbumin from the remaining proteins in egg white. Contrarily to previous works[27–29], we also used a lower molecular weight polymer (PEG 400 instead of PEG 1000) and a biodegradable and less toxic salt (citrate-based instead of phosphate-based) which could justify the high performance obtained in a single-step ABS separation without requiring the multiple stages of equilibrium occurring in CPC and CCC. Finally, we were also able to demonstrate the recovery of ovalbumin from the PEG-rich phase and the viability of recovering and reusing the coexisting phases, which certainly decreases the cost of the process and increases

its sustainable nature. In summary, in this work, it is shown that a simple and easily scalable and recyclable single-step process can be used to purify ovalbumin from egg white without requiring the use of sophisticated chromatographic equipment. The flowchart of the developed process for purifying ovalbumin directly from egg white is shown in Figure 2.3.11. The developed process allows to purify ovalbumin from a crude sample solution prepared from fresh egg white, in an one-step operation and in a relatively short time.

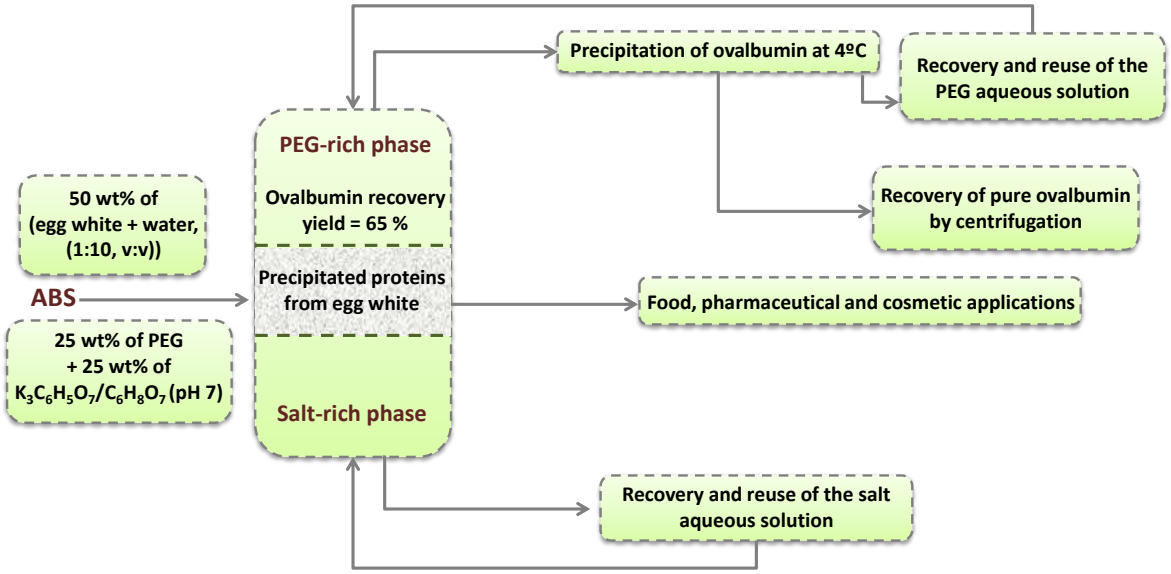

Figure 2.3.11. Flow chart of the developed process for the purification of ovalbumin from egg white.

2.3.5. Conclusions

The extraction and purification of ovalbumin using a cost-effective method based on ABS formed by polymers and a salt, followed by a precipitation step for the protein recovery, is here proposed. The ABS phase diagrams were initially determined, at different pH values and with PEGs of different molecular weight, to ascertain on the biphasic/monophasic regimes. These two-phase systems where then employed in studies concerning the partition of commercial ovalbumin aiming at identifying the best ABS. In all model systems, ovalbumin preferentially migrates to the PEG-rich phase and the best results were obtained with PEGs of lower molecular weight and at pH 7. Extraction efficiencies of ovalbumin to the PEG-rich up to 98.9% were attained in a single-step. After the optimization study conducted with the model systems using a standard solution of ovalbumin, the enhanced ABS were then applied in the extraction and purification of ovalbumin from egg white. The extraction efficiency values obtained range between 90.6% and 97.8%. The separation of albumin was also confirmed by SDS-PAGE and SE-HPLC analysis in the extraction carried out with the ABS constituted by PEG 400. The systems investigated reveal to be a

promising approach to extract ovalbumin from egg white since all contaminant proteins precipitate at the interface while ovalbumin selectively migrates to the polymer-rich phase. The complete purification of ovalbumin from egg white with a recovery yield of 65% was achieved in one-step using an ABS composed of 25 wt% of PEG 400 + 25 wt% of $K_3C_6H_5O_7/C_6H_8O_7$ + 50 wt% of an egg white aqueous solution (1:10, v:v). An induced precipitation step was also optimized to allow the recovery of the protein from the polymer-rich phase aiming at guarantying its further applicability while decreasing the cost of the overall process and enhancing its sustainable nature. The protein stability after the recovery step was confirmed by FT-IR and SE-HPLC. In summary, in this work, it was shown that a simple and easily scalable and recyclable single-step process can be used to purify ovalbumin from egg white without requiring the use of sophisticated chromatographic equipment.

2.3.6. References

1. Omana, D.A., Wang, J., Wu, J.. J Chromatogr B Analyt Technol Biomed Life Sci. 2010;878(21):1771-1776.
2. Mine, Y.. Trends Food Sci Technol. 1995;6(7):225-232.
3. Geng, F., Huang, Q., Wu, X., Ren, G., Shan, Y., Jin, G., Ma, M.. Sep Purif Technol. 2012;96:75-80.
4. Croguennec, T., Nau, F., Pezennec, S., Brule, G.. J Agric Food Chem. 2000;48(10):4883-4889.
5. Stein, P.E., Leslie, A.G.W., Finch, J.T., Turnell, W.G., McLaughlin, P.J., Carrell, R.W.. Nature. 1990;347(6288):99-102.
6. Shah, R.R., Dodd, S., Schaefer, M., Ugozzoli, M., Singh, M., Otten, G.R., Amiji, M.M., O'Hagan D.T., Brito, L. A... J Pharm Sci. January 2015:1-10.
7. Borde, A., Ekman, A., Holmgren, J., Larsson, A.. Eur J Pharm Sci. 2012;47(4):695-700.
8. Misaka, S., Sato, H., Yamauchi, Y., Onoue, S., Yamada, S.. Eur J Pharm Sci. 2009;37(3-4):469-476.
9. Bernkop-Schnurch, A., Gabor, F., Szostak, M.P., Lubitz, W.. Eur J Pharm Sci. 1995;3:293-299.
10. Hopkins, F.G.. J Physiol. 1900;25(4):306–330.
11. Desert, C., Guérin-Dubiard, C., Nau, F., Jan, G., Val, F., Mallard, J.. J Agric Food Chem. 2001;49(10):4553-4561.
12. Noh, K., Imm, J.. Food Chem. 2005;93(1):95-101.
13. Awadé, A.C., Moreau, S., Mollé, D., Brulé, G., Maubois, J.L... J Chromatogr A. 1994;677(2):279-288.
14. Chiu, H., Lin, J., Cheng, T., Chou, S., Huang, C. J Appl Poly Sci. 2012;125:616–621.
15. Chiang, B.H., Su, C.K., Tsai, G.J., Tsao, G.T.. J Food Sci. 1993;58(2):303-306.
16. Tong, X.D, Dong, X.Y, Sun, Y.. Biochem Eng J. 2002;12(2):117-124.
17. Ghosh, R., Silva, S.S., Cui, Z.. Biochem Eng J. 2000;6(1):19-24.
18. Chang, Y.K., Chang, I.P.. Biochem Eng J. 2006;30(1):63-75.
19. Albertsson, P.A. Partition of cell particles and macromolecules: separation and purification of biomolecules, cell organelles, membranes, and cells in aqueous polymer two-phase systems and their use in biochemical analysis and biotechnology. Wiley. 1986;3rd edn:371.
20. Saravanan, S., Rao, J.R., Nair, B.U., Ramasami, T.. Process Biochem. 2008;43(9):905-911.
21. Nerli, B., Espariz, M., Picó, G.. Biotechnol Bioeng. 2001;72(4):468-474.
22. Dallora, N.L.P., Klemz, J.G.D., Filho, P de A.,P... Biochem Eng J. 2007;34(1):92-97.
23. Coen, C.J., Prausnitz, J.M., Blanch, H.W.. Biotechnol Bioeng. 1997;53(6):567-574.
24. Su, C.K., Chiang, B.H.. Process Biochem. 2006;41(2):257-263.
25. Lu, Y., Lu, W., Wang, W., Guo, Q., Yang, Y.. J Chem Technol Biotechnol. 2013;88(3):415-421.
26. Diederich, P., Amrhein, S., Hämmerling, F., Hubbuch, J.. Chem Eng Sci. 2013;104:945-956.
27. Shibusawa, Y., Kihira, S., Ito, Y.. J Chromatogr B Biomed Sci Appl. 1998;709(2):301-305.
28. Shibusawa, Y., Iino, S., Shindo, H., Ito, Y.. J Liq Chromatogr Relat Technol. 2001;24(13):2007-2016.
29. Zhi, W.B., Deng, Q.Y., Song, J.N., Ouyang, F. Chin J Biotechnol. 2005;21(1):129-134.
30. Roy, I., Rao, M.V.S., Gupta, M.N.. Appl Biochem Biotechnol. 2003;111(1):55-63.
31. Abeyrathne, E.D.N.S., Lee, H.Y., Ahn, D.U.. Poult Sci. 2014;93(4):1001-1009.
32. Almeida, M.R., Passos, H., Pereira, M.M., Lima, Á.S., Coutinho, J.A.P., Freire, M.G.. Sep Purif Technol. 2014;128:1–10.
33. Pereira, J.F.B., Lima, Á.S., Freire, M.G., Coutinho, J.A.P.. Green Chem. 2010;12(9):1661-1669.
34. Merchuk, J.C., Andrews, B.A., Asenjo, J.A... J Chromatogr B Biomed Sci Appl. 1998;711(1-2):285-293.
35. Akita, E,M,, Nakai, S.. J Immunol Methods. 1993;160(2):207-214.

36. Marcus, Y.. J Chem Soc.. 1991;87(18):2995-2999.
37. Hofmeister F.. Arch Exp Pathol Pharmacol. 1888;24:247-260.
38. Freire, M.G., Pereira, J.F.B., Francisco, M., Rodríguez, H., Rebelo, L.P.N., Rogers, R.D., Coutinho, J.A.P.. Chemistry. 2012;18(6):1831-1839.
39. Rogers, R.D., Zhang, J.. J Chromatogr B Biomed Appl. 1996;680(1-2):231-236.
40. Piculell, L., Lindman, B.. Adv Colloid Interface Sci. 1992;41(0):149-178.
41. da Silva, L.H.M., Meirelles, A.J.A.. J Chem Eng Data. 2001;46(2):251-255.
42. Cascone, O., Andrews, B.A., Asenjo, J.A.. Enzyme Microb Technol. 1991;13(8):629-635.
43. Rajan, R.S., Li, T., Aras, M., Sloey, C., Sutherland, W., Arai, H., Briddell, R., Kinstler, O., Lueras, A.M.K., Zhang, Y., Yeghnazar, H., Treuheit, M., Brems, D.N.. Protein Sci. 2006;15(5):1063-1075.
44. Muraoka, T., Adachi, K., Ui, M., Kawasaki, S., Sadhukhan, N., Obara, H., Tochio, H., Shirakawa, M., Kinbara, K.. Angew Chem Int Ed Engl. 2013;52(9):2430-2434.
45. Muraoka, T., Sadhukhan, N., Ui, M., Kawasaki, S., Hazemi, E., Adachi, K., Kinbara, K.. Biochem Eng J. 2014;86:41-48.
46. Barth A.. Biochim Biophys Acta. 2007;1767(9):1073-1101.

2.4. Extraction and purification of Major Royal Jelly Proteins from honey in a single step using aqueous biphasic systems formed by ionic liquids and carbohydrates

This chapter is based on an unpublished work with the following authors involved:
Matheus M. Pereira, Maria V. Quental, Sónia N. Pedro, Aminou Mohamadou, João A. P. Coutinho and Mara G. Freire

2.4.1. Abstract

Nowadays there is a strong demand for efficient and sustainable purification processes capable of industrial implementation. Although much interest has been devoted to ionic-liquid-based aqueous biphasic systems (IL-based ABS), most studies rely on inorganic salts and imidazolium-based ILs. In this work we propose novel ABS composed of phosphonium-based ILs, analogues of natural glycine-betaine, and carbohydrates. The respective ternary phase diagrams, as well as the tie-lines and tie-line lengths, were determined at 25°C. This type of systems was then investigated to recover and purify Major Royal Jelly Proteins (MRJPs) from honey. In all systems investigated MRJPs precipitate in the ABS interface, allowing a recovery yield ranging between 84 and 97%, and high levels of purification (80-90%) of MRJP1. This work demonstrates that novel bio-based ABS can be used to extract and/or selectively precipitate proteins from complex samples in a single-step.

2.4.2. Introduction

In recent years, liquid-liquid extractions based on aqueous biphasic systems (ABS) have proved themselves as alternative, more biocompatible and low-cost techniques for the extraction, purification and concentration of several biocompounds, such as proteins[1–5], enzymes[6,7], drugs[8,9] and other biomolecules[10,11]. ABS are "greener" alternatives to the traditional organic solvent-water biphasic systems[12]. In addition to the more traditional ABS composed of polymer-polymer or polymer-salt combinations, more recent and interesting are the ABS formed by ionic liquids (ILs)[12]. The success of ILs has been attributed to their unique physico-chemical characteristics and high adaptive ability under a wide range of conditions and applications[13,14].

Despite the large number of publications dealing with IL-based ABS[12], most of these studies are focused on the determination of the respective ternary phase diagrams, and on extraction studies with model systems/biomolecules to appraise their ability to extract given products. To

Contributions: M.G.F., J.A.P.C. and A.M. conceived and directed this work. M.M.P., S.N.P. and M.V.Q. acquired the experimental data. M.M.P., A.M., J.A.P.C. and M.G.F interpreted the experimental data. The manuscript was mainly written by M.M.P. and M.G.F. with significant contributions from the remaining authors.

move further on this field, as well as to prove their applicability to real systems, it is now crucial that research on IL-based ABS is aimed at the separation and purification of valuable products directly from complex biological media or industry residues. Although a large number of IL-based ABS has been investigated, most of these studies were carried out with ABS formed by imidazolium-based ILs and inorganic salts[12]. This trend is a result of the high ability of inorganic salts to salt-out ILs from aqueous media, and thus their high aptitude to form two-phase systems. Nevertheless, taking into account the use of these systems for the purification and recovery of target products with biological activity, considering the human consumption of the end products, as well as some environmental issues related to the use of non-toxic phase-forming components, it is critical to find alternative IL-based ABS with more benign characteristics. To this end, more benign ILs and alternatives to the widely studied inorganic salts should be appraised. More biocompatible systems were recently proposed through the use of carbohydrates, instead of inorganic salts, as phase separation promoters in aqueous systems comprising ILs[15–18]. This perception arose from special benefits offered by carbohydrates, as non-toxic substances that can be obtained from renewable natural resources. Even though, there is still only a small number of possible IL-carbohydrate-based ABS due to the low salting-out ability of carbohydrates, as well as on their investigation as potential platforms to purify and isolate added-value compounds from real matrices, with published works up to date only addressing ILs composed of fluorinated-based anions and imidazolium- or pyridinium-based cations[15,16,18–25].

Honey is a natural supersaturated solution of sugars (60-80% of the total content) produced by honeybees[26]. In addition to its high carbohydrates content, honey is also rich in phenolic compounds, aliphatic acids, vitamins, amino acids, proteins and inorganic compounds[27]. In the last decade, honey has been the focus of many studies, mostly due to their antioxidant characteristics[28]. Honey was already identified as a product able to reduce the risks of diseases triggered by reactive oxygen species and other free radicals, such as degenerative diseases, including cancer[29]. In addition to the valuable phenolic compounds present in honey, honey proteins display valued properties, namely anti-inflammatory[30], anti-microbial[31], and anti-cancer[32] activities. Several proteins were already identified in honey samples, corresponding to approximately 0.1–0.5% of the honey content, with molecular weights ranging from 22 to 75 kDa[33]. In 1992 it was identified the first royal jelly (RJ) protein in honey, termed as major protein 1, and since then, eight more royal jelly proteins (MRJP) were identified[34]. Among them, MRJP1 is likely to promote liver regeneration and to have a cytoprotective action on hepatocytes[35] , MRJP3 can exhibit potent immunoregulatory effects *in vitro* and *in vivo*[36], and both MRJP4 and MRJP5 are

important sources of essential amino acids[37]**.** Besides their valued properties, the extraction and recovery of proteins from honey samples remain a challenge. During the last decade, several studies on the precipitation of proteins from honey were reported, by the addition of ammonium sulfate, tungstic acid or trichloroacetic acid[38]. Dialysis, centrifugation and chromatographic techniques (adsorption, ion exchange, and affinity chromatography) have also been attempted for the honey proteins separation from sugars and other small compounds[34]. In general, complex multi-step approaches are required, often involving the use of volatile compounds, which also compromise the proteins integrity.

Herein we investigated the formation of more biocompatible ABS formed by phosphonium-based ILs and carbohydrates, and their further use as a strategy to extract and purify MRJP from honey on a single step.

2.4.3. Experimental procedures

Materials. The carbohydrates used were sucrose (>99.5 wt.% pure from Himedia), D-(+)-maltose (>98.0 wt.% pure from Sigma), D-(+)-glucose (>99.5 wt.% pure from Scharlau), D-sorbitol (>99.0 wt.% pure from Fluka), xylitol (>99.0 wt.% pure from Sigma), maltitol (>95.0 wt.% pure from Acros Organics), D(+)-Fructose (>98.0 wt.% pure from Panreac), D(+)-Galactose (>95 wt.% pure from Prolabo), L(+)-Arabinose (>99 wt.% pure from Acros Organics), D-(+)-Mannose (>99.0 wt.% pure from Aldrich), D-(+)-xylose (≥ 99.0 wt% pure,. from Carlo Erba). Commercial honey was purchased at a local market.

The commercial ILs used in this study were tetrabutylphosphonium bromide ($[P_{4444}]Br$, > 96 wt % pure), tetrabutylphosphonium chloride ($[P_{4444}]Cl$, > 95% pure), triisobutylmethylphosphonium tosylate ($[P_{i(444)1}][TOS]$, > 95 wt% pure), and tributylmethylphosphonium methylsulphate ($[P_{4441}][MeSO_4]$, > 99 wt% pure), all kindly provided by Cytec Ind. The tri(n-butyl)[2-ethoxy-2-oxoethyl]phosphonium bromide ($[Bu_3PC_2]Br$) and tri(n-butyl)[2-butoxy-2-oxoethyl]phosphonium bromide ($[Bu_3PC_4]Br$) were synthesized by us and characterized according to protocols described in Appendix D. The materials used in the ILs synthesis were 2-bromoacetic acid ethyl ester, 4-bromobutyric acid ethyl ester, ethyl acetate and tri(n-butyl)phosphine, all purchased from Sigma-Aldrich. The molecular structures of carbohydrates and ILs investigated are depicted in Figure 2.4.1. All ILs were dried in vacuum. The purity of the synthesized ILs is > 98%.

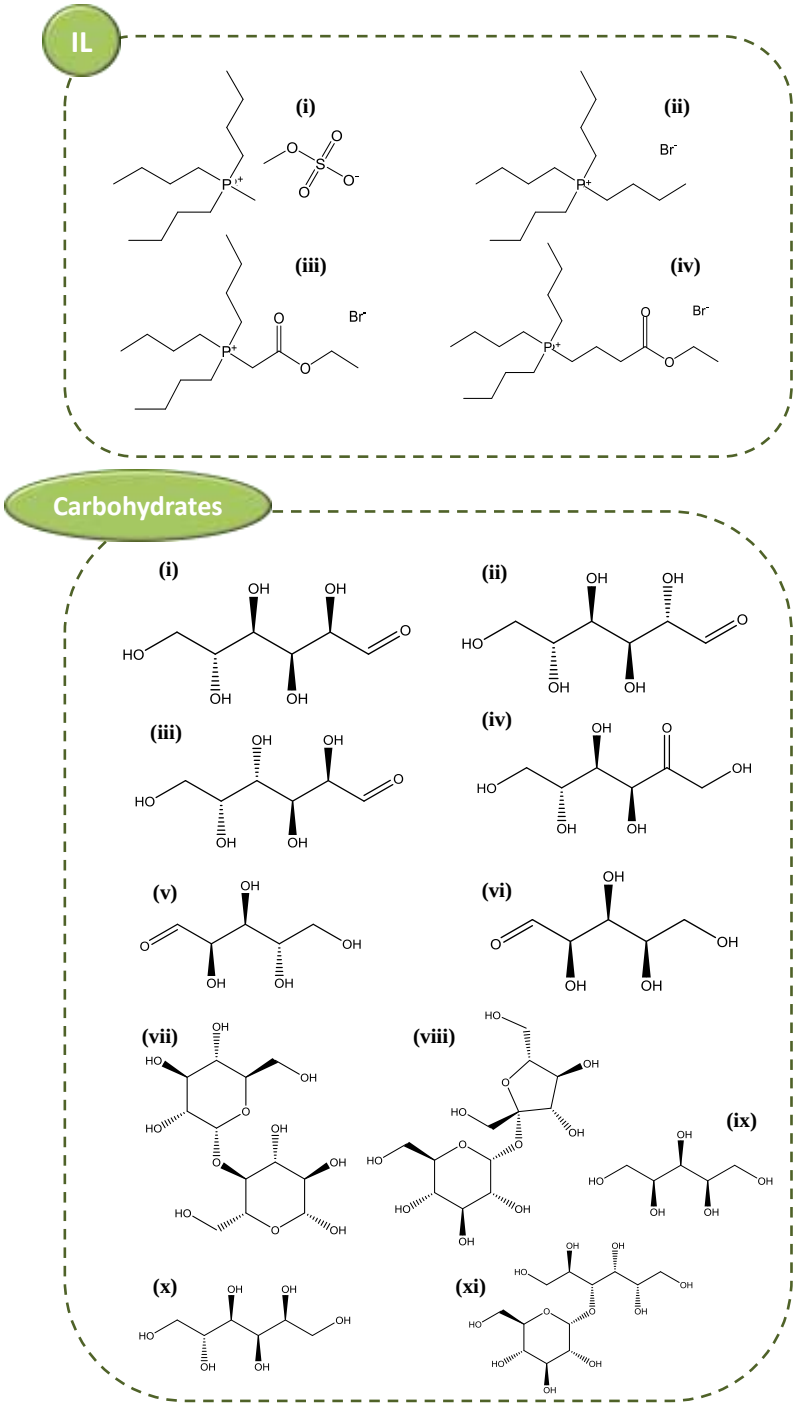

Figure 2.4.1. Chemical structures of the studied ILs: (i) $[P_{4441}][MeSO_4]$, (ii) $[P_{4444}]Br$, (iii) $[Bu_3PC_2]Br$ and (iv) $[Bu_3PC_4]Br$; Chemical structures of the studied carbohydrates: (i) D-(+)-glucose, (ii) D-(+)-mannose, (iii D(+)-galactose, (iv) D(+)-fructose, (v) D(+)-arabinose, (vi) D-(+)-xylose, (vii) D-(+)-maltose, (viii) sucrose, (ix) xylitol, (x) D-sorbitol and (xi) maltitol.

Phase diagrams and tie-lines. Aqueous solutions of each IL ($[P_{4444}]Br$, $[P_{4444}]Cl$, $[P_{i(444)1}][TOS]$, $[P_{4441}][MeSO_4]$, $[Bu_3PC_2]Br$, $[Bu_3PC_4]Br$), at concentrations ranging between 80 and 90 wt%, and aqueous solutions of each carbohydrate, at concentrations between 50 and 80 wt%,

were initially prepared, and used for the determination of the binodal curves. Dropwise addition of the aqueous ionic liquid solution to each carbohydrate aqueous solution was carried out until the detection of a cloudy (biphasic) solution, followed by the dropwise addition of ultrapure water until the formation of a clear and limpid solution (monophasic region). Dropwise additions were carried out under constant stirring. The ternary system compositions were determined by weight quantification of all components within $\pm 10^{-4}$ g, using an analytical balance (Mettler Toledo Excellence XS205 DualRange). The experimental binodal curves were correlated according to the approach proposed by Merchuk *et al.*[39], described by Equation (2.4.1):

$$[CH] = Aexp[(B[IL]^{0.5}) - (C[IL]^3)] \quad (2.4.1)$$

where $[CH]$ and $[IL]$ are the IL and the carbohydrate mass fraction percentages, and *A*, *B* and *C* are constants obtained by the regression of the experimental binodal data. The determination of the TLs was accomplished through the solution of the following system of four equations (Equations (2.4.2) to (2.4.5)) to determine four unknown values ($[CH]_{\mathrm{CH}}$, $[CH]_{\mathrm{IL}}$, $[IL]_{\mathrm{CH}}$ and $[IL]_{\mathrm{IL}}$):

$$[CH]_{IL} = Aexp\left[\left(B[IL]_{PEG}^{0.5}\right) - \left(C[IL]_{CH}^{3}\right)\right] \quad (2.4.2)$$

$$[CH]_{IL} = Aexp\left[\left(B[IL]_{IL}^{0.5}\right) - \left(C[IL]_{IL}^{3}\right)\right] \quad (2.4.3)$$

$$[CH]_{CH} = \frac{[CH]_M}{\alpha} - \frac{1-\alpha}{\alpha}[CH]_{IL} \quad (2.4.4)$$

$$[IL]_{CH} = \frac{[IL]_M}{\alpha} - \frac{1-\alpha}{\alpha}[IL]_{IL} \quad (2.4.5)$$

where the subscripts "CH", "IL" and "M" represent the top and the bottom phases and the mixture composition, respectively. The parameter α is the ratio between the weight of the top phase and the weight of the overall mixture. For the calculation of each tie-line length (TLL), Equation (2.4.6) was used:

$$TLL = \sqrt{([CH]_{IL} - [CH]_{CH})^2 + ([IL]_{IL} - [IL]_{CH})^2} \quad (2.4.6)$$

In all systems the top phase corresponds to the IL-rich phase, whereas the bottom phase is mainly constituted by the carbohydrate and water. In ABS constituted with honey the opposite occurs, been the top phase composed mainly by carbohydrate and the bottom phase correspond to the IL-rich phase.

Purification and Recovery of Proteins from Honey. The ABS mixtures compositions used in the extraction and purification of proteins from honey were chosen based on the phase diagrams determined in this work. It was used a common mixture composition (25 wt% of IL, 25 wt% of water, and 50 wt% of carbohydrates from honey, knowing that honey contains *ca.* 80 wt% of carbohydrates). Each mixture was vigorously stirred, centrifuged for 30 min (7500 rpm), and left to equilibrate for 10 min at 25℃ to allow the complete phase separation and proteins extraction. After, a careful separation of the phases was performed and the amount of total proteins in each phase was quantified by the Bradford's method[40], using a previous calibration curve established with bovine serum albumin (BSA). UV-Vis spectroscopy was carried out for quantification purposes (using a SYNERGYIHT microplate reader, BioTek, at 595 nm). To eliminate the influence of the IL and carbohydrates present on the protein concentration analysis, a blank control for each mixture was used. It should be remarked that a solid interphase is created when preparing these mixtures, mainly composed of proteins as discussed below. This interphase was recovered, resuspended in phosphate-buffered saline (PBS) concentration of 10 mM and pH 6.8, and the proteins content quantified by UV-Vis spectroscopy as described before. At least three independent ABS were prepared for each mixture and three samples of each phase quantified, allowing to determine the associated uncertainty of the recovery yield and purity of proteins.

The recovery yield of honey proteins, $\boldsymbol{RY_{PROT}}\%$, was determined as the percentage ratio between the total amount of proteins as part of the interphase to that in the initial honey, defined according to Equation (2.4.7)**:**

$$RY_{\mathrm{PROT}}\% = \frac{w_{PROT}^{INT}}{w_{PROT}^{Honey}} \boldsymbol{x}100 \qquad (2.4.7)$$

where w_{PROT}^{INT} and w_{PROT}^{Honey} are the total weight of protein in the interphase and in honey, respectively.

The purity level percentage of MRJ1 was determined according to Sodium Dodecyl Sulphate Polyacrylamide Gel Electrophoresis (SDS-PAGE) results, considering the intensity corresponding to the target protein and the total intensity corresponding to all proteins in the interphase (taking into account all the dilution factors applied to each solution), according to Equation (2.4.8):

$$PY_{PROT}\% = \frac{I_{PROT}^{INT}}{I_{PROT}^{Honey}} \times 100 \qquad (2.4.8)$$

where I_{PROT}^{INT} and I_{PROT}^{Honey} are the intensity corresponding to MRJ1 and the total intensity corresponding to all proteins present in the interphase, respectively.

Sodium dodecyl sulphate polyacrylamide gel electrophoresis (SDS-PAGE). Taking into account the UV-spectroscopy quantification of the total amount of proteins in each phase, all samples were diluted so that the amount of total proteins in each gel lane in the SDS-PAGE was *circa* 0.5 μg. Samples of the aqueous phases of each ABS containing ovalbumin were diluted at 2:1 (v:v) in a dissociation buffer consisting of 2.5 mL of 0.5 M Tris-HCl pH 6.8, 4.0 mL of 10 % (w/v) SDS solution, 2.0 mL of glycerol, 2.0 mg of bromophenol blue and 310 mg of dithiothreitol (DTT). This overall solution was heated at 95°C for 5 min to denature the proteins by reducing disulfide linkages, and thus overcoming some forms of the tertiary protein folding and breaking up the quaternary protein structure. Electrophoresis was run on polyacrylamide gels (stacking: 4 % and resolving: 20 %) with a running buffer constituted by 250 mM Tris-HCl, 1.92 M glycine, and 1 % SDS. Proteins were stained with Coomassie Brilliant Blue G-250 0.1 % (w/v), methanol 50 % (v/v), acetic acid 7 % (v/v), and water 42.9 % (v/v). All gels were placed in an orbital shaker at a moderate speed during 2-3 h at room temperature. Gels were further distained in a solution containing acetic acid at 7 % (v/v), methanol at 20 % (v/v), and water at 73 % (v/v) in an orbital shaker at a moderate speed during 3-4 h at room temperature. SDS-PAGE Molecular Weight Standards, namely marker molecular weight full-range from VWR, were used as protein standards. All gels were analyzed using the Image Lab 3.0 (BIO-RAD) analysis tool.

2.4.4. Results and discussion

Phase diagrams and tie-lines. Aiming at the development of more biocompatible ABS, in this work we evaluated the potential of several carbohydrates in the formation of ABS combined with non-fluorinated phosphonium-based ILs. To this end, the ability of two-phase formation was addressed by combining several carbohydrates and ILs, followed by the determination of the corresponding ternary phase diagrams at 25℃. The respective ternary phase diagrams are depicted in Figure 2.4.2 and Figure 2.4.3**.** Detailed weight fraction data are provided in Appendix D. In all phase diagrams, the monophasic region is located below the binodal curve, whereas the biphasic regime is located above. Amongst the studied ILs, $[P_{4444}]Cl$ and $[P_{4441}][TOS]$ were found as not able to form ABS with carbohydrates. Regarding the studied carbohydrates, D-(+)-xylose, D-(+)-maltose and sucrose were not able to form ABS at 25℃ with any of the ILs investigated.

Figure 2.4.2 displays the ternary phase diagrams of the ABS composed of $[Bu_3PC_4]Br$ and several carbohydrates. According to these results, the ability of monosaccharides to create IL-based ABS follows the rank: D-(+)-mannose > D-(+)-galactose > D-(+)-glucose > D-(-)-fructose > D-(-)-arabinose. Taking into account the carbohydrates chemical structures provided in Figure

2.4.1, it seems that the number of –OH groups has a significant impact in the ABS formation. Carbohydrates with 5 –OH groups (D-(+)-mannose, D-(+)-galactose and D-(+)-glucose) have a higher ability to form two phases than carbohydrates with 4 –OH groups (D-(-)-fructose and D-(-)-arabinose). The results obtained in this work are in agreement with the trend previously reported for ABS composed of other ILs and carbohydrates[16]. All the works reported up to date on IL-based ABS formed by the addition of carbohydrates were achieved with fluorinated imidazolium-, or pyridinium-based ILs[15,16,18–25]. However, these fluoride-based ILs display important disadvantages when considering the development of more sustainable processes since besides being more expensive they tend to be recalcitrant to biodegradation and more toxic[41]. Furthermore, some fluorinated ILs are also non-water stable[42].

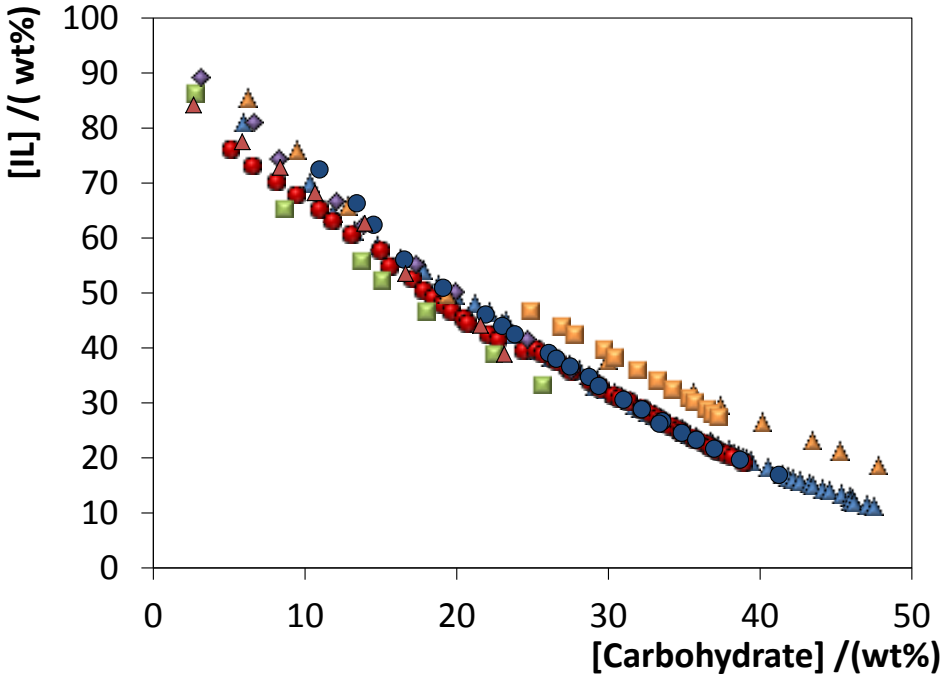

Figure 2.4.2. ABS phase diagrams for the systems composed of $[Bu_3PC_4]Br$ + Carbohydrates + H_2O at 25°C: **(a)** D-(+)-mannose (▲); D(+)-galactose (■); D-(+)-glucose (●); D(+)-fructose (▲); D(+)-arabinose, (◆); maltitol (▲); D-sorbitol (●); xylitol (■).

In Figure 2.4.2 are displayed the phases diagrams for ABS composed of $[Bu_3PC_4]Br$ + polyols + water at 25°C. The polyols ability to undergo liquid–liquid demixing follows the rank: maltitol > D-sorbitol > xylitol. The effect of –OH groups on the ABS formation ability is also important for polyols, as discussed before for monosaccharides. The results here obtained also are in close agreement with the trends previously observed for polyols to act as two-phase promoters of ABS composed of other ILs[15]. From the results obtained, it is clear that hydrogen bonding between carbohydrates and water is essential, and that these compounds act as “salting-out” species.

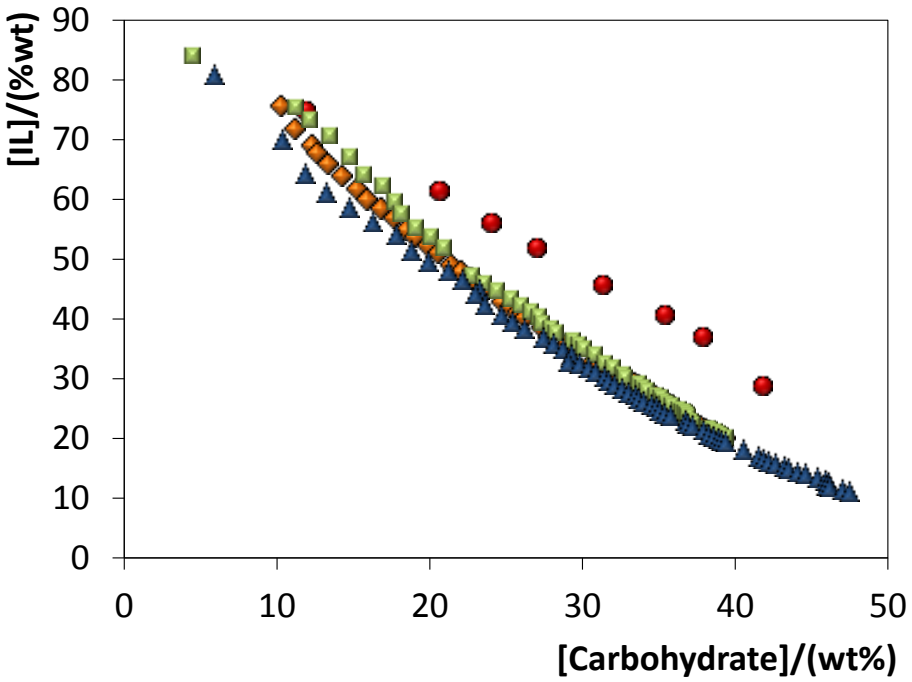

Figure 2.4.3. Phase diagrams for the systems composed of IL + D(+)-fructose + H_2O at 25 °C: $[P_{4441}][MeSO_4]$ (●), $[P_{4444}]Br$ (■), $[Bu_3PC_2]Br$ (◆), $[Bu_3PC_4]Br$ (▲).

Figure 2.4.3. depicts the binodal curves for the systems composed of phosphonium-based ILs + D-(-)-fructose, allowing the evaluation of the effect of the IL on the formation of ABS. The ability of phosphonium-based ILs to form ABS follows the order: $[Bu_3PC_4]Br$ > $[Bu_3PC_2]Br$ > $[P_{4444}]Br$ > $[P_{4441}][MeSO_4]$. Since ILs are constituted by different cations and anions, a comparison of the IL effect as phase-forming agents needs to take into account the contribution of both ions to be hydrated. Generally, ILs with longer alkyl side chains are more hydrophobic and require lower amounts of salting-out agents (in this work the carbohydrates) to form a two-phase system[43]. Accordingly, $[P_{4444}]Br$ requires a higher amount of D-(-)-fructose for the liquid-liquid demixing, when compared with $[Bu_3PC_2]Br$ and $[Bu_3PC_4]Br$. On the other hand, $[P_{4441}][MeSO_4]$ presents the lowest ability to form ABS. This is mostly due to its higher affinity for water, which results in the need to use a larger carbohydrate amount to promote the "salting-out" of the IL.

The experimental data corresponding to the binodal curves were fitted using Equation (2.4.1). The regression parameters estimated by least-squares regression, standard deviations (σ) and correlation coefficients (R^2) are displayed in Table 2.4.1. Equation (2.4.1) is able to correlate the experimental binodal curves, as shown by the high correlation coefficients obtained (R^2 > 0.9934).

Table 2.4.1. Correlation parameters used to describe the experimental binodal data by Equation (2.4.1)

IL	Carbohydrate	$A \pm \sigma$	$B \pm \sigma$	$10^5 (C \pm \sigma)$	R^2
$[Bu_3PC_4]Br$	D(+)-fructose	136.9 ± 1.8	-0.21 ± 0.03	1.02 ± 0.01	0.9988
	D-(+)-mannose	254.0 ± 3.1	-0.46 ± 0.34	0.01 ± 0.25	0.9934
	D(+)-galactose	120.0 ± 1.8	-0.20 ± 0.05	1.56 ± 0.15	0.9992
	D-(+)-glucose	118.7 ± 2.1	-0.18 ± 0.05	1.12 ± 0.04	0.9971
	D(+)-arabinose	120.7 ± 2.9	-0.16 ± 0.08	1.68 ± 0.15	0.9979
	xylitol	82.0 ± 8.8	-0.07 ± 0.02	1.21 ± 0.07	0.9995
	D-sorbitol	178.1 ± 5.6	-0.26 ± 0.08	0.91 ± 0.05	0.9998
	maltitol	100.1 ± 2.9	-0.10 ± 0.01	3.56 ± 0.03	0.9964
$[P_{4441}][MeSO_4]$	D(+)-fructose	118.7 ± 7.5	-0.13 ± 0.01	0.71 ± 0.08	0.9969
$[P_{4444}]Br$		123.5 ± 3.3	-0.15 ± 0.08	1.43 ± 0.05	0.9929
$[Bu_3PC_2]Br$		158.7 ± 2.2	-0.23 ± 0.03	0.99 ± 0.02	0.9994

Extraction and Purification of Proteins from Honey. Aiming to reduce the amount of compounds required to promote the creation of ABS to act as separation platforms, the sugar present in honey was used directly as a phase-forming agent. A common mixture composition of 25 wt% of IL, 50 wt% of honey and 15 wt% of water was prepared. This mixture was prepared considering that honey contains *ca.* 80% (in weight) of carbohydrates according to thr nutritional composition described on the label of the commercial honey used. The results obtained are reported in Figure 2.4.4. Detailed data are given in Appendix D. In all systems, the top phase is mostly composed of carbohydrate and the bottom phase corresponds to the IL-rich phase. For all systems it was observed a large amount of precipitated proteins as an interphase. The protein quantification was carried out only in the top and bottom phases, and the precipitated proteins recovered at the interphase were resuspended in a phosphate buffer solution for further analysis/quantification.

The recovery yield of the total proteins at the interphase ranges between 83.34 and 97.30%, whereas the ILs ability to promote the proteins recovery increases according to the following rank: $[P_{4444}]Br > [P_{4441}][MeSO_4] > [Bu_3PC_4]Br > [Bu_3PC_2]Br$ (based ABS). Phosphonium based-ILs are more hydrophobic than their imidazolium counterparts[44]. Due to their more hydrophobic characteristics it is possible that specific interactions create an unfavorable environment in the aqueous phases for the honey proteins, inducing their precipitation at the ABS interface, creating

thus an interphase rich in proteins. The same behavior was previously observed with other proteins from serum and egg white using IL-salt and polymer-salt-based ABS[45,46]. It was already reported that IL-salt-based ABS allow the complete precipitation of BSA in systems constituted by $[P_{4444}]Br$ and $K_3C_6H_5O_7/C_6H_8O_7$[45]. Polymer-salt-based ABS lead to the extraction and purification of ovalbumin from egg white, while precipitating the major contaminant proteins[46].

The extraction, purification and isolation of honey proteins was already investigated using other physical and/or chemical methods[47,48]. Ultracentrifugation, ion exchange chromatography and dialysis are normally used to obtain amylase from honey[47,48]. Aqueous solutions of sodium tungstate combined with sulfuric acid are usually applied to induce the honey proteins precipitation[48]. However, this method requires not only the use of high temperatures, but is also necessary the sample centrifugation and washing (for several times) until the supernatant becomes sugar-free.

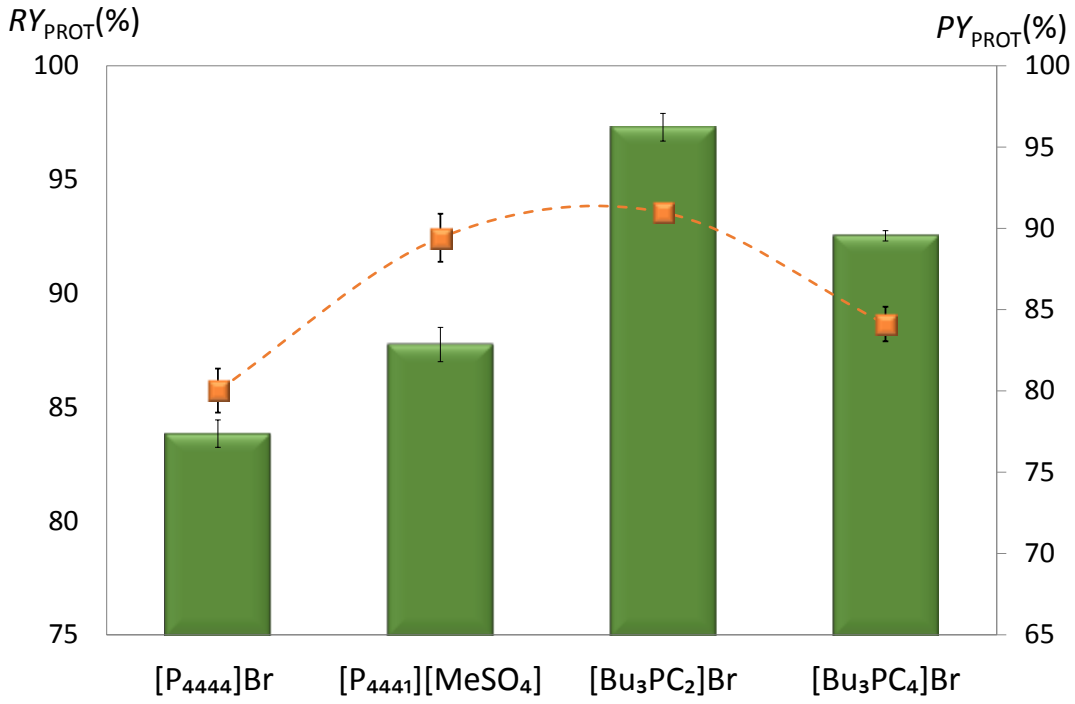

Figure 2.4.4. Recovery yield (RY_{PROT}%, bars) and purification level (PY_{PROT}, symbols) of proteins from honey in ABS composed of 25 wt% of IL + 50 wt% honey + 25 wt% water at 25°C.

Although a large amount of proteins was precipitated, UV spectroscopy quantification did not allow to confirm the purification levels of the proteins isolated. To this end, the precipitated proteins were re-suspended in a 10 mM phosphate buffer solution ($1g.L^{-1}$) and analyzed by SDS-PAGE. The results obtained are given in Figure 2.4.5**.** Detailed data are given in Appendix D. According to molecular weight markers, the precipitated proteins correspond to MRJPs, identified

as MRJP 1, MRJP 3 and MRJP 5. Moreover, according to the bands intensity, the system composed of 25 wt% of $[Bu_3PC_2]Br$ + 50 wt% of honey and 15 wt% of water, was the ABS that results in the MRJP1 precipitation at the interface with the highest purity level (90.98 ± 0.49 %). Despite the loss of others MRJPs, as detected in the aqueous phases of the studied ABS, this ABS allows us to purify and isolate MRJP1, with a recovery yield of 97.30% and a purity level of 90.98%. MRJP1 is particularly relevant because of its antibacterial activity against multi-drug resistant bacteria, been a natural antibacterial compound[49]. MRJP1 was obtained in a single-step using ABS composed of phosphonium-based ILs and carbohydrates, which can be further envisioned as extraction platforms to obtain proteins from other carbohydrate-rich complex matrices.

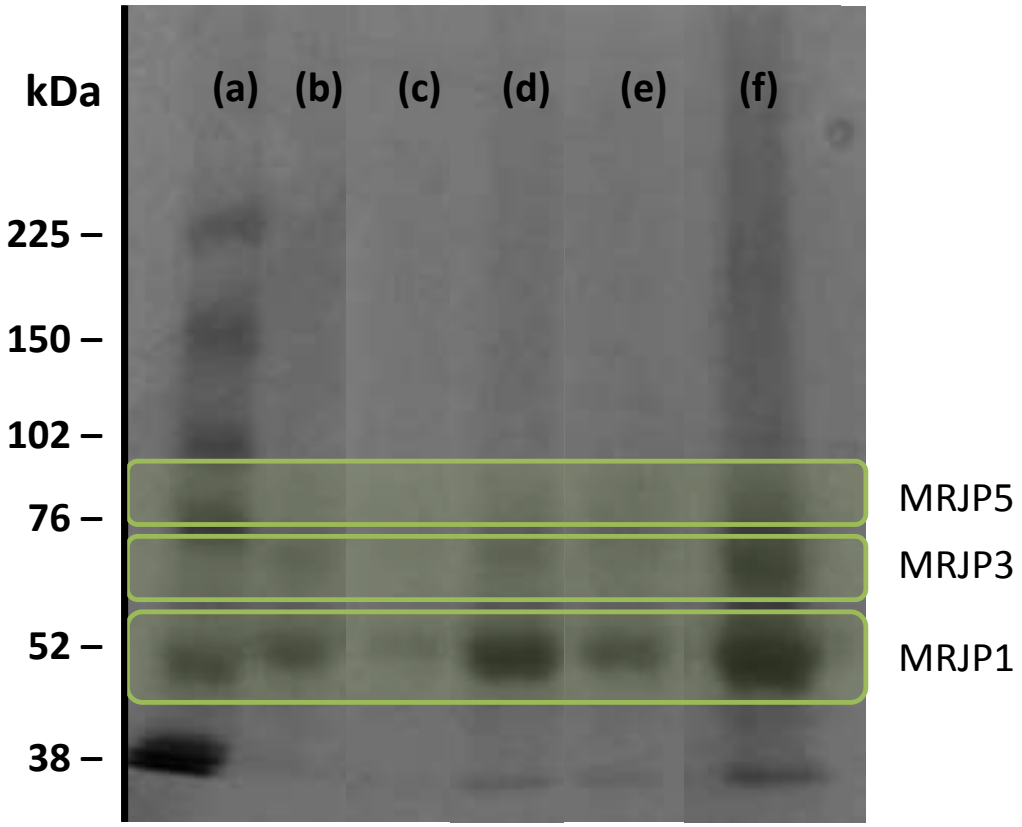

Figure 2.4.5. SDS-PAGE of the (a) protein molecular weight marker, precipitated proteins on interphase and re-dissolved in a buffer solution of the ABS composed of (b) $[P_{4444}]Br$, (c) $[P_{4441}][MeSO_4]$, (d) $[Bu_3PC_2]Br$, (e) $[Bu_3PC_4]Br$ and (f) commercial honey.

As already discussed, processes currently applied to obtain MRJPs are based on the use of less biocompatible solvents and under harsher conditions[47,48]. In addition, significant amounts of wastes are produced due to the several steps required to achieve the proteins extraction, purification and isolation. The advantages of the proposed process are summarized in Figure 2.4.6. It should be remarked that the carbohydrate-rich fraction can proceed to additional

applications, while the IL-rich phase can be used again to create novel ABS to recover MRJPs from honey samples.

The ABS reported in this work have the following advantages: (i) the use of non-fluorinated and non-imidazolium/pyridinium ILs to form ABS with carbohydrates; (ii) the possibility to directly use matrices rich in carbohydrates as phase-forming components of ABS, requiring only the addition of IL and water; (iii) they allow a remarkable recovery and purification of MRJP1 in one-step; and (iv) are a low-cost sustainable process with the possibility of reusing/recycling the applied ILs and to further process the carbohydrate matrix.

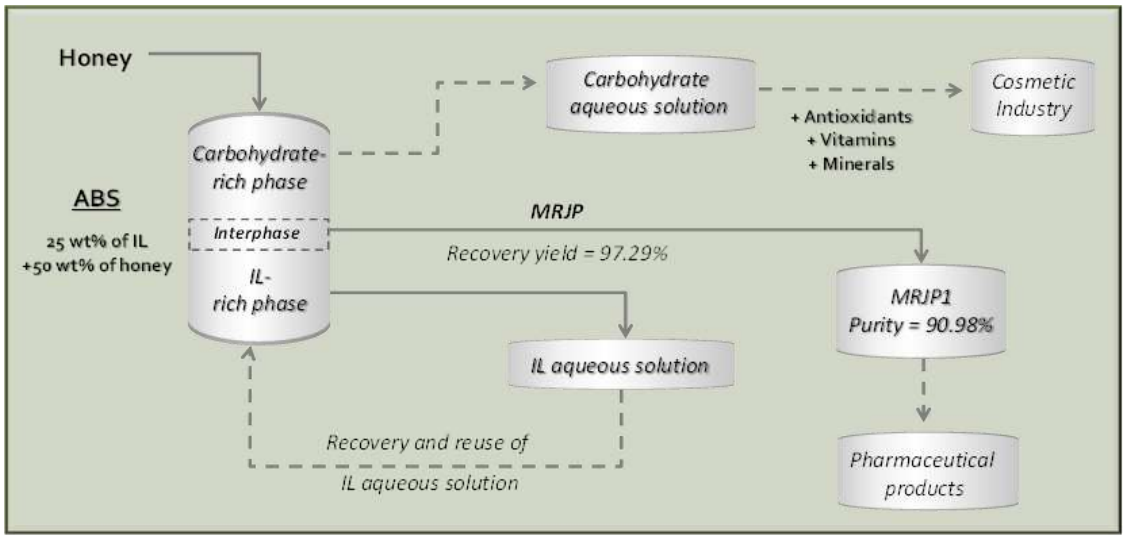

Figure 2.4.6. Flow chart of the developed process for the isolation of proteins from honey, including the steps of the ILs recycling and possible applications of the carbohydrates aqueous solutions.

2.4.5. Conclusions

In this work, novel ABS with more biocompatible characteristics constituted by phosphonium-based ILs and carbohydrates were investigated. The respective ternary phase diagrams, tie-lines and tie-line lengths were determined at 25°C and at atmospheric pressure. The ability of the carbohydrates to promote the two phase separation depends on the number of -OH groups present in the molecule and to establish hydrogen-bonds with water. These systems were then investigated to purify proteins from complex honey samples. Proteins from honey preferentially precipitate at the interphase, with recovery yields of total proteins ranging between 83.84 and 97.30%, and a purity level of MRJP1 ranging from 80.02 to 90.08%. Therefore, the ABS here developed are valuable to recover value-added proteins from complex raw matrices.

2.4.6. References

1. Albertsson, P.A. P. Nature. 1958;182(4637):709-711.
2. Taha, M., e Silva, F.A., Quental, M.V., Ventura, S.P., Freire, M.G., Coutinho, J.A.. Green Chem. 2014;16(6):3149-3159.
3. Quental, M.V., Caban, M., Pereira, M.M., Stepnowski, P., Coutinho, J.A.P., Freire, M.G.. Biotechnol J. 2015;10(9):1457-1466.
4. Passos, H., Luís, A., Coutinho, J.A.P., Freire, M.G.. Sci Rep. 2016;6(February):20276.
5. Martins, M., Vieira, F.A., Correia, I,. Ferreira, R.A.S., Abreu, H., Coutinho, J.A.P., Ventura, S.P.M.. Green Chem. 2016;1:63-68.
6. Li, Z., Liu, X., Pei, Y., Wang, J., He, M.. Green Chem. 2012;14(10):2941.
7. Souza, R.L., Ventura, S.P.M., Soares, C.M.F., Coutinho, J.A.P., Lima, Á.S.. Green Chem. 2015;17(5):3026-3034.
8. Dinis, T.B.V., Passos, H., Lima, D.L.D., Esteves, V.I., Coutinho, J.A.P., Freire, M.G.. Green Chem. 2015;17(4):2570-2579.
9. Zawadzki, M., e Silva, F.A, Domańska, U., Coutinho, J.A.P., Ventura, S.P.M.. Green Chem. 2016;18(12):3527-3536.
10. Santos, J.H.P.M., Martins, M., Silvestre, A.J.D., Coutinho, J.A.P., Ventura, S.P.M.. Green Chem. 2016;34:29-41.
11. Capela, E.V., Quental, M.V., Domingues, P., Coutinho, J.A.P., Freire, M.G.. Green Chem. 2017.
12. Freire, M.G., Cláudio, A.F.M., Araújo, J.M.M., Coutinho, J.A.P,. Marrucho, I.M., Canongia Lopes, J.N., Rebelo, L.P.N.. Chem Soc Rev. 2012;41(14):4966-4995.
13. Seddon, K.R., Early M.J.. Pure Appl. Chem. 2002;72(7):10-25.
14. Wasserscheid, P., Welton, T. Ionic Liquids in Synthesis. Vol 7. Wiley-VCH; 2008.
15. Freire, M.G., Louros, C.L.S., Rebelo, L.P.N., Coutinho, J.A.P.. Green Chem. 2011;13(6):1536.
16. Ferreira, A.M., Esteves, P.D.O, Boal-Palheiros, I., Pereiro, A.B., Rebelo, L.P.N., Freire, M.G.. Green Chem. 2016;18(4):1070-1079.
17. Cardoso G de B., Mourão, T., Pereira, F.M., Freire, M.G., Fricks, A.T., Soares, C.M.F., Lima, Á.S.. Sep Purif Technol. 2013;104:106-113.
18. Chen, Y., Meng, Y., Yang, J., Li, H., Liu, X.. J Chem Eng Data. 2012;57(7):1910-1914.
19. Chen, Y., Wang, Y., Cheng, Q., Liu, X., Zhang, S.. J Chem Thermodyn. 2009;41(9):1056-1059.
20. Chen, Y., Meng, Y., Zhang, S., Zhang, Y., Liu, X., Yang, J.. J Chem Eng Data. 2010;55(9):3612-3616.
21. Wu, B., Zhang, Y.M., Wang, H.P.. J Chem Eng Data. 2008;53(4):983-985.
22. Chen, Y., Zhang, S.. J Chem Eng Data. 2010;55(1):278-282.
23. Zhang, Y., Zhang, S., Chen, Y., Zhang, J.. Fluid Phase Equilib. 2007;257(2):173-176.
24. Wu, B., Zhang, Y., Wang, H.. J Phys Chem B. 2008;112(20):6426-6429.
25. Wu, B., Zhang, Y., Wang, H., Yang, L.. J Phys Chem B. 2008;112(41):13163-13165.
26. Karabagias, I.K., Badeka, A., Kontakos, S., Karabournioti, S., Kontominas, M.G.. Food Res Int. 2014;55:363-372.
27. El Sohaimy, S.A., Masry, S.H.D., Shehata, M.G.. Ann Agric Sci. 2015;60(2):279-287.
28. Beretta, G., Granata, P., Ferrero, M., Orioli, M., Facino, R.M.. Anal Chim Acta. 2005;533(2):185-191.
29. Roleira, F.M.F., Silva, E.J.T. da, Varela, C.L., Costa, S.C., Silva, T., Garrido, J., Borges, F.. Food Chem. 2015;183:235-258.
30. Borsato, D.M., Prudente, A.S., Döll-Boscardin, P.M., Borsato, A.V., Luz, C.F, Maia, B.H., Miguel, O.G.. J Med Food. 2014;17(7):817-825.
31. Aggad, H.G.D.. Med Aromat Plants. 2014;3(2):2-3.
32. Rao, P.V., Krishnan, K.T., Salleh, N., Gan, S.H.. Brazilian J Pharmacogn. 2016;26(5):657-664.
33. Bauer, L., Kohlich, A., Hirschwehr, R., Siemann, U., Ebner, H., Scheiner, O., Kraft, D., Ebner, C.. J Allergy Clin Immunol. 1996;97(1 I):65-73.
34. Won, S.R., Lee, D.C., Ko, S.H., Kim, J.W., Rhee, H.I.. Food Res Int. 2008;41(10):952-956.
35. Simuth, J.. Apidologie. 2001;32:69-80.
36. Okamoto, I., Taniguchi, Y., Kunikata, T., Kohno, K., Iwaki, K., Ikeda, M., Kurimoto, M.. Life Sci. 2003;73(16):2029-2045.
37. Schmitzová, J., Klaudiny, J., Albert, Š., Schröder, W., Schreckengost, W., Hanes, J., Júdová, J., Šimúth, J.. Cell Mol Life Sci. 1998;54(9):1020-1030.
38. Aurangzeb, M., Azim, M.K.. Pakistan J Biochem Mol Biol. 2011;44(3):118-124.
39. Merchuk, J.C., Andrews, B.A., Asenjo, J.A.. J Chromatogr B Biomed Sci Appl. 1998;711(1-2):285-293.
40. Bradford, M.M.. Anal Biochem. 1976;72(1):248-254.
41. Pham, T.P.T., Cho, C.W., Yun, Y.S.. Water Res. 2010;44(2):352-372.
42. Freire, M.G., Neves, C.M.S.S., Marrucho, I.M., Coutinho, J.A.P., Fernandes, A.M.. J Phys Chem A. 2010;114(11):3744-3749.
43. Neves, C.M.S.S., Ventura, S.P.M., Freire, M.G., Marrucho, I.M., Coutinho, J.A.P.. J Phys Chem B. 2009;113(15):5194-5199.
44. Louros, C.L.S., Cláudio, A.F.M., Neves, C.M.S.S., Freire, M.G., Marrucho, I.M., Jérôme, P., Coutinho, J.A.P.. Int J Mol Sci. 2010;11(4):1777-1791.
45. Pereira, M.M., Pedro, S.N., Quental, M.V., Lima, Á.S., Coutinho, J.A.P., Freire, M.G.. J Biotechnol. 2015;206:17-25.

46. Pereira, M.M., Cruz, R.A.P., Almeida, M.R., Lima, Á.S., Coutinho, J.A.P., Freire, M.G.. Process Biochem. 2016;51(6):781-791.
47. Babacan, S., Rand, A.G.. J Food Sci. 2005;70(6):c413-c418.
48. Padovan, G.J., Rodrigues, L.P., Leme, I.A., de Jong, D., Marchini, J.S.. Eurasian J Anal Chem. 2007;2(3).
49. Brudzynski, K., Sjaarda, C., Lannigan, R.. Front Microbiol. 2015;6:711.

3. IL-BASED ABS AS EFFECTIVE CONCENTRATION AND PURIFICATION TOOLS FOR CANCER BIOMARKERS

3.1. Simultaneous depletion of human serum albumin (HSA) and immunoglobulin G (IgG) from human serum using ionic-liquid-based aqueous biphasic systems

This chapter is based on an unpublished work with the following authors involved

Matheus M. Pereira, Sónia N. Pedro, Joana Gomes, Aminou Mohamadou, João A. P. Coutinho and Mara G. Freire

3.1.1. Abstract

In recent years, advances in clinical analysis allowed the identification of several metabolites in human fluids. Nevertheless, the accurate identification and quantification of low-abundance proteins in human serum is still very difficult to achieve due to masking effects exerted by other abundant proteins, namely human serum albumin (HSA) and immunoglobulin G (IgG). Therefore, the development of more efficient, and ideally more sustainable, depletion methods has been a hot topic of research envisaging the accurate quantification of low-abundance human metabolites or proteins. This work aims at the development of novel depletion methods for human serum samples based on aqueous biphasic systems (ABS) composed of ionic liquids (ILs). To this end, novel ABS formed by glycine-betaine-based ILs and buffered aqueous solutions of $K_3C_6H_5O_7/C_6H_8O_7$ (pH=7.0) were investigated. Novel analogous of glycine-betaine-based ILs were synthesized and characterized, followed by their use as phase-forming agents of ABS to be used in the depletion of the human serum most abundant proteins. According to the results here reported, the investigated ABS lead to a complete and simultaneous depletion of HSA and IgG from human serum in a single-step, allowing to identify transferrin, a low abundant protein. The IL-based ABS here reported are thus appropriate systems for the depletion of highly abundant proteins from human serum, a process that can be extended to other biological samples.

3.1.2. Introduction

Human biological samples (serum, plasma, urine, blood and saliva) have been used for long in the diagnosis of several diseases[1–3]. Human serum comprises several proteins, nucleic acids and other metabolites, and thus is one of the most used biological samples for the detection and monitoring of several diseases[4,5]. In fact, this strategy is already applied in clinical practice, such as in the early-stage cancer diagnosis and prognosis[6]. Nevertheless, clinical diagnosis based on biological fluids is not straightforward due to the large diversity of metabolites in biological fluids, therefore requiring the biological samples pretreatment mainly to remove high-abundant proteins which can mask the diagnosis results[7].

Contributions: M.G.F., A.M. and J.A.P.C. conceived and directed this work. M.M.P., S.N.P. and J.G. acquired the experimental data. M.M.P., J.A.P.C., A.M. and M.G.F interpreted the experimental data. The manuscript was mainly written by M.M.P. and M.G.F. with significant contributions from the remaining authors.

The human serum proteomic profile is mostly constituted by human serum albumin (HSA) and immunoglobulin G (IgG), accounting for up to 80% of the total serum proteins content[3]. The high abundance of these two proteins masks the detection of low-abundant ones by the commonly used analytical methods. In order to overcome these problems, depletion methods for abundant serum proteins are a mandatory step. The depletion of HSA and IgG was already investigated applying different methodologies, such as solid-phase extraction[8–12], liquid-liquid extraction[13,14], and precipitation[9]. Amongst these, solid-phase extractions are the most applied pretreatment strategy to reduce the proteomic content of HSA and IgG.

Within the liquid-liquid extraction approaches, aqueous biphasic systems (ABS) are an environmentally-friendly technique (since they are mainly composed of water) that received increased attention in the last decades for extracting and purifying bioactive molecules or compounds[15]. ABS are usually constituted by non-volatile pairs of compounds dissolved in water (a mixture of two polymers, a polymer and a salt or two salts), that undergo liquid-liquid demixing above given concentrations. In the past decade, ionic-liquid-(IL)-based ABS were proposed by Gutowski et al.[16], further receiving a remarkable attention in the separations field[17]. ILs are molten salts composed of a large organic cation and an inorganic/organic anion, usually liquid at temperatures below 100°C. Since ILs display an ionic character, they exhibit a negligible volatility at atmospheric conditions, high thermal and chemical stabilities, and an impressive solvation ability for several compounds[18,19]. However, one of the most important properties that arise from ILs is the large number of possible cation-anion combinations, making possible the IL tailoring for specific applications, being this advantage extended to IL-based ABS. Combining the large content of water and the outstanding features of ILs, IL-based ABS can be envisioned as alternative depletion methods. In addition to the well-studied imidazolium-based ILs[17], more recent studies are focused on the ILs derived from natural sources, mainly cholinium-based ILs[20–22]. Among these more “benign” alternatives, ILs derived from glycine-betaine analogues (AGB-ILs) are also viable phase-forming components of ABS. Glycine-betaine is an amino acid derivative naturally found in plants, already applied in food and cosmetic industries[23,24].

This chapter aims at the study of the development of novel depletion methods using IL-based ABS, and for which ILs derived from glycine-betaine analogues (AGB-ILs) were chosen to increase the biocompatible character of the process.

3.1.3. Experimental procedures

Materials. All tertiary amines, ethyl acetate and 4-bromobutyrate acid ethyl ester were acquired from Sigma-Aldrich. Silver saccharinate, silver lactate, silver pyruvate, silver

dicyanamide, silver salicylate and silver salicylate were prepared from mixtures (mole ratio of = 1:1.1) of $AgNO_3$ and NaX (X = saccharinate, lactate, pyruvate, dicyanamide and salicylate). $AgNO_3$ and all sodium salts were acquired from Sigma-Aldrich. The ABS studied in this work are composed of a buffer aqueous solution constituted by potassium citrate ($K_3C_6H_5O_7 \cdot H_2O$, ≥ 99 wt% pure) from Sigma–Aldrich, and citric acid ($C_6H_8O_7 \cdot H_2O$, 100 wt% pure) from Fisher Scientific.

Synthesis and characterization of AGB-ILs. The synthesis pathway for the AGB-based ILs is provided in Appendix E. The chemical structures of all ILs synthesized were confirmed by ^{1}H and ^{13}C NMR, Infrared spectroscopy and elemental analysis, showing purity levels > 99 %. All ILs were dried in vacuum. The chemical structures and abbreviations of the synthesized ILs are given in Figure 3.1.1.

Microtox® toxicity tests. To evaluate the ecotoxicity of the synthetized ILs, the Standard Microtox® liquid-phase assay was applied. Microtox® is a bioluminescence inhibition method based on the bacterium *Vibrio fischeri* (strain NRRL B- 11177) luminescence after its exposure to each sample solution at 15°C. In this work, the standard 81.9% test protocol was followed[25]. The microorganism was exposed to a range of diluted aqueous solutions of each compound (from 0 to 81.9 wt%), where 100% corresponds to the IL stock solution with a known concentration. After 5, 15, and 30 min of exposure to each aqueous solution, the bioluminescence emission of *Vibrio fischeri* was measured and compared with the bioluminescence emission of a blank control. The corresponding 5 min-, 15 min- and 30 min-EC_{50} values (EC_{50} being the estimated concentration yielding a 50% of inhibition effect) were then determined with a 95% confidence interval, by non-linear regression using the least-squares method to fit the data.

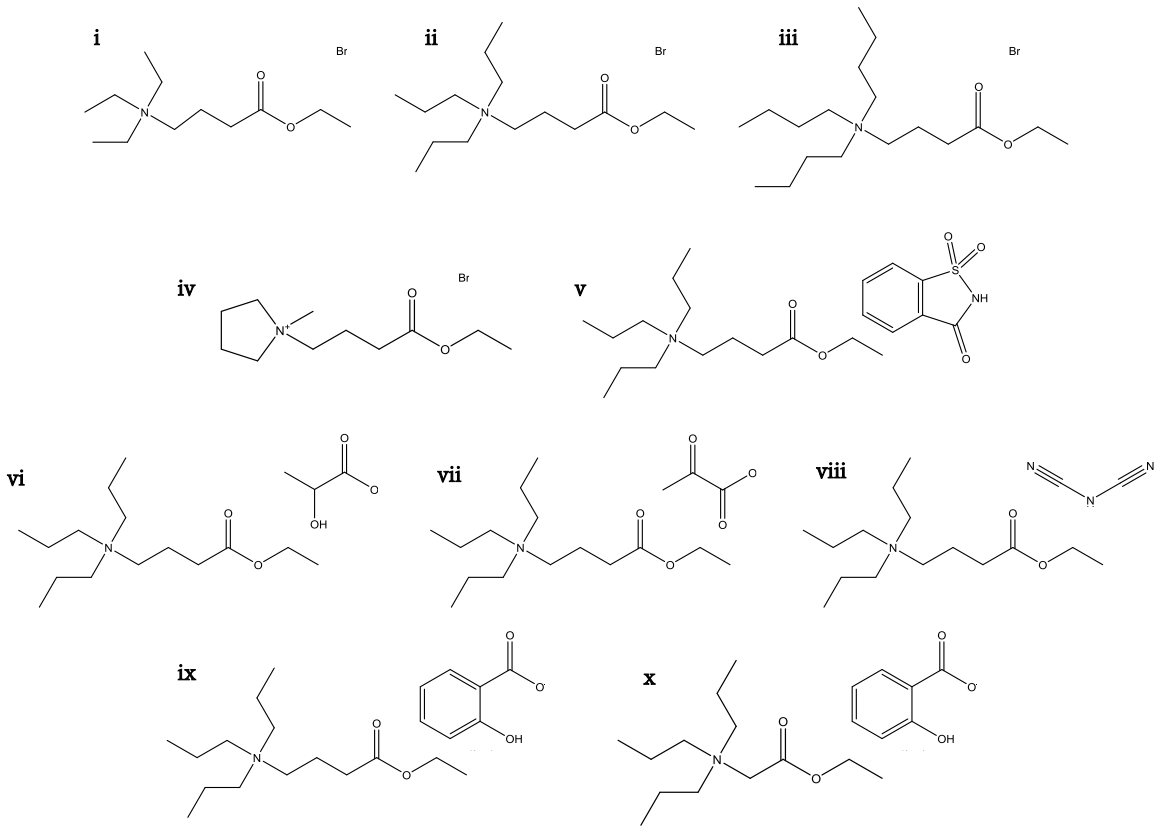

Figure 3.1.1. Chemical structures of the synthesized ILs: (i) $[Et_3NC_4]Br$, (ii) $[Pr_3NC_4]Br$, (iii) $[Bu_3NC_4]Br$, (iv) $[MepyrNC_4]Br$, (v) $[Pr_3NC_4][Sac]$, (vi) $[Pr_3NC_4][Lac]$, (vii) $[Pr_3NC_4][Pyr]$, (viii) $Pr_3NC_4][Dca]$, (ix) $[Pr_3NC_2][Sal]$ and (x) $[Pr_3NC_4][Sal]$,

ABS phase diagrams and tie-lines. Aqueous solutions of each IL ($[MepyrNC_4]Br$, $[Et_3NC_4]Br$, $[Pr_3NC_4]Br$, $[Bu_3NC_4]Br$, $[Pr_3NC_4][Pyr]$, $[Pr_3NC_4][Lac]$, $[Pr_3NC_2][Sal]$, $[Pr_3NC_4][Sal]$, $[Pr_3NC_4]][Sac]$ and $[Pr_3NC_4][Dca]$) at *circa* 90 wt% and aqueous solutions of the mixture $K_3C_6H_5O_7/C_6H_8O_7$ (as a buffer solution at pH = 7.0, mole ratio of ≈ 15:1) at ≈ 50 wt% were prepared and used for the determination of the binodal curves. The phase diagrams were determined through the cloud point titration method[26,27] at 25°C and atmospheric pressure. The system compositions were determined by the weight quantification of all components added within $\pm 10^{-4}$ g. Further details on the experimental procedure can be found elsewhere[27,28].

Tie-lines (TLs) were determined by a gravimetric method originally proposed by Merchuk et al.[29]. Different mixture points at the biphasic region were prepared, vigorously stirred, centrifuged for 10 min and allowed to reach equilibrium by the separation of the phases for at least 10 min at 25°C. After separation of the two phases, both the top and bottom phases were weighted. Each individual TL was determined by application of the lever-arm rule to the

relationship between the top weight phase composition and the overall system composition. The experimental binodal curves were correlated using Equation (3.1.1):

$$[IL] = Aexp[(B[salt]^{0.5}) - (C[salt]^3)] \quad (3.1.1)$$

where $[IL]$ and $[salt]$ are the IL and the salt weight fraction percentages, respectively, and A, B, and C are constants obtained by the regression of the experimental data (see Appendix E).

The determination of the TLs was then accomplished through the solution of the following system of four equations (Equation (3.1.2) to (3.1.5)) aiming at determining four unknown values ($[IL]_{\mathrm{IL}}$, $[IL]_{\mathrm{salt}}$, $[salt]_{\mathrm{IL}}$ and $[salt]_{\mathrm{salt}}$):

$$[IL]_{salt} = Aexp\left[\left(B[salt]_{IL}^{0.5}\right) - \left(C[salt]_{IL}^{3}\right)\right] \quad (3.1.2)$$

$$[IL]_{salt} = Aexp\left[\left(B[salt]_{salt}^{0.5}\right) - \left(C[salt]_{salt}^{3}\right)\right] \quad (3.1.3)$$

$$[IL]_{IL} = \frac{[IL]_M}{\alpha} - \frac{1-\alpha}{\alpha}[IL]_{salt} \quad (3.1.4)$$

$$[salt]_{IL} = \frac{[salt]_M}{\alpha} - \frac{1-\alpha}{\alpha}[salt]_{salt} \quad (3.1.5)$$

where the subscripts "IL", "salt" and "M" represent the top and the bottom phases and the mixture composition, respectively. The parameter α is the ratio between the weight of the top phase and the weight of the overall mixture. For the calculation of each tie-line length (TLL), Equation (3.1.6) was employed:

$$TLL = \sqrt{([salt]_{IL} - [salt]_{salt})^2 + ([IL]_{IL} - [IL]_{salt})^2} \quad (3.1.6)$$

Depletion of human serum albumin (HSA) and Immunoglobulin G (IgG). The ternary mixtures compositions used in the depletion experiments were chosen based on the phase diagrams determined in this work for each IL-salt-water system. Human serum was directly used as the aqueous solution. Each mixture was vigorously stirred, centrifuged for 10 min, and left to equilibrate for 10 min at 25°C to reach the HSA and IgG depletion, that precipitates at the ABS interface. After, a careful separation of the phases was performed and the amount of HSA and IgG in each phase was quantified by SE-HPLC (Size Exclusion High-Performance Liquid Chromatography). Each phase was diluted at a 1:10 (v:v) ratio in a phosphate buffer solution before injection. A Chromaster HPLC (VWR, Hitachi) coupled to an UV detector was used. SE-HPLC

was performed with an analytical column (25 cm × 2 mm i.d., 25 μm), Lichrospher 100 RP-18, from Merck. A 100 mM phosphate buffer in MiliQ water (mobile phase) was run isocratically with a flow rate of 1 mL·min^{-1}. The temperature of the column and auto-sampler was kept constant at 25°C. The injection volume was of 25 μL. The wavelength was set at 280 nm whereas the retention time of IgG and HSA was found to be *circa* 15.7 and 17.1 min, respectively, within an analysis time of 40 min. The quantification of HSA and IgG in each phase was carried out by an external standard calibration method (R^2=0.9997 and R^2=0.9991) - *cf.* the Appendix E with the established calibration curves.

The depletion efficiency of HSA and IgG, $\boldsymbol{DE_{BSA}}\%$, and $\boldsymbol{DE_{IgG}}\%$ are the percentage ratio between the amount of protein in the solid interface to that in the total mixture, and is defined according to Equation (3.1.7) and Equation (3.1.8):

$$DE_{\mathrm{HSA}}\% = \frac{w_{HSA}^{Int}}{w_{HSA}^{IL} + +w_{HSA}^{Salt} + w_{HSA}^{Int}} \times 100 \quad (3.1.7)$$

$$DE_{\mathrm{IgG}}\% = \frac{w_{IgG}^{Int}}{w_{IgG}^{IL} + +w_{IgG}^{Salt} + w_{IgG}^{Int}} \times 100 \quad (3.1.8)$$

where w_{HSA}^{IL}, w_{HSA}^{Salt} ,w_{HSA}^{Int} , w_{IgG}^{IL}, w_{IgG}^{Salt} and $w_{IgG}^{Int}$are the total weight of HSA or IgG in the IL-rich aqueous phases, salt-rich aqueous phases and solid interphase, respectively. For all systems the top phase corresponds to the IL-rich phase whereas the bottom phase is mainly constituted by the citrate-based salt and water.

Sodium dodecyl sulphate polyacrylamide gel electrophoresis (SDS-PAGE). Taking into account the UV-spectroscopy quantification of the total amount of proteins in each phase, all samples were diluted so that the amount of total protein in each gel lane in the SDS-PAGE was *circa* 0.5 μg. Samples of the aqueous phases of each ABS were diluted at 2:1 (v:v) in a dissociation buffer consisting of 2.5 mL of 0.5 M Tris-HCl pH 6.8, 4.0 mL of 10 % (w/v) SDS solution, 2.0 mL of glycerol, 2.0 mg of bromophenol blue and 310 mg of dithiothreitol (DTT). This overall solution was heated at 95°C for 5 min to denature proteins by reducing disulfide linkages, and thus overcoming some forms of the tertiary protein folding and breaking up the quaternary protein structure. Electrophoresis was run on polyacrylamide gels (stacking: 4 % and resolving: 20 %) with a running buffer constituted by 250 mM Tris-HCl, 1.92 M glycine, and 1 % SDS. The proteins were stained with Coomassie Brilliant Blue G-250 0.1 % (w/v), methanol 50 % (v/v), acetic acid 7 % (v/v) and water 42.9 % (v/v). All gels were placed in an orbital shaker at a moderate speed during 2-3 h at

room temperature. The gels were further distained in a solution containing acetic acid at 7 % (v/v), methanol at 20 % (v/v) and water at 73 % (v/v) in an orbital shaker at a moderate speed during 3-4 h at room temperature. SDS-PAGE Molecular Weight Standards, namely molecular weight full-range marker from VWR, were used as protein standards. All gels were analyzed using the Image Lab 3.0 (BIO-RAD) analysis tool.

Molecular Docking. The interaction sites of HSA, IgG and transferrin with the IL ions were identified using the Auto-dock vina 1.1.2 program[30]. The crystal structures of HSA (PDB:1e71), IgG (PDB:1hzh) and Transferrin (PDB:1d3k) were used in the molecular docking, where the Auto DockTools (ADT)[31] was used to prepare the proteins input files by merging non-polar hydrogen atoms, adding partial charges and atom types. Ligand (IL ions) 3D atomic coordinates were computed by Gaussian 03w and ligand rigid root was generated using AutoDockTools (ADT), setting all possible rotatable bonds defined as active by torsions. The grid center at the center of mass (x-, y-, and z-axes, respectively) to cover the whole interaction surface of HSA was 94 Å × 64 Å × 90 Å, of IgG was 126 Å × 112 Å × 126 Å and of transferrin was 100 Å × 124 Å × 102 Å. The binding model that has the lowest binding free energy was searched out from 9 different conformers for each ligand (IL ions).

3.1.4. Results and discussion

Ecotoxicity of AGB-ILs. In order guarantee the development of more sustainable depletion procedures, the ecotoxicity of the AGB-based ILs was evaluated by exposition of aqueous solutions of each IL to marine bacterium *Vibrio fischeri.* EC_{50} values were determined after 5, 15 and 30 min of exposure applying different concentrations of ILs. The EC_{50} values obtained at 30 min are displayed in Figure 3.1.2. The EC_{50} data for 5 and 15 min, as well as the EC_{50} detailed data for 30 min, are given in Appendix E**.** After the exposure time of 30 min, the EC_{50} values of the synthesized GB-ILs decrease according to the following sequence: $[MepyrNC_4]Br > [Et_3NC_4]Br \approx [Pr_3NC_4]Br > [Bu_3NC_4]Br \approx [Pr_3NC_4][Pyr] > [Pr_3NC_4][Sac] \approx [Pr_3NC_4][Dca] > [Pr_3NC_4][Lac] \approx [Pr_3NC_2][Sal] > [Pr_3NC_4][Sal]$. Since not all GB-based ILs cations and anions are common there is a balanced effect of both ions in bacterium luminescence deactivation. All studied ILs share the common central atom (N); nevertheless, the different structures synthesized allow to evaluate the effect of the alkyl side chain length, cyclic *vs.* non-cyclic cations, and anion nature.

According to the results obtained (Figure 3.1.2.) the alkyl side chain length effect in the IL ecotoxic nature follows the rank: $[MepyrNC_4]Br < [Et_3NC_4]Br \approx [Pr_3NC_4]Br < [Bu_3NC_4]Br$. More

hydrophobic ILs, particularly with longer alkyl side chains, have a higher ability to interact and permeate within the membrane phospholipid bilayers, leading to a decrease on the *Vibrio fischeri* bioluminescence. In summary, ILs that exhibit longer alkyl side chains in their structure have a more toxic character, in agreement with the literature[32].

Figure 3.1.2. also depicts the ecotoxicity for ILs with a common cation and different anions, following the rank: $[Pr_3NC_4]Br$ < $[Pr_3NC_4][Pyr]$ < $[Pr_3NC_4][Sac]$ ≈ $[Pr_3NC_4][Dca]$ < $[Pr_3NC_4][Lac]$ < $[Pr_3NC_4][Sal]$. The addition of hydroxyl groups into AGB-ILs ($[Lac]^-$ *vs.* $[Pyr]^-$) increases the ecotoxic nature of ILs, in agreement with the literature [33]. The changes in the IL polarity induced by the addition of aromatic rings ($[Sal]^-$ *vs.* $[Lac]^-$) have no major effects towards the IL toxicity for *V. fischeri*. It should, however, be remarked that the toxic effect afforded by phenolic groups in the IL anion structure has not been well-understood[33]. Overall, in comparison to low-toxic and commercial ammonium based-ILs ($[N_{4444}]Br$)[34], as shown in Figure 3.1.2., most AGB-ILs prepared in this work display an even lower toxicity. All the synthesized ILs are classifiable as harmless or practically harmless according to Passino and Smith[35].

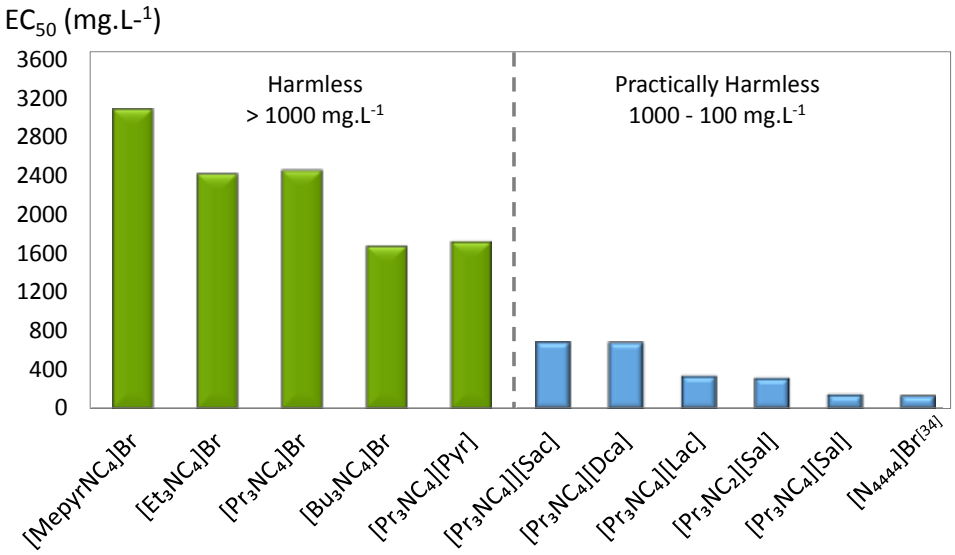

Figure 3.1.2. EC_{50} values, in mg L^{-1}, for 30 min of exposure of the marine bacteria *Vibrio fischeri* to IL aqueous solutions and values obtained from literature for $[N_{4444}]Br$ [34].

Phase diagrams and tie-lines. Novel phase diagrams for several ternary systems consisting of glycine-betaine IL analogues + water + $K_3C_6H_5O_7/C_6H_8O_7$ buffer (pH = 7.0) at 25°C and atmospheric pressure were determined. The respective phase diagrams are displayed in Figure 3.1.3 and Figure 3.1.4. The corresponding experimental data are available in the Appendix E. All values considering the weight fraction of the phase-forming components were carried out taking into account the complexed water in the citrate-based salt. In all ternary phase diagrams, the biphasic and

monophasic regions are above and below the solubility curve, respectively. Phase diagrams with the lowest area above the binodal curve correspond to ILs with a lower ability to undergo phase separation, *i.e.* the IL is less easily salted-out in aqueous solution[17]. Figure 3.1.3 also shows the phase diagrams for the commercial $[N_{4444}]Br$, under the same conditions. In general, most AGB-ILs here prepared present a higher ability to create ABS with $K_3C_6H_5O_7/C_6H_8O_7$ buffer (pH = 7.0) than commercial tetraalkylammonium-based ILs with similar alkyl chain, *i.e.*, they require a lower amount of IL and salt to undergo liquid-liquid demixing. The high hydrophobicity of ammonium-based ILs, and particularly of the AGB-ILs studied in this work, is reflected in the larger biphasic area of the respective systems.

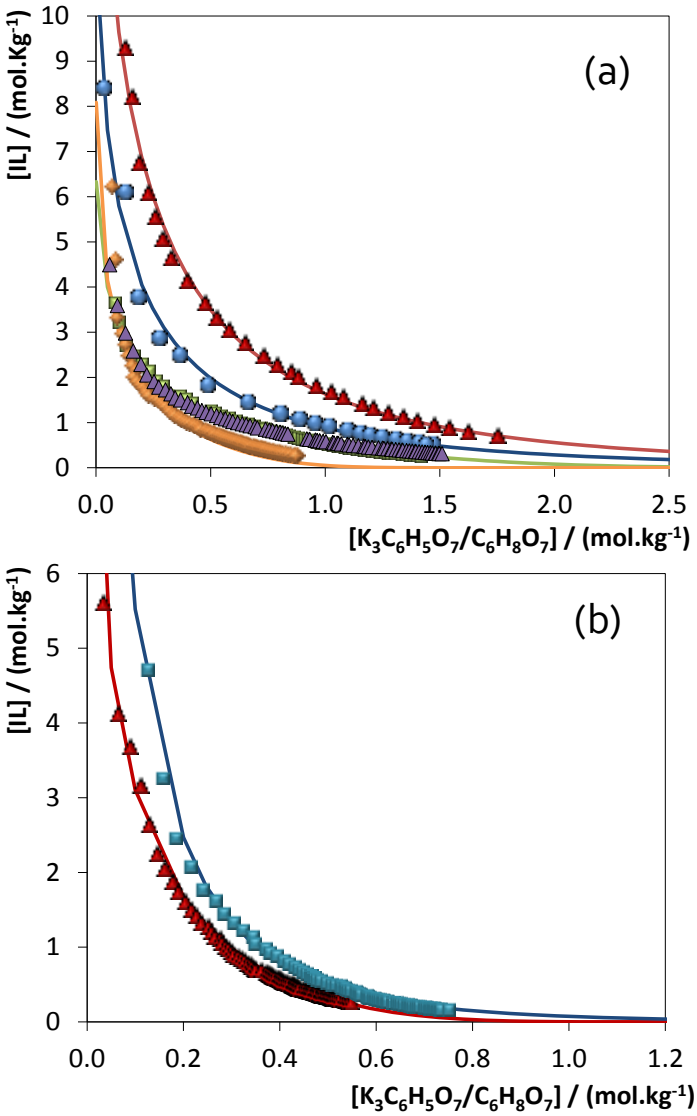

Figure 3.1.3. Phase diagrams for the systems composed of IL + $K_3C_6H_5O_7/C_6H_8O_7$ + H_2O at 25°C and pH 7.0: (a) $[MepyrNC_4]Br$ (▲); $[Et_3NC_4]Br$ (●); $[Pr_3NC_4]Br$ (■); $[Bu_3NC_4]Br$ (◆); $[N_{4444}]Br$ (▲)[37]; (b) $[Pr_3NC_2][Sal]$ (■); $[Pr_3NC_4][Sal]$ (▲); and adjusted binodal data through Equation 3.1.1. (—).

In Figure 3.1.3a are depicted the phase diagrams for the systems composed of $[Bu_3NC_4]Br$, $[Pr_3NC_4]Br$, $[Et_3NC_4]Br$ and $[MepyrNC_4]Br$, and in Figure 3.1.3b for $[Pr_3NC_2][Sal]$ and $[Pr_3PC_4][Sal]$, allowing the evaluation of the cation alkyl chain length for liquid-liquid demixing. The ability of AGB-ILs to form ABS with the citrate-based salt follows the order: $[Bu_3NC_4]Br$ > $[Pr_3NC_4]Br$ > $[Et_3NC_4]Br$ > $[MepyrNC_4]Br$. ILs that contain cations and/or anions with longer alkyl side chains are of a higher hydrophobicity (lower ability to form hydration complexes) and more easily undergo phase separation in aqueous solution, or are salted-out by the organic salt. Therefore, $[Bu_3NC_4]Br$ requires a lower amount of $K_3C_6H_5O_7/C_6H_8O_7$ to create an ABS. In the same line, $[Pr_3NC_2][Sal]$ displays a lower ability to promote ABS than $[Pr_3PC_4][Sal]$ (Figure 3.1.3b). The trend observed is in agreement with previous reports[28,36]. Furthermore, $[MepyrNC_4]Br$ displayed the lowest capacity to create ABS, due to a lower number of CH_2 groups than the remaining ILs shown in Figure 3.1.3a.

Figure 3.1.4 shows the IL anion nature impact on ABS formation, following the rank: $[Pr_3NC_4][Pyr]$ > $[Pr_3NC_4][Lac]$ > $[Pr_3NC_4]Br$ > $[Pr_3NC_4][Sal]$ ≈ $[Pr_3NC_4][Sac]$ > $[Pr_3NC_4][Dca]$. According to the results here presented, ABS formation is driven by the IL anion hydrogen-bond ability with water[38].

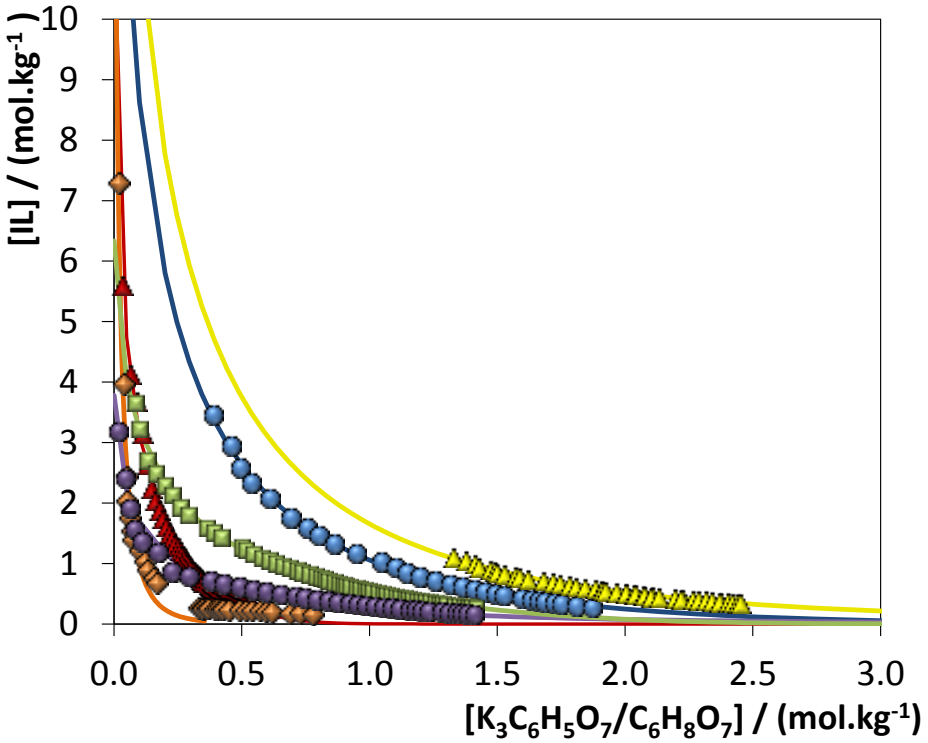

Figure 3.1.4. Phase diagrams for the systems composed of IL + $K_3C_6H_5O_7/C_6H_8O_7$ + H_2O at 25°C and pH 7.0: (a) $[Pr_3NC_4][Pyr]$ (▲); $[Pr_3NC_4][Lac]$ (●); $[Pr_3NC_4]Br$ (■); $[Pr_3NC_4][Sal]$ (▲); $[Pr_3NC_4]][Sac]$ (●); $Pr_3NC_4][Dca]$ (◆); and adjusted binodal data through Equation 3.1.1. (—).

In summary, the AGB-ILs here synthesized display two remarkable advantages when compared with commercial tetraalkylammonium-based ILs ([N_{4444}]Br): (i) most AGB-ILs display a higher ability to undergo phase separation in ABS; and (ii) most AGB-ILs display a lower ecotoxicity. These two features contribute to the development of more sustainable and biocompatible separation processes.

Table 3.1.1. Correlation parameters of Equation (3.1.1) used to describe the experimental binodal data at 25°C.

IL + salt + water					
IL	**Salt**	$A \pm \sigma$	$B \pm \sigma$	$10^5 (C \pm \sigma)$	R^2
[$MepyrNC_4$]Br	$K_3C_6H_5O_7$/ $C_6H_8O_7$	95.36 ± 2.44	-0.245 ± 0.009	1.79 ± 1.45	0.9994
[Et_3NC_4]Br		81.02 ± 4.04	-0.214 ± 0.020	2.29 ± 0.43	0.9915
[Pr_3NC_4]Br		81.40 ± 1.84	-0.264 ± 0.009	3.25 ± 0.23	0.9952
[Bu_3NC_4]Br		103.38 ± 2.52	-0.372 ± 0.011	6.92 ± 0.54	0.9937
[Pr_3NC_4][Pyr]		91.64 ± 1.465	-0.290 ± 0.007	2.78 ± 0.17	0.9904
[Pr_3NC_4][Lac]		128.16 ± 9.66	-0.268 ± 0.021	2.31 ± 0.01	0.9995
[Pr_3NC_2][Sal]		138.70 ± 8.83	-0.472 ± 0.027	0.21 ± 1.39	0.9985
[Pr_3NC_4][Sal]		108.30 ± 1.87	-0.403 ± 0.009	0.35 ± 1.08	0.9951
[Pr_3NC_4][Sac]		93.89 ± 2.70	-0.212 ± 0.020	3.11 ± 0.36	0.9939
[Pr_3NC_4][Dca]		126.75 ± 5.91	-0.875 ± 0.036	0.19 ± 5.50	0.9926

The experimental data corresponding to the solubility curves were fitted using Equation (3.1.1)**,** as shown in Figure 3.1.3. and Figure 3.1.4**.** The regression parameters estimated by least-squares regression, standard deviations (σ) and correlation coefficients (R^2) are given in Table 3.1.1**.** The experimental TLs in each system, along with their respective length, and at the compositions for which the depletion studies of HSA and IgG were conducted, are reported in Table 3.1.2**.**

Table 3.1.2. Experimental TLs and TLLs of the ABS composed of IL + $K_3C_6H_5O_7/C_6H_8O_7$ + H_2O at 25°C.

Weight fraction composition / (wt %)							
IL + $K_3C_6H_5O_7/C_6H_8O_7$ + water							
IL	**$[IL]_{IL}$**	**$[salt]_{IL}$**	**$[IL]_M$**	**$[salt]_M$**	**$[IL]_{salt}$**	**$[salt]_{salt}$**	**TLL**
$[MepyrNC_4]Br$	57.83	4.15	30.25	24.63	4.05	44.07	66.97
	59.63	3.66	30.38	29.17	0.79	54.98	78.07
$[Et_3NC_4]Br$	58.23	2.38	34.65	20.05	2.85	43.86	69.20
	76.07	0.09	30.02	29.57	1.51	47.83	88.54
$[Pr_3NC_4]Br$	66.80	0.56	39.73	20.18	0.30	48.75	82.13
	72.38	0.20	30.22	29.57	0.19	50.51	87.96
$[Bu_3NC_4]Br$	60.31	2.09	25.33	19.69	1.39	31.73	65.95
	62.76	1.80	29.64	29.53	$9.88E^{-05}$	54.35	81.85
$[Pr_3NC_4][Pyr]$	53.85	3.35	30.02	19.98	2.93	38.89	62.10
	68.09	1.05	30.26	30.31	0.15	53.60	85.89
$[Pr_3NC_4][Lac]$	57.88	8.49	32.93	22.38	9.07	35.67	55.87
	67.62	5.62	30.00	29.31	1.84	47.04	77.73
$[Pr_3NC_2][Sal]$	67.09	2.35	29.56	29.61	$2.90E^{-12}$	51.08	82.92
	61.34	2.95	29.01	16.16	0.11	27.97	66.14
$[Pr_3NC_4][Sal]$	71.14	1.08	19.81	20.59	$4.60E^{-03}$	28.12	76.10
	79.33	0.60	29.52	29.75	$5.12E^{-16}$	47.03	91.92
$[Pr_3NC_4][Sac]$	55.17	6.12	30.16	20.06	13.79	29.18	47.37
	80.30	0.54	29.62	29.99	0.94	46.65	91.79
$[Pr_3NC_4][Dca]$	64.59	0.59	20.11	15.63	2.15	21.70	65.91
	80.33	0.27	30.54	29.17	0.32	46.71	92.51

Depletion of human serum albumin (HSA) and Immunoglobulin G (IgG). The depletion efficiencies of HSA and IgG in all AGB-IL-based ABS were investigated for a common mixture composition in the biphasic area (30 wt% of AGB-IL, 30 wt% of $K_3C_6H_5O_7/C_6H_8O_7$ and 40 wt% of human serum). The results obtained are displayed in Figure 3.1.5. In all systems, the top phase is mostly constituted by IL and water, and the bottom phase by water and the citrate-based salt.

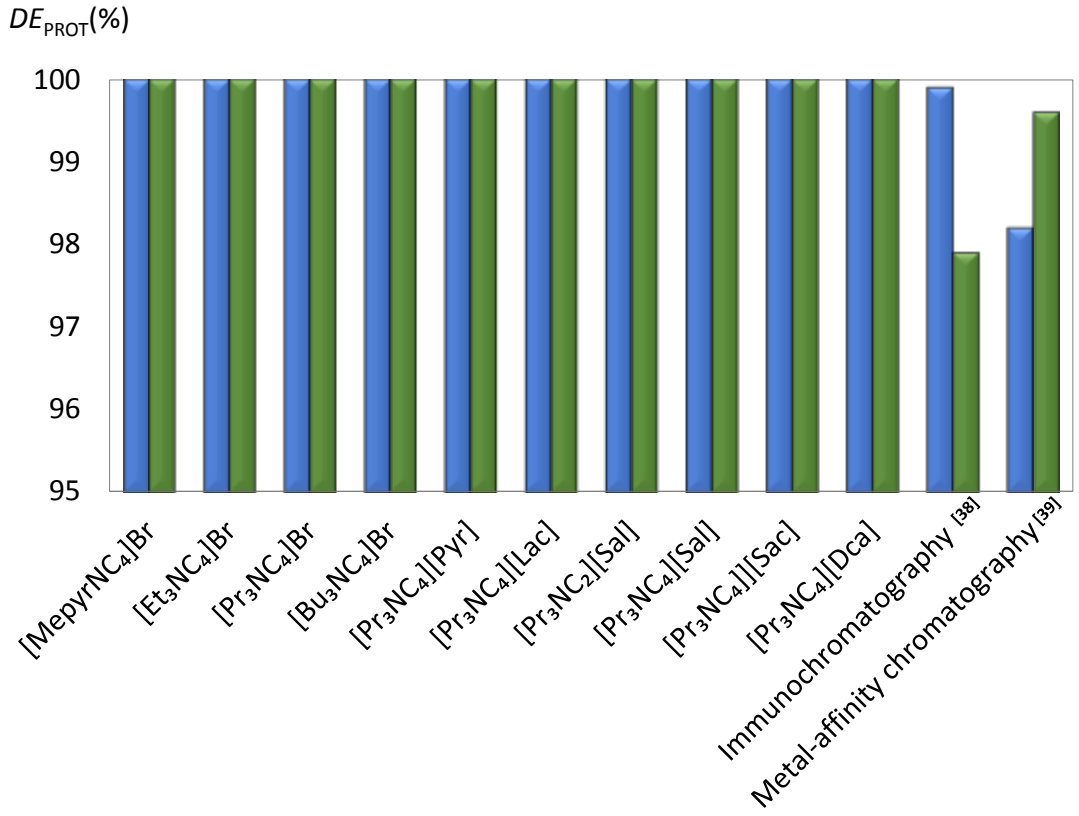

Figure 3.1.5. Depletion efficiency (DE_{PROT}%) of IgG (blue bars) and HSA (green bars) in ABS composed of 30 wt% of IL + 30 wt% of $K_3C_6H_5O_7/C_6H_8O_7$ at 25°C and pH = 7.0. The comparison with other protocols is also included: Dye-affinity chromatography (HSA) + immunochromatography (IgG)[39] and metal-affinity chromatography[39].

The ABS constituted by $[Pr_3NC_4][Sac]$ and $[Pr_3NC_4][Dca]$ lead to the creation of a large solid interphase that also jellifies the IL-rich phase. However, even in these ABS, HSA and IgG were not detected in the phases, at least at levels quantifiable by SE-HPLC with an UV detector. These ILs are amongst the most hydrophobic (according to the ILs ability to promote ABS displayed in Figure 3.1.4), with a low water content in the IL-rich phase at the studied mixture composition. This low water content seems to be the main reason behind the observed IL-rich phase jellification. Remarkably, all remaining ILs or ABS are able to precipitate the abundant serum proteins at the interphase and present well defined IL-rich and salt-rich phases. These show depletion efficiencies of 100% for HSA and IgG, obtained in a single-step. In all systems, the SE-HPLC chromatograms were applied for HSA and IgG quantification, which can confirm the absence of HSA and IgG at the IL-rich phase, as well as at salt-rich phase. The high hydrophobic nature of the ILs investigated seems to be the main responsible for the protein precipitation, favoring protein-protein interactions (protein-protein aggregation) in low water content environments, as shown before with other ABS[40].

The depletion efficiencies obtained by IL-based ABS are higher than those by traditional depletion methods[39,41], which are also shown in Figure 3.1.5 for comparison purposes. For instance, Altıntasü et al.[39,41] developed a modified poly-(glycidyl methacrylate) [poly(GMA)] monosize beads with chelated Cu^{2+} ions to remove IgG from human serum, for which the metal affinity adsorption method allows 98.2% of IgG depletion. However, this method needs to be combined with the anti-HSA antibody-Sepharose column. Vestergaard *et al.* also described IgG and HSA depletion protocols[39,41]. For the removal of HSA, the authors applied a dye-based method (Cibacron Blue 3G-A Sepharose (SB)), and for IgG an immunochromatography method (sepharose beads cross-linked with protein G (S-PG)). Even with a high depletion efficiency (> 97%), this method requires 2 steps to remove each of the highly abundant proteins in serum, namely IgG and HSA. Thus, the IL-based ABS here reported outstands as remarkable depletion methods able to simultaneously perform the depletion of two highly abundant proteins.

As previously mentioned, HSA and IgG were not found in the IL- and salt-rich phases; nevertheless. a low abundance protein was identified at the IL-rich phase (Figure 3.1.6). In order to guarantee the applicability of these new IL-based ABS for the pretreatment of samples for diagnosis purposes, the IL-rich phase was analyzed by SDS-PAGE. According to Figure 3.1.7, the protein present in IL-rich phase after the depletion procedure is identified as transferrin, according to the molecular weight and serum proteomic profile. Transferrin is a glycoprotein (679 amino acids) present in human serum (2.0–3.5 $g.mL^{-1}$) with a relevant physiological function that consists in iron transport[42]. Transferrin levels in human serum are higher for individuals with habits of alcohol consumption, being thus an important biomarker for alcohol abuse and dependence[43,44]. According to previous reports regarding the quantification of transferrin in human serum, sample preparation always required several steps and a long period of storage[45–47]. Attempting the development of a HPLC measurement procedure for transferrin glycoforms, Helanderi and co-workers developed a serum samples treatment procedure based on salt precipitation, storage at low temperature (overnight), and centrifugation[45,46]. In another work focused on transferrin quantification, a similar sample treatment procedure was applied[47]. Renner and Kanitz pretreated human serum samples before the transferrin quantification by ion-exchange chromatography, additionally requiring 2 more steps of storage and centrifugation[47]. Therefore, the outstanding results here reported with IL-based ABS constituted by biocompatible ILs and benign organic salts prove the remarkable potential of ABS for the depletion of abundant proteins from human serum in a single-step, allowing to identify other low-abundance proteins with potential as biomarkers.

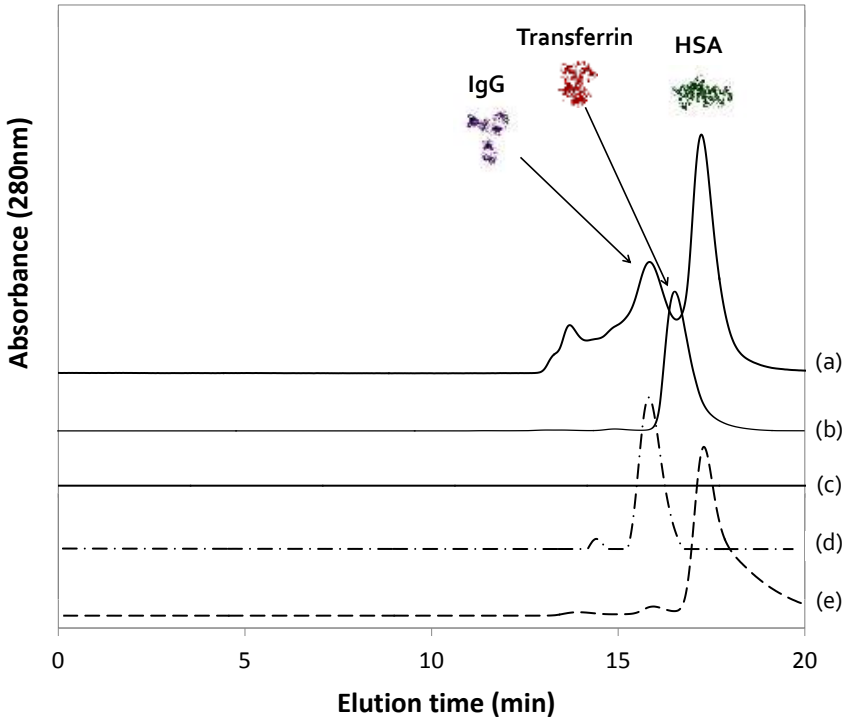

Figure 3.1.6. Size exclusion chromatography results of Human Serum (a); IL rich-phase (b); salt rich-phase (c); IgG standard solution (d); and HSA standard solution (e); corresponding to the ABS composed of $[Bu_3NC_4]Br$ (30 wt%) + $K_3C_6H_5O_7/C_6H_8O_7$ (30 wt%).

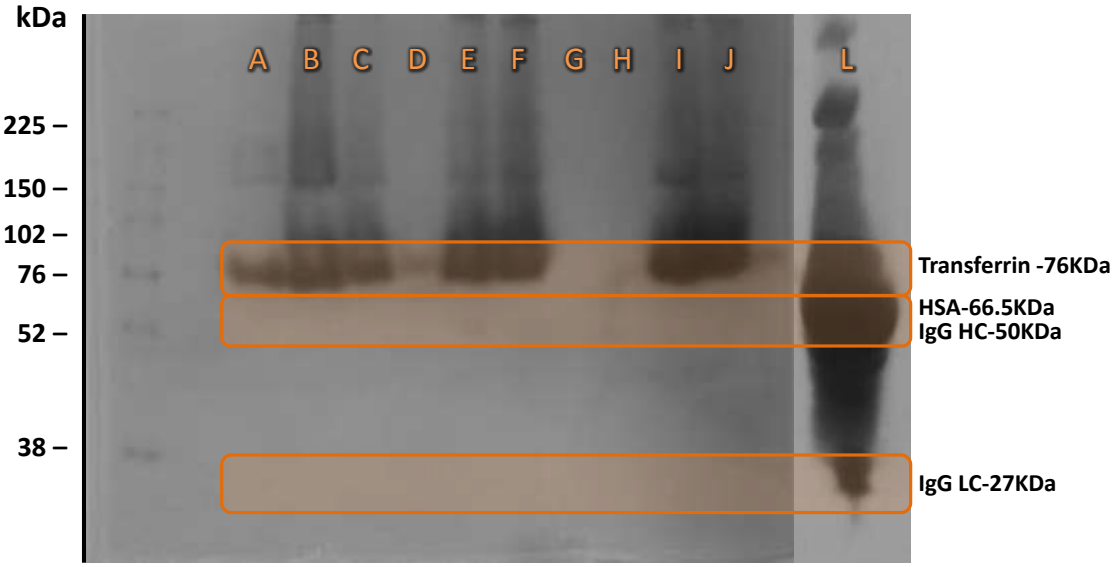

Figure 3.1.7. SDS-PAGE of proteins on IL-rich phase of the ABS composed of (a) $[MepyrNC_4]Br$ (b) $[Et_3NC_4]Br$, (c) $[Pr_3NC_4]Br$, (d) $[Bu_3NC_4]Br$, (e) $[Pr_3NC_4][Lac]$, (f) $[Pr_3NC_4][Pyr]$, (g) $[Pr_3NC_4]][Sac]$, (h) $[Pr_3NC_4][Dca]$, (i) $[Pr_3NC_4][Sal]$, (j) $[Pr_3NC_2][Sal]$ and (L) human serum in PBS (1:10 (v:v, human serum)).

Molecular Docking. The molecular docking of HSA, IgG and transferrin were carried out for each IL ion, in order to evaluate at a molecular level the preferential depletion of HSA and IgG over other proteins present in serum. The role of each IL cation and anion binding on HSA, IgG and transferrin surfaces were studied. The IL ions bind pose with lowest absolute value of affinity (kcal/mol) for HSA, IgG and transferrin with $[MepyrNC_4]^+$, $[Bu_3NC_4]^+$, $[Lac]^-$ and $[Dca]^-$ are displayed in Figures 3.1.8 and 3.1.9, while the pose for all others IL ions is shown in Apendix E. Moreover, the molecular interactions diagrams are displayed in Apendix E. The best binding pose and docking affinities, interacting amino acids residues, type of interaction and geometry distance (Å) of each ILs ions individually are also exhibited in the Apendix E. Molecular docking analysis was carried out in previous works providing specific insights on the molecular interactions occurring between IL ions and proteins[22,48,49].

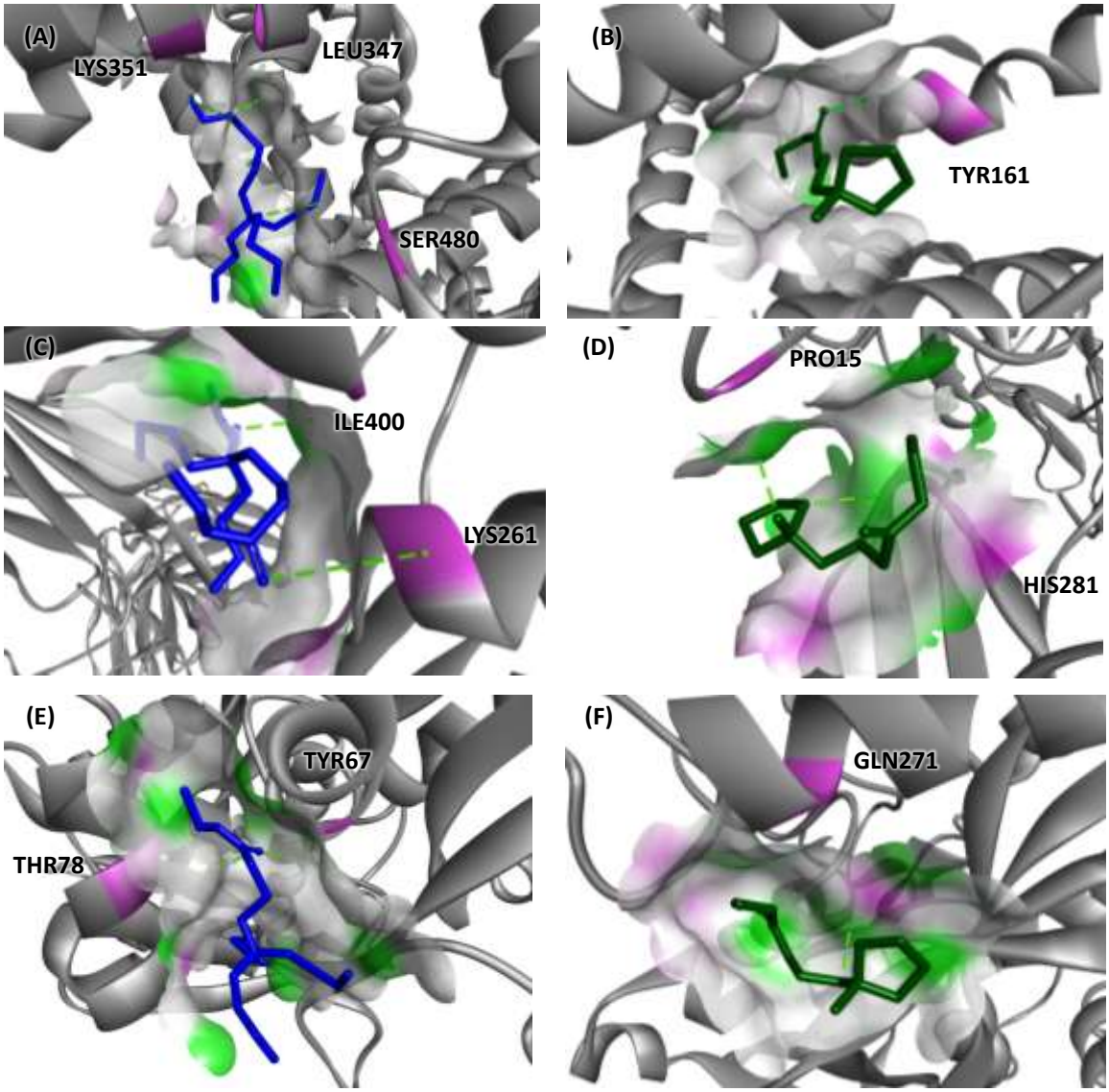

Figure 3.1.8. Molecular docking with AGB-IL cations of HSA and (a) $[MepyrNC_4]^+$ or (b) $[Bu_3NC_4]^+$; IgG and (c) $[MepyrNC_4]^+$ or (d) $[Bu_3NC_4]^+$; and Transferrin and (e) $[MepyrNC_4]^+$ or (f) $[Bu_3NC_4]^+$.

The bind pose with lowest absolute value of affinity (kcal/mol) for HSA, IgG and transferrin for $[Bu_3NC_4]^+$and $[MepyrNC_4]^+$ is shown in Figure 3.1.8 to demonstrate the effect of the most hydrophilic and hydrophobic IL cation (according to the data given in Figure 3.1.3) on protein stability. The IL cation docking affinities to HSA follow the rank: $[MepyrNC_4]^+$ > $[Et_3NC_4]^+$ = $[Pr_3NC_4]^+$ > $[Bu_3NC_4]^+$ > $[Pr_3NC_2]^+$; for IgG they are according to: $[Bu_3NC_4]^+$ > $[MepyrNC_4]^+$ > $[Pr_3NC_4]^+$ >$[Pr_3NC_2]^+$ > $[Et_3NC_4]^+$; and for transferrin they follow the order: $[MepyrNC_4]^+$ > $[Pr_3NC_4]^+$ > $[Bu_3NC_4]^+$ > $[Et_3NC_4]^+$ = $[Pr_3NC_2]^+$. No major differences have been found between the several IL cations and the several anions, with no well-defined trends found for the alkyl chain length effect. Therefore, the studied IL cations present similar interactions and interaction strength with HSA, IgG and Transferrin.

A molecular docking study was also carried out to investigate the binding affinity of the IL anions to HSA, IgG and transferrin. In Figure 3.1.9**.** are depicted the $[Lac]^-$ and $[Dca]^-$ docking bind poses, while the others anions docking bind poses are displayed in Appendix E. The IL anion binding energies for the 3 proteins follows the same rank: $[Sac]^-$ > $[Sal]^-$ > $[Lac]^-$ > $[Pyr]^-$ > $[Dca]^-$ > Br. All IL anions show preferential interactions by hydrogen-bonding with the proteins. In summary, the molecular docking results allow to conclude that no specific IL-protein interactions are responsible for the depletion of the highly abundant proteins. It seems that the low hydrated environment in the IL-rich phase combined with the high salting-out effect exerted by the salt mostly present at the bottom phase play the major role to promote protein-protein interactions and their precipitation. The ions in aqueous solution may disrupt the hydration layer on the protein surface, inducing the depletion of the highly abundant proteins in serum (HSA and IgG), enabling low abundant proteins, in particular Transferrin, to be maintained in the IL-rich phase.

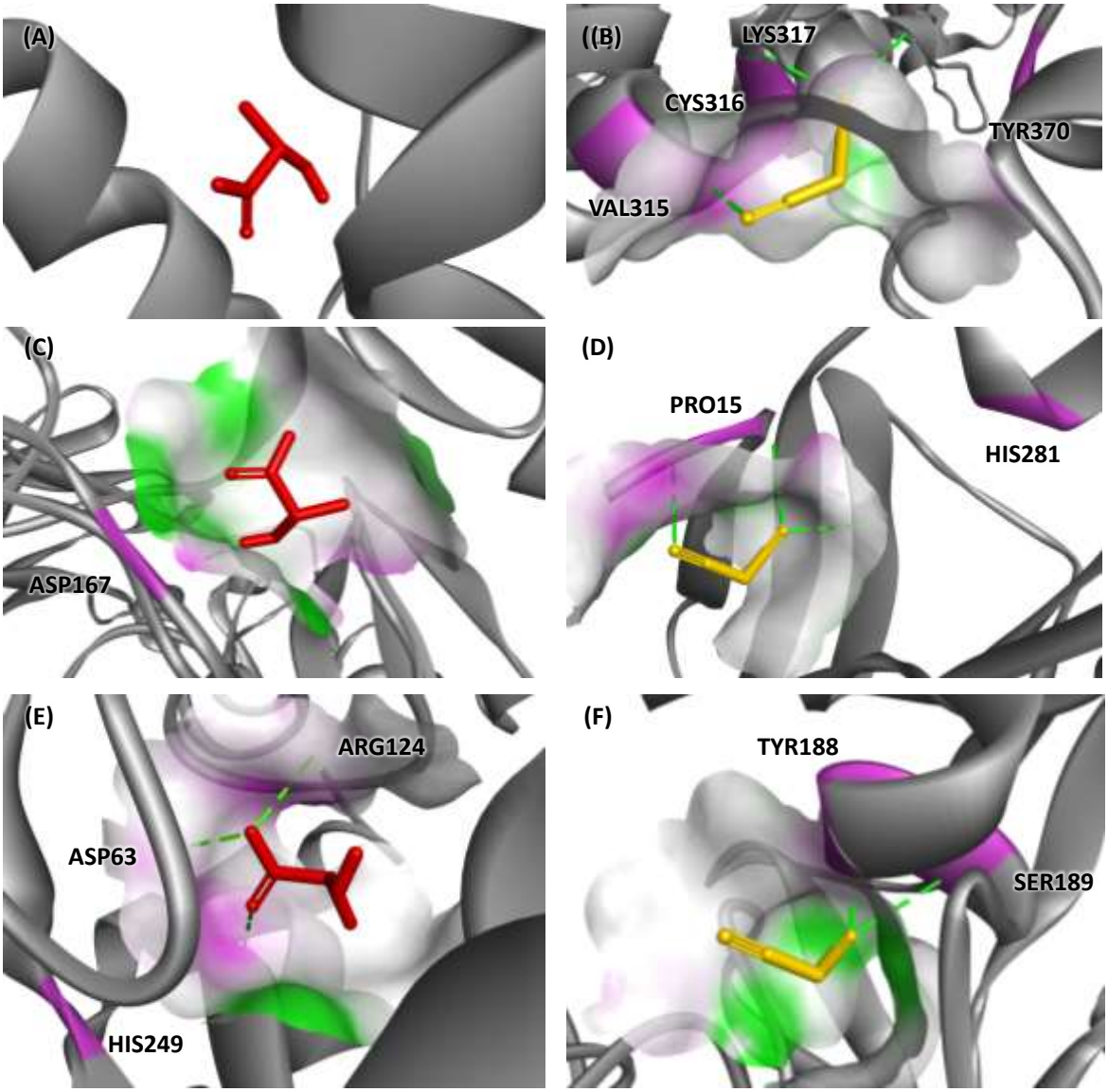

Figure 3.1.9. Molecular docking with AGB-IL cations for HSA and (a) $[Lac]^-$ or (b) $[Dca]^-$; for IgG and (c) $[Lac]^-$ or (d) $[Dca]^-$; and for transferrin and (e) $[Lac]^-$ or (f) $[Dca]^-$.

3.1.5. Conclusions

The depletion of HSA and IgG using a cost-effective method based on ABS formed by AGB-ILs and a salt is here proposed. Novel AGB-ILs were synthesized and characterized, and further used as phase-forming agents combined with $K_3C_6H_5O_7/C_6H_8O_7$ to create two-phase systems. The respective ABS phase diagrams, tie-lines and tie-line lengths were initially determined at 25°C. All studied ABS induce the simultaneous depletion of HSA and IgG. Remarkable depletion efficiencies of 100% of HSA and IgG were obtained in a single-step, allowing to identify low-abundance proteins in the IL-rich phase, such as transferrin. The IL-based ABS depletion method here developed provides higher depletion efficiencies and requires less steps than more traditional depletion methods. According to results here achieved, IL-based ABS represent a sustainable and cost-effective alternative for the pretreatment of biological samples.

3.1.6. References

1. Zhang ,Z., Bast, R.C.J., Yu, Y., Li, J., Soko,l.l.L.J., Ra,I.A.J., Rosenzweig, J.M., Cameron, B., Wang, Y.Y., Meng, X.Y., Berchuck, A., van Haaften-Day, C, Hacker, N.F., de Bruijn, H.W.A., van der Zee, A.G.J., Jacobs, I.J., Fung, E.T., Chan, D.W.. Cancer Res. 2004;64(16):5882-5890.
2. Coon, J.J., Zürbig, P., Dakna, M., Dominiczak, A.F., Decramer, S., Fliser, D., Frommberger, M., Golovko, I., Good, D.M., Herget-Rosentha, l.S., Jankowski, J., Julian, B.A., Kellmann, M., Kolch, W., Massy, Z., Novak, J., Rossing, K., Schanstra, J.P., Schiffer, E., Theodorescu, D., Vanholder, R., Weissinger, E.M., Mischak, H., Schmitt-Kopplin, P.. Proteomics - Clin Appl. 2008;2(7-8):964-973.
3. Anderson, N.L., Anderson, N.G.. Mol Cell Proteomics. 2002;1(11):845-867.
4. Henry, N.L., Hayes, D.F.. Mol Oncol. 2012;6(2):140-146.
5. Mayeux, R.. NeuroRx. 2004;1(2):182-188.
6. Ludwig, J.A., Weinstein, J.N.. Nat Rev Cancer. 2005;5(11):845-856.
7. Peng, J., Tang, F., Zhou, R., Xie, X., Li, S., Xie, F., Yu, P., Mu, L.. Acta Pharm Sin B. 2016;6(6):540-551.
8. Bormotova, E.A., Mil'man, B.L., Gupalova, T.V.. Prikl Biokhim Mikrobiol. 2015;51(3):354-360.
9. Fu, Q., Garnham, C.P., Elliott, S.T., Bovenkamp, D.E., Van Eyk, J.E.. Proteomics. 2005;5(10):2656-2664.
10. Björhall, K., Miliotis, T., Davidsson, P.. Proteomics. 2005;5(1):307-317.
11. Zolotarjova, N., Martosella, J., Nicol, G., Bailey, J., Boyes, B.E., Barrett, W.C.. Proteomics. 2005;5(13):3304-3313.
12. Mei, N., Seale, B., Ng, A.H.C., Wheeler, A.R., Oleschuk, R.. Anal Chem. 2014;86(16):8466-8472.
13. Kim, J., Shin, H., Kim, J., Kim, J., Park, J.. PLoS One. 2015;10(6):1-16.
14. Shin, H., Han, C., Labuz, J.M., Kim, J., Kim, J., Cho, S., Gho, Y.S., Takayama, S., Park, J.. Sci Rep. 2015;5:1-11.
15. Iqbal, M., Tao, Y., Xie, S., Zhu, Y., Chen, D., Wang, X., Huang, L., Peng, D., Sattar, A., Shabbir, M.A.B., Hussain, H.I., Ahmed, S., Yuan, Z.. Biol Proced Online. 2016;18:18.
16. Gutowski, K.E., Broker, G.A., Willauer, H.D., Huddleston, J.G., Swatloski, R.P., Holbrey, J.D., Rogers, R.D.. J Am Chem Soc. 2003;125(22):6632-6633.
17. Freire, M.G., Cláudio, A.F.M., Araújo, J.M.M., Coutinho, J.A.P., Marrucho, I,M,, Canongia Lopes, J.N., Rebelo, L.P.N.. Chem Soc Rev. 2012;41(14):4966-4995.
18. Crowhurst, L., Mawdsley, P.R., Perez-Arlandis, J.M., Salter, P.A., Welton, T.. Phys Chem Chem Phys. 2003;5(13):2790-2794.
19. Plechkova, N.V., Seddon, K.R.. Chem Soc Rev. 2008;37(1):123-150.
20. Huang, S., Wang, Y., Zhou, Y., Li, L., Zeng, Q., Ding, X.. Anal Methods. 2013;5(13):3395-3402.
21. Quental, M.V., Caban, M., Pereira, M.M., Stepnowski, P., Coutinho, J.A.P., Freire, M.G.. Biotechnol J. 2015;10(9):1457-1466.
22. Taha, M., Quental, M.V., Correia, I., Freire, M.G., Coutinho, J.A.P.. Process Biochem. 2015;50(7):1158-1166.
23. Hoffman, J.R., Ratamess, N.A., Kang, J., Rashti, S.L., Faigenbaum, A.D.. J Int Soc Sports Nutr. 2009;6:7.
24. Nsimba, Z.F., Paquot, M., Mvumbi, L.G., Deleu, M.. Biotechnol Agron Soc Environ. 2010;14(4):737-748.
25. A. Environmental, Carlbad CA, USA, 1998.
26. Mourão, T., Cláudio, A.F.M., Boal-Palheiros, I., Freire, M.G., Coutinho, J.A.P.. J Chem Thermodyn. 2012;54:398-405.
27. Passos, H., Trindade, M.P., Vaz, T.S.M., da Costa, L.P., Freire, M.G., Coutinho, J.A.P.. Sep Purif Technol.

2013;108:174-180.
28. Passos, H., Ferreira, A.R., Cláudio, A.F.M., Coutinho, J.A.P., Freire, M.G.. Biochem Eng J. 2012;67:68-76.
29. Merchuk, J.C., Andrews, B.A., Asenjo, J.A.. J Chromatogr B Biomed Sci Appl. 1998;711(1-2):285-293.
30. Trott, O., Olson, A.. J Comput Chem. 2010;31(2):455-461.
31. Morris, G., Huey, R.. J Comput Chem. 2009;30(16):2785-2791. doi:10.1002/jcc.21256.AutoDock4.
32. Stolte, S., Matzke, M., Arning, J., Boschen, A., Pitner, W.R., Welz-Biermann, U., Jastorff, B., Ranke, J.. Green Chem. 2007;9(11):1170-1179.
33. Ventura, S.P.M., e Silva, .F.A., Gonçalves, A.M.M., Pereira, J.L., Gonçalves, F., Coutinho, J.A.P.. Ecotoxicol Environ Saf. 2014;102:48-54.
34. Couling, D.J., Bernot, R.J., Docherty, K.M., Dixon, J.K., Maginn, E.J.. Green Chem. 2006;8(1):82-90.
35. Passino, D.R.M., Smith, S.B.. Environ Toxicol Chem. 1987;6(11):901-907.
36. Ventura, S.P.M., Sousa, S.G., Serafim, L.S., Lima, Á.S., Freire, M.G., Coutinho, J.A.P.. J Chem Eng Data. 2011;56(11):4253-4260.
37. Sintra, T.E., Cruz, R., Ventura, S.P.M., Coutinho, J.A.P.. J Chem Thermodyn. 2014;77:206-213.
38. Cláudio, A.F.M., Swift, L., Hallett, J.P., Welton, T., Coutinho, J.A.P, Freire, M.G.. Phys Chem Chem Phys. 2014;16(14):6593-6601.
39. Altintaş, E.B., Tüzmen, N., Uzun, L., Denizli, A.. Ind Eng Chem Res. 2007;46(23):7802-7810.
40. Pereira, M.M., Pedro, S.N., Quental, M.V., Lima, Á.S., Coutinho, J.A.P., Freire, M.G.. J Biotechnol. 2015;206:17-25.
41. Vestergaard, M., Tamiya, E.. Anal Sci. 2007;23(12):1443-1446.
42. de Jong, G., van Dijk, J.P., van Eijk, H.G. T. Clin Chim Acta. 1990;190(1):1-46.
43. Arndt, T.. Clin Chem. 2001;47(1):13-27.
44. Bortolotti, F., Paoli, G. de, Tagliaro, F.. J Chromatogr B. 2006;841(1):96-109.
45. Helander, A., Wielders, J., Anton, R., Arndt, T., Bianchi, V., Deenmamode, J., Jeppsson, J.O., Whitfield, J.B., Weykamp, C., Schellenberg, F.. Clin Chim Acta. 2016;459:19-24.
46. Helander, A., Wielders, J., Anton, R., Arndt, T., Bianchi, V., Deenmamode, J., Jeppsson, J.O., Whitfield, J.B., Weykamp, C., Schellenberg, F.. Clin Chim Acta. 2017;467:15-20.
47. Jeppsson, J.O., Kristensson, H., Fimiani, C.l. Clin Chem. 1993;39(10):2115-2120.
48. Taha, M., e Silva, F.A., Quental, M.V., Ventura, S.P.M., Freire, M.G., Coutinho, J.A.P.. Green Chem. 2014;16(6):3149.
49. Taha, M., Almeida, M.R., e Silva, F.A., Domingues, P., Ventura, S.P.M., Coutinho, J.A.P., Freire, M.G.. Chem - A Eur J. 2015;21(12):4781-4788.

3.2. Concentration of tumour biomarkers for an early-stage diagnosis of prostate cancer using ionic-liquid-based aqueous biphasic systems

This chapter is based on an unpublished work with the following authors involved

Matheus M. Pereira, João D. Calixto, Ana C. A. Sousa, Bruno J. Pereira, Álvaro S. Lima, João A. P. Coutinho and Mara G. Freire

3.2.1. Abstract

Prostate cancer (PCa) is the second most common type of cancer in men, being responsible for more than 300,000 annual deaths. Prostate specific antigen (PSA) quantification in serum is still the "gold standard" procedure for an initial screening on PCa. Immunoassays are commonly used for PSA quantification, therefore requiring an extensive sample processing and the use of sophisticated technical equipment, not available in all laboratories, particularly in those from developing nations where PCa mortality is higher. Furthermore, the current diagnosis methods require the collection of blood; yet, PSA also occurs in other biological fluids, including urine. This work aims to develop a cost-effective method for the extraction and concentration of PSA from urine samples using aqueous biphasic systems (ABS) composed of Good's buffers ionic liquids (GB-ILs). Initially, the phase diagrams of a set of aqueous biphasic systems were determined and their ability to extract PSA ascertained. The protein-friendly properties of GB-ILs were confirmed by molecular docking analysis, showing that the IL ions binding sites are far from the PSA catalytic center. After demonstrating that PSA can be completely extracted to the IL-rich phase in a single step, with no losses of protein, the applicability of the investigated ABS for the concentration of PSA was evaluated, first from model aqueous solutions and afterwards from urine samples. The obtained results demonstrated that it is possible to extract and concentrate PSA up to 250 times in a single-step. Given the high concentration factors achived, the quantification of PSA may be performed in urine samples using less expensive laboratory equipment and methods. Overall, these new ABS can be foreseen as alternative and cost-effective platforms for the extraction and concentration of cancer biomarkers from non-invasive samples (urine), while allowing their identification and quantification by more expedite equipment.

3.2.2. Introduction

Prostate cancer (PCa) is the second most common type of cancer in men and the fifth leading cause of cancer death worldwide, with the highest mortality rates found in the Caribbean and Southern and Middle Africa[1]. Age is considered the greatest risk factor[2,3] with 97% of PCa cases occuring in men over 50 years old. Thus, in an aging society, the incidence of PCa is likely to

Contributions: M.G.F. and J.A.P.C. conceived and directed this work. M.M.P. and J.D.C. acquired the experimental data. M.M.P., A.S.L, A.C.A.S., B.J.P., J.A.P.C. and M.G.F interpreted the experimental data. The manuscript was mainly written by M.M.P., A.C.A.S. and M.G.F. with significant contributions from the remaining authors.

increase. In order to decrease the burden associated with the increasing incidence of PCa, effective diagnosis and treatment monitoring are of utmost relevance.

In the last decades, the importance of biomarkers in cancer diagnosis and prognosis increased significantly[4]. A wide range of cancer biomarkers are currently used in clinical practice, and are approved by the Food and Drug Administration (FDA)[5]. For prostate cancer, the "gold standard" biomarker is the prostate-specific antigen (PSA). This glycoprotein, produced by the prostate gland, is usually found at higher levels in the blood of prostate cancer patients. It was approved by FDA as a biomarker of PCa in 1986 in the United States, and since then it has been used for the early-stage diagnosis of PCa. Over more recent years, conflicting studies have debated the accuracy of PSA as a biomarker, mainly as a consequence of overdiagnosis[6]. Nevertheless, PSA is still the most reliable clinical biomarker recurrently used in PCa diagnosis[7], before proceeding to more invasive diagnostic tests, such as transrectal ultrasound (TRUS) guided biopsy. Currently, there are several commercial techniques for the PSA quantification in blood samples, but they generally require the use of immunoassay-specific antibodies and skilled technical operators[8–11].

In addition to blood, PSA can also be found in other human fluids, including semen and urine. Some authors proposed the use of urinary PSA levels as a useful biomarker for the differential diagnosis of PCa, particularly when serum PSA levels are between 2.5 and 10 $ng.mL^{-1}$, the so called "grey zone", in which the differentiation between PCa and benign prostate hyperplasia (BPH) is difficult[12]. Furthermore, urine biomarkers possess a set of unique advantages, mainly associated to the non-invasive collection of urine, further reducing sampling costs and the need of trained personnel to collect samples. Thus, the evaluation of PSA levels in urine using simpler and cost-effective techniques is highly desirable for PCa screening. However, in order to quantify PSA using equipment not based on immunoassays, such as size-exclusion HPLC (SE-HPLC), it is necessary to perform the pretreatment of the urine sample to increase its levels. However, the total recovery and simultaneous concentration of PSA is not an easy task given the labile nature of proteins. In this context, it is required to find cost-effective alternatives to traditional liquid-liquid extraction strategies, which in the past mainly comprised organic-solvent-water systems or polymer-based aqueous biphasic systems (ABS)[13,14]. ABS are formed by two structurally different compounds that undergo phase separation when dissolved in water above given concentrations. Although these systems are seen as amenable media for proteins due to their high water content (up to 70-90%), they display a high viscosity, which hinders the mass transfer and also lead to a slower phase separation, and a limited polarity range between the two phases, hampering high

extraction efficiencies and high selectivity to be achieved in one-step. This limited tailoring of the phase polarities can be however overwhelmed by the introduction of ionic liquids (ILs) as phase-forming components of ABS[15–17]. ILs belong to the molten salts group (with melting temperatures below 100°C) and are usually constituted by a large organic cation and an inorganic/organic anion[18]. Due to their large chemical diversity and high number of possible cation-anion combinations, the ABS phases' polarities can be tailored by an appropriate choice of the IL ions[16]. Therefore, it is expected that IL-based ABS can be properly designed for the effective extraction of a multitude of proteins, while being able to keep their native form and stability. However, most of the ILs investigated up to date for the formation of IL-based ABS to carry out extraction of proteins are of low biocompatible nature and do not allow the pH control[16], a crucial request when aiming the total recovery and the stability maintenance of protein biomarkers such as PSA. To both increase the biocompatible nature and the control of the medium pH, ionic liquids derived from biological Good's buffers (GBs)[19–21], with self-buffering characteristics, appear as promising alternatives[22]. Up to date, no works have been published aiming the extraction of PSA (or other cancer biomarkers) with IL-based ABS, and to the best of our knowledge, there is only one work in which the PSA partition coefficient using polymer-based ABS[23] was addressed, but with limited results[23]. The main goal of this work is to develop a new pretreatment strategy for increasing the concentration of PSA from human urine samples using IL-based ABS, so that the cancer biomarker at the IL-rich phase may be detectable and quantified using less laborious techniques.

3.2.3. Experimental procedures

Materials. Potassium citrate tribasic monohydrate ($K_3C_6H_5O_7 \cdot H_2O$, purity ≥ 99 wt%) was obtained from Sigma-Aldrich Chemical Co. (USA). Prostate Specific Antigen from human semen (purity ≥ 95 %) was obtained from Sigma-Aldrich Chemical Co. Methanol (purity > 99.9%) was obtained from Fisher Scientific. Acetonitrile (purity > 99.7%) was supplied from Lab-Scan. The buffers required for the ILs synthesis, namely n-Cyclohexyl-2-aminoethanesulfonic acid (CHES, purity > 99 wt%), 4-(2-hydroxyethyl)-1-piperazineethanesulfonic acid (HEPES, purity > 99.5 wt%), 2-(N-morpholino)ethanesulfonic acid (MES, purity> 99 wt%), n-(Tri(hydroxymethyl)methyl)glycine (Tricine, purity > 99 wt%) and 2-[[1,3-dihydroxy-2-(hydroxymethyl)propan-2-yl]amino]ethanesulfonic acid (TES, purity > 99 wt%) were purchased from Sigma-Aldrich Chemical Co. The cation precursor, tetrabutylphosphonium hydroxide ($[P_{4444}][OH]$, 40 wt% in H_2O) was supplied by Sigma–Aldrich Chemical Co. Tetramethylsilane (TMS, purity > 99.9 wt%) and deuterium oxide (D_2O purity > 99.9 wt%) were obtained from Sigma–Aldrich Chemical Co. Purified

water passed through a reverse osmosis and a Milli-Q plus 185 water purifying system was used in all experiments. For the quantification of PSA using the BLItz Pro System, Super Streptavidin biosensors acquired from VWR were used.

Synthesis of Good-buffers-ionic liquids (GB-ILs). The GB-ILs ([P_{4444}][MES], [P_{4444}][TES], [P_{4444}][CHES], [P_{4444}][HEPES] and [P_{4444}][Tricine] – chemical structures and complete descriptions (given in Figure 3.2.1) were synthesized via neutralization of the base with the appropriate acid, according to previously reported protocols[22]. Briefly, a slightly excess of an equimolar aqueous solution (1:1.1) of buffer was added drop-wise to a tetrabutylphosphonium hydroxide solution. The mixture was stirred continuously for at least 12 h at room temperature (≈ 25°C) to produce the IL and water as by-product. The mixture was then subjected to 50-60°C under reduced pressure, resulting in a viscous liquid. A mixture of acetonitrile and methanol (1:1, v:v) was added and vigorously stirred at room temperature for 1 h. The solution was then filtered to remove any excess buffer. The organic solvents were evaporated and the GB-IL products dried under vacuum (10 Pa) for 3 days at room temperature. The water content in each GB-IL was measured by Karl-Fischer (KF) titration, using a KF coulometer (Metrohm Ltd., model 831) – data given in Appendix F. The chemical structures or purity of the GB-ILs were confirmed by ^{1}H and ^{13}C NMR spectroscopy (Bruker AMX 300) operating at 300.13 and 75.47 MHz, respectively. Chemical shifts are expressed in δ (ppm) using tetramethylsilane (TMS) as internal reference and D_2O as deuterated solvent. The ILs synthetized in this work showed high purity levels without signs of decomposition. The chemical structures of the synthesized ILs are shown in Figure 3.2.1., while the respective ^{1}H and ^{13}C NMR spectra are provided in Appendix F.

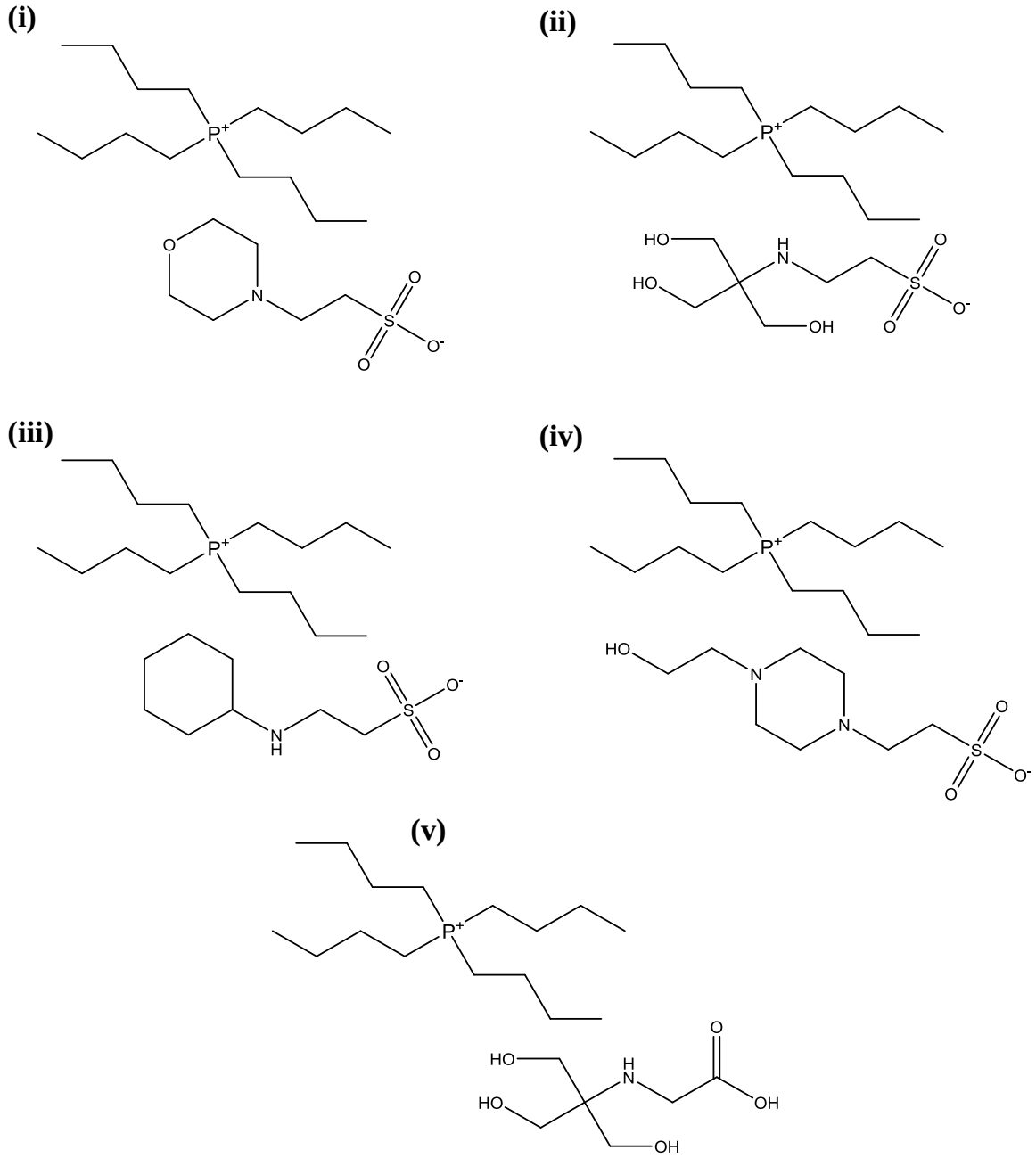

Figure 3.2.1. Chemical structures of the studied GB-ILs: (i) $[P_{4444}][MES]$; (ii) $[P_{4444}][TES]$; (iii) $[P_{4444}][CHES]$; (iv) $[P_{4444}][HEPES]$; (v) $[P_{4444}][Tricine]$.

Phase diagrams and tie-lines. To ascertain the mixture compositions required to form two-phase systems that can be used as extraction/concentration platforms, the binodal curve of each ABS were initially determined through the cloud point titration method[16] at 25°C (± 1°C) and atmospheric pressure. Aqueous solutions of $K_3C_6H_5O_7$ at *circa* 60 wt % and aqueous solutions of the different ILs (≈ 80 wt %) were prepared and used for the determination of the binodal curves, followed by the drop-wise addition of water until the finding of the monophasic region. The

opposite procedure also was carried out to better describe the binodal curves, particularly at the salt-rich region, which is of extreme relevance to deal with ABS as concentration strategies. The ternary system compositions were determined by weight quantification within ± 10^{-4} g. The experimental binodal curves at 25°C were fitted by Equation (3.2.1)[24]:

$$[IL] = Aexp[(B[salt]^{0.5}) - (C[salt]^3)] \quad (3.2.1)$$

where $[IL]$ and $[salt]$ are the IL and the salt weight fraction percentages, respectively, and A, B, and C are constants obtained by the regression of the experimental data.

Tie-lines (TLs), *i.e.* the composition of each phase for a given initial mixture composition at the biphasic region, were determined through the solution of the following system of four equations (Equation (3.2.2) to (3.2.5)) with four unknown values ($[IL]_{\mathrm{IL}}$, $[IL]_{\mathrm{salt}}$, $[salt]_{\mathrm{IL}}$ and $[salt]_{\mathrm{salt}}$):

$$[IL]_{salt} = Aexp\left[\left(B[salt]_{IL}^{0.5}\right) - \left(C[salt]_{IL}^{3}\right)\right] \quad (3.2.2)$$

$$[IL]_{salt} = Aexp\left[\left(B[salt]_{salt}^{0.5}\right) - \left(C[salt]_{salt}^{3}\right)\right] \quad (3.2.3)$$

$$[IL]_{IL} = \frac{[IL]_M}{\alpha} - \frac{1-\alpha}{\alpha}[IL]_{salt} \quad (3.2.4)$$

$$[salt]_{IL} = \frac{[salt]_M}{\alpha} - \frac{1-\alpha}{\alpha}[salt]_{salt} \quad (3.2.5)$$

where the subscripts "IL", "salt" and "M" represent the top and the bottom phases and the mixture composition, respectively. The parameter α is the ratio between the weight of the top phase and the weight of the overall mixture. The respective tie-line lengths (TLLs were determined by Equation (3.2.6):

$$TLL = \sqrt{([salt]_{IL} - [salt]_{salt})^2 + ([IL]_{IL} - [IL]_{salt})^2} \quad (3.2.6)$$

Extraction of Prostate Specific Antigen (PSA) using IL-based ABS. An initial screening on the several ILs performance and mixture compositions was carried out, particularly to appraise the ABS ability to extract PSA from aqueous solutions without protein losses. To this end, different ABS, involving all the prepared ILs, and two mixture compositions (30 wt% salt + 30 wt% IL + 40 wt% H_2O and 30 wt% salt + 40 wt% IL + 30 wt% H_2O) were studied to evaluate the effect of the

concentration of the phase-forming components. Aqueous solutions of PSA at concentrations *circa* 50 ng.mL^{-1} were used as the "water" added to each ABS. The used PSA concentration was chosen after optimization using the BLItz® Pro system. This type of quantification was chosen since it allows also to address the PSA stability and activity, since only active PSA binds with PSA-antibody. After, a careful separation of the phases was performed and the amount of PSA in each phase was quantified using the BLItz® Pro system equipment, by an external standard calibration method using protein concentrations ranging from 1 to 100 ng.mL^{-1} (calibration curve given in Appendix F)**.** At least three independent ABS were prepared and 2 samples of each phase quantified. The percentage extraction efficiency of PSA ($\boldsymbol{EE_{PSA}}\%$) is the percentage ratio between the amount of PSA in the IL-rich aqueous phase to that in the total mixture, and is defined according to Equation (3.2.7)**:**

$$EE_{\mathrm{PSA}}\% = \frac{w_{PSA}^{IL}}{w_{PSA}^{IL} + w_{PSA}^{Salt}} \times 100 \qquad (3.2.7)$$

where w_{PSA}^{IL} and w_{PSA}^{Salt} are the total weight of PSA in the IL-rich and in the salt-rich aqueous phases, respectively. In all systems the top phase corresponds to the IL-rich phase whereas the bottom phase is mainly constituted by the salt and water.

***Lever-arm Rule*.** The lever-arm rule was used to determine the weight percentages ratio of the coexisting phases in the respective phase diagrams for given mixture compositions. Several extractions were carried out at different compositions in the same TL, allowing to work with different concentration factors. A fixed and long TL was initially selected, and the lever-arm rule was used to determine the weight fraction of each phase-forming component (IL and $K_3C_6H_5O_7$) to be used in each extraction corresponding to a given concentration factor (*CF*). The CF is defined as the ability along the same TL to maintain the composition of each phase while varying only the volume or weight ratio of the phases. Several ternary mixtures were prepared within the biphasic region with the "theoretical" weight percentages of salt, IL and H_2O/PSA, corresponding to *CF* of 5, 20, 50, 100, 150, 200 and 250-fold. ABS were first prepared as a control without adding PSA, and once achieved the *CF* of 250-fold, the extractions were performed adding an aqueous solution of PSA at a concentration of 150 ng. mL^{-1} (the cut-off value found in urine[12]). Each mixture was vigorously stirred, centrifuged for 10 min, and left to equilibrate for at least 10 min at (25 ± 1)°C.

Size-exclusion HPLC (SE-HPLC). After a careful separation of the phases, both were analyzed by SE-HPLC. Each phase was diluted at a 1:9 (v:v) ratio in a phosphate buffer solution before injection. A Chromaster HPLC (VWR Hitachi) was used. The SE-HPLC was performed on an analytical column Shodex Protein KW- 802.5 (8 mm x 300 mm). A 100 mM phosphate buffer + NaCl 0.3 M was run isocratically with a flow rate of 0.5 $mL.min^{-1}$. The column oven and autosampler temperatures were kept at 25°C and at 10°C, respectively. The injection volume was 25 µL. The wavelength was set at 280 nm using a DAD detector. The obtained chromatograms were treated and analyzed using the OriginPro8 software.

Molecular Docking. The interaction sites of PSA with the GB-ILs ions were identified using the Auto-dock vina 1.1.2 program[25]. The crystal structure of PSA (PDB:1hrc) was adapted and used in the molecular docking. Auto DockTools (ADT)[26] was used to prepare the protein input files by merging non-polar hydrogen atoms, adding partial charges and atom types. Ligand (GB-IL cation and anions) 3D atomic coordinates were computed by Gaussian 03w and ligand rigid root was generated by AutoDockTools (ADT), setting all possible rotatable bonds defined as active by torsions. The grid center at the center of mass (x-, y-, and z-axes, respectively) to cover the whole interaction surface of PSA was 86 Å × 100 Å × 86 Å. The binding model that has the lowest binding free energy was searched out from 9 different conformers for each ligand (GB-ILs cation and anions).

3.2.4. Results and discussion

Phase diagrams and tie-lines. The ABS phase-diagrams at 25°C and at atmospheric pressure, for the systems composed of water, $K_3C_6H_5O_7$ and GB-ILs, are illustrated in Figure 3.2.2. The experimental data are shown in weight fraction to allow a direct screening of the mixture compositions required to form two-phase systems to further carry out the PSA extraction and concentration.

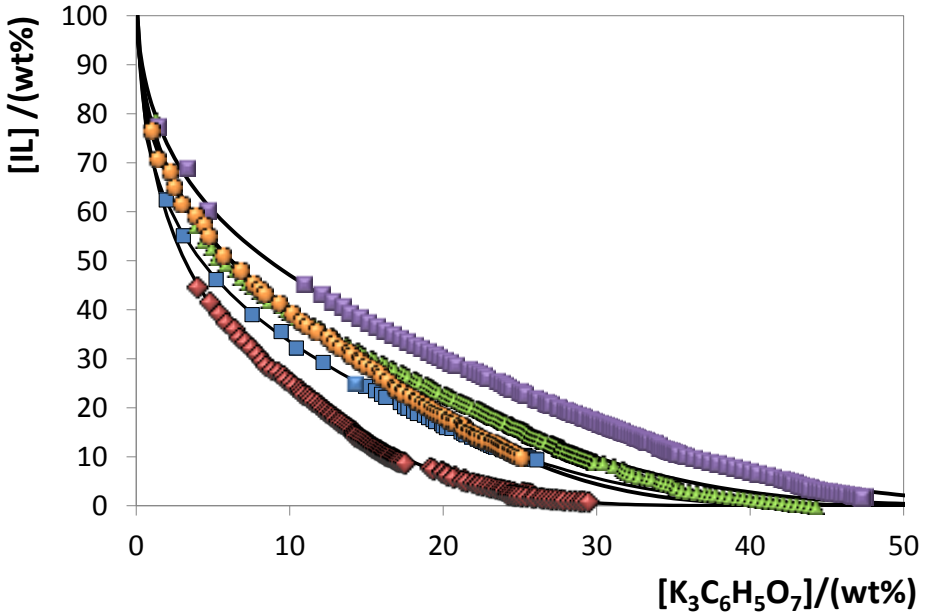

Figure 3.2.2. Phase diagrams for the systems composed of GB-IL + $K_3C_6H_5O_7$ + H_2O at 25°C: $[P_{4444}]$[Tricine] (■); $[P_{4444}]$[HEPES] (▲); $[P_{4444}]$[TES] (●); $[P_{4444}]$[MES] (■); $[P_{4444}]$[CHES] (◆); and adjusted binodal data through Equation 3.2.1 (—).

In all ABS, the biphasic region is positioned above the solubility curve while the monophasic region is localized below. Diagrams with the largest area above the binodal curve have therefore a higher ability to form two phases, *i.e*. the IL is more easily salted-out by the salt. The citrate-based salt used is composed of a trivalent charged anion and is a strong salting-out species according to the Hofmeister series[27]. Therefore, it has a high affinity for water, and thus, there is a preferential exclusion of the IL ions from the aqueous solution, promoting the two-phases separation.

Since the salt, temperature, pressure and pH are constants in the studied two-phase systems, the ABS formation ability is a result of the type of IL. For instance, at 10 wt% of $K_3C_6H_5O_7$, the ability of GB-ILs to create ABS follows the order: $[P_{4444}]$[CHES] > $[P_{4444}]$[MES] > $[P_{4444}]$[HEPES] ≈ $[P_{4444}]$[TES] > $[P_{4444}]$[Tricine]. The ILs investigated are formed by a tetrabutylphosphonium ($[P_{4444}]^+$) cation and GB-derived anions. The cation is the same for all the investigated ILs and its effect cannot be appraised from the obtained phase diagrams. However, it was already demonstrated that $[P_{4444}]$-based ILs display a high ability to promote the phase split when compared with ammonium-, pyridinium- and imidazolium-based ionic liquids[28]. $[P_{4444}]$-based salts have highly shielded charges, located mostly on the heteroatom surrounded by four alkyl chains, thus leading to a higher tendency towards their salting-out from aqueous media. On the other hand, the anions have a higher aptitude for creating hydration complexes because they are more polarizable and present more diffuse valence electronic distribution[29]. This means that anions,

when compared with cations, have a more relevant influence in ABS formation and behavior. Anions with lower hydrogen-bond basicity values present lower ability to form coordinative hydrogen-bonds and to create hydration complexes, and therefore are more easily salted-out by conventional salts[29]. The hydrogen-bond basicity values for the ILs used in this work have not been reported up to date; yet, relevant conclusions can be achieved using the octanol-water partition coefficients (*K*ow) of each GB. The higher the value of log(*K*ow) the higher the affinity of the anion for the octanol-rich phase, meaning that it has a lower affinity for the water-rich phase and to be hydrated. In this context, higher log(*K*ow) values correspond to anions that are more easily separated by a salting-out phenomenon. As expected, the ILs composed of anions with –OH groups and lower values of log(*K*ow) ([Tricine]$^-$: -5.25; [TES]$^-$: -4.48; [HEPES]$^-$: -3.11)[30] are those that correspond to ILs that are more distant from the axis in Figure 3.2.2. Thus, these GB-ILs require higher amounts of salt for phase separation. On the other hand, GBs with no –OH groups display higher log(*K*ow) values ([MES]$^-$: -2.48; [CHES]$^-$: -0.59)[30] reflecting their lower aptitude to hydrogen-bond with water and higher ability for liquid-liquid demixing in ABS.

The detailed experimental data corresponding to the ternary phase diagrams with the compositions of the coexisting phases are presented in Appendix F. For the studied systems, the experimental binodal data were fitted by the empirical relationship described by Equation (3.2.1). The regression parameters *A*, *B* and *C*, were estimated by the least-squares regression method, and their values and corresponding standard deviations (σ), as well as the respective tie-lines and tie-line lengths are provided in Table 3.2.1. and Table 3.2.2.

Table 3.2.1. Correlation parameters of Equation (3.2.1) used to describe the experimental binodal data at 25°C.

IL + salt + water					
IL	**Salt**	$A \pm \sigma$	$B \pm \sigma$	$10^5 (C \pm \sigma)$	R^2
$[P_{4444}][MES]$	$K_3C_6H_5O_7$	98.33 ± 0.54	-0.327 ± 0.022	3.96 ± 0.06	0.9996
$[P_{4444}][CHES]$		111.92 ± 2.49	-0.450 ± 0.009	10.50 ± 0.44	0.9929
$[P_{4444}][HEPES]$		105.17 ± 1.19	-0.295 ± 4.257	2.78 ± 0.08	0.9978
$[P_{4444}][Tricine]$		105.15 ± 5.10	-0.248 ± 0.016	1.71 ± 0.02	0.9992
$[P_{4444}][TES]$		99.63 ± 0.51	-0.356 ± 0.007	5.40 ± 0.29	0.9971

Table 3.2.2. Experimental TLs and TLLs of the ABS composed of IL + $K_3C_6H_5O_7$ + H_2O at 25°C.

Weight fraction composition / (wt %)							
IL + $K_3C_6H_5O_7$ + water							
IL	**$[IL]_{IL}$**	**$[salt]_{IL}$**	**$[IL]_M$**	**$[salt]_M$**	**$[IL]_{salt}$**	**$[salt]_{salt}$**	**TLL**
$[P_{4444}][MES]$	65.71	1.51	29.42	20.48	2.89	34.36	70.89
	90.81	0.06	29.36	30.33	0.37	44.12	100.60
	94.29	0.01	30.21	39.87	$0.27.10^{-3}$	58.64	111.04
$[P_{4444}][CHES]$	67.45	1.26	29.70	19.83	0.11	34.38	75.04
	75.58	0.76	29.64	30.25	0.17×10^{-4}	49.27	89.81
	93.56	0.16	30.11	39.95	0.18×10^{-8}	58.83	110.44
$[P_{4444}][HEPES]$	57.51	4.14	29.89	20.14	6.59	33.63	57.80
	83.11	0.63	30.24	29.49	0.95	46.00	93.84
	90.97	0.24	29.72	40.13	0.03	59.46	108.52
$[P_{4444}][Tricine]$	52.11	7.75	30.08	24.73	4.42	44.50	60.20
	70.02	2.64	30.45	29.71	2.53	48.78	81.75
	94.31	0.19	29.78	40.11	0.54	58.20	110.26
$[P_{4444}][TES]$	50.61	5.97	30.28	19.70	0.39	39.87	60.59
	93.58	0.05	30.69	29.89	0.08	44.32	103.45
	96.00	0.02	30.43	39.48	0.11×10-3	57.80	112.05

Extraction and concentration of prostate specific antigen (PSA). The extraction efficiencies of PSA in ABS composed of $[P_{4444}][GB]$ + $K_3C_6H_5O_7$ at given mixture compositions are shown in Table 3.2.3. PSA was added to each system as an aqueous solution at a concentration *circa* 50 $ng.mL^{-1}$. The obtained results show the absence of PSA in the bottom phase, demostrating that PSA is completely extracted to the top phase (IL-rich) in all the studied systems. Furthermore, only small losses of PSA were obtained. In fact, because PSA is a labile protein some denaturation is possible. Nevertheless, as displayed in Appendix F the mass balance of protein reveals losses of PSA below 10%. Given that only those systems with the lowest losses (<5%) were selected for the future concentration step, these values are negligible and will not have an impact in the PSA quantification by SE-HPLC. To optimize the procedure, several ABS without PSA were prepared at different compositions along the same TLL (Figure 3.2.3) in order to reduce the IL-rich phase and to attain the required *CF*. The representation of each system with the corresponding TLs and real *CF* is depicted in Appendix F. With the exception of $[P_{4444}][Tricine]$, concentration factors up to

250-fold were achieved for all the IL-based ABS investigated. $[P_{4444}][Tricine]$ is the most hydrophilic GB-IL used in this work and, the respective phase diagram is the farthest from the axis. Consequently, it has a smaller biphasic region and the theoretical information provided by the lever-arm rule is only valid up to concentration factors of 150-fold.

Table 3.2.3. Extraction efficiency of PSA (EE_{PSA}%) at 25° C in the ABS composed of ILs and $K_3C_6H_5O_7$.

IL	Weight fraction composition / (wt %)		*EE*PSA%
	$[IL]_{IL}$	$[salt]_{IL}$	
$[P_{4444}][MES]$	30.35 ± 0.15	30.84 ± 0.53	100
	30.01 ± 0.04	40.03 ± 0.14	100
$[P_{4444}][CHES]$	30.13 ± 0.25	30.54 ± 0.63	100
	29.94 ± 0.13	40.12 ± 0.57	100
$[P_{4444}][HEPES]$	30.16 ± 0.35	30.44 ± 0.29	100
	30.09 ± 0.34	39.97 ± 0.27	100
$[P_{4444}][Tricine]$	30.90 ± 0.28	30.70 ± 0.31	100
	30.37 ± 0.17	39.98 ± 0.07	100
$[P_{4444}][TES]$	29.95 ± 0.24	30.08 ± 0.69	100
	30.63 ± 0.37	39.85 ± 0.17	100

After validating the *CF* achievable with each system, the procedure was repeated by adding an aqueous solution of PSA (at 150 ng/mL) for the mixtures able to lead to a *CF* of 250. These mixture compositions allow to reduce the volume of the IL-rich phase down to a minimum capable of concentrate PSA in a factor of interest while allowing its detection and quantification by SE-HPLC. *CFs* of 250-fold were also achieved in the presence of PSA for all ABS, except for that composed of $[P_{4444}][Tricine]$. The *CFs* were experimentally confirmed by weighting both the IL-rich phase and the aqueous solutions containing PSA (Appendix F). For comparison the HPLC spectrum of an aqueous solution of pure PSA is also provided, with the PSA peak appearing 13.5 minutes under the operational conditions used (Figure 3.2.5**)**. The HPLC peak corresponding to PSA is not seen in the bottom phase of any extraction. However, the system composed of $[P_{4444}][Tricine]$ results in no peak of PSA detectable by HPLC since the *CF* of 250-fold was not achieved with this system. In addition, a tendency is clearly seen in the HPLC spectra; the peak intensity, and thus, the PSA concentration, decreases in the following order: $[P_{4444}][CHES] > [P_{4444}][MES] > [P_{4444}][TES] > [P_{4444}][HEPES] > [P_{4444}][Tricine]$. This trend is in close agreement with the PSA losses discussed before and that depend on the hydrophobic character of each IL. It is possible to see that the

most intense peak corresponds to the more hydrophobic IL, $[P_{4444}][CHES]$, with the highest log(*Kow*) value and thus this IL is the most promising one to be used in PSA extraction and concentration from real urine samples.

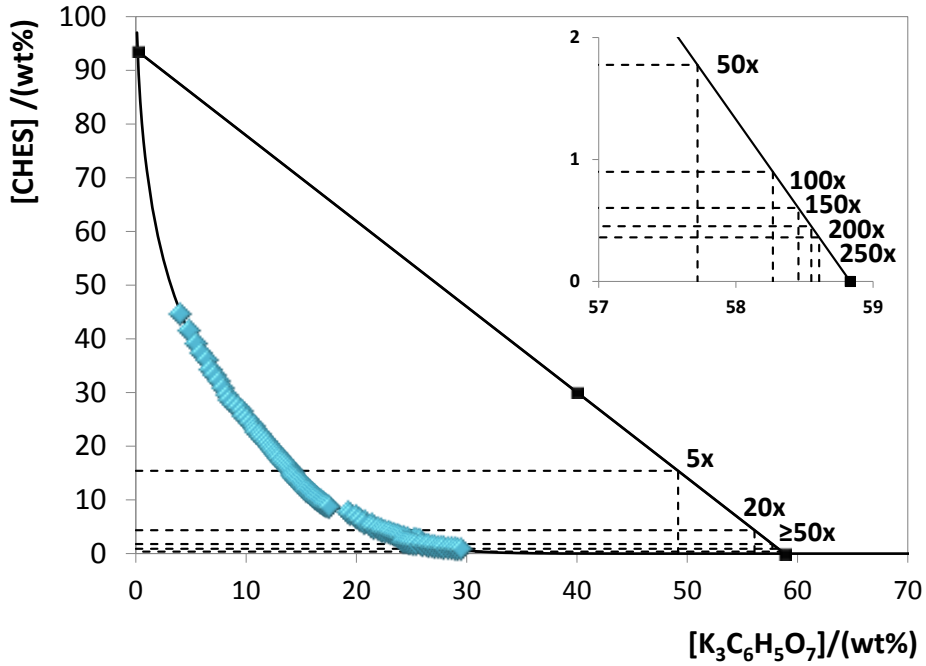

Figure 3.2.3. Schematic representation of lever-arm rule for the systems composed of $[P_{4444}][MES]$ + $K_3C_6H_5O_7$ + H_2O at 25°C, and adjusted binodal data through Equation (3.2.1) (—).

Molecular docking. Aiming at elucidating the molecular interactions that drive the remarkable extraction efficiency of PSA to IL-rich phase, it was carried out a molecular docking analysis. Binding sites of each GB-IL ions in PSA were selected from the lowest binding energy structure amongst 9 different chemical conformers. PSA is a 30 kDa serine protease (kallikrein family)[31], with a proteolytic mechanism based on three amino acids (HIS57/ASP102/SER195) that constitute PSA catalytic triad[32].

The lowest absolute value of affinity bind pose (kcal/mol) for all GB-ILs ions ($[P_{4444}]^+$,$[CHES]^-$, $[MES]^-$, $[TES]^-$, $[HEPES]^-$ and $[Tricine]^-$) and the molecular interactions diagrams are exhibited in Appendix F. The best binding pose and docking affinities, interacting amino acids residues, type of interaction and geometry distance (Å) of each GB-IL ion also are provided in Appendix F. All GB-ILs studied in this work are constitued by a coomom tetrabutylphosphonium-based cation; therefore, the docking affinity values of GB-ILs on PSA were ranked according to IL anion, following the sequence: $[TES]^- > [MES]^- > [CHES]^- > [HEPES]^- > [Tricine]^-$. According to docking affinity values, all anions present higher binding energies than $[P_{4444}]^+$ (-3.1 kcal/mol), with exception of $[Tricine]^-$ that displays the same docking affinity energy (Appendix F).

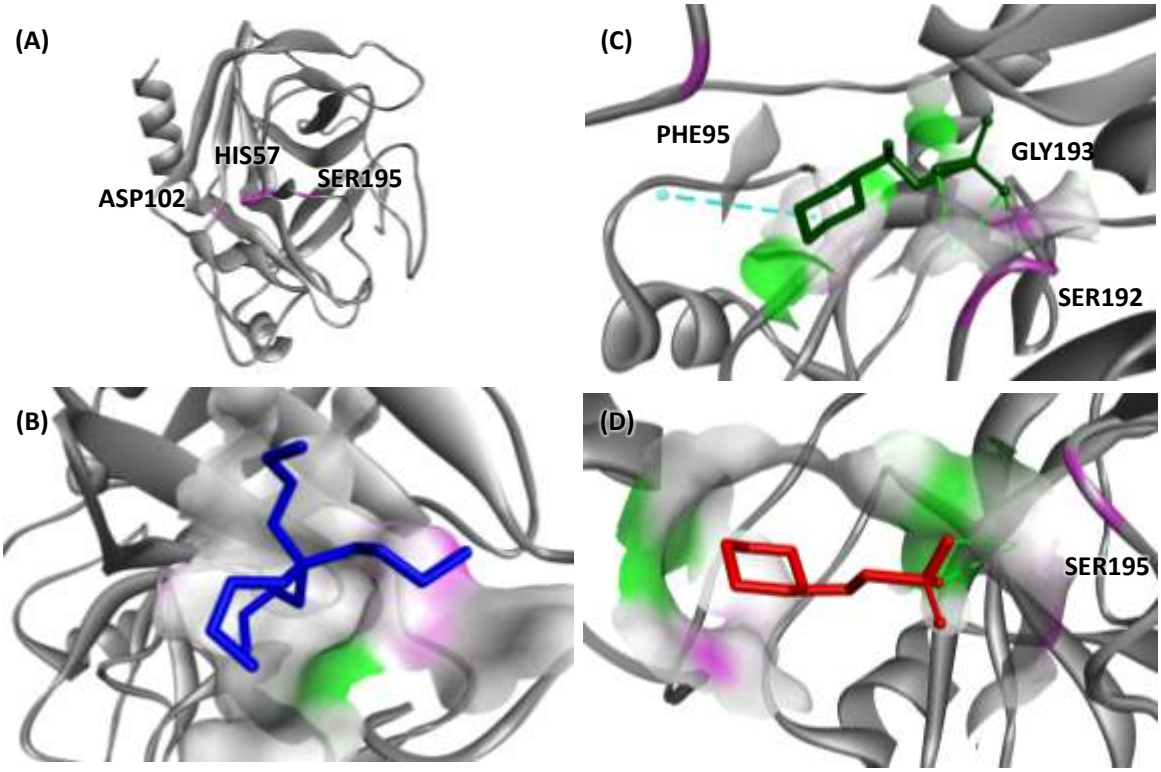

Figure 3.2.4. Catalytic triad and molecular docking of PSA with GB-IL ions: (a) PSA Catalytic triad, (b) $[P_{4444}]^+$, (c) $[CHES]^-$, and (d) $[MES]^-$.

The specific interactions (hydrogen bonding, electrostatic and hydrophobic interactions) between the GB-IL ions and PSA amino acids residues were also analyzed by molecular docking. In Figure 3.2.4 the PSA catalytic triad and binding of $[P_{4444}]^+$ and $[CHES]^-$ are displayed. According to the results obtained, GB-IL anions bind amino acids residues not surrounding the PSA catalytic triad, with the exception of $[MES]^-$ that binds in SER195. On the other hand, in Figure 3.2.4c the $[CHES]^-$ best binding position is also presented. $[CHES]^-$ binds adjacent to PHE95, SER192 and GLY193. The anions $[TES]^-$, $[CHES]^-$, $[HEPES]^-$ and $[Tricine]^-$ display binding sites in amino acids residues that do not affect the PSA stability (Appendix F). Overall, the molecular docking results disclose that the synthesized GB-ILs do not exibit specific interactions with the PSA catalytic site, being therefore protein-friendly.

Extraction and concentration of prostate specific antigen (PSA) from human urine. It has been demonstrated that PSA can be concentrated up to 250-fold in ABS composed of $K_3C_6H_5O_7$ and $[P_{4444}][CHES]$, $[P_{4444}][MES]$, $[P_{4444}][HEPES]$ or $[P_{4444}][TES]$. However, HPLC analyses of the IL-rich phase reveal a tendency for obtaining higher peaks with the ABS composed of more hydrophobic

GB-ILs, meaning lower losses of protein. Taking into account these results, $[P_{4444}][CHES]$ was the IL selected to extract and concentrate (*CF* = 250) PSA from real human urine samples.

At first we analyzed PSA in pure water and afterwards we evaluated the extraction and concentration of PSA in real human urine samples donated by healthy volunteers (male and female). The top and the bottom phases were analyzed by SE-HPLC, together with a sample of pure PSA in water and human urine for terms of comparison. Because women do not produce PSA, the female urine sample maybe regarded as a negative control. As expected, the analysis of the female urine sample revealed no peak in both phases (see Appendix F). The SE-HPLC profile of pure PSA in water, of human urine from a healthy man and of the top and bottom phases of an extraction performed with $[P_{4444}][CHES]$ + salt + urine is depicted in Figure 3.2.5. The peak of standard PSA in aqueous solution appears at 13.5 min. No peak corresponding to PSA can be observed in the urine sample (Figure 3.2.5b) from a healthy male donor as its levels cannot be identified by SE-HPLC. Remarkably, after extraction and concentration, the PSA peak is clearly seen in the top phase of the $[P_{4444}][CHES]$-based ABS (Figure 3.2.5.c), while it is not found in the respective bottom phase (Figure 3.2.5.d). Therefore, PSA from healthy male donors has been extracted to the GB-IL-rich phase and concentrated up to a factor that allows it to be analyzed by SE-HPLC.

The HPLC profiles also revealed that there is another small peak, between 16 and 17 min. A previous study already revealed a similar profile of PSA by SE-HPLC, where this small band was identified as bPSA[33]. PSA is a glycoprotein that can be found in different forms, and the levels of those different forms and their respective ratio have been used in PCa differential diagnosis [33]. Thus, our system composed of GB-ILs is able not only to concentrate PSA but also bPSA which opens new perspectives for the use of IL-GB-based ABS in PCa differential diagnosis.

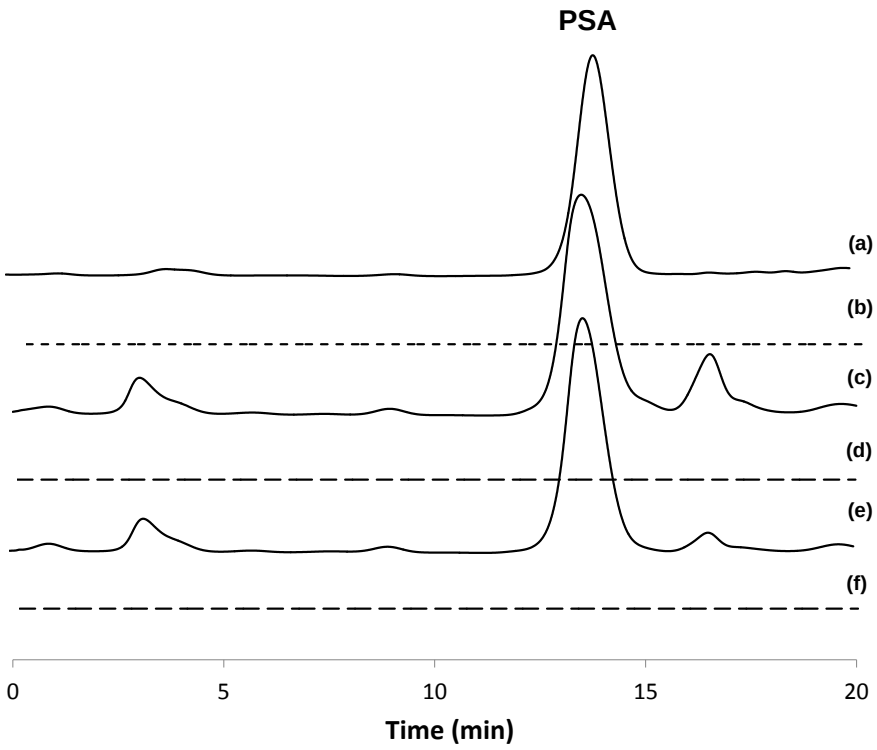

Figure 3.2.5. SE-HPLC profile of pure PSA in aqueous solution, human urine (from a healthy male donor) and in the top and bottom phases of an ABS composed of $[P_{4444}][CHES]$ + salt + human urine: (a) PSA in aqueous solution (150 mg/ml); (b) Urine sample; (c) IL rich-phase (pure urine); (d) Salt rich-phase (pure urine); (e) IL rich-phase (150 ng/mL of PSA added to urine); (f) Salt rich-phase (150 ng/mL of PSA added to urine).

3.2.5. Conclusions

In this work we described the ability of IL-based ABS to act as concentration platforms of PSA from urine samples. GB-ILs were synthesized and the respective phase diagrams, tie-lines and tie-line lengths were determined. The ability of GB-ILs to form ABS follows the order: $[P_{4444}][CHES]$ > $[P_{4444}][MES]$ > $[P_{4444}][HEPES]$ ≈ $[P_{4444}][TES]$ > $[P_{4444}][Tricine]$. In all the studied ABS systems, PSA migrates to the IL-rich phase. Remarkable extraction efficiencies of 100% were obtained in a single-step. Molecular docking results demonstrate that GB-ILs do not interact with the PSA catalytic site and therefore are protein-friendly. The most promising ABS were finally used to concentrate PSA from human urine samples, for which a concentration factor was successfully achieved allowing its quantification by more expedite equipment. Furthermore, the urine samples pretreatment with ABS allowed to detect a peak that probably corresponds to different forms of PSA. The possibility to extract and concentrate different PSA forms with IL-based ABS opens an exciting new possibility for future research on the prostate cancer differential diagnosis.

3.2.6. References

1. Torre, L.A., Bray, F., Siegel, R.L., Ferlay, J., Lortet-tieulent, J., Jemal, A.. CA a cancer J Clin. 2015;65(2):87-108.
2. Hodson, R... Nature. 2015;528(7582):118-119.
3. Siegel, R.L., Miller, K.D., Jemal, A.. CA Cancer J Clin. 2015;65(1):5-29.
4. Cameron, S.J.S., Lewis, K.E., Beckmann, M., Allison, G.G., Ghosal, R., Lewis, P.D., Mur, L.A.J.. Lung Cancer. 2016;94:88-95.
5. Füzéry, A.K., Levin, J., Chan, M.M., Chan, D.W.. Clin Proteomics. 2013;10(1):13.
6. Sohn, E.. Nature. 2015;528(7582):120-122.
7. Stephan, C., Ralla, B., Jung, K. Biochim Biophys Acta - Rev Cancer. 2014;1846(1):99-112.
8. Kalyvas, M., Zammit, S., Chem, C.. Clin Chem. 1996;42(5):675-684.
9. Peter, J., Unverzagt, C., Lenz, H., Hoesel, W.. Anal Biochem. 1999;273(1):98-104.
10. Oh, S.W., Kim, Y.M., Kim, H.J., Kim, S.J., Cho, J.S., Choi, E.Y.. Clin Chim Acta. 2009;406(1-2):18-22.
11. Poon, C., Chan, H., Li, H.. Sensors Actuators B Chem. 2014;190:737-744.
12. Bolduc, S., Lacombe, L., Naud, A., Grégoire, M., Fradet, Y., Tremblay, R.R.. Can Urol Assoc J. 2007;1(4):377-381.
13. Pereira, D.Y., Chiu, R.Y.T., Zhang, S.C.L., Wu, B.M., Kamei, D.T.. Anal Chim Acta. 2015;882:83-89.
14. Mashayekhi, F., Meyer, A.S., Shiigi, S.A., Nguyen, V., Kamei, D.T.. Biotechnol Bioeng. 2009;102(6):1613-1623.
15. Gutowski, K.E., Broker, G.A., Willauer, H.D., Huddleston, J.G., Swatloski, R.P., Holbrey, J.D., Rogers, R.D.. J Am Chem Soc. 2003;125(22):6632-6633.
16. Freire, M.G., Cláudio, A.F.M., Araújo, J.M.M., Coutinho, J.A.P., Marrucho, I.M., Canongia Lopes, J.N., Rebelo, L.P.N.. Chem Soc Rev. 2012;41(14):4966-4995.
17. Pereira, J.F.B., Rebelo, L.P.N., Rogers, R.D., Coutinho, J.A.P, Freire, M.G.. Phys Chem Chem Phys. 2013;15(45):19580-19583.
18. Seddon, K.R.. Nat Mater. 2003;2(6):363-365.
19. Taha, M., e Silva, F.A., Quental, M.V., Ventura, S.P.M., Freire, M.G., Coutinho, J.A.P.. Green Chem. 2014;16(6):3149.
20. Lee, S.Y., Vicente, F.A., e Silva, F.A., Sintra, T.E., Taha, M., Khoiroh, I., Coutinho, J.A.P., Show, P.L., Ventura, S.P.M.. ACS Sustain Chem Eng. 2015;3(12):3420-3428.
21. Taha, M,, Almeidam M.R., e Silva, F.A., Domingues, P., Ventura, S.P.M., Coutinho, J.A.P., Freire, M.G.. Chem - A Eur J. 2015;21(12):4781-4788.
22. Taha, M., Quental, M.V., e Silva, F.A., Capela, E.V., Freire, M.G., Ventura, S.P.M, Coutinho, J.A.P.. J Chem Technol Biotechnol. 2017;92(9):2287-2299.
23. Taylor, P., Fedotoff, O., Mikheeva, L.M., Chait, A., Uversky, V.N., Boris, Y.. J Biomol Struct Dyn. 2012;29(5):1051-1064.
24. Merchuk, J.C., Andrews, B.A., Asenjo, J.A.. J Chromatogr B Biomed Sci Appl. 1998;711(1-2):285-293.
25. Trott, O., Olson, A.. J Comput Chem. 2010;31(2):455-461.
26. Morris, G., Huey, R.. J Comput Chem. 2009;30(16):2785-2791.
27. Pegram, L.M., Record, M.T.. J Phys Chem B. 2007:5411-5417.
28. Bridges, N.J., Gutowski, K.E., Rogers, R.D.. Green Chem. 2007;9(2):177.
29. Ventura, S.P.M., Neves, C.M.S.S., Freire, M.G., Marrucho, I.M., Oliveira, J., Coutinho, J.A.P.. J Phys Chem B. 2009;113(27):9304-9310.
30. Mourão, T., Cláudio, A.F.M., Boal-Palheiros, I., Freire, M.G., Coutinho, J.A.P.. J Chem Thermodyn. 2012;54:398-405.
31. Suzuki, K., Kise, H., Nishioka, J., Hayashi, T.. Semin Thromb Hemost. 2007;33(1):46-52.
32. Watt, K.W., Lee, P.J., M'Timkulu, T., Chan, W.P., Loor, R.. Proc Natl Acad Sci U S A. 1986;83(10):3166-3170.
33. Mikolajczyk, S.D., Millar, L.S., Wang, T.J., Rittenhouse, H.G., Wolfert, R.L., Marks, L.S., Song, W., Wheeler, T.M., Slawin, K.M.. Urology. 2000;55(1):41-45.

3.3. Extraction of lactate dehydrogenase (LDH) from human serum using ionic-liquid-based systems

This chapter is based on an unpublished work with the following authors involved

Matheus M. Pereira, Sónia N. Pedro, João A. P. Coutinho and Mara G. Freire

3.3.1. Abstract

Most cancer biomarkers are proteins and their accurate quantification in human serum is a difficult task due to the presence of highly abundant proteins, such as human serum albumin (HSA) and immunoglobulin G (IgG). Therefore, in order to accurately quantity biomarkers the deplection of high abundant proteins is necessary. In this work, a series of liquid-liquid systems, in particular aqueous biphasic systems (ABS) composed of phosphonium-based ionic liquids (ILs) and buffered aqueous solutions of $K_3C_6H_5O_7/C_6H_8O_7$ (pH=7.0), were investigated as novel extraction/purification platforms for Lactate Dehydrogenase (LDH), a prognostic biomarker of melanoma, lung cancer, prostate cancer, osteosarcoma and kidney cell carcinoma, from human serum. ABS were evaluated through their ability to simultaneously promote the HSA and IgG depletion and the extraction of LDH. According to results here reported, IL-based ABS lead to a complete depletion of HSA and IgG and to the extraction of LDH to the IL-rich phase in a single-step, allowing a better identification and quantification of the cancer biomarker and thus contributing to more accurate cancer diagnosis and prognosis.

3.3.2. Introduction

Cancer is one of the worldwide leading causes of death, with approximately 14 million new cases each year[1]. By 2012, 8.2 million deaths have been reported, being this number expected to increase up to 70% in the next two decades[2]. Given these values, in the last years, the interest on the use of biological markers to evaluate the risk of cancer has significantly increased, accompanied by the search on new and more specific biomarkers[3]. These biomolecules can be used for the patient's helath assessment in multiple clinical settings, including diagnosis, in the estimation of the disease risk, to distinguish between benign and malignant tumours, and in the prognosis and follow-up of patients who have been diagnosed with cancer[4]. Cancer biomarkers can be detected in several biological fluids, such as whole blood (and serum or plasma), urine, saliva and tears, for which threshold values usually exist and are well-established[5,6]. In addition to the research of more specific and reliable biomarkers, the development of pretreatment strategies of human fluids is also an area of increasing interest. These pretreatment strategies by

Contributions: M.G.F. and J.A.P.C. conceived and directed this work. M.M.P. and S.N.P. acquired the experimental data. M.M.P., J.A.P.C. and M.G.F interpreted the experimental data. The manuscript was mainly written by M.M.P., J.A.P.C. and M.G.F. with significant contributions from the remaining authors.

increasing the accuracy in biomarker quantification will avoid a significant number of false-positive results and as a consequence unnecessary biopsies, and underestimated or overtreatment[7].

Within the cancer biomarkers, lactate dehydrogenase (LDH) is usually associated with several anaerobic types of cancer, such as myeloma, lung cancer, prostate cancer, osteosarcoma and kidney cell carcinoma, and is particularly used in prognosis[8–11]. In these cancer types, LDH levels in biological fluids increase due to the upregulation of LDH by tumor cells and by tumor cell necrosis, causing the spillover of the enzyme into bloodstream[12]. Therefore, contrarily to normal levels in healthy patients serum, which range between 100 and 300 U/L, levels higher than 300 U/L might be associated with cancer[13]. Currently, the LDH enzyme is quantified by kinetic assay systems under reversible reactions[14]. Although spectrophotometric assays are easy to perform and robust, they have some limitations. The reading must occur in the first seconds of reaction after adding the serum samples since most of the times all NADH is consumed before the first reading[15]. Furthermore, interferences display a significant role over the kinase activity when dealing with biological fluids[16]. Therefore, preliminary steps of sample preparation, such as protein precipitation are usually performed[17]. Based on the exposed, there is an essential need for the development of alternative pretreatment strategies to avoid interferences of the main proteins present in serum samples when the identification and quantification of cancer biomarkers is required for diagnosis and prognosis.

Aqueous biphasic systems (ABS) constituted by ionic liquids (ILs) have recently emerged as new platforms for the extraction and purification of biomolecules of interest, such as proteins[18]. IL-based ABS have been reported for the extraction of lysozyme, trypsin, myoglobin, bovine serum albumin, peroxidase, cytochrome c, γ-globulins, hemoglobin, among others, without compromising the enzymatic activity or the protein stability[19,20]. Although most of these works are focused on providing high extraction abilities while keeping the proteins stability, in a previous work[21] we found that ABS formed by phosphonium-based ILs are capable not only of extracting proteins of interest, but also of selectively denaturating proteins, like albumin. These results support the idea that it is possible to tailor the IL chemical structure and ABS composition to induce the precipitation of target proteins from complex matrices. ILs composed of chaotropic ions were already used in the pretreatment of liquid biological sample to the analysis of xenobiotics[17,22]. Li et al.[23] successfully reported a pretreatment method for the quantitative determination of glycocholic acid (GCA) in urine and plasma samples, thereby supporting the potential use of IL-based ABS in clinical diagnosis.

Although protein extraction and serum pretreatment to identify small metabolites have been reported with IL-based ABS, to the best of our knowledge, there are no works on IL-based ABS to simultaneous act as a depletion method, induding the precipitation of highly abundant proteins, and to completely extract cancer biomarkers from serum samples. In this work we investigate IL-based ABS as a pretreatment strategy of serum samples envisioning the extraction and improved quantification of LDH. This step allows the use of more accurate equipment, such as size exclusion high performance liquid chromatography (SE-HPLC), for the quantification of the enzyme effective concentration instead of its activity as typically carried out[14,24].

3.3.3. Experimental procedures

Materials. The ABS studied in this work are composed of a buffer aqueous solution constituted by potassium citrate ($K_3C_6H_5O_7 \cdot H_2O$, ≥ 99 wt% pure) from Sigma–Aldrich, and citric acid ($C_6H_8O_7 \cdot H_2O$, 100 wt% pure from Fisher Scientific), and the ILs tetrabutylphosphonium chloride ($[P_{4444}]Cl$, > 96 % pure) and tetrabutylphosphonium bromide ($[P_{4444}]Br$, > 96 % pure) from Cytec Ind. Phosphate buffered saline (PBS), 100 wt% pure from Sigma-Aldrich, aqueous solutions were also used. For HPLC analysis, sodium phosphate monobasic (NaH_2PO_4, purity 99- 100.5 %), sodium phosphate dibasic heptahydrated ($Na_2HPO_4.7H_2O$, purity 98.2- 102.0 %) and sodium chloride (NaCl), acquired from Sigma Aldrich, were used.

Simultaneous extraction of lactate dehydrogenase (LDH) and depletion of human serum albumin (HSA) and immunoglobulin G (IgG). The ternary mixtures compositions used in the partitioning experiments were chosen based on the phase diagrams determined in a previous work[21]. Aqueous solutions containing LDH (100 $U.L^{-1}$) and human serum were used as the aqueous solution. Each mixture was vigorously stirred, centrifuged for 10 min, and left to equilibrate for 10 min at 25°C to reach the LDH complete extraction and the HSA and IgG complete depletion (that precipitate as a solid interphase between the two liquid phases). After, a careful separation of the phases was performed and the amount of LDH, HSA and IgG in each phase was quantified by SE-HPLC (Size Exclusion High-Performance Liquid Chromatography). Each phase was diluted at a 1:10 (v:v) ratio in a phosphate buffer solution before injection. A Chromaster HPLC (VWR, Hitachi) coupled to an UV detector was used. SE-HPLC was performed with an analytical column (25 cm × 2 mm i.d., 25 μm), Lichrospher 100 RP-18, from Merck. A 100 mM phosphate buffer in MiliQ water (mobile phase) was run isocratically with a flow rate of 1 $mL \cdot min^{-1}$. The temperature of the column and auto-sampler was kept constant at 25°C. The injection volume was of 25 μL. The wavelength was set at 280 nm whereas the retention time of IgG, LDH and HSA was found to be *circa* 15.7, 16.2 and 17.1 min, respectively, within an analysis time of 40 min. The quantification of

LDH, HSA and IgG in each phase was carried out by an external standard calibration method (R^2=0.9993 R^2=0.9997 and R^2=0.9991, respectively) - *cf.* Appendix G with the established calibration curves. The extraction efficiency of LDH ($\boldsymbol{EE_{LDH}}\%$) and the depletion efficiencies of HSA and IgG, $\boldsymbol{DE_{BSA}}\%$, and $\boldsymbol{DE_{IgG}}\%$, respectively, are defined according to Equation (3.3.1), Equation (3.3.2) and Equation (3.3.3):

$$EE_{\mathrm{LDH}}\% = \frac{w_{LDH}^{IL}}{w_{LDH}^{IL} + +w_{LDH}^{Salt} + w_{LDH}^{Int}} \times 100 \quad (3.3.1)$$

$$DE_{\mathrm{HSA}}\% = \frac{w_{HSA}^{Int}}{w_{HSA}^{IL} + +w_{HSA}^{Salt} + w_{HSA}^{Int}} \times 100 \quad (3.3.2)$$

$$DE_{\mathrm{IgG}}\% = \frac{w_{IgG}^{Int}}{w_{IgG}^{IL} + +w_{IgG}^{Salt} + w_{IgG}^{Int}} \times 100 \quad (3.3.3)$$

where $w_{Protein}^{IL}$, $w_{Protein}^{Salt}$ and $w_{Protein}^{Int}$ are the total weight of protein in the IL-rich aqueous phase, salt-rich aqueous phase and solid interphase, respectively. In all systems the top phase corresponds to the IL-rich phase whereas the bottom phase is mainly constituted by the citrate-based salt and water. In the cases were depletion occurs, the solid middle phase is mostly composed of proteins.

The percentage recovery yield of LDH, $\boldsymbol{RY_{LDH}}\%$, is the percentage ratio between the amount of protein in the IL-rich aqueous phase to that in the initial LDH aqueous solution, and is defined according to Equation (3.3.4)**:**

$$RY_{\mathrm{LDH}}\% = \frac{w_{LDH}^{IL}}{w_{LDH}^{Aqueous\ solution}}\ \boldsymbol{x}100 \quad (3.3.4)$$

where $w_{LDH}^{Aqueous\ solution}$ and w_{LDH}^{IL} are the total weight of LDH in the LDH aqueous solution and in the IL-rich phase, respectively.

Molecular Docking. The interaction sites of HSA, IgG and LDH with the IL ions were identified using the Auto-dock vina 1.1.2 program[25]. The crystal structure of HSA (PDB:1e71), IgG (PDB:1hzh) and LDH (PDB:5ixs) were adapted and used in the molecular docking. Auto DockTools (ADT)[26] was used to prepare the proteins input files by merging non-polar hydrogen atoms, adding partial charges and atom types. Ligand (IL cation and anions) 3D atomic coordinates were computed by Gaussian 03w and ligand rigid root was generated using AutoDockTools (ADT), setting all possible rotatable bonds defined as active by torsions. The grid center at the center of mass (x-, y-, and z-axes, respectively) to cover the whole interaction surface of HSA was 94 Å × 64 Å × 90 Å, of IgG

was 126 Å × 112 Å × 126 Å and of LDH was 94 Å × 90 Å × 98 Å. The binding model that has the lowest binding free energy was searched out from 9 different conformers for each ligand (IL ions).

3.3.4. Results and discussion

Extraction of lactate dehydrogenase (LDH) and depletion of human serum albumin (HSA) and immunoglobulin G (IgG). The extraction of LDH and the depletion efficiencies of HSA and IgG in $[P_{4444}]$Br-based ABS were investigated at a common mixture composition (30 wt% of $K_3C_6H_5O_7/C_6H_8O_7$ + and 30 wt% of $[P_{4444}]$-based ILs + 40 wt% of an aqueous solution containing LDH at 100 $U.L^{-1}$ or serum spiked with LDH at the same concentration) in the biphasic area according to phase diagrams previously reported[21].

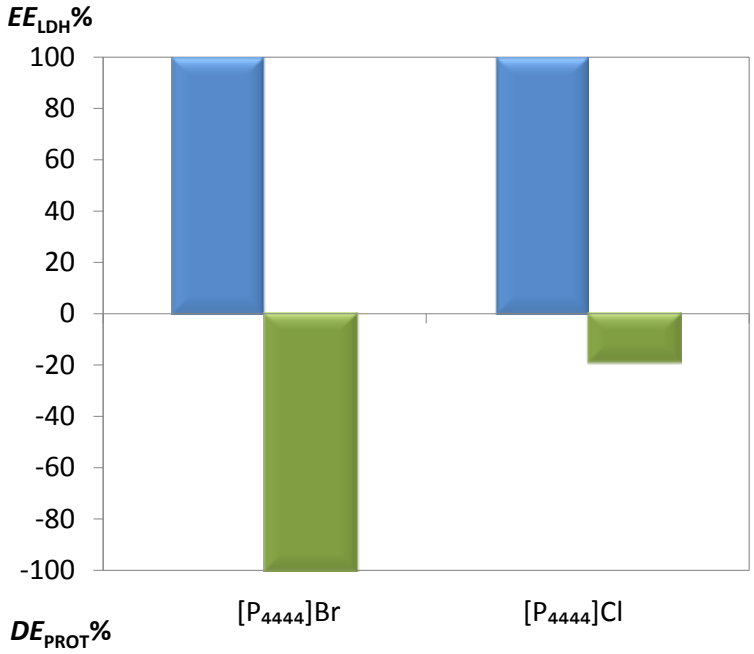

Figure 3.3.1. Extraction efficiency of LDH ($EE_{LDH\%}$■) and simultaneous depletion efficiency of IgG and HSA ($DE_{PROT}\%$■) using ABS composed of 30 wt% of IL + 30 wt% $K_3C_6H_5O_7/C_6H_8O_7$ at 25°C and pH = 7.0.

Figure 3.3.1. displays the effect of the IL anion on the extraction of LDH and on the simultaneous depletion efficiencies of HSA and IgG. The ABS investigated are composed of 30 wt% of $K_3C_6H_5O_7/C_6H_8O_7$ + and 30 wt% of $[P_{4444}]$-based ILs + 40 wt% of an aqueous solution containing LDH at 100 $U.L^{-1}$ or serum spiked with LDH. For the two IL-based ABS, LDH is completely extracted to the top phase (IL-rich phase) - extraction efficiencies of 100% attained in a single-step (Figure 3.3.1.). However, only the ABS constituted by $[P_{4444}]$Br induces the precipitation of proteins

creating a solid interphase, with depletion efficiencies of 100% for HSA and IgG obtained in a single-step.

In Figure 3.3.2 and Figure 3.3.3. are depicted the SE-HPLC chromatograms corresponding to the extractions carried out with LDH, and corresponding to the depletion efficiencies studies from human serum allowing to confirm the effect of the IL on the proteomic profile, respectively. According to the results obtained, both IL-based ABS allow the complete partitioning of LDH to the IL-rich phase in a single-step. Moreover, no losses of protein by precipitation at the interface where observed. The chromatographic peak of LDH is visible between 15 and 17 min.

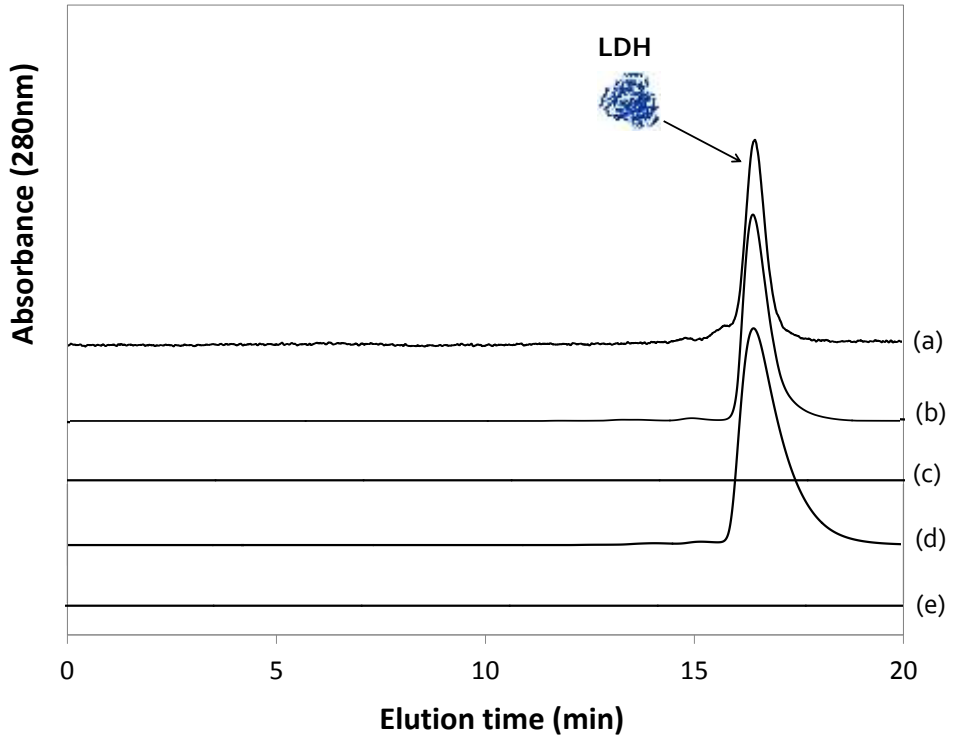

Figure 3.3.2. Size exclusion chromatography results of a aqueous solution containing LDH at 100 $U.L^{-1}$ (a); $[P_{4444}]Cl$-rich phase (b); salt rich-phase; (c) $[P_{4444}]Br$-phase (d); salt rich-phase; Corresponding to the ABS composed of IL (30 wt%) + $K_3C_6H_5O_7/C_6H_8O_7$ (30 wt%) at 25°C and pH = 7.0.

In the $[P_{4444}]Cl$-based ABS an evident peak between 17 and 18 min is detected, which mainly corresponds to the highly abundant protein HSA (Figure 3.3.3b**)**. However, in the the ABS composed of $[P_{4444}]Br$ a complete precipitation of the highly abundant serum proteins was observed (HSA and IgG) (Figure 3.3.3d**)**. No proteins have been identified in the ABS bottom phases (salt-rich phases). $[P_{4444}]Br$ is more hydrophobic, which may justify the complete precipitation and/or denaturation observed. The changes in the protein structure leading to precipitation may result from specific interactions occurring between the protein and the IL.

Hydrophobic interactions responsible for proteins precipitation have been reported with polymers, organic solvents and salts[27,28]. The protein behaviour in presence of ions is in part explained by the Hofmeister series[29]. Therefore, protein stability and enzyme activity can be strongly influenced by the type of salts or ILs present in aqueous solution[30]. In this case, Br^- has a weaker ability to hydrogen-bond with water and to form hydration complexes; therefore, the respective IL-rich phase has a lower water content when compared with the chloride-based system – *cf.* the Appendix G with the compositions of the phases. This low water content seems not appropriate to dissolve proteins while keeping them stable, leading thus to their precipitation.

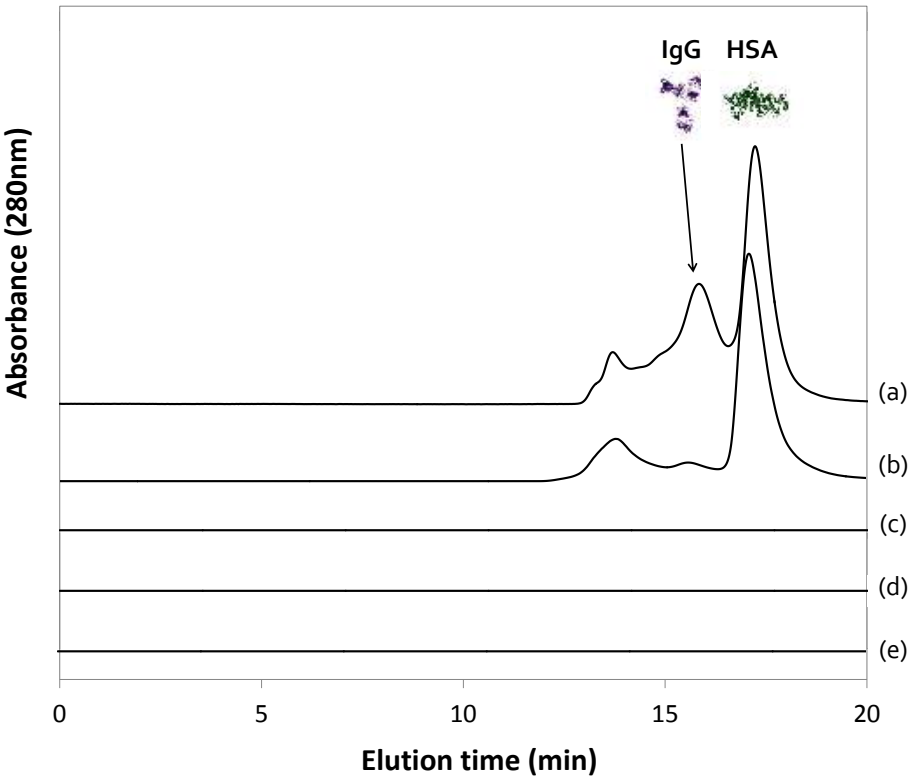

Figure 3.3.3. Size exclusion chromatography results of human serum samples (a); $[P_{4444}]$Cl-rich phase (b); salt-rich phase; (c) $[P_{4444}]$Br-phase (d); salt-rich-phase; corresponding to the ABS composed of IL (30 wt%) + $K_3C_6H_5O_7/C_6H_8O_7$ (30 wt%) at 25°C and pH = 7.0.

Given that the best results were obtained with $[P_{4444}]$Br + $K_3C_6H_5O_7/C_6H_8O_7$ (pH=7) (which imply the extraction of LDH to the IL-rich phase and simultaneous depletion of HSA and IgG from serum samples), further mixtures for various concentrations of $[P_{4444}]$Br (from 15 to 45 wt%) and $K_3C_6H_5O_7/C_6H_8O_7$ (from 10 to 30 wt%) were investigated and their impact on the LDH partition and HSA and IgG depletion evaluated. Figure 3.3.5 depicts the effect of the $K_3C_6H_5O_7/C_6H_8O_7$ and IL concentrations. Interestingly, independently of the salt or IL concentration employed, the same trends is observed. All compositions studied allow the complete extraction of LDH to the IL-rich

phase, without observing the precipitation and/or denaturation of the target biomarker, and the complete depletion of HSA and IgG. However, in systems composed of 30 wt% of IL and 10 wt% of salt it was observed the formation of a relatively small top-phase compared to the bottom phase, which did not allow to separate the interphase (depleted serum proteins).

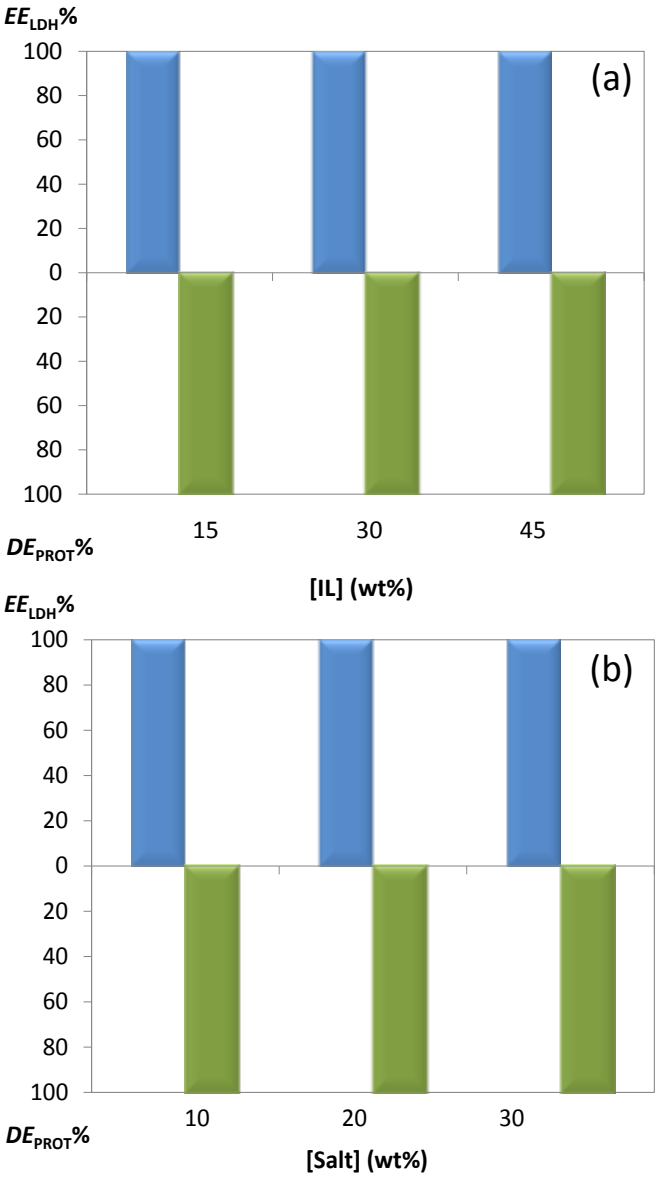

Figure 3.3.4. Extraction efficiency of LDH ($EE_{LDH\%}$■) and depletion efficiency of IgG and HSA ($DE_{PROT}\%$■) of: (a) ABS composed of 20 wt% of $K_3C_6H_5O_7/C_6H_8O_7$ + different concentrations of $[P_{4444}]Br$ and (b) 30 wt% of $[P_{4444}]Br$ + different concentrations of $K_3C_6H_5O_7/C_6H_8O_7$ at 25°C and pH = 7.0.

On the other hand, the mixture composed of 20 wt% of $K_3C_6H_5O_7/C_6H_8O_7$ + 15 wt% $[P_{4444}]Br$ + serum leads to small top-phase, not allowing its separation from the interphase. However, in these situations it was not observed the presence of proteins in the opposite phase, assuming

that 100% of precipitation of LDH and HSA occurs. Even so, in all the evaluated situations for the salt and IL effect, LDH preferentially migrates to the IL-rich phase confirming that protein-IL interactions and salting-out effects play a significant role.

The mixtures studied lead however to different recovery yields of LDH, as shown in Figure 3.3.5. The mixture formed by 20 wt% of salt+ 30wt % IL is the one that leads to lower losses of LDH. However, the mixture composed of 20 wt% of $K_3C_6H_5O_7/C_6H_8O_7$ and 45 wt% of $[P_{4444}]Br$ appears as the most promising in terms of handling, due to the larger volume of the top-phase (IL-rich phase where LDH is enriched), and due to a well-defined third phase corresponding to precipitated HSA and IgG.

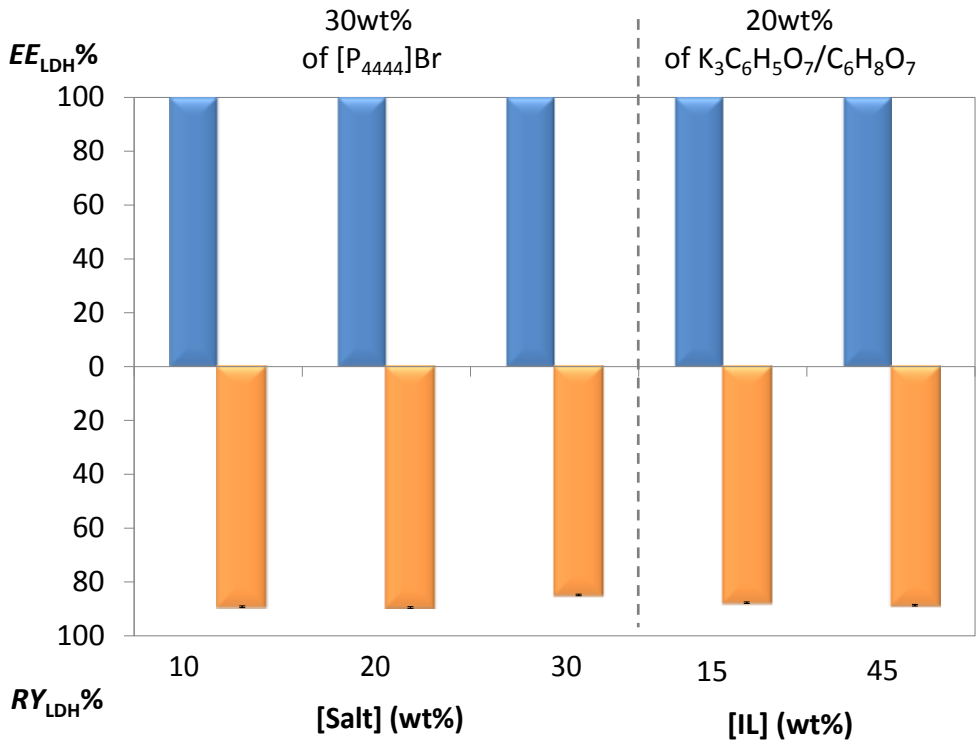

Figure 3.3.5. Extraction efficiency of LDH ($EE_{LDH\%}$■) and recovery yields of LDH ($RY_{LDH}\%$■) of in ABS composed of different concentrations of $K_3C_6H_5O_7/C_6H_8O_7$ and $[P_{4444}]Br$ at 25°C and pH = 7.0.

The ABS contituted by 45 wt% of $[P_{4444}]Br$ + 20 wt% of $K_3C_6H_5O_7/C_6H_8O_7$ was finally investigated to extract LDH directly from serum samples, with the simultaneous depletion of HSA and IgG. To this end, serum samples were spiked with LDH in a concentration of 100 U/L. LDH was added at a know concentration since the commercial serum samples acquired correspond to healthy volunteers. Figure 3.3.6**.** displays the SE-HPLC chromatograms corresponding to non-treated serum samples, standard LDH, and to the ABS top and bottoms phases. At the IL-rich phase, only LDH is identified, with the absence of LDH aggregates or the protein fragmentation.

The peak of LDH in aqueous solution for concentration of 100 U/L at around 16.2 minutes is clearly seen in the LDH standard aqueous solution and in the IL-rich phase after the sample pre-treatment. Given that LDH has an intermediate molecular weight between IgG and HSA, remarkably, HSA and IgG were not detected in the HPLC chromatograms, thereby not acting as interferents in the quantification.

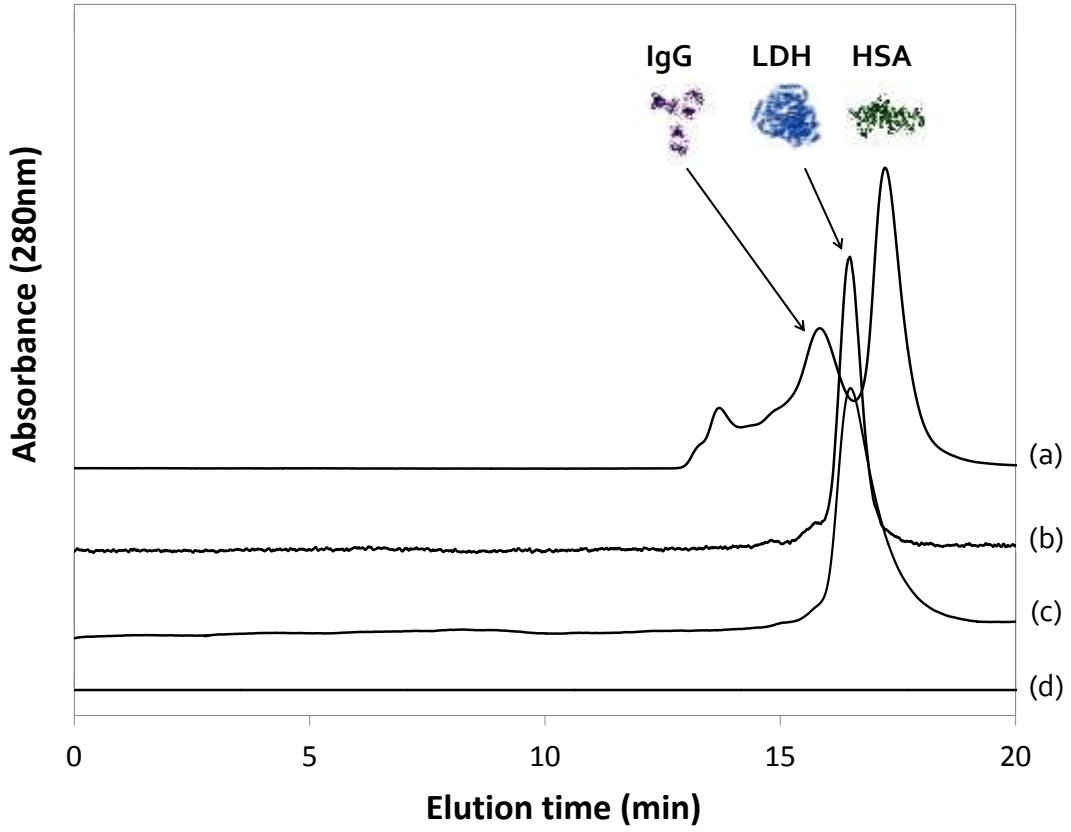

Figure 3.3.6. SE-HPLC chromatograms of human serum without pre-treatment (a), standard LDH (b), IL-rich phase after extraction (c), and salt-rich phase (d) of the ABS composed of 45 wt% [P4444]Br + 20 wt% $K_3C_6H_5O_7/C_6H_8O_7$ + serum samples with LDH at 100 U/L.

Molecular Docking. The molecular docking of HSA, IgG and LDH for each IL ion were carried out, allowing to better understand the preferencial depletion of HSA and IgG. Molecular docking analysis was carried out in previous works, providing valuable insights on the interactions occuring betwen ILs and proteins[31–33]. The IL cation ($[P_{4444}]^+$) and anion (Cl^- and Br^-) binding on HSA, IgG and LDH surfaces were studied. The IL ions bind pose with lowest absolute value of affinity (kcal/mol) for HSA, IgG and LDH with Cl^- and Br^- are displayed in Figure 3.3.7, while the pose corresponding to the IL cation is shown in Apendix G. The molecular interactions diagrams, the best binding pose

and docking affinities, interacting amino acids residues, type of interaction and geometry distance (Å) of each IL ion individually also are provided in Apendix G.

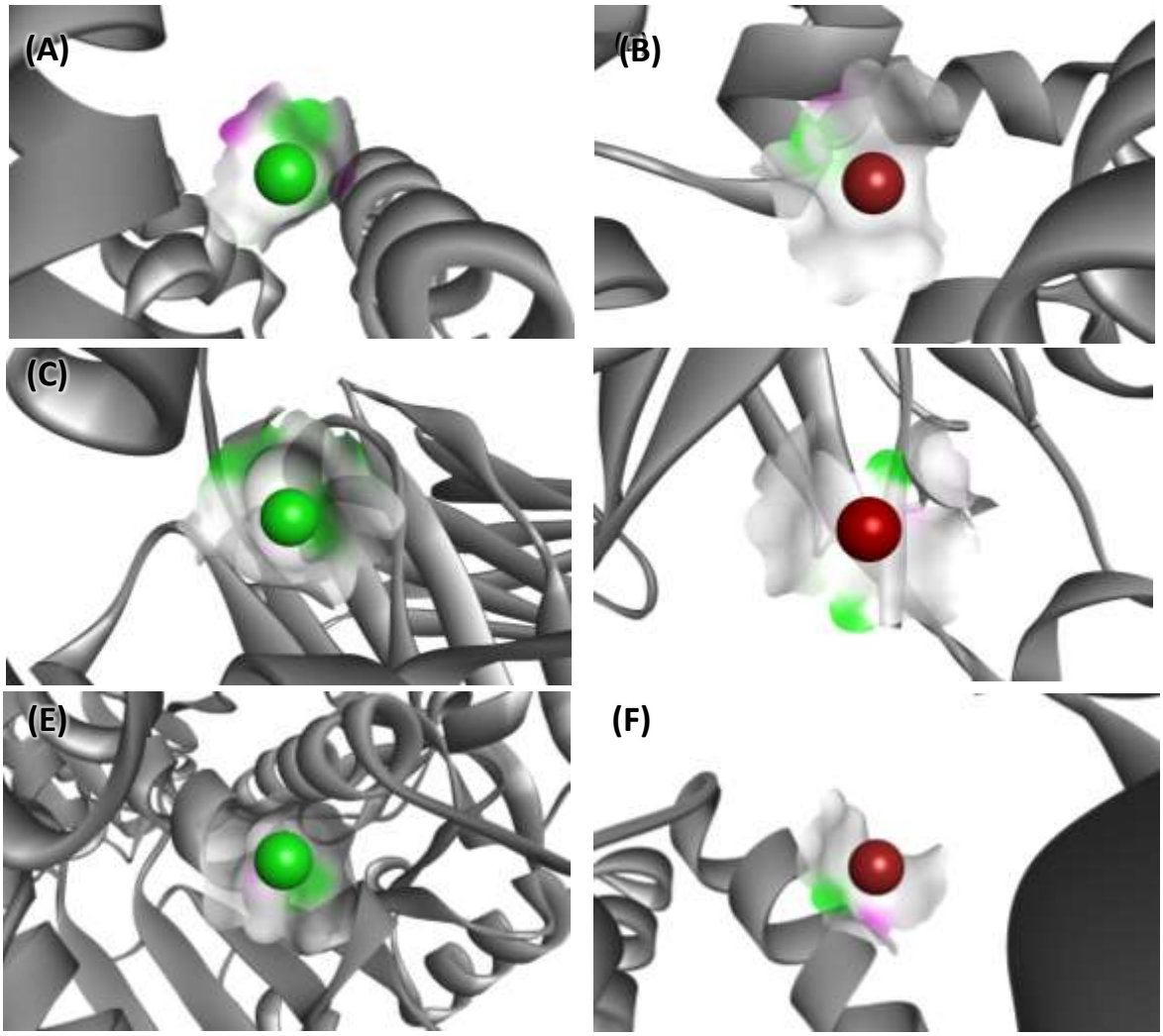

Figure 3.3.7. Molecular docking of has and (a) Cl^- and (b) Br^-; IgG and (c) Cl^- and (d) Br^-; and LDH and (e) Cl^- and (f) Br^-.

The $[P_{4444}]^+$ binding energies with the 3 proteins follow the rank: HSA > LDH > IgG. For Br^- and Cl^- the trend is as follows: HSA > LDH > IgG and HSA > LDH = IgG, respectively. However, there are no stronger binding energies between each ion and each protein, demonstrating that IL-protein preferential interactions are not the major ones responsible for the HSA and IgG precipitation. Therefore, the molecular docking results allow to conclude that low hydrated enviroments in the IL-rich phase combined to the high salting-out effect exerted by the salt promote protein-protein interactions, which are more relevant for high abundant proteins.

3.3.5. Conclusions

The depletion of HSA and IgG and extraction of LDH using ABS formed by phosphonium-based ILs and salts is here proposed. Remarkable depletion efficiencies of 100% to HSA and IgG were obtained, whereas LDH can be completely extracted to the IL-rich phase, in a single-step. This possibility only occurs with more hydrophobic ILs with a low water content at the IL-rich phase. No specific IL-protein interactions have been found to be responsible for this behavior. Low water contents promote protein-protein interactions and their further precipitation. According to results here achieved, these studied IL-based ABS represent a cost-effective alternative for the pretreatment of biological samples before clinical analysis, particularly in cancer diagnosis and prognosis. The proposed method reduces other proteins interferences in the LDH quantification, thus allowing to use SE-HPLC chromatography for its quantification instead of the commonly applied enzymatic activity assays, therefore leading to more accurate results.

3.3.6. References

1. Cancer. WHO (2015). World Health Organization (2015) Cancer. :Accessed on February 3, 2017; Available from: http://www.who.int/mediacentre/factsheets/fs297/en/.
2. Ferlay, J., Soerjomataram, I., Dikshit, R., Eser, S., Mathers, C., Rebelo, M., Parkin, D.M., Forman, D., Bray, F.. Int J Cancer. 2015;136(5):359-386.
3. Hawksworth, D., Ravindranath, L., Chen, Y., Furusato, B., Sesterhenn, I.A., McLeod, D.G., Srivastava, S., Petrovics, G.. Prostate Cancer Prostatic Dis. 2010;13(4):311-315.
4. Ward, J.B., Henderson, R.E.. Environ Health Perspect. 1996;104(5):895-900.
5. Henry, N.L., Hayes, D.F.. Mol Oncol. 2012;6(2):140-146..
6. Füzéry, A.K., Levin, J., Chan, M.M., Chan, D.W.. Clin Proteomics. 2013;10(1):13.
7. Lilja, H.. Urology. 2003;62(5):27-33.
8. Ziaian, B,, Saberi, A., Ghayyoumi, M.A., Safaei, A., Ghaderi, A., Mojtahedi, Z.. Asian Pacific J Cancer Prev. 2014;15(4):1617-1620.
9. Chen, J., Sun, M.X., Hua, Y.Q., Cai, Z.D.. J Cancer Res Clin Oncol. March 2014:0-5.
10. Naruse, K., Yamada, Y., Aoki, S., Taki, T., Nakamura, K., Tomiume, M., Zennami, K., Katsuda, R., Sai, S.,Nishio, Y., Inoue, Y., Noguchi, H., Honda N. Hinyokika Kiyo. 2007;53(5):287-92.
11. Sidaway, P.. Nat Rev Urol. 2015;12(5):241..
12. Weinstein, D., Leininger, J., Hamby, C., Safai, B.. J Clin Aesthet Dermatol. 2014;7(6):13-24.
13. Girgis, H., Masui, O., White, N.M., Scorilas, A., Rotondo, F., Seivwright, A., Gabril, M., Filter, E.R., Girgis, A.H., Bjarnason, G.A., Jewett, M.A., Evans, A., Al-Haddad, S., Siu, K.M., Yousef, G.M.. Mol Cancer. 2014;13(1):101.
14. Buonocore, R., Avanzini, P., Aloe, R., Lippi, G.. Ann Clin Biochem. 2015;53(3):405-408.
15. Martinek, R.G.. Clin Chim Acta. 1972;40(1):91-99.
16. Bisswanger, H.. Perspect Sci. 2014;1(1):41-55.
17. Flieger, J., Czajkowska-Żelazko, A.. J Liq Chromatogr Relat Technol. 2015;38(2):182-189.
18. Freire, M.G., Cláudio, A.F.M., Araújo, J.M.M., Coutinho, J.A.P, Marrucho, I.M., Canongia Lopes, J.N., Rebelo, L.P.N.. Chem Soc Rev. 2012;41(14):4966-4995.
19. Raja, S., Murty, V.R., Thivaharan, V., Rajasekar, V., Ramesh, V.. Sci Technol. 2012;1(1):7-16.
20. Ventura, S.P.M., e Silva, F.A., Quental, M.V., Mondal, D., Freire, M.G., Coutinho, J.A.P.. Chem Rev. 2017;117(10):6984-7052.
21. Pereira, M.M., Pedro, S.N., Quental, M.V,, Lima, Á.S., Coutinho, J.A.P., Freire, M.G.. J Biotechnol. 2015;206:17-25.
22. Flieger, J., Czajkowska-Żelazko, A.. J Sep Sci. 2013;36(18):3035-3041.
23. Li, H., Zhao, H., Li, Q., Meng, D., Li, Z.. Chromatographia. 2017;80(2):209-215.
24. Yu, S.L., Xu, L.T., Qi, Q., Geng, Y.W., Chen, H., Meng, Z.Q., Wang, P., Chen, Z.. Sci Rep.. 2017;7:45194.
25. Trott, O., Olson, A.. J Comput Chem. 2010;31(2):455-461.
26. Morris, G,, Huey, R.. J Comput Chem. 2009;30(16):2785-2791.
27. Arakawa, T., Kita, Y., Timasheff, S.N.. Biophys Chem. 2007;131(1-3):62-70.
28. Kumar, V., Sharma, V.K., Kalonia, D.S.. Int J Pharm. 2009;366(1-2):38-43.

29. Kumar, A., Venkatesu, P.. Int J Biol Macromol. 2014;63:244-253.
30. Zhang, Y., Furyk, S., Sagle, L. B., Cho, Y., Bergbreiter, D. E., Cremer, P.S.. J Phys Chem C Nanomater Interfaces. 2008;111(25):8916-8924.
31. Taha, M., Quental, M. V., Correia, I., Freire, M.G., Coutinho, J.A.P.. Process Biochem. 2015;50(7):1158-1166.
32. Taha, M., e Silva, F.A., Quental, M.V., Ventura, S.P.M., Freire, M.G., Coutinho, J.A.P.. Green Chem. 2014;16(6):3149.
33. Taha, M., Almeida, M.R., Silva, F.A.E., Domingues, P., Ventura, S.P.M., Coutinho, J.A.P., Freire, M.G.. Chem - A Eur J. 2015;21(12):4781-4788.

4. FINAL REMARKS AND FUTURE WORK

Investments on the development of effective techniques for the early-stage diagnosis of cancer is a crucial priority in order to decrease the burden associated to cancer epidemics. In this context, this thesis was focused on the development of pretreatment strategies of biological fluids to improve the identification and quantification of cancer biomarkers, while allowing the use of more versatile equipment. Aqueous biphasic systems (ABS) were investigated for this purpose. Since the target cancer biomarkers are proteins, initially, the ability of IL-based and polymer-based ABS for the extraction of amino acids, model proteins and proteins from biological complex media was investigated. Novel ABS composed of commercial ILs or novel AGB-ILs with salts, as well as novel ABS formed by ILs and carbohydrates were evaluated, aiming at developing more sustainable separation/isolation strategies. The recovery of the proteins from IL-rich phase, followed by the recyclability/reusability of the ILs, was also demonstrated. This set of results allowed to better understand the proteins behavior in IL-based ABS, namely which factors allow their extraction with no denaturation or those that induce the proteins precipitation.

Based on the first set of results, IL-based ABS were then investigated as pretreatment strategies of human fluids envisaging a more accurate cancer diagnosis and prognosis. Novel AGB-ILs were synthesized and characterized, followed by their use as phase-forming agents of ABS for the depletion of human serum highly abundant proteins, allowing the analysis of low abundance proteins such as transferrin, a biomarker for several diseases and alcohol abuse and dependence. Given the labile nature of proteins, ABS constituted by GB-based ILs were then investigated to extract and concentrate PSA from human urine samples. After the ABS pretreatment, PSA can be identified and quantified by SE-HPLC in a non-invasive sample (urine), contributing to improvements on CaP diagnosis. Finally, IL-based ABS were investigated for the depletion of highly abundant serum proteins, such as IgG and HSA, with the simultaneous extraction of LDH from human serum to the IL-rich phase. The gathered results allow to quantify the cancer biomarker LDH in serum samples by SE-HPLC, instead of the commonly used enzymatic assays, thus leading to better clinical diagnosis and prognosis.

Based on the results achieved in this thesis, the following steps should be further addressed towards improved cancer diagnosis and prognosis:

- To extend the use of IL-based ABS for the extraction of PSA from human urine of a significant number of PaC patients aiming at validating the developed technique, as well as to validate the use of urine as a relevant fluid for PCa diagnosis;
- To carry out studies on the extraction of LDH and simultaneous depletion of HSA and IgG with other ILs to better understand the IL effect on the proteins depletion;

- To extend the use of IL-based ABS for the extraction of LDH from cancer patients serum samples;
- To appraise the use of IL-based ABS to extract and concentrate several cancer biomarkers from human samples envisioning a more accurate diagnosis;
- To test IL-based ABS as pre-treatment strategies of other human fluids (serum, saliva, tears, etc.) relevant for diagnosis purposes.

5. LIST OF PUBLICATIONS

5.1. Thesis publications

Research Papers:

1. Matheus M. Pereira, Sónia N. Pedro, Maria V. Quental, Álvaro S. Lima, João A. P. Coutinho, Mara G. Freire. Enhanced extraction of bovine serum albumin with aqueous biphasic systems of phosphonium- and ammonium-based ionic liquids. Journal of Biotechnology, 2015, 206, 17-25.
2. Matheus M. Pereira, Rafaela A. P. Cruz, Mafalda R. Almeida, Álvaro S. Lima, João A. P. Coutinho, Mara G. Freire. Single-Step Purification of Ovalbumin from Egg White Using Aqueous Biphasic Systems. Process Biochemistry, 2016, 51, 781-791.

5.2. Other publications

Book chapter:

1. Matheus M. Pereira, João A. P. Coutinho, Mara G. Freire. CHAPTER 8: Ionic Liquids as Efficient Tools for the Purification of Biomolecules and Bioproducts from Natural Sources. *In:* Ionic Liquids in the Biorefinery Concept: Challenges and Perspectives. RSC Green Chemistry. 1ed.The Royal Society of Chemistry, 2015, v. 1, p. 227-257.
2. Álvaro S. Lima, Nilmara S. de O. Plácido, Regina L. S. França, Igor A. O. Reis, Matheus M. Pereira, Mara G. Freire. Aplicação de Sistemas Aquosos Bifásicos na Purificação de Biomoléculas. Processos de Extração e Purificação de Biomoléculas. 1ed. Aracaju: Editora Universitária Tiradentes, 2017, v. 1, p. 113-140.

Research Papers:

1. Carlos E. Barão, Leandro D. Paris, João H. Dantas, Matheus M. Pereira, Lucio C. Filho, Heizir F. Castro, Gisella M. Zanin, Flavio F. Moraes, Cleide M. F. Soares. Characterization of Biocatalysts Prepared with Thermomyces lanuginosus Lipase and Different Silica Precursors, Dried using Aerogel and Xerogel Techniques. Applied Biochemistry and Biotechnology, 2014, 172, 263-274.
2. Gustavo de B. Cardoso, Isabela N. Souza, Matheus M. Pereira, Mara G. Freire, Cleide M. F. Soares, Álvaro S. Lima. Aqueous Two-Phase Systems formed by Biocompatible and Biodegradable Polysaccharides and Acetonitrile. Separation and Purification Technology, 2014, 136, 74-80.
3. Mafalda R. Almeida, Helena Passos, Matheus M. Pereira, Álvaro S. Lima, João A.P. Coutinho, Mara G. Freire. Ionic liquids as additives to enhance the extraction of antioxidants in aqueous two-phase systems. Separation and Purification Technology, 2014, 128, 1-10.
4. Rebeca Y. Cabrera-Padilla, Elvio B. Melo, Matheus M. Pereira, Renan T. Figueiredo, Alini T. Fricks, Elton Franceschi, Álvaro S. Lima, Daniel P. Silva, Cleide M. F. Soares. Use of ionic liquids as additives for the immobilization of lipase from Bacillus sp.. Journal of Chemical Technology and Biotechnology, 2015, 90, 1308-1316.

5. Matheus M. Pereira, Kiki A. Kurnia, Filipa L. Sousa, Nuno J. Silva, José A. L. Silva, João A. P. Coutinho, Mara G. Freire. Contact Angles and Wettability of Ionic Liquids on Polar and Non-polar Surfaces. PCCP. Physical Chemistry Chemical Physics, 2015, 17, 31653-31661.
6. Maria V. Quental, Magda Caban, Matheus M. Pereira, Priot Stepnowski, João A. P. Coutinho, Mara G. Freire. Enhanced extraction of proteins using cholinium-based ionic liquids as phase-forming components of aqueous biphasic systems. Biotechnology Journal, 2015, 10, 1457-1466.
7. Gustavo de B. Cardoso, Isabela N. Souza, Matheus M. Pereira, Luis P. Costa, Mara G. Freire, Cleide M. F. Soares, Álvaro S. Lima. Poly(Vinyl Alcohol) as a Novel Constituent to form Aqueous Two-Phase Systems with Acetonitrile: Phase Diagrams and Partitioning Experiments. Chemical Engineering Research & Design, 2015, 94, 317-323.
8. Erika S. Vieira, Tâmara K. De Oliveira Fontes, Matheus M. Pereira, Hofsky V. Alexandre, Daniel P. da Silva, Cleide M. F. Soares, Álvaro S. Lima. New strategy to apply perfluorodecalin as an oxygen carrier in lipase production: minimisation and reuse. Bioprocess and Biosystems Engineering, 2015, 38, 721-728.
9. Rebeca Y. Cabrera-Padilla, Milena C. Lisboa, Matheus M. Pereira, Renan T. Figueiredo, Elton Franceschi, Alini T. Fricks, Álvaro S. Lima, Daniel P. Silva, Cleide M. F. Soares. Immobilization of Candida rugosa lipase onto an eco-friendly support in the presence of ionic liquid. Bioprocess and Biosystems Engineering, 2015, 38, 805-814.
10. Anderson S. Barbosa, Jessica A. Lisboa, Matheus A. O. Silva, Nayara B. Carvalho, Matheus M. Pereira, Alini T. Fricks, Silvana Mattedi, Álvaro S. Lima; Elton Franceschi; Cleide M. F. Soares. The Novel Mesoporous Silica Aerogel Modified With Protic Ionic Liquid For Lipase Immobilization. Química Nova, 2016, 37, 969-976.
11. Acenine L. Balieiro, Rafalea A. Santos, Matheus M. Pereira, Renan T. Figueiredo, Lisiane S. Freitas, Odelsia L. S. Alsina, Álvaro S. Lima, Cleide M. F. Soares. Adsorption Process of Molecularly Imprinted Silica for Extraction of Lactose from Milk. Brazilian Journal of Chemical Engineering, 2016, 33, 361-372.
12. Rosilene dos S. Oliveira; Juliana da S. Rocha; Keren H. Pinheiro; Matheus M. Pereira, Carlos E. Barão. Application of an ultrasound process to extract catechins from green tea wastes. Brazilian Journal of Food Research, 2016, 7, 29-34.
13. Nripat Singh, Mukesh Sharma, Dibyendu Mondal, Matheus M. Pereira, Kamalesh Prasad. Very high concentration solubility and long term stability of DNA in an ammonium-based ionic liquid: a suitable media for nucleic acid packaging and preservation. ACS Sustainable Chemistry & Engineering, 2017, 5, 1998-2005.
14. Rita Superbi, Matheus M. Pereira, Mara G. Freire, João A. P. Coutinho. Evaluation of the effect of ionic liquids as adjuvants in polymer-based aqueous biphasic systems using biomolecules as molecular probes. Separation and Purification Technology, 2017, DOI:10.1016/j.seppur.2017.07.018.

Appendix A

Table A1. Experimental weight fraction data for the systems composed of IL (1) + Na_2SO_4 (2) + H_2O (3) at 25°C.

[MepyrNC$_2$]Br		[Et$_3$NC$_2$]Br		[Pr$_3$NC$_2$]Br	
100 w_1	100 w_1	100 w_2	100 w_2	100 w_1	100 w_2
33.1378	8.3559	29.1670	8.9985	20.3311	10.9583
34.4708	7.6320	31.6004	7.8192	21.3152	10.0477
36.6415	6.7211	33.5676	6.9598	22.4079	9.2350
38.4450	6.0902	34.9656	6.2954	23.1188	8.8211
40.1111	5.4507	36.9211	5.5339	24.0998	8.3795
42.3150	4.6771	38.8827	4.8770	25.1633	7.7507
44.0663	4.1646	40.9810	4.1975	26.5713	7.1643
45.2233	3.8143	43.3685	3.5852	27.6955	6.6495
46.9720	3.3929	44.8294	3.2435	28.7305	6.1966
50.3730	2.7154	46.7899	2.8111	29.7898	5.7869
		49.1203	2.3680	30.7546	5.4067
				32.2404	4.9226
				33.5973	4.4774
				34.9715	4.0738
				36.4336	3.6577
				37.7549	3.3447
				39.1167	3.0236
				40.0246	2.7756
				41.4645	2.4928
				42.7144	2.2365

Table A2. Experimental weight fraction data for the systems composed of IL (1) + Na_2SO_4 (2) + H_2O (3) at 25°C.

$[Bu_3NC_2]Br$		$[Bu_3PC_2]Br$		$[Bu_3PC_4]Br$	
100 w_1	100 w_1	100 w_2	100 w_2	100 w_1	100 w_2
13.6713	12.0942	31.0361	4.2511	44.5013	1.7572
15.7194	11.2106	29.7960	4.3385	42.3530	2.0145
17.6766	10.4290	28.4314	4.6051	40.7760	2.2385
19.2316	9.8090	26.8843	5.0331	35.2482	3.0600
20.2670	9.0821	25.1688	5.4887	32.7655	3.4429
21.2023	8.6881	23.9059	5.8683	29.8216	4.1393
21.6827	8.4006	22.4596	6.2975	28.5463	4.4000
22.3581	8.0770	20.6246	6.8615	26.3769	4.9503
23.4242	7.6979	18.5541	7.5297	24.0975	5.4856
23.7964	7.4287	16.6607	8.1858	21.7522	6.0716
24.9692	7.0591	14.4647	8.9694	21.0798	6.1874
25.7420	6.7887	11.6045	10.1799	19.4257	6.6259
26.4669	6.4900			17.7823	7.1037
27.0642	6.2875			17.1462	7.2825
27.7519	6.0275			16.4858	7.4956
28.3946	5.7589			15.7395	7.7325
29.3150	5.5259			15.2055	7.8885
31.1238	4.7654			14.4151	8.1583
31.9612	4.5799			13.7455	8.3643
33.0661	4.3011			12.3650	8.9083
34.3332	4.0105			11.7141	9.1611
35.2187	3.7924			10.5113	9.6710
36.3686	3.5531				
37.4250	3.3252				

Table A3. Extraction efficiencies (*EE*%$_{TRY}$) of tryptophan, pH and weight fraction compositions of the initial mixtures at 25 °C.

IL	Weight fraction composition / (wt %)		pH		*EE*%$_{TYR}$ ± *σ*
	IL	Na_2SO_4	IL-rich phase	$NaSO_4$-rich phase	
[MepyrNC$_2$]Br	39.87 ± 0.02	7.53 ± 0.03	3.14 ± 0.01	3.31 ± 0.01	98.52 ± 0.22
[Et$_3$NC$_2$]Br	39.67 ± 0.05	7.53 ± 0.01	4.04 ± 0.08	4.76 ± 0.05	98.78 ± 0.19
[Pr$_3$NC$_2$]Br	39.95 ± 0.01	7.51 ± 0.02	4.23 ± 0.07	4.40 ± 0.01	99.08 ± 0.01
[Bu$_3$NC$_2$]Br	40.09 ± 0.10	7.57 ± 0.04	6.24 ± 0.05	5.12 ± 0.16	100
[Bu$_3$PC$_2$]Br	39.94 ± 0.13	7.55 ± 0.04	3.24 ± 0.04	3.61 ± 0.05	93.65 ± 0.72
[Bu$_3$PC$_4$]Br	39.87 ± 0.28	7.58 ± 0.01	4.68 ± 0.01	4.49 ± 0.01	76.09 ± 0.10

Table A4. Extraction efficiencies (*EE*%$_{TYR}$) of tyrosine, pH and weight fraction compositions of the initial mixtures at 25 °C.

IL	Weight fraction composition / (wt %)		pH		*EE*%$_{TYR}$ ± *σ*
	IL	Na_2SO_4	IL-rich phase	$NaSO_4$-rich phase	
[MepyrNC$_2$]Br	39.80 ± 0.11	7.57 ± 0.02	3.14 ± 0.01	3.31 ± 0.01	96.70 ± 0.62
[Et$_3$NC$_2$]Br	39.88 ± 0.05	7.59 ± 0.05	4.04 ± 0.08	4.76 ± 0.05	97.06 ± 0.29
[Pr$_3$NC$_2$]Br	39.78 ± 0.11	7.52 ± 0.04	4.23 ± 0.07	4.40 ± 0.01	94.70 ± 0.31
[Bu$_3$NC$_2$]Br	40.36 ± 0.09	7.53 ± 0.07	6.24 ± 0.05	5.12 ± 0.16	88.59 ± 0.73
[Bu$_3$PC$_2$]Br	40.03 ± 0.07	7.52 ± 0.12	3.24 ± 0.04	3.61 ± 0.05	79.42 ± 0.25
[Bu$_3$PC$_4$]Br	40.08 ± 0.07	7.55 ± 0.07	4.68 ± 0.01	4.49 ± 0.01	70.63 ± 0.83

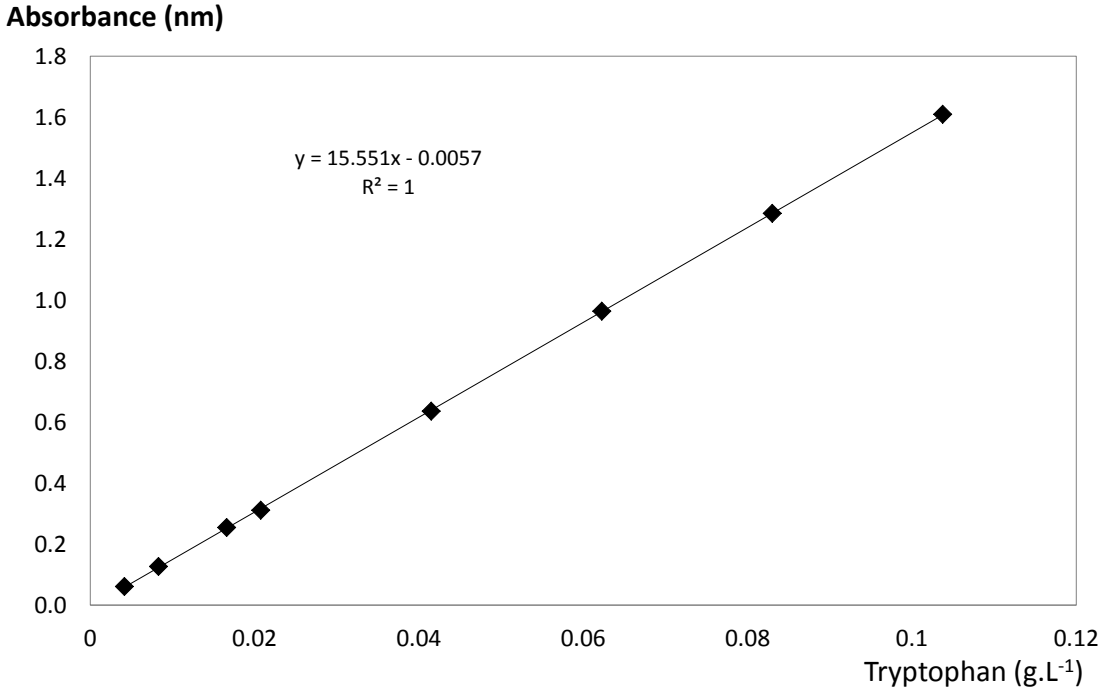

Figure A1. Tryptophan calibration curve by UV-Vis.

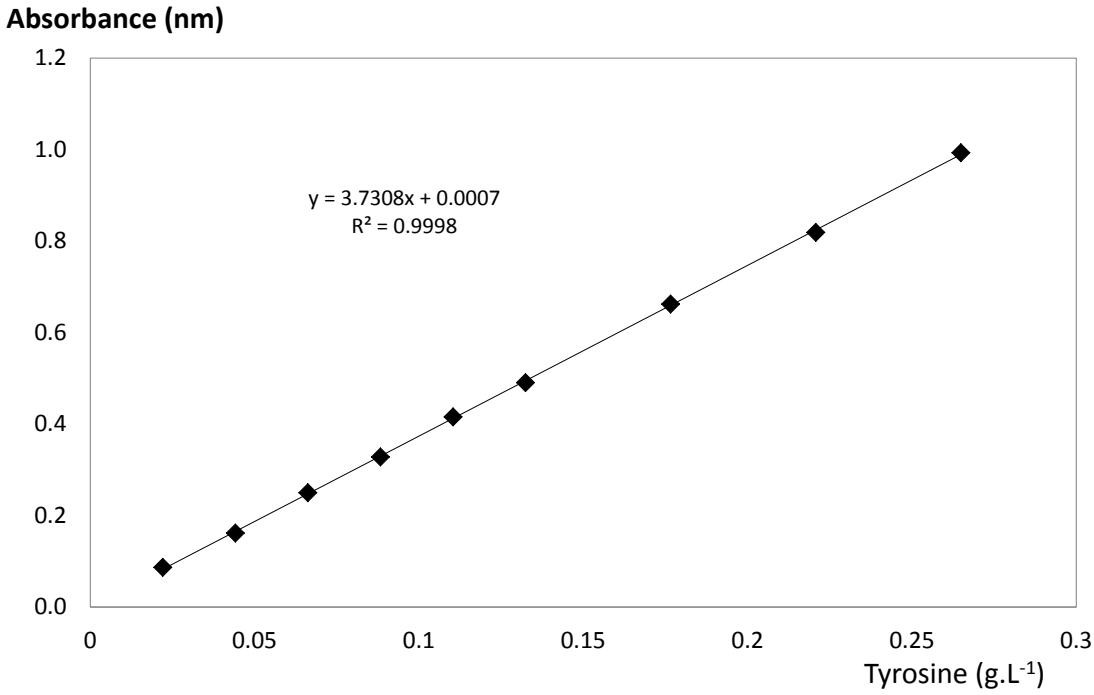

Figure A2. Tyrosine calibration curve by UV-Vis.

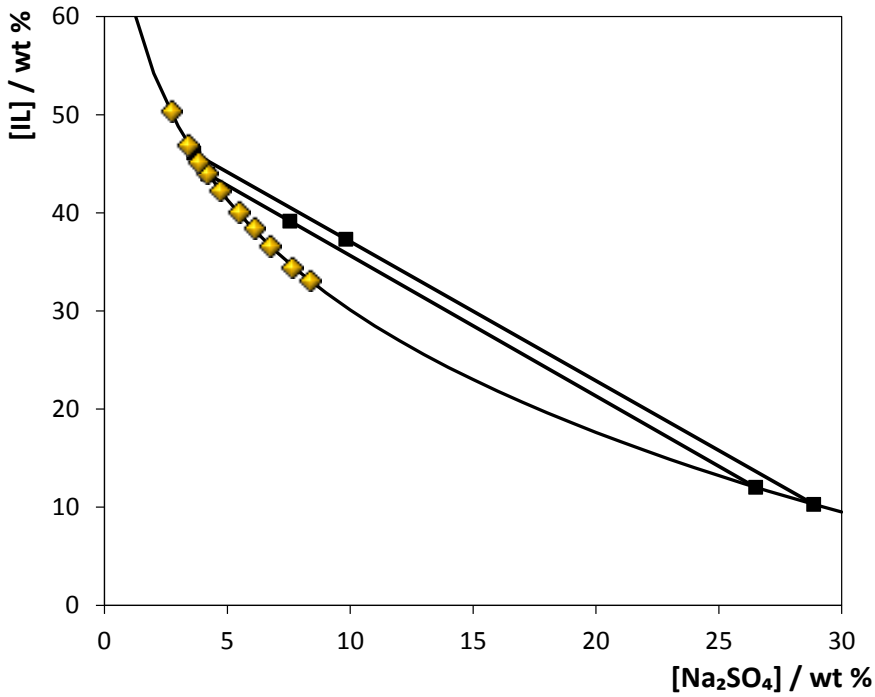

Figure A3. Phase diagram for the system composed of $[MepyrNC_2]Br + Na_2SO_4 + H_2O$ at 25 °C: binodal curve data (◆); TL data (●); and adjusted binodal data through Eq. (1) (—).

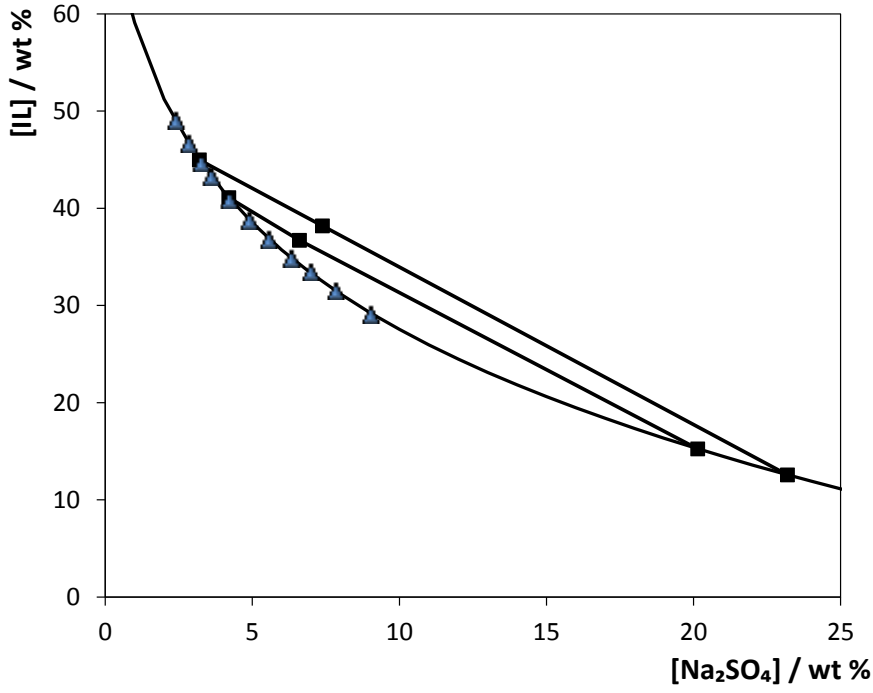

Figure A4. Phase diagram for the system composed of $[Et_3NC_2]Br + Na_2SO_4 + H_2O$ at 25 °C: binodal curve data (▲); TL data (●); and adjusted binodal data through Eq. (1) (—).

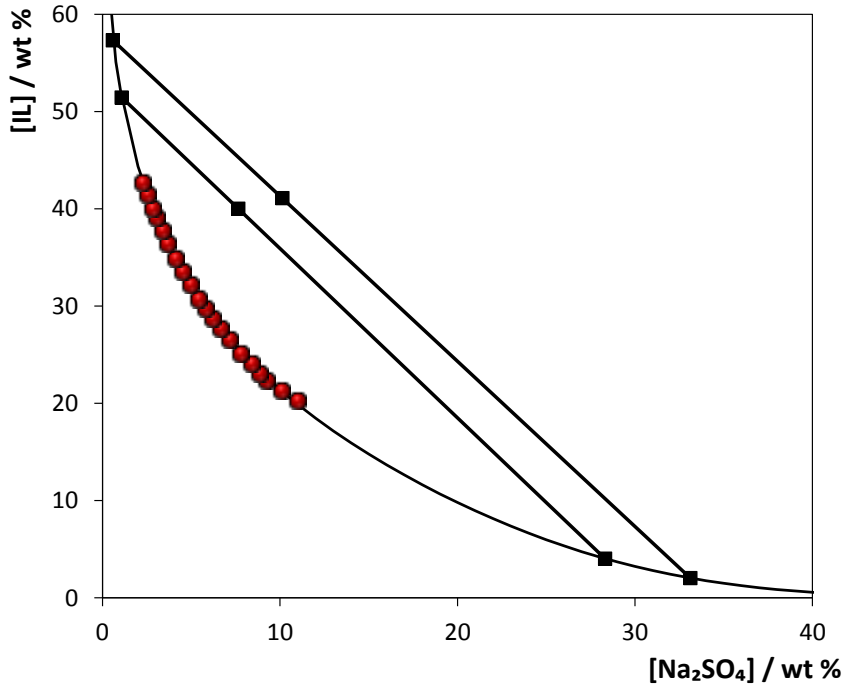

Figure A5. Phase diagram for the system composed of $[Pr_3NC_2]Br + Na_2SO_4 + H_2O$ at 25 °C: binodal curve data (●); TL data (●); and adjusted binodal data through Eq. (1) (—).

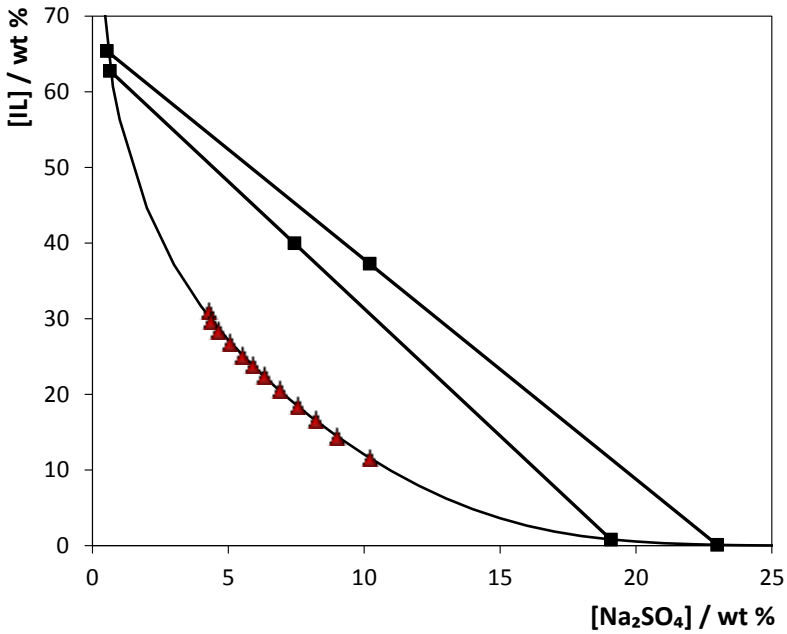

Figure A6. Phase diagram for the system composed of $[Bu_3PC_2]Br + Na_2SO_4 + H_2O$ at 25 °C: binodal curve data (▲); TL data (●); and adjusted binodal data through Eq. (1) (—).

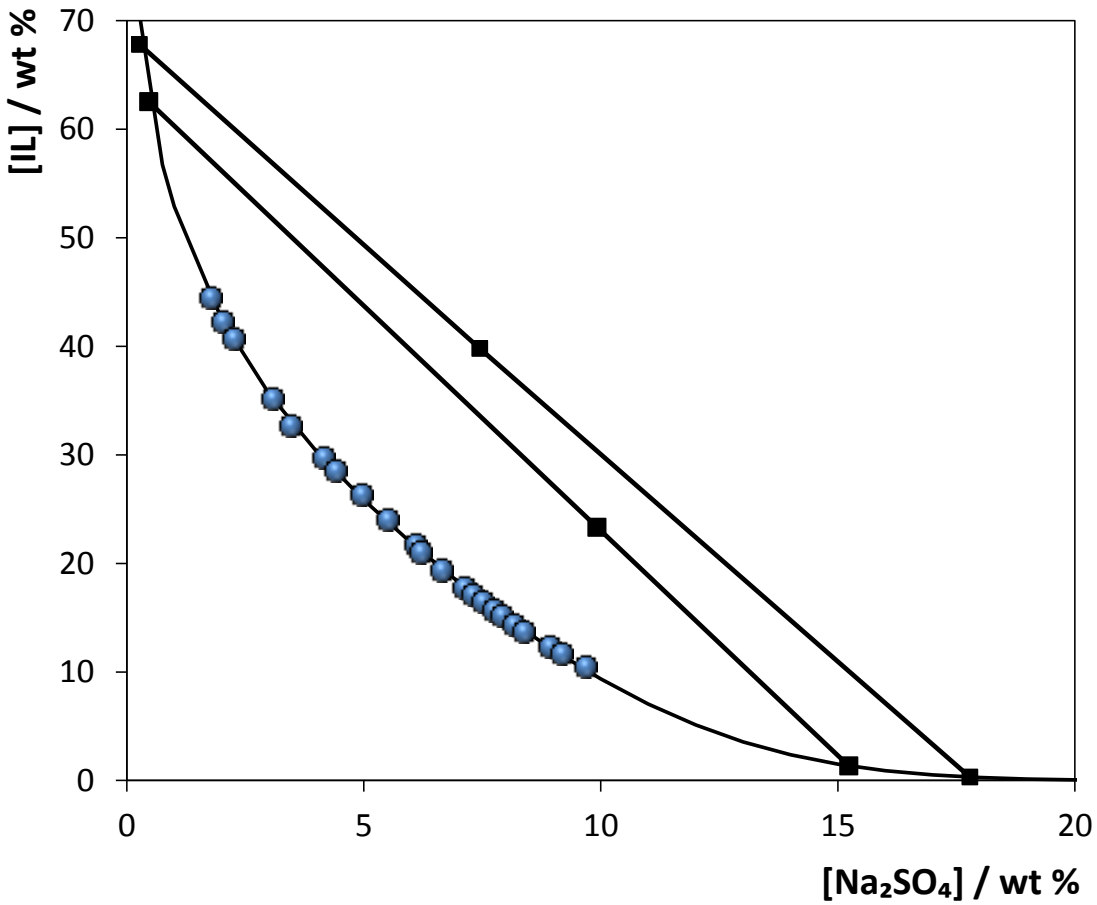

Figure A7. Phase diagram for the system composed of $[Bu_3PC_4]Br + Na_2SO_4 + H_2O$ at 25 °C: binodal curve data (●); TL data (●); and adjusted binodal data through Eq. (1) (—).

Appendix B

Table B1. Experimental weight fraction data for the systems composed of IL (1) + $C_6H_5K_3O_7$/$C_6H_8O_7$ (2) + H_2O (3) at 25°C.

[P_{4444}]Br		[P_{4441}][$MeSO_4$]		[$P_{i(444)1}$][Tos]	
100 w_1	100 w_1	100 w_2	100 w_2	100 w_1	100 w_2
47.8388	0.4370	56.6986	1.3192	75.0208	4.9219
43.1597	0.6590	47.4375	2.9804	59.0400	8.4023
40.1121	0.8976	41.1468	4.2037	51.2389	11.3257
38.1240	1.0659	38.3272	5.4815	46.1956	12.6033
36.3785	1.1897	35.7905	6.0568	44.0170	13.6880
33.5144	1.6411	31.0666	7.5380	39.8392	15.9586
30.2567	2.1531	29.4275	8.1733	35.8389	16.3896
19.2260	5.1635	28.1825	9.0201	33.8655	17.9247
9.5022	15.0050	26.9444	9.6570	32.6041	18.6099
5.7890	23.2343	25.5742	9.9455	32.0466	18.9232
5.2514	26.3552	23.9893	11.2778	30.9711	19.3291
4.6391	26.5561	23.0484	11.7249	29.5810	20.2982
3.9429	28.3602	22.4124	12.0319	28.3531	20.4044
3.2088	29.3497	21.2283	12.9313	26.3549	21.7354
3.0881	31.0576	20.5209	13.3704	25.6420	21.9617
2.0531	40.2288	19.9960	13.9119	24.9033	22.2586
1.6293	42.9543	19.3293	14.1657	24.0632	23.0090
1.4306	43.0913	18.5344	14.8994	23.4145	23.2715
1.1906	43.9595	18.0235	15.1199	22.5863	24.0136
		17.2124	15.9367	20.8279	24.6423
		16.7184	16.2356	20.3996	24.8575
		16.0916	16.7175	19.9438	25.0807
		15.6444	17.0013	19.5664	25.3059
		15.2076	17.3501	18.9791	25.8348
		14.6634	17.8620	18.5981	26.0797
		14.4839	17.6352	18.2917	26.1410
		13.7880	18.6043	17.9134	26.3303
		13.2213	18.8075	17.6349	26.4507
		12.7655	19.2995	17.2022	26.8071
		12.2857	19.7923	16.7512	27.1170
		12.2565	19.1829	16.4947	27.2218
		11.4734	19.0956	16.2380	27.2667
		10.8963	19.6156	15.6235	27.8635
		10.4880	19.6969	15.4141	28.0551
		9.9797	20.5787	15.2192	28.0490
		9.7096	20.9184	14.9494	28.4711

9.2204	21.5358	14.6383	28.7265
8.8098	21.9017	14.3991	29.0902
8.4510	22.3908	14.1926	29.1553
8.0010	23.2081	13.9835	29.1822
		13.6886	29.4696
		13.4918	29.5053
		12.9818	29.9173
		12.7009	30.1312
		12.5818	30.1172
		12.4371	30.1693
		12.3459	30.0383
		12.2228	30.2212
		12.0441	30.4163
		11.5321	31.1580
		11.2065	31.1134
		10.9317	31.1274
		10.6328	31.4308
		10.3840	31.6882
		10.1343	31.8178
		9.8418	31.9182
		9.4906	32.2824
		9.0729	33.1904
		8.8289	33.2905
		8.3966	33.0807

Table B2. Experimental weight fraction data for the systems composed of IL (1) + $C_6H_5K_3O_7$/$C_6H_8O_7$ (2) + H_2O (3) at 25°C and pH 7.

[P_{4444}]Cl		[N_{4444}]Cl	
100 w_1	100 w_2	100 w_1	100 w_2
86.4924	1.0557	50.1620	1.9141
63.9963	2.1215	45.2156	3.4470
54.1184	3.0299	42.0719	5.0582
48.8418	3.8526	38.4429	7.4342
45.1634	4.9749	36.2246	8.6956
41.6605	5.6622	34.5441	9.5152
38.3788	6.9352	32.5062	10.6393
35.4859	8.1447	29.6917	12.9078
33.2368	9.1887	27.6777	14.3710
32.0140	10.4540	25.3324	16.1640
31.2483	10.8314	23.7616	17.2831
30.5379	11.2235	21.2843	19.2403
29.8257	11.5870	19.5450	19.3433
28.8400	12.3574	18.0172	21.1155
28.2796	12.6258	15.9995	23.1501
27.6475	12.9362	14.0455	25.3000
27.0681	13.2758	12.9804	26.3039
25.1693	14.1107	11.6673	28.1300
24.0642	14.9879	11.0443	28.5202
23.5031	15.3220	10.0017	29.7699
22.8671	15.6276	9.0441	30.9635
22.0932	16.1253	8.2642	31.9726
21.4158	16.5200	7.8630	32.5237
20.6174	17.1369	7.2713	33.2358
19.8613	17.7528	6.8774	33.9086
19.4211	17.9311	6.3816	34.5217
18.8651	18.2848	6.0857	34.9466
18.2412	18.8202		
17.8484	19.0146		
17.2806	19.4545		
16.9682	19.6283		
16.4548	20.0527		
15.9250	20.4714		
15.4629	20.8920		
15.1644	21.0156		
14.7427	21.3710		

14.3337	21.7670
14.0974	21.8658
13.7232	22.1883
13.3256	22.5398
12.9924	22.8022
12.6610	23.0760
12.3382	23.3616
12.0179	23.6156
11.6960	23.8891
11.3895	24.2068
11.2217	24.2950
10.9611	24.5733
10.8120	24.6647
10.4943	25.0120
10.2971	25.1279
10.0704	25.3459
9.9706	25.3551
9.7907	25.5576
9.5933	25.7322
9.4068	25.9006
9.2592	26.0450
9.0738	26.2066
8.9031	26.3534
8.7424	26.4771
8.6448	26.5315
8.5041	26.6767
8.3424	26.8247
8.1868	26.9672
8.0522	27.1411
7.9174	27.2373
7.7751	27.3717
7.6558	27.5242
7.4726	27.7560
7.3972	27.7587
7.2689	27.8644
7.0996	28.0967
7.0320	28.1204
6.9784	28.1906
6.9154	28.2171
6.7833	28.3706
6.6517	28.5458

6.5472	28.6451
6.4414	28.7360
6.3508	28.8701
6.2583	28.9889
6.1654	29.0779
6.0494	29.2289
5.9604	29.3077
9.5933	25.7322
9.4068	25.9006
9.2592	26.0450
9.0738	26.2066
8.9031	26.3534
8.7424	26.4771
8.6448	26.5315
8.5041	26.6767
8.3424	26.8247
8.1868	26.9672
8.0522	27.1411
7.9174	27.2373
7.7751	27.3717
7.6558	27.5242
5.7127	30.3562
5.2826	31.1830
4.2756	32.3747
3.8831	33.5204
3.3983	34.9449
2.2193	36.3959
1.9091	39.8339
1.7341	43.2143
1.5590	45.9750
1.4739	48.4673

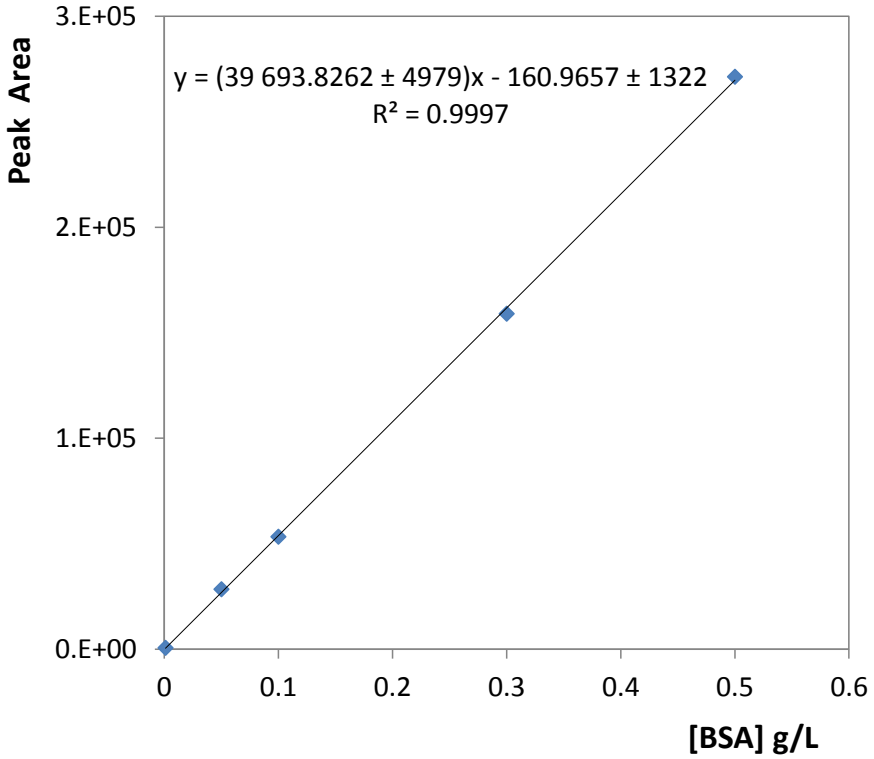

Figure B1. BSA calibration curve by SE-HPLC.

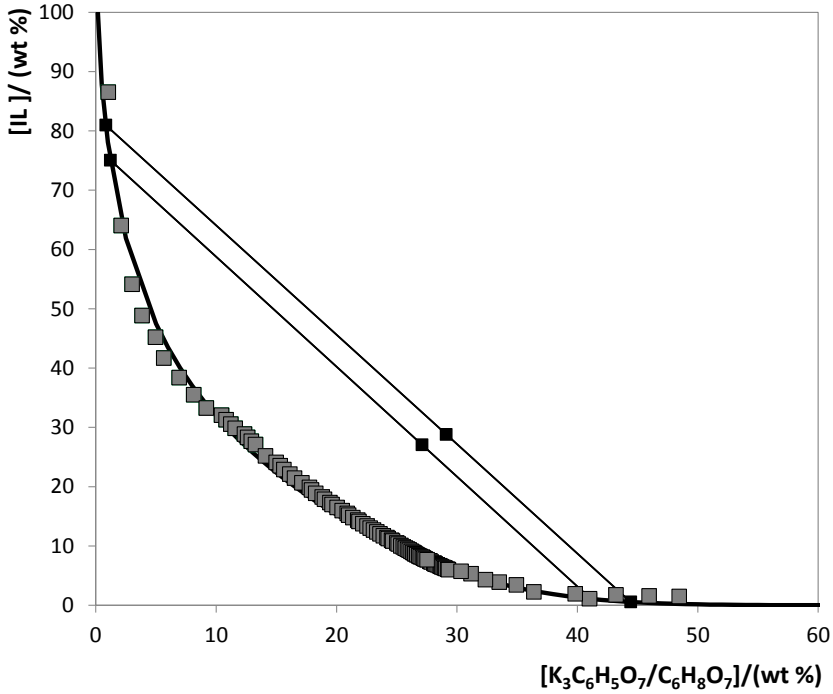

Figure B2. Phase diagram for the system composed of $[P_{4444}]Cl + K_3C_6H_5O_7/C_6H_8O_7 + H_2O$ at 25°C and pH 7.0: binodal curve data (■); TL data (■); adjusted binodal data through Equation 1 (—).

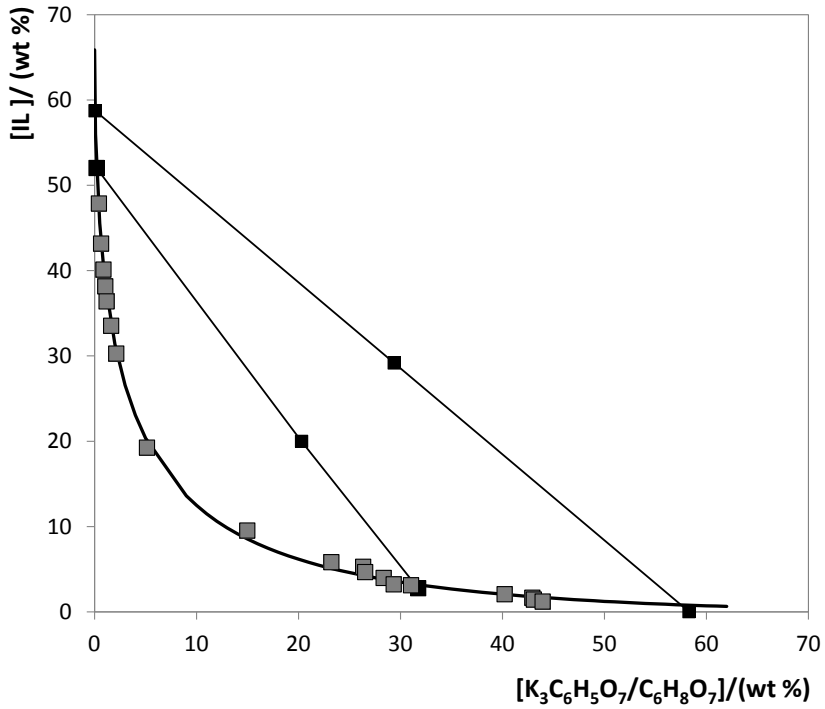

Figure B3. Phase diagram for the system composed of $[P_{4444}]Br + K_3C_6H_5O_7/C_6H_8O_7 + H_2O$ at 25°C and pH 7.0: binodal curve data (■); TL data (■); adjusted binodal data through Equation 1 (—).

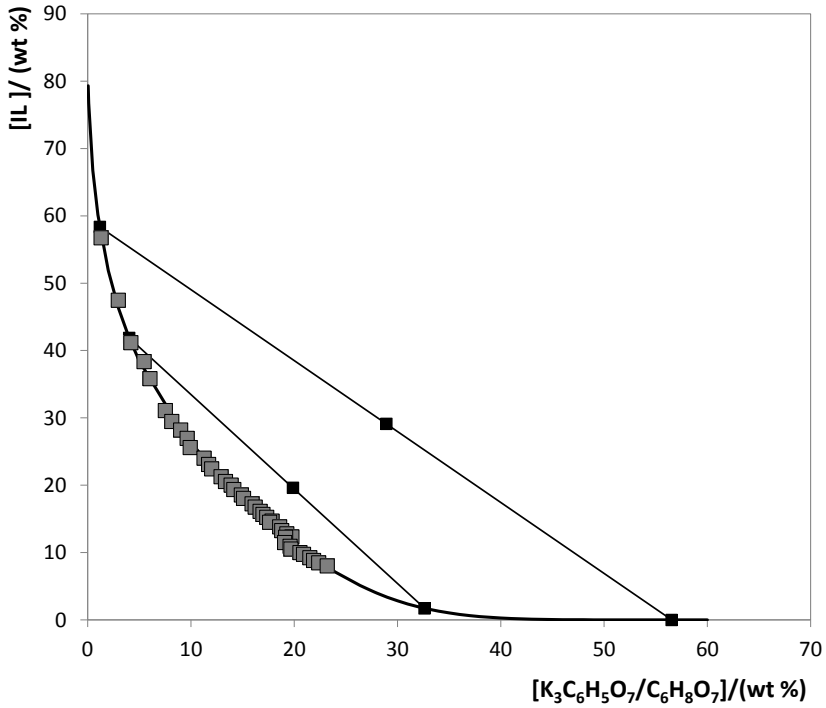

Figure B4. Phase diagram for the system composed of $[P_{4441}][MeSO_4] + K_3C_6H_5O_7/C_6H_8O_7 + H_2O$ at 25°C and pH 7.0: binodal curve data (■); TL data (■); adjusted binodal data through Equation 1 (—).

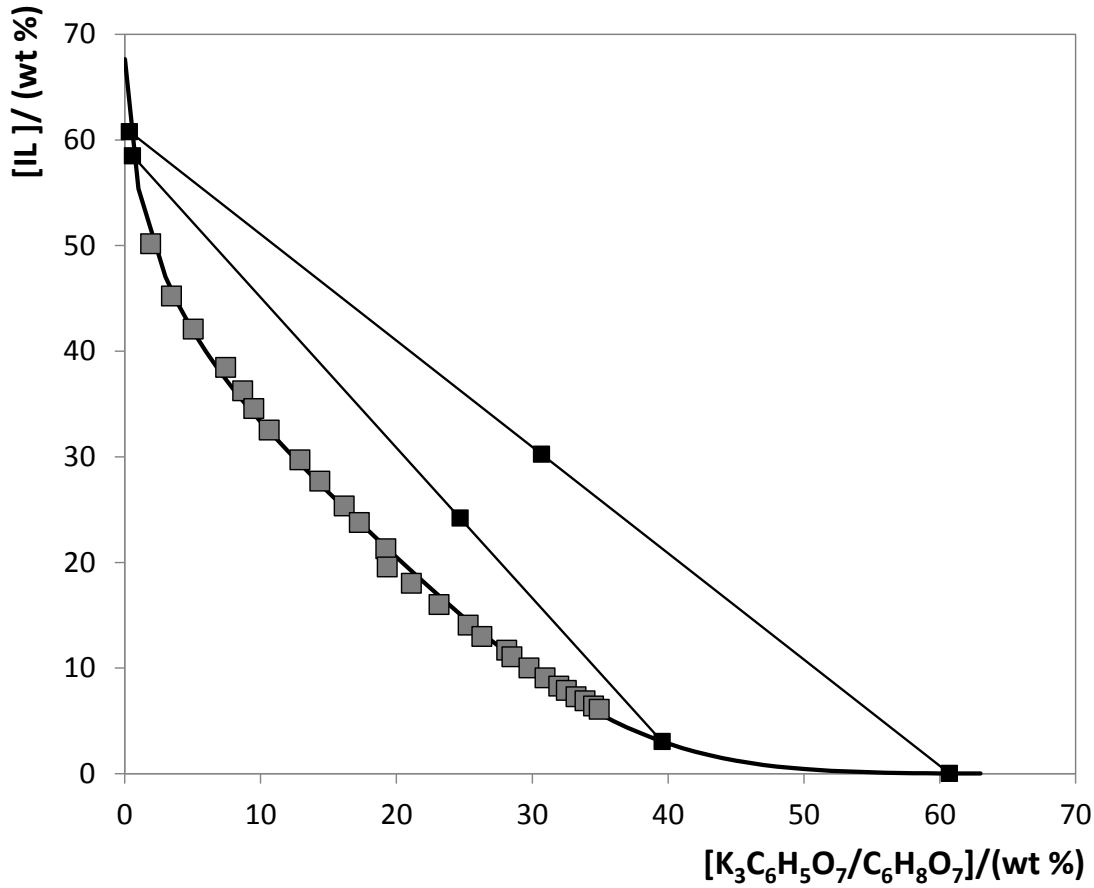

Figure B5. Phase diagram for the system composed of $[N_{4444}]Cl + K_3C_6H_5O_7/C_6H_8O_7 + H_2O$ at 25°C and pH 7.0: binodal curve data (■); TL data (■); adjusted binodal data through Equation 1 (—).

Appendix C

Table C2. Experimental weight fraction data for the systems composed of PEG 400 (1) + $C_6H_5K_3O_7$/$C_6H_8O_7$ (2) + H_2O (3) at 25°C.

pH 5		pH 6		pH 8	
100 w_1	100 w_2	100 w_1	100 w_2	100 w_1	100 w_2
13.8784	44.0714	12.7242	41.2876	68.0207	1.4982
15.8030	41.1839	13.5478	39.3030	60.6933	2.8980
17.1646	38.9245	14.7701	37.6565	57.5232	3.7124
19.3922	36.7353	15.7787	35.3873	54.2955	4.3635
21.0099	34.8396	16.2211	34.0678	51.6291	5.1016
23.5517	32.7621	17.5670	32.2227	48.3830	6.0044
25.2393	31.1759	18.7109	30.6367	44.8083	6.9456
26.8034	29.9046	19.9625	29.1688	40.2519	8.2738
28.2945	28.6035	21.6725	27.7436	39.5334	8.5822
29.5790	27.4259	23.4239	26.5159	38.7919	8.9058
31.3389	26.2354	23.8886	25.6818	38.0258	9.2458
32.3955	25.2020	25.2992	24.6300	37.2332	9.6035
32.6902	24.6885	26.6489	23.6464	36.3949	9.9819
34.1753	23.6390	27.8100	22.7248	35.5420	10.3786
35.7246	22.6037	28.9584	21.9689	34.6619	10.7976
36.4717	21.9259	29.8614	21.2308	33.7523	11.2408
37.6852	21.0508	30.7524	20.4976	32.8105	11.7106
39.0763	20.1973	32.3364	19.6229	31.8337	12.2092
41.3708	19.1531	33.2482	18.9739	30.7015	12.7517
42.1115	18.5689	34.3542	18.2869	29.8047	13.3088
44.3205	17.4301			28.9110	13.8516
				27.2947	14.6005
				26.3131	15.2395
				25.7023	15.7740
				25.1869	16.2964
				23.8576	17.0889
				22.5121	17.9341
				21.8801	18.5595
				20.4643	19.4835
				19.2419	20.3042
				18.4269	21.1170
				16.6452	22.2122
				15.7167	23.1358
				13.7114	24.4315
				11.3638	25.9401
				10.3368	27.0210
				6.4377	31.3587

Table C2. Experimental weight fraction data for the systems composed of PEG (1) + $C_6H_5K_3O_7/C_6H_8O_7$ (2) + H_2O (3) at 25°C and pH 7.

PEG 400		PEG 600		PEG 1000	
100 w_1	100 w_2	100 w_1	100 w_2	100 w_1	100 w_2
82.6364	2.7688	85.9890	1.7175	57.8766	5.9077
75.1384	3.7415	75.6691	3.2334	52.8615	6.5404
69.3176	4.8225	66.0885	4.1373	47.5771	7.0310
64.5254	5.9201	61.2011	5.2283	43.2552	8.0531
60.4327	6.9732	57.0016	6.2553	40.5045	9.0397
56.8465	7.0909	53.3512	7.1548	38.5181	9.3272
53.6422	8.1477	48.9937	7.7503	37.3214	9.7977
50.7347	9.1522	45.9932	8.3937	36.3024	10.2048
50.3763	9.2678	43.8617	9.0435	34.8850	10.7059
44.9721	10.9316	41.6540	9.5154	33.3928	11.0325
42.1959	12.4068	40.2461	10.0757	32.4179	11.4377
40.9067	12.9465	38.8544	10.6452	31.5184	11.7518
39.3859	13.5980	37.2160	11.0289	30.6611	12.1286
37.4982	14.6429	36.0051	11.5597	29.8253	12.4888
36.3936	15.1547	34.9330	12.0149	29.0518	12.8247
35.2881	15.5759	34.0072	12.4572	28.2799	13.2131
33.4970	16.6700	33.1104	12.8165	27.6278	13.4697
32.0660	17.4791	32.2384	13.1799	26.9766	13.6716
30.7214	18.2968	31.3807	13.4793	26.3515	13.9313
29.4833	19.0725	30.5355	13.8412	24.6438	14.6031
28.5894	19.5448	29.4578	14.5832	24.1790	14.9130
27.4451	20.3323	27.6537	15.0870	23.3543	15.3366
26.1742	21.1703	25.0088	16.1531	22.7360	15.7350
25.2695	21.6338	22.7269	17.7926	21.5921	16.2943
24.0984	22.5744	22.2983	18.1895	20.3070	16.8851
23.0210	23.3475	21.4583	18.7162	19.3895	17.4345
22.9418	24.0731	20.7102	19.2075	17.9807	18.1916
22.1722	24.6153	19.8200	19.7896	16.8277	18.8238
21.4621	25.0926	18.8294	20.4667	15.9315	19.3771
20.9712	25.4513	18.6367	21.3598	14.7080	20.0678
20.8230	25.7781	16.6079	22.1350	13.0007	20.8642
20.3333	26.0970	16.0212	22.5600	11.7033	21.7123
20.4662	26.1916	14.8776	23.3935	10.9790	22.2316
19.9953	26.5007	13.5874	24.3492	9.4577	23.0413
19.4360	26.9010	12.1340	25.3038	8.8034	23.6258
17.7018	29.0287	10.4744	26.5086	7.1315	24.5652

16.9222	30.0241	9.6662	27.1884	6.3816	25.3675
15.8030	32.5812	8.6476	28.1055	5.3984	26.0209
15.3813	32.7344	7.5462	29.1223	3.4627	28.1891
14.1924	33.5291	6.5676	30.2392		
13.3104	35.7602	5.6147	31.3011		
12.4501	37.8980	3.6603	33.7064		
11.8434	39.2537				

Table C3. Partition coefficients (K_{Ova}) and extraction efficiencies ($EE\%_{Ova}$) of ovalbumin and weight fraction compositions of the initial mixtures at 25°C.

PEG	pH	Weight fraction composition / (wt %)		$K_{Ova} \pm \sigma$	$EE\%_{Ova} \pm \sigma$
		PEG	$C_6H_5K_3O_7/C_6H_8O_7$		
400	5	30.01	29.99	12.6 ± 0.3	94.8 ± 0.7
	6	29.99	29.85	32.8 ± 0.3	96.1 ± 0.1
	7	29.98	29.97	54.7 ± 0.1	97.7 ± 0.7
	8	30.13	29.84	52.4 ± 0.1	96.5 ± 0.5

Table C4. Partition coefficients (K_{Ova}) and extraction efficiencies ($EE\%_{Ova}$) of ovalbumin and weight fraction compositions of the initial mixtures at 25°C and pH 7.

PEG	Weight fraction composition / (wt %)		$K_{Ova} \pm \sigma$	$EE\%_{Ova} \pm \sigma$
	PEG	$C_6H_5K_3O_7/C_6H_8O_7$		
400	24.75	25.28	76.4 ± 0.4	98.8 ± 0.7
	29.98	19.97	89.5 ± 0.2	98.9 ± 0.1
	30.05	24.97	76.4 ± 0.6	98.8 ± 0.8
	30.01	29.84	54.7 ± 1.0	97.6 ± 0.5
	35.72	24.97	74.4 ± 0.4	98.4 ± 0.7
600	25.05	24.98	54.5 ± 0.1	97.1 ± 0.4
	30.13	20.38	55.7 ± 0.4	96.1 ± 0.3
	30.21	25.44	54.7 ± 0.5	97.1 ± 0.3
	29.79	30.01	52.7 ± 0.9	97.8 ± 0.1
	35.06	24.98	34.7 ± 0.6	97.7 ± 0.5
1000	24.93	25.42	35.5 ± 0.6	95.6 ± 0.4
	29.94	20.01	12.7 ± 0.2	93.6 ± 0.8
	29.87	25.06	35.5 ± 0.3	95.6 ± 0.7
	30.10	29.93	51.6 ± 0.9	97.8 ± 0.4
	34.95	25.15	22.1 ± 0.2	95.2 ± 0.9

Table C5. Partition coefficients (K_{Ova}) and extraction efficiencies ($EE\%_{Ova}$) of ovalbumin from egg white and weight fraction compositions of the initial mixtures at 25°C and pH 7.

PEG	Weight fraction composition / (wt %)		$K_{Ova} \pm \sigma$	$EE\%_{Ova} \pm \sigma$
	PEG	$C_6H_5K_3O_7/C_6H_8O_7$		
400	25.43	25.28	74.4 ± 0.6	98.4 ± 0.3
600	24.65	25.05	34.7 ± 0.6	97.7 ± 0.1
1000	25.16	25.35	22.1 ± 0.1	95.2 ± 0.9

Appendix D

Section D3. Synthesis of GB-ILs

Tri(n-butyl)[2-ethoxy-2-oxoethyl]phosphonium bromide ([Bu_3PC_2]Br)

Tri(n-butyl)[2-ethoxy-2-oxoethyl]phosphonium bromide ([Bu_3PC_2]Br) was synthesized by the reaction : A solution of tri(n-butyl)phosphine (131.7 mL, 102.5 g 0.55 mol) in ethyl acetate (150 mL) cooled to 4 C was added dropwise 2-bromoacetic acid ethyl ester (37.5 g, 0.22 mol). The mixture was then stirred at room temperature for 1 day. Precipitate produced during the reaction was filtered and washed with ethyl acetate. Recrystallization of the residue by ethanol/ethyl acetate (10:90, V:V) gave a white powder which was filtered, washed with ethyl acetate and dried in vacuum yield 90%.

Tri(n-butyl)[2-butoxy-2-oxoethyl]phosphonium bromide ([Bu_3PC_4]Br)

Tri(n-butyl)[2-butoxy-2-oxoethyl]phosphonium bromide ([Bu_3PC_4]Br), was synthesized by the reaction : A solution of tri(n-butyl)phosphine (83.8 mL, 65.2 g, 0.35 mol) in ethyl acetate (150 mL) was added a solution of 4-bromobutyric acid ethyl ester (29.6 mL, 37.5 g, 0.22 mol) in 50 mL of ethyl acetate. The mixture was refluxed for 2 days and then stirred at room temperature for one day. The brownish oil which separated was recovered and washed three times with ethyl acetate and kept in a freezer. The white product, which crystallised after 48 hours, was washed with ethyl acetate and diethyl ether and then dried in vacuum yield 85%.

Section D2 . Characterization of GB-ILs

Tri(n-butyl)[2-ethoxy-2-oxoethyl]phosphonium bromide ([Bu_3PC_2]Br)

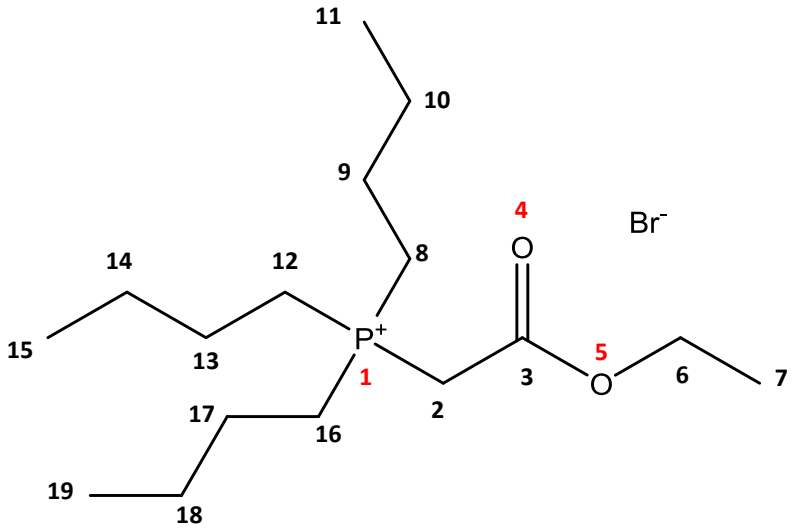

^{1}H and ^{13}C NMR

1H NMR (300 MHz, D_2O) δ 0.83 (t, *J* = 7.3 Hz, 9H, 11, 15, 19), 1.20 (t, *J* = 7.3 Hz, 3H, 7), 1.36 - 1.50 (p, *J* = 7.1 Hz, 8H, 8, 9, 10, 12, 13, 14, 16, 17, 18), 3.5 (m, 2H, 2), 4.14 – 4.22 (q, 2H, 6).

^{13}C NMR (75 MHz, D_2O) δ 12.44 (11, 15, 19), 13.14 (7), 17.97 (12, 16), 18.61 (8), 22.61 (13, 17), 22.67 (9), 23.05 (10, 14, 18), 23.26 (2), 62.78 (6), 166.49 (3).

Elemental Analysis ($C1_6H_{34}BrO_2P$)

Calculated: C 55.5, H 9.8%.

Experimental: C 55.2, H 9.8%.

Molecular Weight: 369.32

Melting Point: 95.8

Tri(n-butyl)[2-butoxy-2-oxoethyl]phosphonium bromide ([Bu_3PC_4]Br)

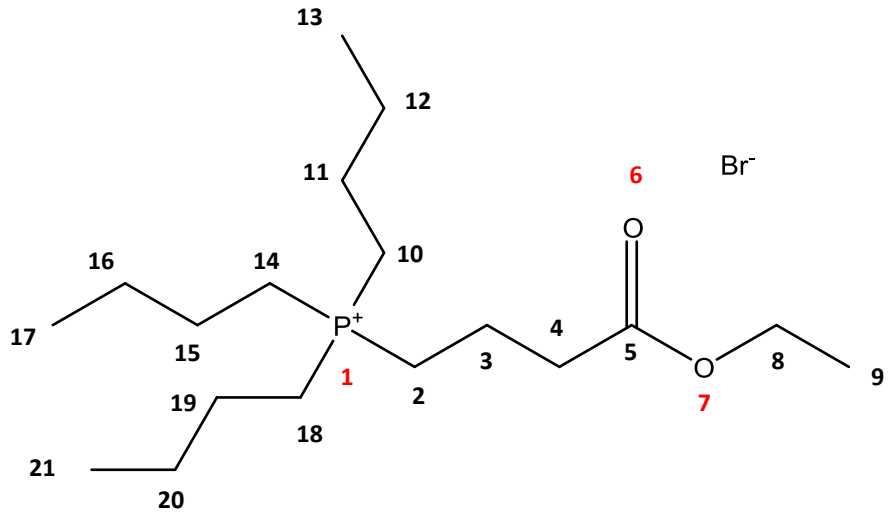

^{1}H and ^{13}C NMR

1H NMR (300 MHz, D_2O) δ 0.90 – 0.95 (t, *J* = 7.3 Hz, 12H, 9, 12, 13), 1.19 -1.24 (t, *J* = 7.3 Hz, 10H, 10, 11, 17, 21), 2.10 – 2.21 (p, *J* = 7.1 Hz, 16H, 2, 3, 14, 15, 16, 18, 19, 20), 2.51 (m, 2H, 4), 4.09 (m, 2H, 8).

^{13}C NMR (75 MHz, D_2O) δ 12.48 (3), 13.28 (13, 17, 21), 16.39 (9), 17.13 (1, 14, 18), 17.77 (2), 22.59 (11, 15, 19), 23.32 (12, 16, 20), 34.14 (4), 61.85 (8), 174.90 (5).

Elemental Analysis ($C1_6H_{34}BrO_2P$)

Calculated: C 52.0, H 9.3%.

Experimental: C 52.0, H 9.6%.

Molecular Weight: 411.41

Melting Point: 94.7

Table D1. Experimental weight fraction data for the systems composed of $[Bu_3PC_4]Br$ (1) + monosaccharide (2) + H_2O (3) at 25°C.

Glucose		Galactose		Fructose	
100 w_1	100 w_1	100 w_2	100 w_2	100 w_1	100 w_2
76.2046	5.0596	86.4755	2.7075	81.0714	5.8724
73.2867	6.4879	65.4044	8.5725	70.0528	10.2726
70.3418	8.0306	55.9454	13.6487	64.4838	11.7857
67.9864	9.3671	52.3490	15.0090	61.2938	13.1946
65.2930	10.9041	46.7844	17.9298	58.6819	14.7057
63.1966	11.7704	39.0503	22.4056	56.3363	16.2181
60.7889	13.0084	33.4223	25.6102	54.2426	17.7576
57.8404	14.9106			51.6018	18.7345
54.9762	15.5047			49.7134	19.8538
52.6854	17.0264			48.1657	21.1593
50.5807	17.7259			46.6294	22.1071
49.2381	18.3758			44.9965	23.1818
48.0083	18.9905			44.4269	22.9080
46.7947	19.5899			42.5833	23.5524
45.5004	20.3919			40.7628	24.6571
44.6287	20.6342			39.6606	25.3565
42.5999	22.0201			38.4632	26.1339
41.5802	22.6659			37.0386	27.3864
39.7049	24.3325			36.0612	28.0336
39.8876	25.1501			35.0727	28.6690
39.0395	25.6132			34.2016	29.2380
38.2413	26.2935			33.0209	29.0094
37.6174	26.6062			32.5855	29.7378
36.6315	27.2277			31.9066	30.3246
35.8935	27.4931			31.2262	30.8089
34.0561	28.7371			30.5431	31.3683
33.3432	29.1957			29.7131	31.6630
32.7902	29.4116			29.0761	32.0630
31.5541	30.2995			28.4713	32.5281
30.9390	30.6830			27.8662	32.9669
30.3576	31.2917			27.3673	33.3752
29.1455	32.1477			26.7592	33.5980
28.8277	32.1836			26.2775	33.9657
28.1429	32.7437			25.7862	34.4290
27.3083	33.1985			25.3592	34.8020
26.8415	33.4510			24.7911	34.9796
25.8495	34.0921			24.3317	35.3268
25.2260	34.5496			23.8808	35.7083
24.7896	34.7633			23.0314	36.6734
23.8139	35.4569			22.5850	36.7906

23.4198	35.6896		22.2003	37.1706
22.8737	36.1996		21.5038	37.8895
22.3249	36.5749		20.7676	38.2198
22.0319	36.7009		20.4619	38.5160
21.5407	37.1031		20.1317	38.8125
21.2088	37.2917		19.8242	39.0483
20.7509	37.7042		19.5373	39.3276
20.3274	38.0959		18.2939	40.4776
19.2686	38.8309		17.0756	41.4320
			16.6399	41.7835
			16.2663	42.1000
			15.8836	42.5766
			15.3841	43.1937
			15.0166	43.4171
			14.4681	44.0375
			14.1448	44.5302
			13.5399	45.2959
			12.9954	45.8808
			12.6921	46.0258
			12.2120	45.9004
			11.9714	46.1179
			11.5435	46.9953
			11.2149	47.4557
			10.8681	47.9758

Table D2. Experimental weight fraction data for the systems composed of $[Bu_3PC_4]Br$ (1) + monosaccharide (2) + H_2O (3) at 25°C.

Arabinose		Mannose	
100 w_1	100 w_1	100 w_1	100 w_2
89.3082	3.0736	55.2097	11.0407
81.1093	6.5802	48.8483	12.1263
74.5095	8.2243	31.9643	18.358
66.8030	12.0018	30.0462	20.2357
62.3798	13.7638	28.7566	21.4988
55.3122	17.2569	26.8592	23.3556
50.3365	19.8645	21.2481	29.0164
41.7202	24.5921	20.0189	30.3467
36.0764	27.5139	18.3509	32.1399
31.3416	30.1302	17.2262	33.433
		13.7316	37.7718

Table D3. Experimental weight fraction data for the systems composed of $[Bu_3PC_4]Br$ (1) + polyols (2) + H_2O (3) at 25°C.

Sorbitol		Xylitol		Maltitol	
100 w_1	100 w_1	100 w_2	100 w_2	100 w_1	100 w_2
72.4437	10.9600	46.8773	24.7859	84.1690	2.6551
66.2891	13.4174	44.0246	26.8282	77.4722	5.8590
62.3754	14.5225	42.5740	27.7236	72.8268	8.3624
56.0517	16.5497	39.8600	29.6525	68.2169	10.6647
50.9498	19.1093	38.3747	30.3143	62.6544	13.9464
46.0666	21.9108	36.1221	31.8845	53.5050	16.6306
43.9932	23.0065	34.1760	33.1498	44.0870	21.5703
42.4734	23.8344	32.6039	34.1942	38.8360	23.1351
39.0671	26.0704	31.0706	35.2508		
37.9997	26.5721	30.2977	35.6006		
36.6341	27.4801	29.0750	36.4170		
34.7270	28.7261	28.2436	36.8143		
33.0946	29.3649	27.5806	37.2200		
30.5595	30.9903				
28.8375	32.1999				
26.6611	33.5567				
26.2328	33.3580				
24.5632	34.8383				
23.2952	35.7921				
21.6718	36.9803				
19.6494	38.6823				
16.8948	41.2389				

Table D4. Experimental weight fraction data for the systems composed of IL (1) + Fructose (2) + H_2O (3) at 25°C.

$[Bu_3PC_2]Br$		$[P_{4444}]Br$		$[P_{4441}][MeSO_4]$	
100 w_1	100 w_1	100 w_2	100 w_2	100 w_1	100 w_2
75.7834	10.2019	84.2115	4.4238	74.9300	11.8629
72.0334	11.1339	75.6491	11.1818	61.6603	20.5770
69.1868	12.2178	73.6149	12.0880	56.1941	23.9891
67.9224	12.5751	70.9021	13.3861	51.9984	26.9508
66.0813	13.2470	67.4206	14.6601	45.8537	31.2701
64.1281	14.2136	64.3379	15.6287	40.7686	35.3375
61.8875	15.1468	62.5354	16.8775	37.1898	37.8258
60.1951	15.8499	59.8745	17.6634	28.9239	41.7419
58.6611	16.7380	57.7749	18.0574		
57.1024	17.5773	55.5168	19.0153		
55.0136	18.3791	53.8827	20.0039		
53.9019	18.9999	52.0864	20.8428		
52.4493	19.8369	47.4227	22.7050		
51.2373	20.4755	46.1664	23.4870		
49.2666	21.3005	44.8703	24.3147		
48.0859	22.0121	43.5547	25.2103		
47.0433	22.6688	42.5047	25.8726		
46.2350	22.9879	41.4130	26.5294		
45.0880	23.4559	40.5985	27.0383		
43.0300	24.6652	39.4686	27.2633		
42.1324	25.1793	38.5371	27.8256		
41.3223	25.7135	37.8072	28.1850		
40.4144	26.1943	36.5153	29.2882		
38.7647	27.2626	35.8154	29.6643		
37.3133	27.7620	35.1540	30.0182		
35.7667	28.8755	34.2505	30.7381		
35.0560	29.3385	32.7716	31.4154		
32.9650	30.6197	32.0337	31.9249		
31.3947	31.7700	30.7980	32.5882		
29.5128	33.3363	30.2783	32.7269		
29.1112	33.5484	29.3915	33.6025		
28.5566	33.8660	28.6963	33.8523		
27.2457	34.6656	28.1910	34.1209		
26.6039	35.1869	27.3901	34.7376		
26.2451	35.3693	26.9654	35.0214		
25.6839	35.8097	26.4075	35.1627		
25.5170	35.6890	25.9604	35.4735		
24.9670	35.5465	25.6112	35.7525		

24.4053	35.9948	25.0761	36.2587	
24.0864	36.1904	24.7190	36.4571	
23.3689	36.7681	24.4384	36.6312	
22.7950	37.1854	24.1011	36.7437	
22.5760	37.2453	23.7848	36.8359	
22.1595	37.6368	23.2568	36.7869	
21.7242	37.9415	22.9557	37.0007	
21.4078	38.1918	22.8625	36.9975	
21.1537	38.3460	22.5518	37.1308	
20.2877	39.2589	21.8672	38.1219	
		21.6282	38.2370	
		21.2399	38.6251	
		20.9871	38.7536	
		20.7307	38.9909	
		20.3015	39.3040	
		20.0824	39.4197	

Table D5. Correlation parameters of Eq. (1) used to describe the experimental binodal data at 298 K.

IL + carbohydrate + water					
IL	**Carbohydrate**	$A \pm \sigma$	$B \pm \sigma$	$10^5 (C \pm \sigma)$	R^2
$[P_{4441}][MeSO_4]$	D(+)-fructose	118.7±7.59	-0.130±0.01	0.71±0.08	0.9969
$[P_{4444}]Br$		123.5±3.38	-0.155±0.08	1.43±0.05	0.9929
$[Bu_3PC_2]Br$		158.7±2.24	-0.232±0.03	0.99±0.02	0.9994
$[Bu_3PC_4]Br$		136.9±1.76	-0.211±0.03	1.02±0.01	0.9988
	D-(+)-mannose	254.0±3.13	-0.468±0.34	0.01±0.25	0.9934
	D(+)-galactose	120.0±1.81	-0.200±0.05	1.56±0.15	0.9992
	D-(+)-glucose	118.7±2.16	-0.185±0.05	1.12±0.04	0.9971
	D(+)-arabinose	120.7±2.92	-0.163±0.08	1.68±0.15	0.9979
	xylitol	82.0±8.88	-0.075±0.02	1.21±0.07	0.9995
	D-sorbitol	178.1±5.60	-0.268±0.08	0.91±0.05	0.9998
	maltitol	100.1±2.93	-0.104±0.01	3.56±0.03	0.9964

Table D6. Recovery yield ($RY\%_{PROT}$) and purification yield ($PY\%_{PROT}$) of MRJP and weight fraction compositions of the initial mixtures at 25 °C.

IL	**Weight fraction composition / (wt %)**		$RY\%_{PROT} \pm \sigma$	$PY\%_{PROT} \pm \sigma$
	IL	**Honey**		
$[P_{4444}]Br$	24.95 ± 0.02	60.86 ± 0.12	83.84 ± 0.60	80.02 ± 1.36
$[P_{4441}][MeSO_4]$	25.05 ± 0.07	60.83 ± 0.09	87.75 ± 0.75	89.42 ± 1.48
$[Bu_3PC_2]Br$	24.97 ± 0.04	60.96 ± 0.07	97.30 ± 0.61	90.98 ± 0.49
$[Bu_3PC_4]Br$	24.92 ± 0.11	60.15 ± 0.04	92.53 ± 0.23	84.12 ± 1.07

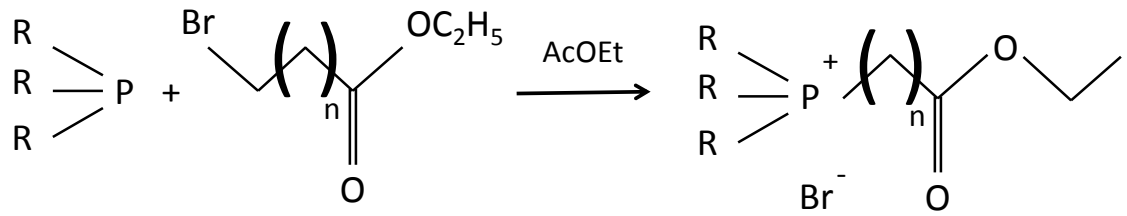

n = 1 or 3 R = *n*-C_4H_9

Figure D1. Synthetic route of GB-ILs.

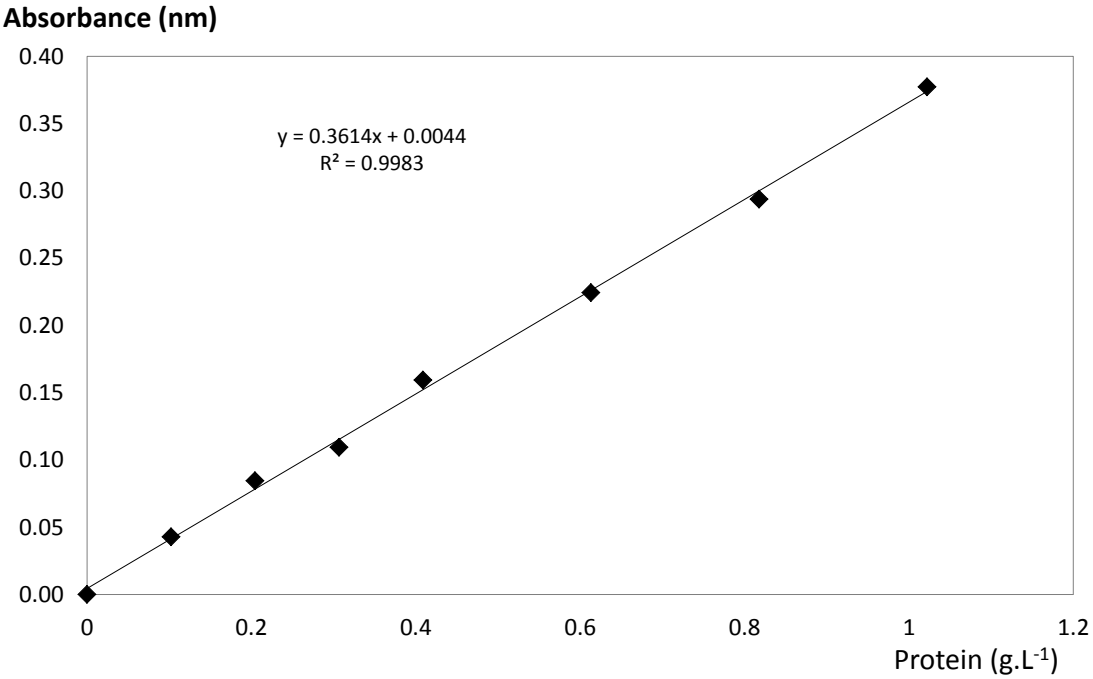

Figure D2. Proteins calibration curve (UV-Vis - 595 nm) determined by the Bradford's method.

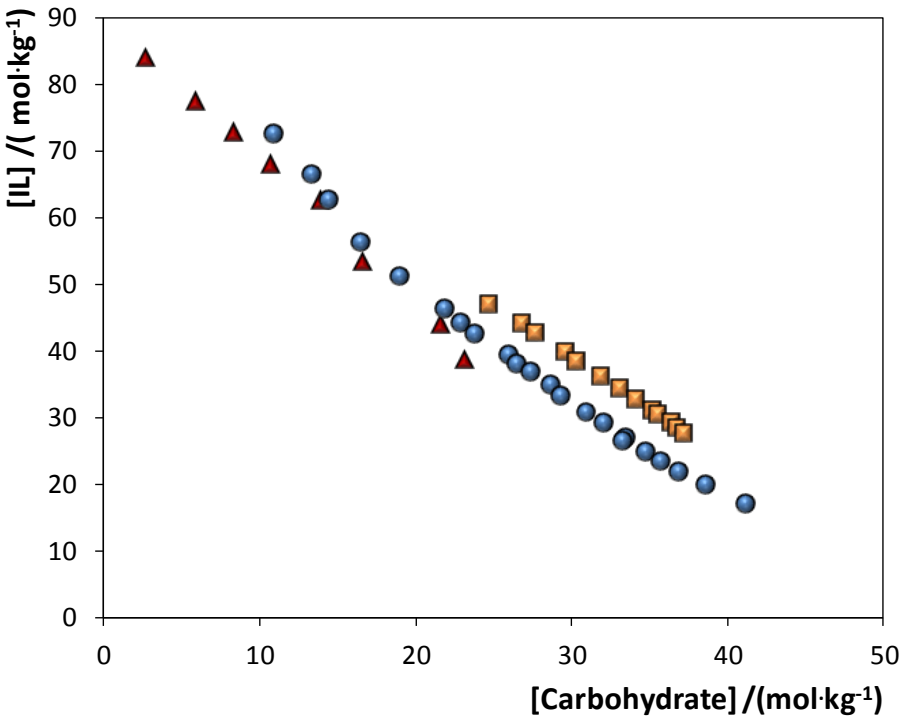

Figure D3. Phase diagrams for the systems composed of $[Bu_3PC_4]Br$ + Carbohydrates + H_2O at 25°: maltitol (▲); D-sorbitol (●), xylitol (■).

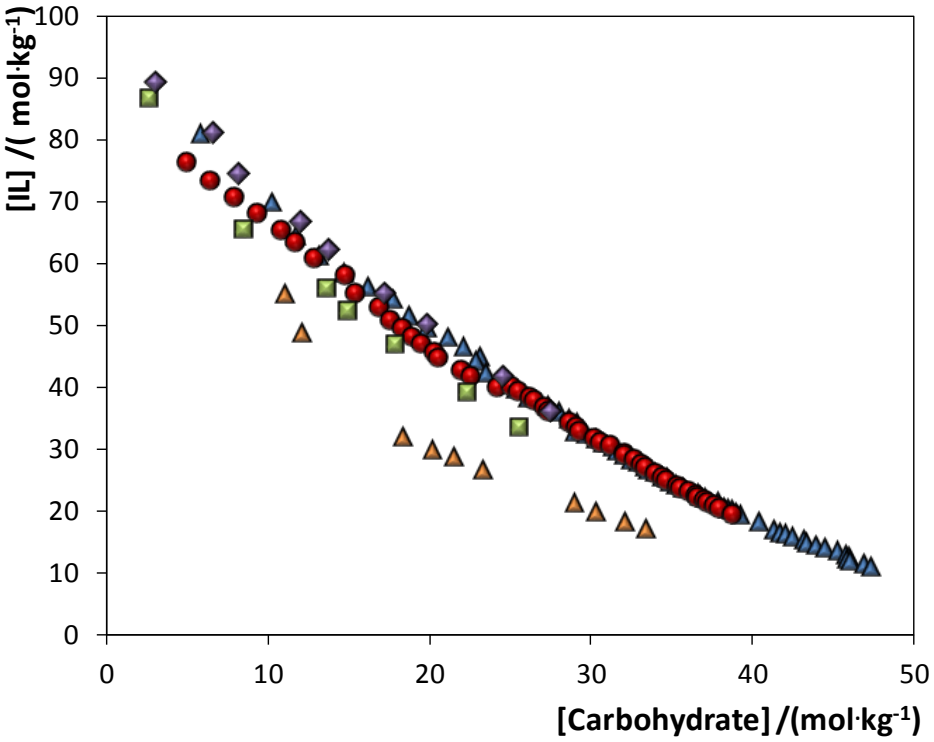

Figure D4. Phase diagrams for the systems composed of $[Bu_3PC_4]Br$ + Carbohydrates + H_2O at 25°: D-(+)-mannose (▲), D(+)-galactose (■), D-(+)-glucose (●), D(+)-fructose (▲), D(+)-arabinose, (◆).

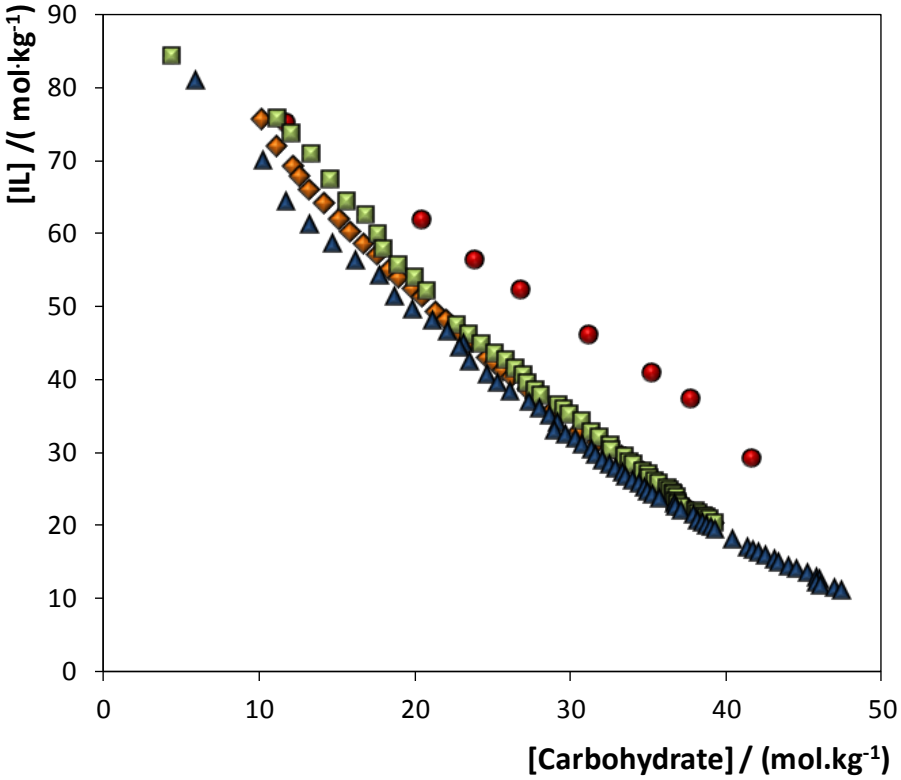

Figure E5. Phase diagrams for the systems composed of IL + D(+)-fructose + H_2O at 25°: $[P_{4441}][MeSO_4]$ (●), $[P_{4444}]Br$ (■), $[Bu_3PC_2]Br$ (◆), $[Bu_3PC_4]Br$ (▲).

Appendix E

Section E4. Synthesis of GB-ILs

n-(1-methylpyrrolidyl-2-butoxy-2-oxoethyl)ammonium bromide ([MePyrNC$_4$][Br])

n-(1-methylpyrrolidyl-2-butoxy-2-oxoethyl)ammonium bromide ([MePyrNC$_4$][Br]) was synthesized by the reaction : (90 mL , 68.85 g, 0.81 mol) in ethyl acetate (150 mL) was added 4-bromobutyrate acid ethyl ester (68 mL, 98.7 g, 0.51 mol) whilst stirring. The mixture was refluxed for 12h and the stirred at room temperature for 2h. Precipitate produced was filtered and washed twice with ethyl acetate and then with ethyl ether, and dried in vacuum.

Tri(n-ethyl)[2-butoxy-2-oxoethyl]ammonium bromide ([Et$_3$NC$_4$]Br)

Tri(n-ethyl)[2-butoxy-2-oxoethyl]ammonium bromide ([Et$_3$NC$_4$]Br) was synthesized by the reaction: trialkylamine (120 mL , 81.96 g, 0.81 mol) in ethyl acetate (160 mL) was added 4-bromobutyrate acid ethyl ester (68 mL, 98.7 g, 0.51 mol) whilst stirring. The mixture was refluxed for 12h and the stirred at room temperature for 2h. Precipitate produced was filtered and washed twice with ethyl acetate and then with ethyl ether, and dried in vacuum.

Tri(n-propyl)[2-butoxy-2-oxoethyl]ammonium bromide ([Pr$_3$NC$_4$]Br)

Tri(n-propyl)[2-butoxy-2-oxoethyl]ammonium bromide ([Pr$_3$NC$_4$]Br) was synthesized by the reaction : trialkylamine (160 mL , 116.03 g, 0.81 mol) in ethyl acetate (200 mL) was added 4-bromobutyrate acid ethyl ester (68 mL, 98.7 g, 0.51 mol) whilst stirring. The mixture was refluxed for 12h and the stirred at room temperature for 2h. Precipitate produced was filtered and washed twice with ethyl acetate and then with ethyl ether, and dried in vacuum.

Tri(n-butyl)[2-butoxy-2-oxoethyl]ammonium bromide ([Bu$_3$NC$_4$]Br)

Tri(n-butyl)[2-butoxy-2-oxoethyl]ammonium bromide ([Bu$_3$NC$_4$]Br) was synthesized by the reaction : trialkylamine (210 mL , 159.49 g, 0.81 mol) in ethyl acetate (250 mL) was added 4-bromobutyrate acid ethyl ester (68 mL, 98.7 g, 0.51 mol) whilst stirring. The mixture was refluxed for 48h and the stirred at room temperature for 2h. At rest the solution separates into two phases, the bottom phase was recovered and dissolved in 100 mL of ethyl acetate and kept in the freezer for 48 h. The crystallized residue is filtered, washed with ethyl acetate and then with ethyl ether, and dried in vacuum.

Tri(n-butyl)[2-butoxy-2-oxoethyl]phosphonium bromide ([Bu_3PC_4]Br)

Tri(n-butyl)[2-butoxy-2-oxoethyl]phosphonium bromide ([Bu_3PC_4]Br) was synthesized by the reaction : A solution of tri(n-butyl)phosphine (83.8 mL, 65.2 g, 0.35 mol) in ethyl acetate (150 mL) was added a solution of 4-bromobutyrate acid ethyl ester (29.6 mL, 37.5 g, 0.22 mol) in 50 mL of ethyl acetate. The mixture was refluxed for 2 days and then stirred at room temperature for one day. The brownish oil which separated was recovered and washed three times with ethyl acetate and kept in a freezer. The white product, which crystallized after 48 hours, was washed with ethyl acetate and diethyl ether and then dried in vacuum.

Tri(n-propyl)[2-butoxy-2-oxoethyl]ammonium saccharinate ([Pr_3NC_4][Sac])

Tri(n-propyl)[2-butoxy-2-oxoethyl]ammonium saccharinate ([Pr_3NC_4][Sac]) was synthesized by the reaction : Tri(n-propyl)[2-butoxy-2-oxoethyl]ammonium bromide (16 g, 0.05 mol) in water (150 mL) was added silver saccharinate (17.4 g, 0.06 mol) whilst stirring. The mixture was refluxed for 12h and the stirred at room temperature for 2h. Precipitate produced was filtered and washed with ethyl acetate and ethyl ether, then was removed from the supernatant. Therefore, the supernatant was dried in vacuum to remove the organic solvents and water.

Tri(n-propyl)[2-butoxy-2-oxoethyl]ammonium lactate ([Pr_3NC_4][Lac])

Tri(n-propyl)[2-butoxy-2-oxoethyl]ammonium lactate ([Pr_3NC_4][Sac]) was synthesized by the reaction : Tri(n-propyl)[2-butoxy-2-oxoethyl]ammonium bromide (16 g, 0.05 mol) in water (150 mL) was added silver lactate (11.8 g, 0.06 mol) whilst stirring. The mixture was refluxed for 12h and the stirred at room temperature for 2h. Precipitate produced was filtered and washed with ethyl acetate and ethyl ether, then was removed from the supernatant. Therefore, the supernatant was dried in vacuum to remove the organic solvents and water.

Tri(n-propyl)[2-butoxy-2-oxoethyl]ammonium pyruvate ([Pr_3NC_4][Pyr])

Tri(n-propyl)[2-butoxy-2-oxoethyl]ammonium pyruvate ([Pr_3NC_4][Pyr]) was synthesized by the reaction : Tri(n-propyl)[2-butoxy-2-oxoethyl]ammonium bromide (16 g, 0.05 mol) in water (150 mL) was added silver pyruvate (11.6 g, 0.06 mol) whilst stirring. The mixture was refluxed for 12h and the stirred at room temperature for 2h. Precipitate

produced was filtered and washed with ethyl acetate and ethyl ether, then was removed from the supernatant. Therefore, the supernatant was dried in vacuum to remove the organic solvents and water.

Tri(n-propyl)[2-butoxy-2-oxoethyl]ammonium dicyanamide ([Pr_3NC_4][Dca])

Tri(n-propyl)[2-butoxy-2-oxoethyl]ammonium dicyanamide ([Pr_3NC_4][Dca]) was synthesized by the reaction : Tri(n-propyl)[2-butoxy-2-oxoethyl]ammonium bromide (16 g, 0.05 mol) in water (150 mL) was added silver dicyanamide (10.4 g, 0.06 mol) whilst stirring. The mixture was refluxed for 12h and the stirred at room temperature for 2h. Precipitate produced was filtered and washed with ethyl acetate and ethyl ether, then was removed from the supernatant. Therefore, the supernatant was dried in vacuum to remove the organic solvents and water.

Tri(n-propyl)[2-butoxy-2-oxoethyl]ammonium salicylate ([Pr_3NC_4][Sal])

Tri(n-propyl)[2-butoxy-2-oxoethyl]ammonium salicylate ([Pr_3NC_4][Sal]) was synthesized by the reaction : Tri(n-propyl)[2-butoxy-2-oxoethyl]ammonium bromide (16 g, 0.05 mol) in water (150 mL) was added silver salicylate (14.7 g, 0.06 mol) whilst stirring. The mixture was refluxed for 12h and the stirred at room temperature for 2h. Precipitate produced was filtered and washed with ethyl acetate and ethyl ether, then was removed from the supernatant. Therefore, the supernatant was dried in vacuum to remove the organic solvents and water.

Tri(n-ethyl)[2-butoxy-2-oxoethyl]ammonium salicylate ([Pr_3NC_2][Sal])

Triethyl[2-ethoxy-2-oxoethyl]ammonium bromide ([Pr_3NC_2]Br) was synthesized according to previously reported protocols[1]. Triethyl[2-ethoxy-2-oxoethyl]ammonium salicylate ([Et_3NC_4][Sal]) was synthesized by the reaction : Triethyl[2-ethoxy-2-oxoethyl]ammonium bromide ([Et_3NC_2]Br) (14.1 g, 0.05 mol) in water (150 mL) was added silver salicylate (14.7 g, 0.06 mol) whilst stirring. The mixture was refluxed for 12h and the stirred at room temperature for 2h. Precipitate produced was filtered and washed with ethyl acetate and ethyl ether, then was removed from the supernatant. Therefore, the supernatant was dried in vacuum to remove the organic solvents and water.

Section E2. Characterization of GB-ILs

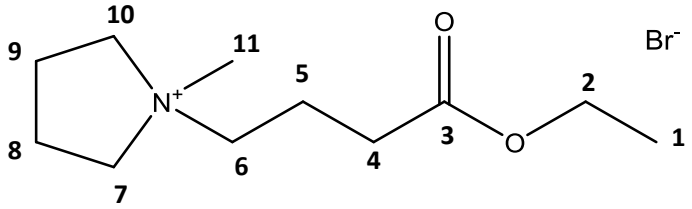

n-(1-methylpyrrolidyl-2-butoxy-2-oxoethyl)ammonium bromide ([MePyrNC$_4$][Br])

^{1}H and ^{13}C NMR

^{1}H NMR (300 MHz, DMSO): δ 1.20 (3 H, t, *J*=7.1 Hz, H1), 1.91-2.01 (2 H, m, H5), 2.08 (2 H, s, H11) 2.41 (2 H, t, *J*=7.2 Hz, H4), 3.27-3.38 (2 H, m, H8, H9), 3.39-3.56 (4 H, m, H6, H7, H10) 4.09 (2 H, q, *J*=7.1 Hz, H2).

^{13}C NMR (75,47 MHz, DMSO): δ 11.2 (C1), 14.8 (C8, C9), 19.1 (C5), 21.7 (C4), 23.0 (C6), 31.3 (C7, C10), 56.9 (C11), 60.5 (C2), 172.5 (C3).

Elemental Analysis ($C_{11}H_{22}BrO_2N$)

Calculated: C 47.1%, H 7.9%, Br 28.5%, N 5%, O 11.42%.

Experimental: C 44.4%, H 7.8%, N 4.7%.

Molecular Weight: 280.21

Melting Point: 73.24

Temperature of Decomposition: 179.52

Solubility in water (25 ° C): 77.40 g/ 100 ml

Tri(n-ethyl)[2-butoxy-2-oxoethyl]ammonium bromide ([Et_3NC_4]Br)

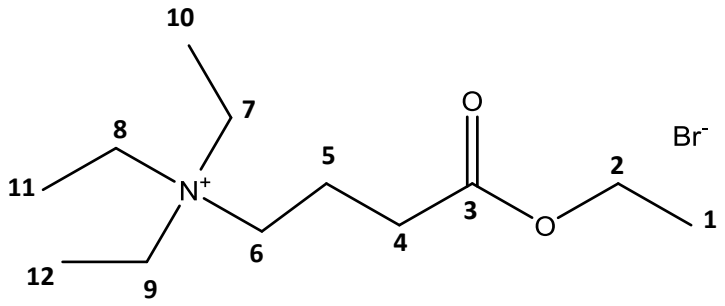

^{1}H and ^{13}C NMR

^{1}H NMR (300 MHz, DMSO): δ 1.19 (12 H, m, H1, H10, H11, H12), 1.77-1.88 (2 H, m, H5), 2.45 (2 H, t, *J*=6.9 Hz, H4), 3.09-3.15 (2H, m, H6), 3.24 (6H, q, J=7.7 Hz, H7, H8, H9), 4.08 (2 H, q, *J*=7.2 Hz, H2).

^{13}C NMR (75,47 MHz, DMSO): δ 14.1 (C10, C11, C12), 19.6 (C1), 23.5 (C5), 33.1 (C4), 56.8 (C6), 58.0 (C7, C8, C9), 60.7 (C6), 62.7 (C2), 139.2 (C3).

Elemental Analysis ($C_{15}H_3BrO_2N$)

Calculated: C 48.6%, H 8.9%, Br 26.9%, N 4.7%, O 10.8%.

Experimental: C 48.0%, H 8.9%, N 4.5%.

Molecular Weight: 296.25

Melting Point: 77.97

Temperature of Decomposition: 187.63

Solubility in water (25 ° C): 72.50 g/ 100 ml

Tri(n-propyl)[2-butoxy-2-oxoethyl]ammonium bromide ([Pr_3NC_4]Br)

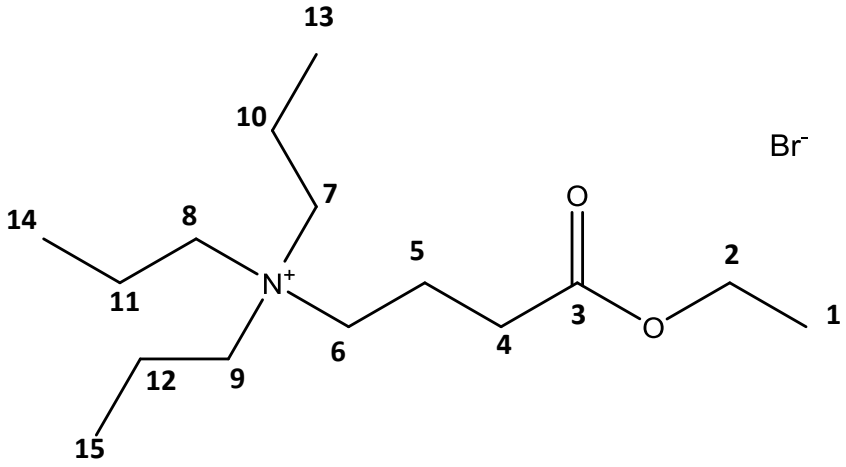

^{1}H and ^{13}C NMR

^{1}H NMR (300 MHz, DMSO): δ 0.90 (9 H, t, *J*=7.2 Hz, H13, H14, H15), 1.20 (3 H, t, *J*=7.1 Hz, H1), 1.57-1.70 (6 H, m, H10, H11, H12), 1.79-1.81 (2 H, m, H5), 2.43 (2 H, t, *J*=7.2 Hz, H4), 3.12-3.20 (8 H, m, H6, H7, H8, H9) 4.08 (2 H, q, *J*=7.2 Hz, H2).

^{13}C NMR (75,47 MHz, DMSO): δ 11.1 (C13, C14, C15), 14.4 (C1), 15.2 (C10, C11, C12), 16.8 (C5), 30.1 (C4), 59.7 (C6, C7, C8, C9), 60.7 (C2), 172.4 (C3).

Elemental Analysis ($C_{15}H_{32}BrO_2N$)

Calculated: C 53.2%, H 9.5%, Br 23.6%, N 4.1%, O 9.4%.

Experimental: C 51.5%, H 9.6%, N 4.2%.

Molecular Weight: 338.33

Melting Point: 78.18

Temperature of Decomposition: 184.63

Solubility in water (25 ° C): 73.20 g/ 100 ml

Tri(n-butyl)[2-butoxy-2-oxoethyl]ammonium bromide ($[Bu_3NC_4]Br$)

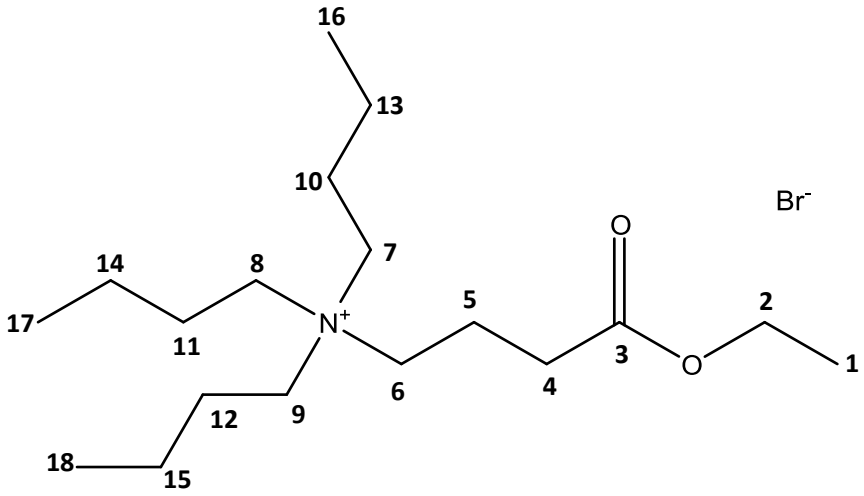

^{1}H and ^{13}C NMR

^{1}H NMR (300 MHz, DMSO): δ 0.94 (9 H, t, *J*=7.3 Hz, H16, H17, H18), 1.21 (3 H, t, *J*=7.4 Hz, H1), 1.25-1.37 (6 H, m, H13, H14, H15), 1.54-1.64 (6 H, m, H10, H11, H12), 1.79-1.89 (2 H, m, H5), 2.43 (2 H, t, *J*=6.7 Hz, H4), 3.15-3.21 (8 H, m, H6, H7, H8, H9), 4.09 (2 H, q, *J*=7.1 Hz, H2).

^{13}C NMR (75,47 MHz, DMSO): δ 14.1 (C16, C17, C18), 19.6 (C1), 23.5 (C13, C14, C15), 33.1 (C5), 56.8 (C10, C11, C12), 58.0 (C4), 60.7 (C6, C7, C8, C9), 62.7 (C2), 139.2 (C3).

Elemental Analysis ($C_{19}H_{40}BrO_2N$)

Calculated: C 57.8%, H 10.2%, Br 20.2%, N 3.5%, O 8.1%.

Experimental: C 57.1%, H 9.9%, N 3.5%.

Molecular Weight: 394.44

Melting Point: 79.64

Temperature of Decomposition: 153.53

Solubility in water (25 ° C): 79.50 g/ 100 ml

Tri(n-ethyl)[2-butoxy-2-oxoethyl]ammonium saccharinate ([Pr_3NC_4][Sac])

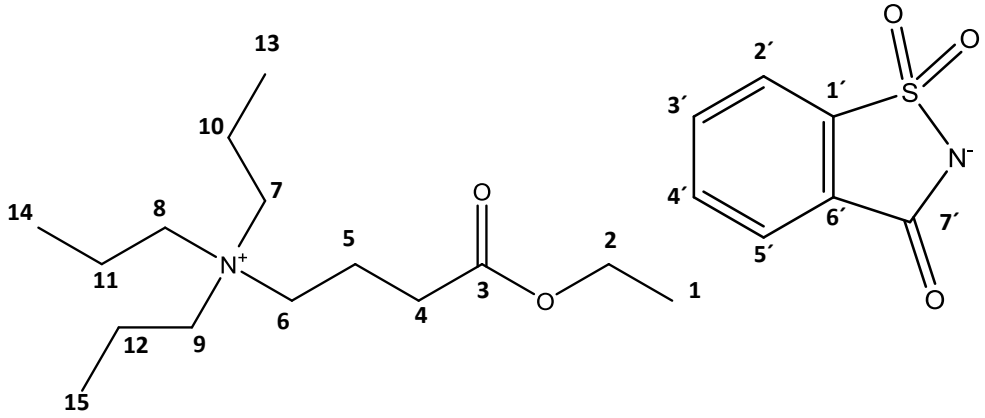

^{1}H and ^{13}C NMR

^{1}H RMN (300 MHz, DMSO): δ 0.89 (9 H, t, J=7.2 Hz, H13, H14, H15), 1.20 (3 H, t, *J*=7.1 Hz, H1), 1.56-1.69 (6 H, m, H10, H11, H12), 1.79-1.89 (2 H, m, H5), 2.42 (2 H, t, *J*=6.8 Hz, H4), 3.11-3.20 (8 H, m, H6, H7, H8, H9) 4.08 (2 H, q, *J*=7.1 Hz, H2), 7.61 (2H, m, H2', H5'), 7,68 (2H, m, H3', H4').

^{13}C NMR (75,47 MHz, DMSO): δ 10.9 (C13, C14, C15), 14.6 (C1), 15.3 (C10, C11, C12), 17.2 (C5), 30.2 (C4), 59.8 (C6, C7, C8, C9), 60.6 (C2), 119.6 (C2'), 123.0 (C5'), 131.6 (C6'), 132.3 (C4'), 135.0 (C3'), 145.6 (C1'), 168.0 (C7'), 172.4 (C3).

Elemental Analysis ($C_{22}H_{36}N_2O_5S$)

Calculated: C 59.9%, H 8.2%, N 6.3%, O 18.1%, S 7.2%.

Experimental: C 56.1, H 8.2%, %, N 6.2%, O 7.0%.

Molecular Weight: 440.60

Melting Point: 98.51

Temperature of Decomposition: 178.81

Solubility in water (25 ° C): 78.02 g/ 100 ml

Tri(n-ethyl)[2-butoxy-2-oxoethyl]ammonium lactate ([Pr_3NC_4][Lac])

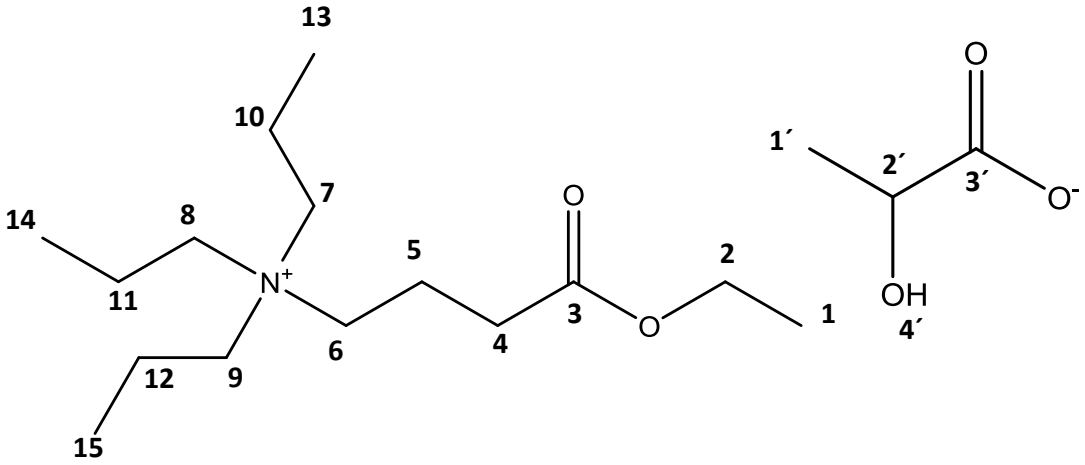

^{1}H and ^{13}C NMR

^{1}H NMR (300 MHz, DMSO): δ 0.90 (9 H, t, *J*=7.2 Hz, H13, H14, H15), 1.04 (3 H, d, *J*=7.0 Hz, H1'), 1.20 (3H, q, *J*=7.1 Hz, H1), 1.22 (1 H, q, *J*=7.1 Hz, H2'), 1.57-1.69 (6 H, m, H10, H11, H12), 1.79-1.81 (2 H, m, H5), 2.42 (2 H, t, *J*=6.8 Hz, H4), 3.12-3.20 (8 H, m, H6, H7, H8, H9) 4.08 (2 H, q, *J*=7.1 Hz, H2).

^{13}C NMR (75,47 MHz, DMSO): δ 11.1 (C13, C14, C15), 14.4 (C1), 15.2 (C10, C11, C12), 22.4 (C1'), 30.4 (C5), 31.2 (C4), 59.6 (C7, C8, C9), 61.1 (C6), 67.6 (C2), 154.1 (C2'), 172.7 (C3, C3').

Elemental Analysis ($C_{18}H_{37}NO_5$)

Calculated: C 62.2%, H 10.7%, N 4.0%, O 23.0%.

Experimental: C 62.8, H 10.0%, %, N 3.7%.

Molecular Weight: 347.50

Melting Point: 33.25

Temperature of Decomposition: 189.64

Solubility in water (25 ° C): 95.90 g/ 100 ml

Tri(n-ethyl)[2-butoxy-2-oxoethyl]ammonium pyruvate ([Pr_3NC_4][Pyr])

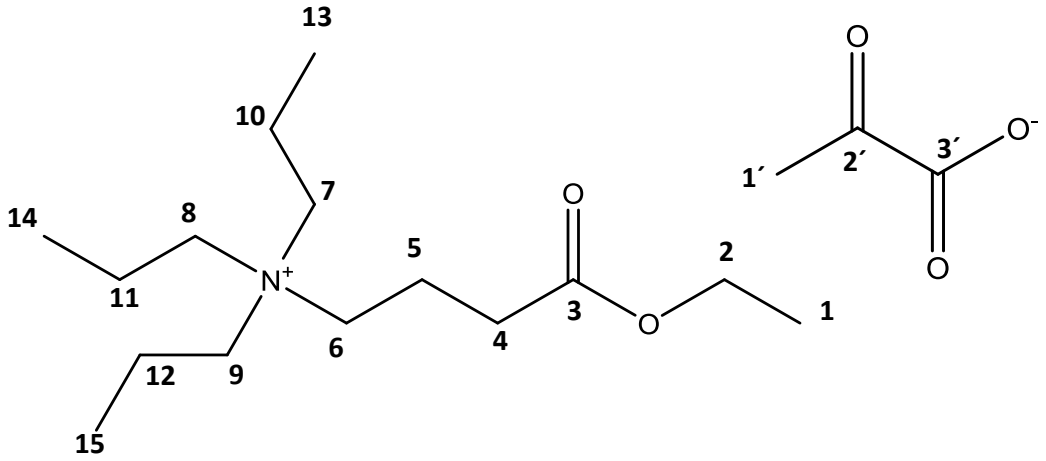

^{1}H and ^{13}C NMR

^{1}H NMR (300 MHz, DMSO): δ 0.90 (9 H, t, *J*=7.2 Hz, H13, H14, H15), 1.20 (3 H, t, *J*=7.1 Hz, H1), 1.57-1.70 (6 H, m, H10, H11, H12), 1.79-1.81 (2 H, m, H5), 2.00 (3H, s, H1'), 2.42 (2 H, t, *J*=6.8 Hz, H4), 3.12-3.20 (8 H, m, H6, H7, H8, H9) 4.08 (2 H, q, *J*=7.1 Hz, H2).

^{13}C NMR (75,47 MHz, DMSO): δ 11.1 (C13, C14, C15), 14.4 (C1), 15.2 (C10, C11, C12), 17.2 (C5), 28.9 (C1'), 30.2 (C4), 59.7 (C6, C7, C8, C9), 60.7 (C2), 172.4 (C3, C3'), 207.6 (C2').

Elemental Analysis ($C_{18}H_{35}NO_5$)

Calculated: C 62.5%, H 10.2%, N 4.0%, O 23.1%.

Experimental: C 49.5, H 8.9%, %, N 4.7%.

Molecular Weight: 345.48

Melting Point: 30.58

Temperature of Decomposition: 172.33

Solubility in water (25 ° C): 84.30 g/ 100 ml

Tri(n-ethyl)[2-butoxy-2-oxoethyl]ammonium dicyanamide ([Pr_3NC_4][Dca])

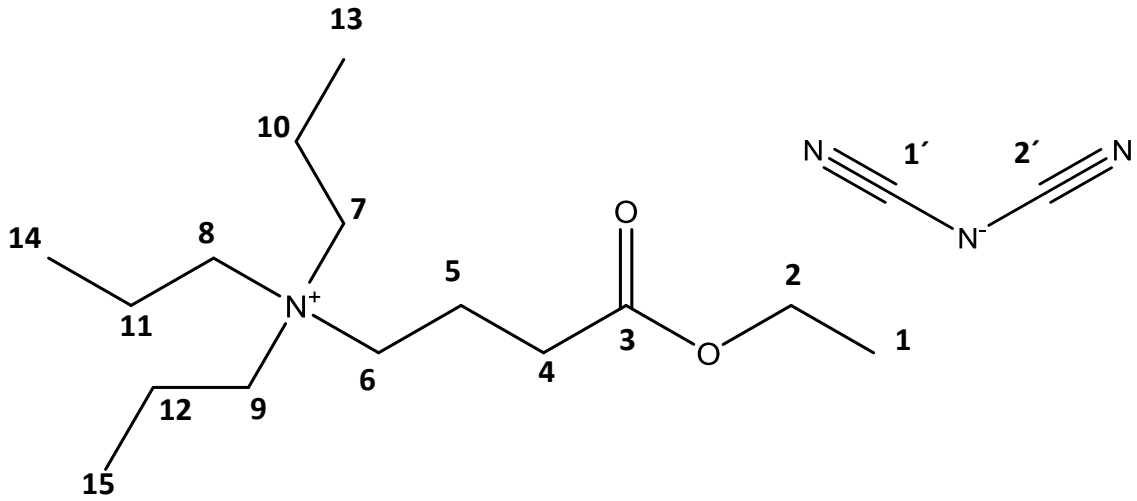

^{1}H and ^{13}C NMR

^{1}H NMR (300 MHz, DMSO): δ 0.90 (9 H, t, *J*=7.2 Hz, H13, H14, H15), 1.20 (3 H, t, *J*=7.1 Hz, H1), 1.57-1.70 (6 H, m, H10, H11, H12), 1.79-1.81 (2 H, m, H5), 2.43 (2 H, t, *J*=7.2 Hz, H4), 3.12-3.20 (8 H, m, H6, H7, H8, H9) 4.08 (2 H, q, *J*=7.2 Hz, H2).

^{13}C NMR (75,47 MHz, DMSO): δ 11.1 (C13, C14, C15), 14.4 (C1), 15.2 (C10, C11, C12), 17.2 (C5), 30.2 (C4), 59.7 (C6, C7, C8, C9), 60.7 (C2), 120.0 (C1'), 172.4 (C3).

Elemental Analysis ($C_{17}H_{32}N_4O_2$)

Calculated: C 62.9%, H 9.9%, N 17.2%, O 9.8%.

Experimental: C 60.1, H 9.8%, %, N 16.5%.

Molecular Weight: 324.47

Melting Point: 35.99

Temperature of Decomposition: 156.59

Solubility in water (25 ° C): 74.70 g/ 100 ml

Tri(n-ethyl)[2-butoxy-2-oxoethyl]ammonium salicylate ([Pr_3NC_4][Sal])

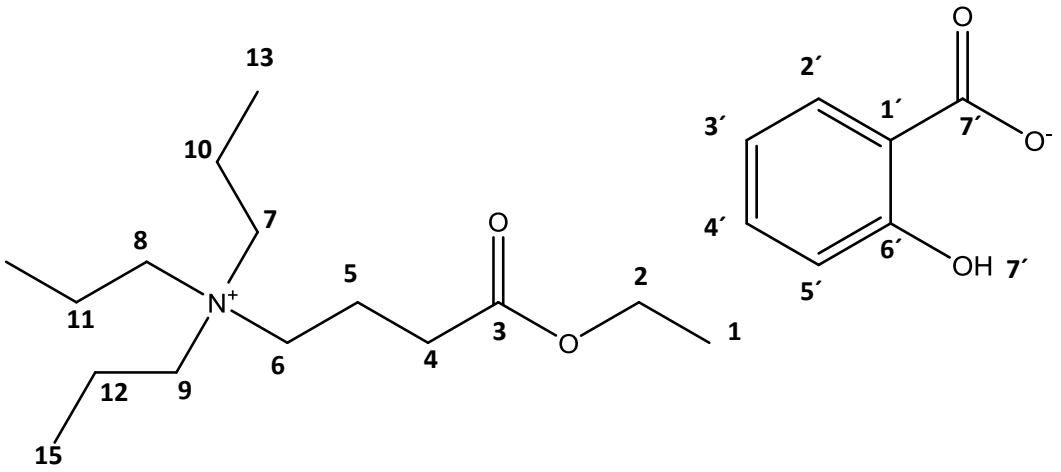

^{1}H and ^{13}C NMR

^{1}H NMR (300 MHz, DMSO): δ 0.89 (9 H, t, *J*=7.2 Hz, H13, H14, H15), 1.20 (3H, t, *J*=7.1 Hz, H1), 1.56-1.68 (6 H, m, H10, H11, H12), 1.79-1.89 (2 H, m, H5), 2.40 (2 H, t, *J*=7.1 Hz, H4), 3.11-3.20 (8 H, m, H6, H7, H8, H9) 4.08 (2 H, q, *J*=7.1 Hz, H2), 6.54 (1H, dd, J=7.4, 1.2 Hz, H3'), 6.59 (1H, dd, J=8.1, 1.0 Hz, H5'), 7.10 (1H, ddd, J= 8.1, 7.1, 1.9, H4'), 7.63 (1H, dd, J=7.6, 1.9 Hz, H2').

^{13}C NMR (75,47 MHz, DMSO): δ 11.1 (C13, C14, C15), 14.4 (C1), 15.1 (C10, C11, C12), 17.2 (C5), 30.2 (C4), 59.7 (C1'), 60.8 (C5), 116.0 (C5'), 116.2 (C3'), 121.5 (C1'), 130.2 (C4'), 131.8 (C2'), 163.6 (C6'), 171.6 (C3), 172.7 (C1'').

Elemental Analysis ($C_{22}H_{37}NO_5$)

Calculated: C 66.8%, H 9.4%, N 3.5%, O 20.2%.

Experimental: C 61.4, H 9.6%, %, N 3.2%.

Molecular Weight: 395.54

Melting Point: 60.78

Temperature of Decomposition: 151.23

Solubility in water (25 ° C): 77.95 g/ 100 ml

Triethyl[2-ethoxy-2-oxoethyl]ammonium salicylate ([Pr_3NC_2][Sal])

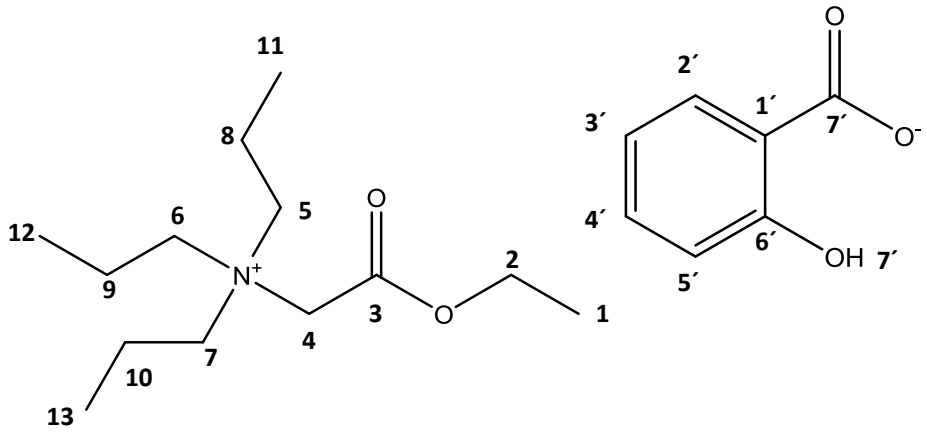

^{1}H and ^{13}C NMR

^{1}H NMR (300 MHz, DMSO): δ 0.88 (9 H, t, *J*=7.2 Hz, H11, H12, H13), 1.24 (3H, t, *J*=7.1 Hz, H1), 1.59-1.72 (6 H, m, H8, H9, H10), 3.35-3.40 (6 H, m, H2) 4.23 (2 H, q, *J*=7.1 Hz, H2), 4.36 (2H, s, H4), 6.56 (1H, dd, J=7.4, 1.1 Hz, H3'), 6.60 (1H, dd, J=8.1, 0.8 Hz, H5'), 7.12 (1H, ddd, J= 8.1, 7.1, 1.9, H4'), 7.64 (1H, dd, J=7.6, 1.7 Hz, H2').

^{13}C NMR (75,47 MHz, DMSO): δ 10.9 (C11, C12, C13), 14.2 (C1), 15.5 (C8, C9, C10), 61.5 (C4), 62.5 (C2, C5, C6, C7), 116.2 (C5'), 116.3 (C3'), 120.8 (C1'), 130.3 (C2'), 131.8 (C4'), 163.6 (C6'), 165.2 (C3) 171.6 (C1'').

Elemental Analysis ($C_{20}H_{33}NO_5$)

Calculated: C 65.3%, H 9.0%, N 3.8%, O 21.7%.

Experimental: C 62.8, H 8.9%, %, N 3.7%.

Molecular Weight: 367.49

Melting Point: 50.76

Temperature of Decomposition: 176.97

Solubility in water (25 ° C): 94.60 g/ 100 ml

Table E1. Experimental weight fraction data for the systems composed of IL (1) + $K_3C_6H_5O_7/C_6H_8O_7$ (2) + H_2O (3) at 25°C.

[MepyrNC$_4$]Br		[Et$_3$NC$_4$]Br		[Pr$_3$NC$_4$]Br		[Bu$_3$NC$_4$]Br	
100 w_1	100 w_1	100 w_2	100 w_2	100 w_1	100 w_2	100 w_1	100 w_2
62.561	3.612	71.388	0.901	68.296	1.377	71.145	1.942
59.620	4.436	64.445	3.595	63.890	1.665	64.578	2.334
54.880	5.301	52.891	5.155	55.345	2.423	56.869	2.569
52.305	6.323	46.082	7.548	52.219	2.892	54.145	3.178
50.025	7.159	42.637	9.830	47.855	3.736	51.950	3.614
47.703	7.952	37.676	12.528	45.762	4.670	49.646	3.983
45.567	8.885	35.427	12.677	43.724	5.615	47.373	4.398
42.686	10.595	30.399	16.473	42.033	6.403	46.115	4.870
39.766	12.436	26.509	19.341	39.542	7.198	44.447	4.606
37.536	13.565	24.643	20.932	38.013	8.000	43.296	4.981
35.529	14.797	23.053	22.209	35.076	9.823	42.383	5.378
33.289	16.292	21.754	23.300	33.984	10.464	41.559	5.766
30.995	17.916	20.183	24.675	32.727	11.188	40.732	6.046
29.235	19.081	19.028	25.631	30.069	13.029	39.950	6.116
27.745	20.241	18.191	26.313	29.272	13.398	39.083	6.293
26.785	20.833	17.259	27.126	28.238	14.053	37.773	7.046
24.839	22.314	16.273	28.087	27.166	14.777	37.429	7.390
23.274	23.476	15.431	28.809	26.297	15.410	36.598	7.742
22.061	24.379	14.615	29.607	25.398	15.957	35.797	8.012
20.360	25.770	13.789	30.511	24.681	16.533	35.034	8.246
19.386	26.518	13.336	30.078	23.923	17.074	34.211	8.612
18.161	27.604			23.185	17.677	33.303	8.721
17.002	28.598			22.522	18.066	32.574	9.075
15.949	29.548			21.806	18.627	31.613	9.241
14.858	30.626			21.161	19.103	30.930	9.600
13.905	31.563			20.589	19.520	30.381	9.818
12.836	32.694			20.115	19.829	29.927	9.911
11.384	34.382			19.613	20.096	29.341	10.270
				18.996	20.519	28.828	10.454
				18.491	20.869	28.257	10.827
				18.029	21.189	27.653	11.196
				17.659	21.389	27.310	11.298
				17.216	21.671	26.758	11.588
				16.712	22.122	26.308	11.799
				16.352	22.367	25.941	11.932
				15.946	22.706	25.656	11.940
				15.544	22.973	24.834	12.420
				15.135	23.252	24.484	12.654
				14.712	23.598	24.222	12.739
				14.306	23.975	23.864	12.970
				13.984	24.194	23.521	13.210

	13.596	24.492	23.263	13.273
	13.260	24.819	23.015	13.364
	12.956	25.094	22.623	13.594
	12.592	25.420	22.250	13.827
	12.299	25.659	21.867	13.993
	11.990	25.911	21.504	14.163
	11.683	26.191	21.278	14.204
	11.390	26.468	20.938	14.380
	11.106	26.737	20.650	14.523
	10.836	27.020	20.382	14.685
	10.546	27.368	20.195	14.768
	10.324	27.580	19.965	14.953
	10.098	27.798	19.780	14.976
	9.900	28.045	19.534	15.170
	9.427	28.522	19.321	15.280
	9.190	28.799	19.078	15.464
	8.960	29.082	18.614	15.653
	8.764	29.300	18.352	15.772
	8.570	29.514	18.106	15.922
	8.359	29.796	17.833	15.958
			17.596	16.108
			17.391	16.213
			17.199	16.329
			16.993	16.470
			16.665	16.567
			16.460	16.654
			16.264	16.747
			16.038	16.963
			15.849	17.076
			15.668	17.179
			15.486	17.284
			15.312	17.359
			15.123	17.453
			14.946	17.590
			14.782	17.670
			14.604	17.759
			14.445	17.861
			14.282	17.943
			14.090	18.085
			13.905	18.255
			13.631	18.364
			13.365	18.473
			13.155	18.683
			12.928	18.775
			12.676	18.947
			12.469	19.098

			12.253	19.270
			12.037	19.373
			11.786	19.547
			11.542	19.758
			11.233	19.982
			10.911	20.222
			10.603	20.482
			10.292	20.744
			10.069	20.625

Table E2. Experimental weight fraction data for the systems composed of IL (1) + $K_3C_6H_5O_7/C_6H_8O_7$ (2) + H_2O (3) at 25°C.

[Pr_3NC_4][Lac]		[Pr_3NC_4][Dca]		[Pr_3NC_4][Pyr]		[Pr_3NC_4][Sac]	
100 w_1	100 w_1	100 w_2	100 w_2	100 w_1	100 w_2	100 w_1	100 w_2
54.633	10.399	70.322	0.506	34.046	26.369	58.403	0.516
50.605	12.069	56.293	1.081	32.658	27.454	51.549	1.328
47.311	12.874	44.247	1.472	30.827	28.060	45.777	1.808
44.876	13.864	39.884	1.480	29.131	28.354	40.895	2.288
42.044	15.416	36.306	1.840	27.785	28.452	37.451	3.156
38.018	17.146	33.305	2.016	26.921	29.193	34.358	4.869
35.643	18.465	31.123	2.151	25.800	29.709	27.706	6.334
33.885	19.373	70.322	0.506	24.628	29.932	25.881	8.066
31.650	20.522	56.293	1.081	23.850	30.601	23.979	10.197
28.991	22.111	44.247	1.472	23.330	30.861	22.724	11.416
26.350	23.847	39.884	1.480	22.868	30.958	21.403	12.846
24.700	24.817	36.306	1.840	22.301	31.389	20.179	14.017
22.809	25.548	33.305	2.016	21.759	31.987	19.012	15.148
21.505	26.388	31.123	2.151	21.266	32.188	17.884	16.364
20.042	27.355	28.264	2.963	20.678	32.659	16.867	17.551
18.680	28.287	25.178	3.511	20.086	33.456	16.103	18.282
17.687	28.977	22.629	3.736	19.504	33.956	15.228	19.188
16.682	29.690	20.001	4.450	18.955	34.312	14.508	20.063
15.758	30.305	18.081	4.790	18.456	34.781	13.887	20.782
14.991	30.874	28.264	2.963	17.780	35.101	13.172	21.600
14.322	31.366	25.178	3.511	17.380	35.561	12.623	22.187
13.038	32.332	8.152	9.026	17.022	36.058	12.065	22.785
12.398	32.853	7.806	9.355	16.420	36.343	11.533	23.406
11.891	33.245	7.718	9.434	16.176	36.400	11.043	23.993
11.487	33.537	7.929	9.446	15.958	36.530	10.583	24.544
10.904	34.037	7.840	9.782	15.659	37.055	10.163	25.095
10.478	34.391	7.834	9.952	15.344	37.502	9.724	25.738
9.656	35.147	7.643	10.551	15.095	37.486	9.399	26.131
8.835	35.916	7.484	10.800	14.801	37.842	9.076	26.522
		7.376	11.110	14.663	37.932	8.798	26.946
		7.389	11.297	14.395	38.273	8.163	27.746
		7.254	12.790	14.221	38.338	7.856	28.190
		7.110	11.833	13.995	38.692	7.566	28.630
		6.932	13.348	13.656	38.625	7.324	28.962
		6.863	13.917	13.479	38.976	7.090	29.282
		6.869	14.556	13.106	39.668	6.840	29.694
		6.474	15.091	12.908	39.969		
		6.228	15.583	12.758	39.920		
		5.514	17.046	12.472	40.406		
		5.634	17.902	12.294	40.632		
		4.995	18.918	12.119	40.948		

	11.684	41.189
	11.502	41.554
	11.379	41.508
	11.236	41.830
	11.065	42.018
	10.923	42.209
	10.775	42.322

Table E3. Experimental weight fraction data for the systems composed of IL (1) + $K_3C_6H_5O_7/C_6H_8O_7$ (2) + H_2O (3) at 25°C.

[Pr_3NC_4][Sal]		[Pr_3NC_2][Sal]	
100 w_1	100 w_2	100 w_1	100 w_2
68.963	0.961	63.426	3.602
62.076	1.847	54.584	4.453
59.345	2.595	47.568	5.162
55.627	3.192	43.422	5.999
51.132	3.680	39.607	6.649
47.180	4.160	37.519	7.355
44.902	4.566	34.857	7.772
42.803	5.019	32.916	8.301
40.931	5.341	31.254	8.788
39.043	5.699	29.760	9.316
37.478	6.057	28.023	9.427
36.139	6.321	26.660	9.955
34.579	6.599	25.525	10.166
33.766	6.970	24.644	10.531
32.589	7.126	23.453	10.853
31.310	7.316	22.506	11.121
30.666	7.604	21.627	11.394
29.628	7.688	20.828	11.582
28.635	7.860	20.059	11.783
28.139	8.054	19.361	11.998
27.219	8.176	18.727	12.197
26.415	8.312	18.119	12.343
25.959	8.534	17.556	12.479
25.169	8.725	17.120	12.674
24.574	8.884	16.535	12.939
23.937	9.035	15.788	13.153
23.392	9.177	15.549	13.349
22.804	9.256	15.234	13.588
22.287	9.377	14.827	13.637
21.779	9.436	14.495	13.785
21.737	9.738	14.101	13.822
21.013	9.986	13.723	13.920
20.435	10.087	13.495	14.044
20.168	10.165	13.113	14.270
19.863	10.232	12.776	14.346
19.600	10.283	12.484	14.422
19.310	10.408	12.242	14.443
19.036	10.530	11.948	14.490
18.771	10.617	11.635	14.795
18.513	10.663	11.423	14.832
18.245	10.743	11.258	14.844

17.809	10.772	11.055	14.881
17.587	10.878	10.842	14.935
17.364	10.994	10.717	15.074
17.146	11.094	10.542	15.145
16.935	11.215	10.342	15.180
16.725	11.311	10.224	15.277
16.379	11.269	10.075	15.374
16.218	11.344	9.873	15.496
16.052	11.397	9.660	15.504
15.889	11.458	9.583	15.531
15.745	11.516	9.499	15.657
15.464	11.488	9.377	15.698
15.292	11.563	9.262	15.732
15.144	11.602	9.063	15.959
14.954	11.766	8.922	15.958
14.779	11.868	8.734	16.111
14.629	11.970	8.574	16.185
14.490	12.031	8.341	16.290
14.334	12.097	8.140	16.432
14.117	12.107	7.964	16.575
13.976	12.178	7.857	16.613
13.869	12.279	7.694	16.676
13.672	12.327	7.604	16.711
13.546	12.413	7.490	16.730
13.371	12.437	7.418	16.823
13.182	12.611	7.290	16.920
13.015	12.606	7.188	17.012
12.868	12.609	7.079	17.119
12.757	12.641	6.920	17.349
12.676	12.693	6.816	17.307
12.565	12.762	6.745	17.305
12.476	12.842	6.710	17.328
12.327	12.868	6.654	17.415
12.214	12.913	6.576	17.557
12.115	12.954	6.517	17.518
12.001	13.008	6.483	17.527
11.896	13.055	6.441	17.580
11.805	13.088	6.397	17.641
11.701	13.145	6.349	17.695
11.629	13.204	6.283	17.713
11.475	13.186	6.243	17.757
11.408	13.237	6.203	17.809
11.239	13.339	6.148	17.881
11.084	13.436	6.106	17.941
10.899	13.507	6.046	17.978
10.702	13.691	5.993	18.012

10.462	13.811	5.884	18.343
10.262	13.908	63.426	3.602
10.096	13.962	54.584	4.453
9.923	14.087	47.568	5.162

Table E6. Recovery yield ($RY\%_{PROT}$) and purification yield ($PY\%_{PROT}$) of MRJP and weight fraction compositions of the initial mixtures at 25 °C.

IL	Weight fraction composition / (wt %)		$DE\%_{HSA} \pm \sigma$	$DE\%_{IgG} \pm \sigma$
	IL	$K_3C_6H_5O_7/C_6H_8O_7$		
[MepyrNC$_4$]Br	30.38 ± 0.03	29.17 ± 0.05	100	100
[Et$_3$NC$_4$]Br	30.02 ± 0.04	29.57 ± 0.02	100	100
[Pr$_3$NC$_4$]Br	30.22 ± 0.01	29.57 ± 0.08	100	100
[Bu$_3$NC$_4$]Br	30.22 ± 0.05	29.55 ± 0.02	100	100
[Pr$_3$NC$_4$][Pyr]	30.26 ± 0.01	30.31 ± 0.07	100	100
[Pr$_3$NC$_4$][Lac]	29.62 ± 0.11	29.91 ± 0.06	100	100
[Pr$_3$NC$_2$][Sal]	29.56 ± 0.05	29.61 ± 0.11	100	100
[Pr$_3$NC$_4$][Sal]	29.52 ± 0.01	29.75 ± 0.09	100	100
[Pr$_3$NC$_4$][Sac]	29.62 ± 0.04	29.99 ± 0.11	100	100
[Pr$_3$NC$_4$][Dca]	30.54 ± 0.05	29.17 ± 0.02	100	100

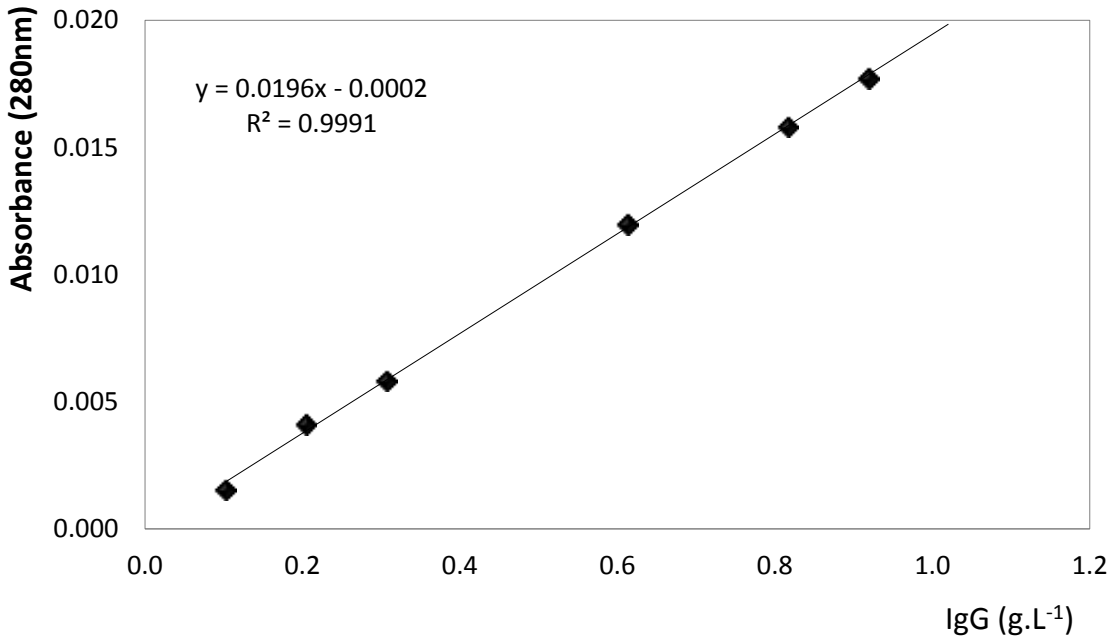

Figure E2. IgG calibration curve by SE-HPLC.

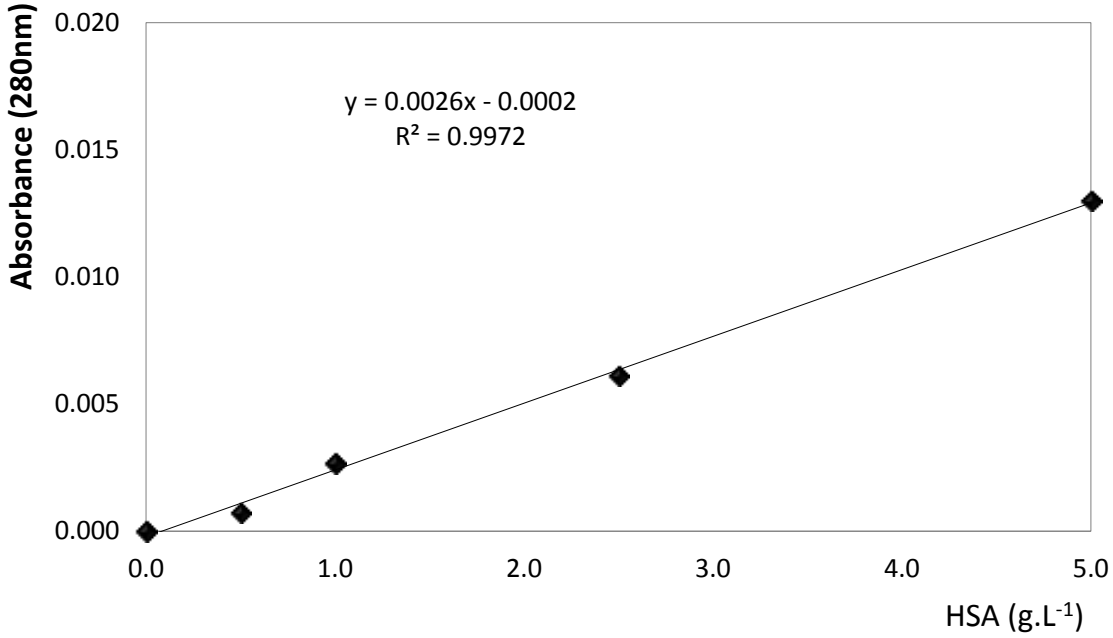

Figure E3. HSA calibration curve by SE-HPLC.

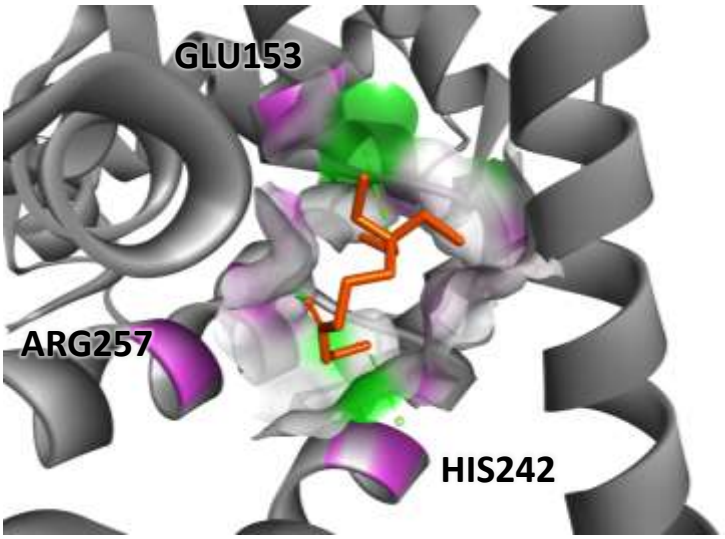

Figure E4. Docking pose with the lowest absolute value of affinity (kcal/mol) for HSA with $[Et_3NC_4]^+$.

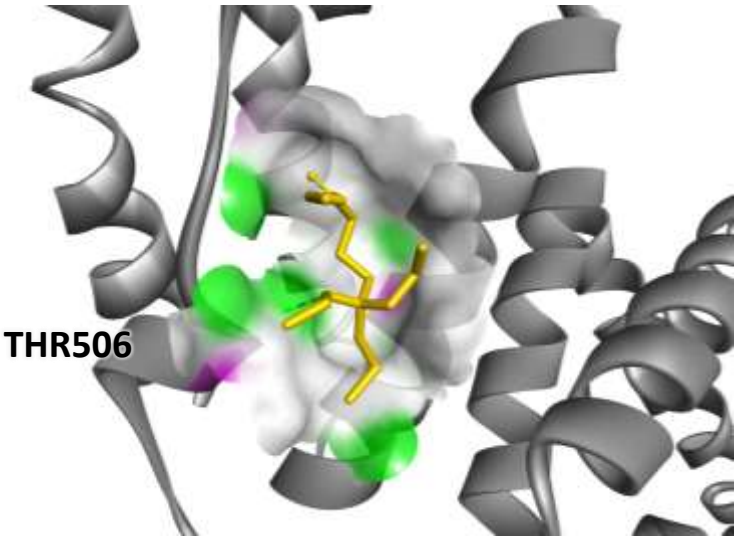

Figure E5. Docking pose with the lowest absolute value of affinity (kcal/mol) for HSA with $[Pr_3NC_4]^+$.

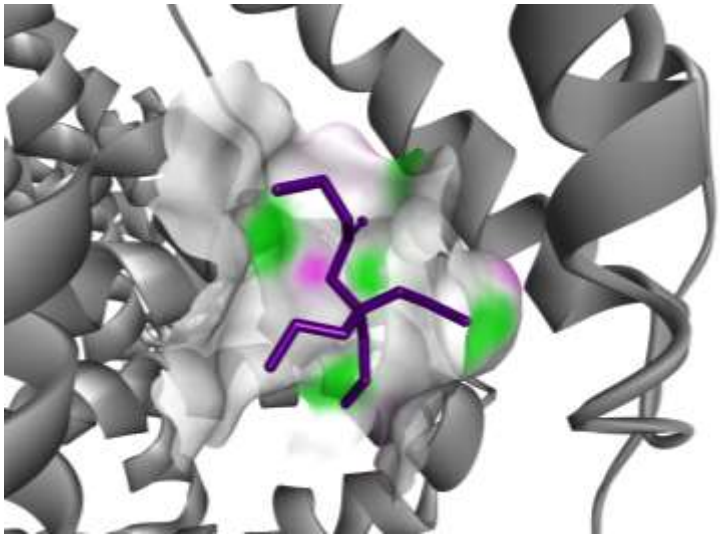

Figure E6. Docking pose with the lowest absolute value of affinity (kcal/mol) for HSA with $[Pr_3NC_2]^+$.

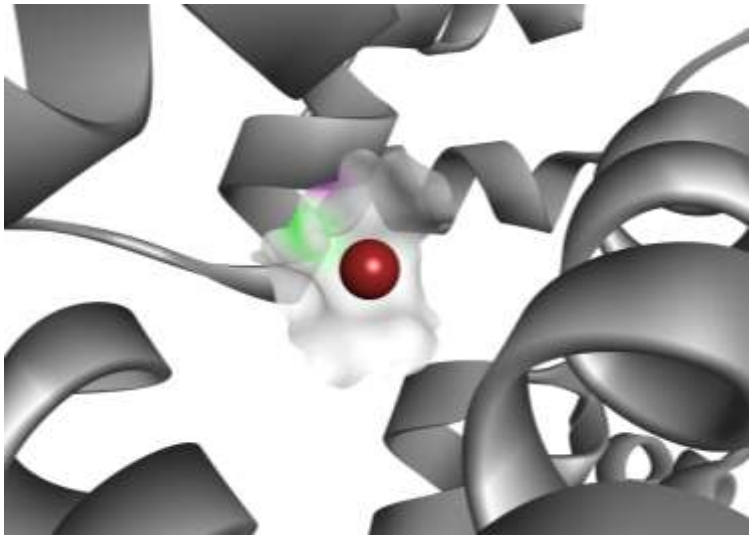

Figure E7. Docking pose with the lowest absolute value of affinity (kcal/mol) for HSA with Br^-.

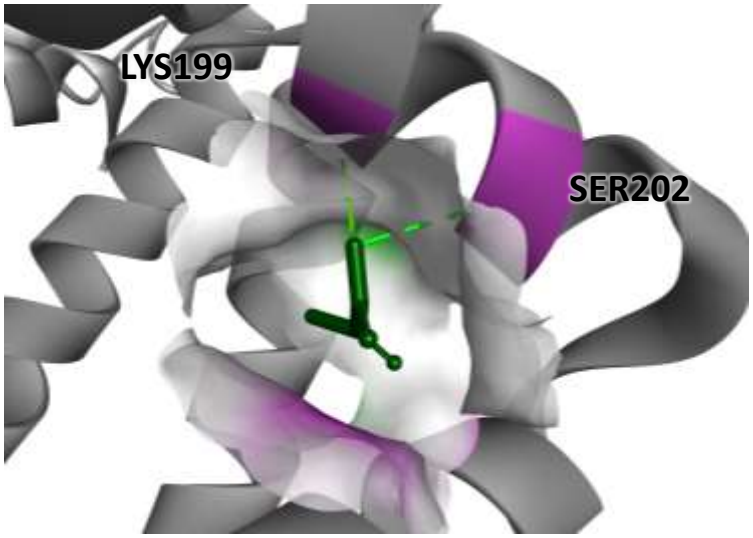

Figure E8. Docking pose with the lowest absolute value of affinity (kcal/mol) for HSA with $[Pyr]^-$.

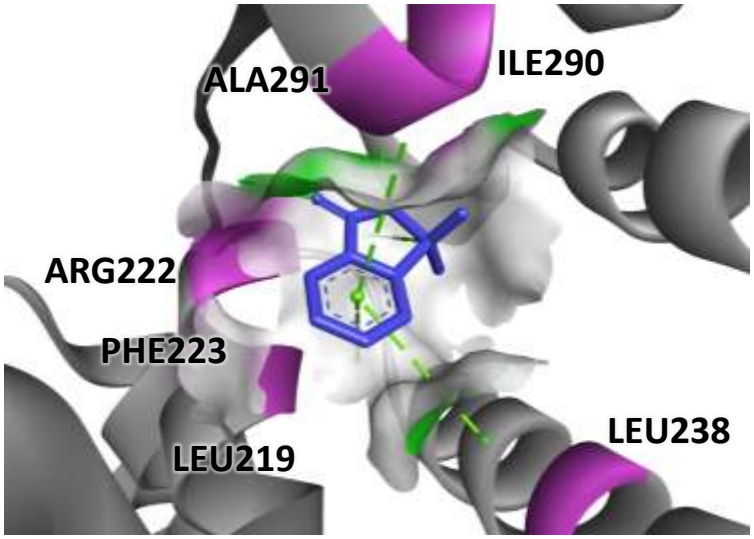

Figure E9. Docking pose with the lowest absolute value of affinity (kcal/mol) for HSA with $[Sac]^-$.

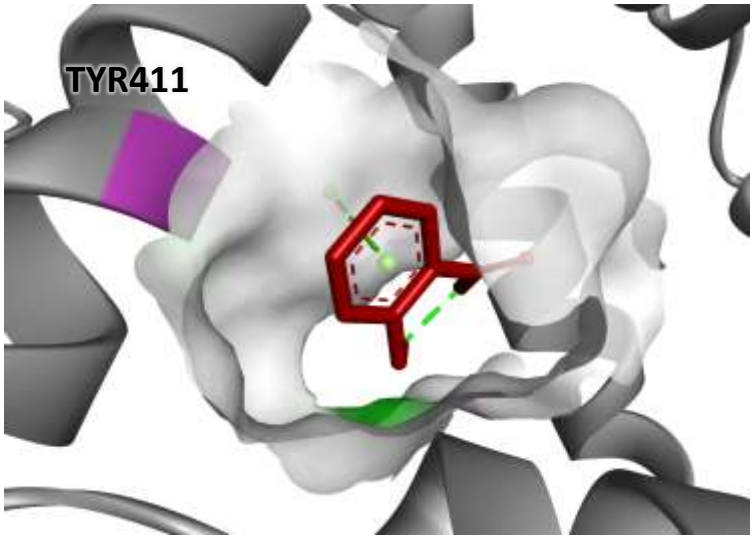

Figure E10. Docking pose with the lowest absolute value of affinity (kcal/mol) for HSA with $[Sal]^-$.

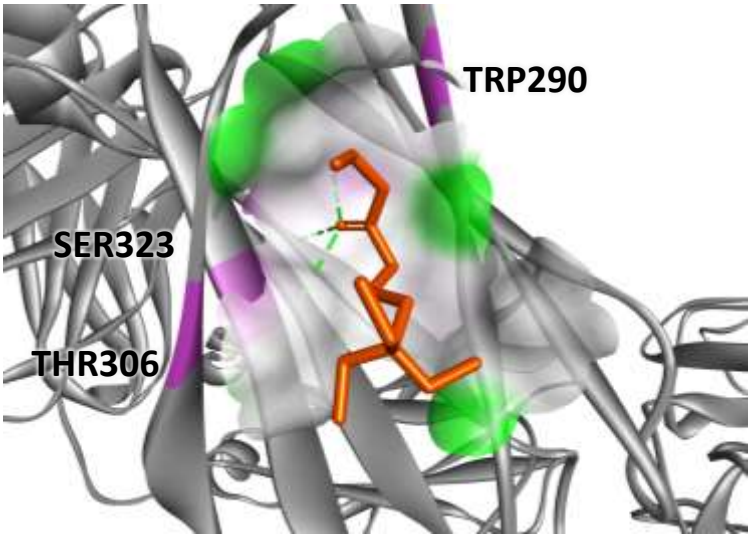

Figure E11. Docking pose with the lowest absolute value of affinity (kcal/mol) for IgG with $[Et_3NC_4]^+$.

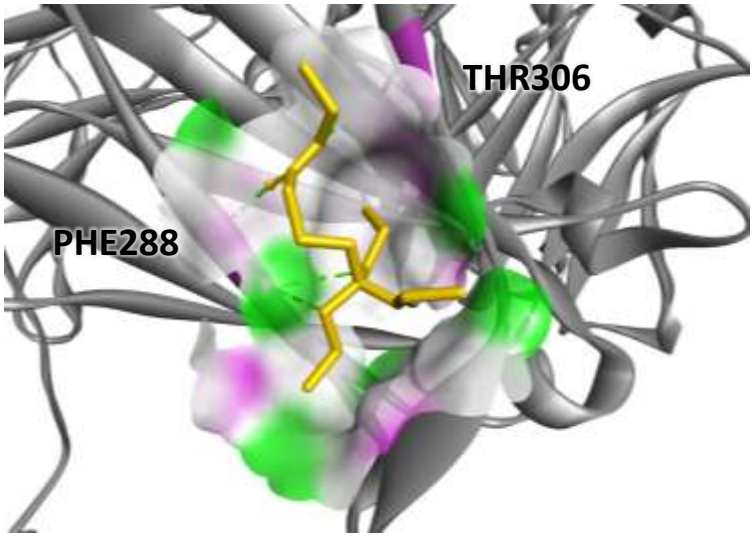

Figure E12. Docking pose with the lowest absolute value of affinity (kcal/mol) for IgG with $[Pr_3NC_4]^+$.

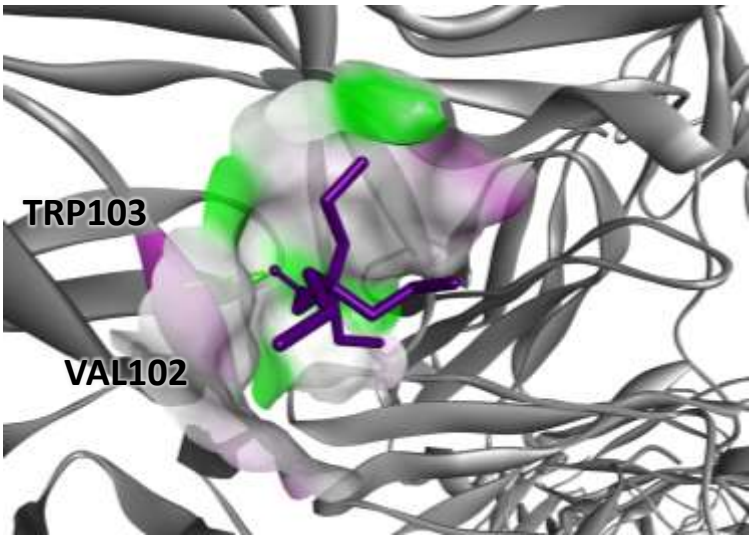

Figure E13. Docking pose with the lowest absolute value of affinity (kcal/mol) for IgG with $[Pr_3NC_2]^+$.

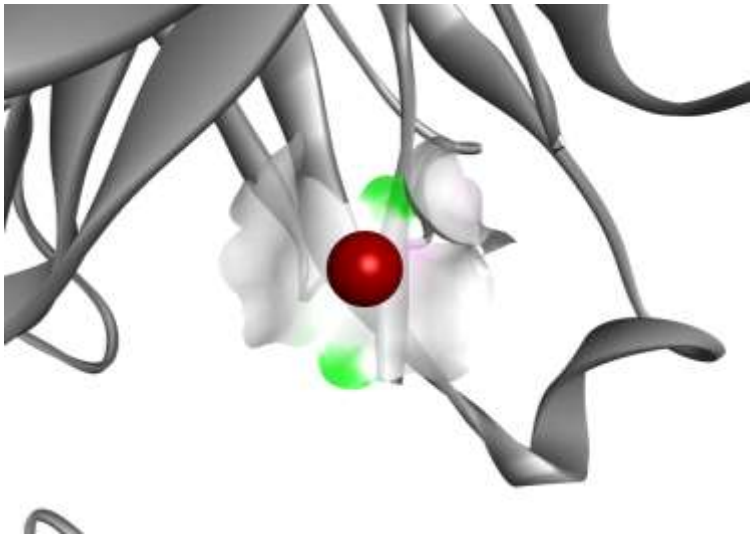

Figure E14. Docking pose with the lowest absolute value of affinity (kcal/mol) for IgG with Br^-.

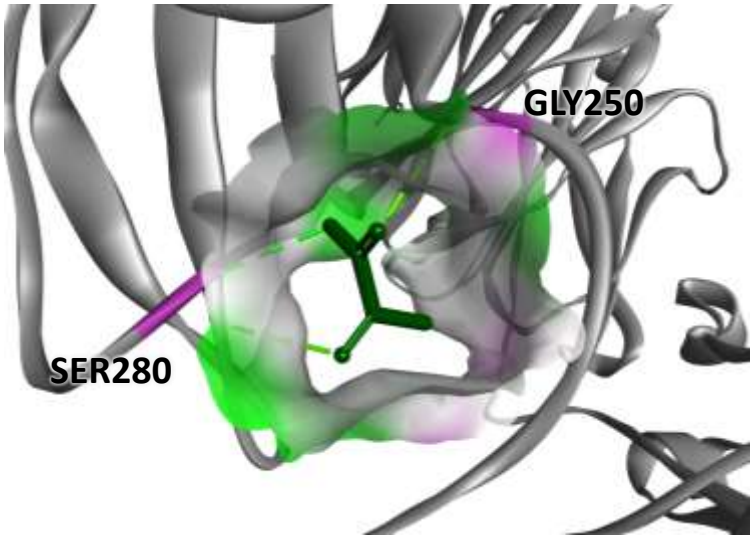

Figure E15. Docking pose with the lowest absolute value of affinity (kcal/mol) for IgG with $[Pyr]^-$.

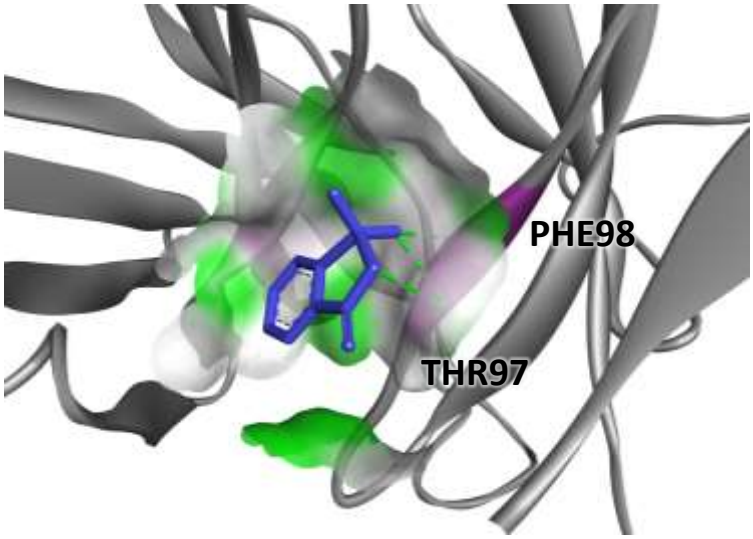

Figure E16. Docking pose with the lowest absolute value of affinity (kcal/mol) for IgG with $[Sac]^-$.

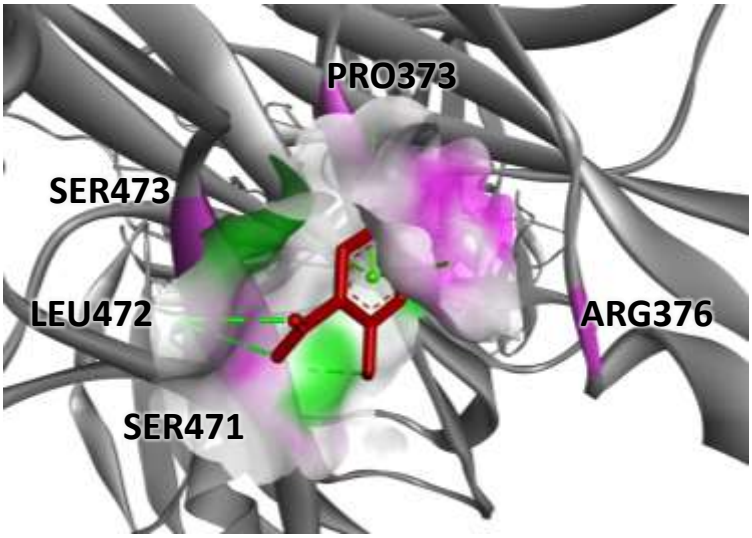

Figure E17. Docking pose with the lowest absolute value of affinity (kcal/mol) for IgG with $[Sal]^-$.

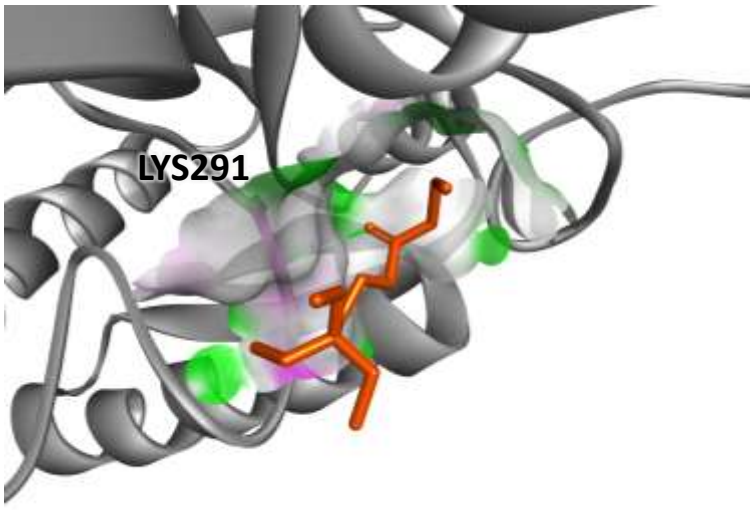

Figure E18. Docking pose with the lowest absolute value of affinity (kcal/mol) for Transferrin with $[Et_3NC_4]^+$.

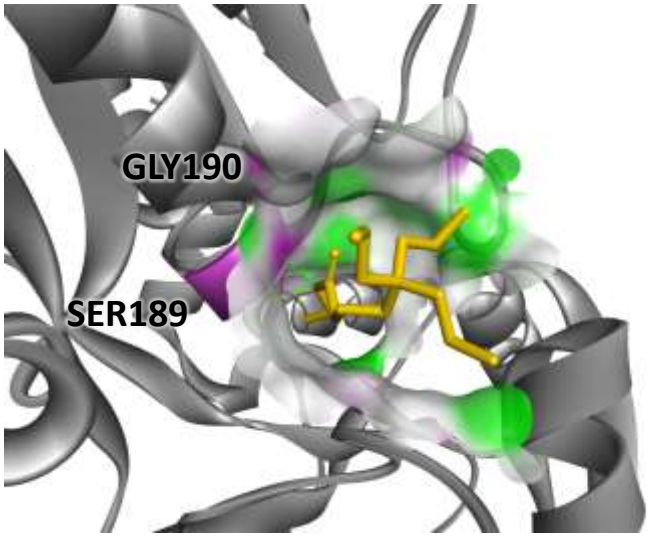

Figure E19. Docking pose with the lowest absolute value of affinity (kcal/mol) for Transferrin with $[Pr_3NC_4]^+$.

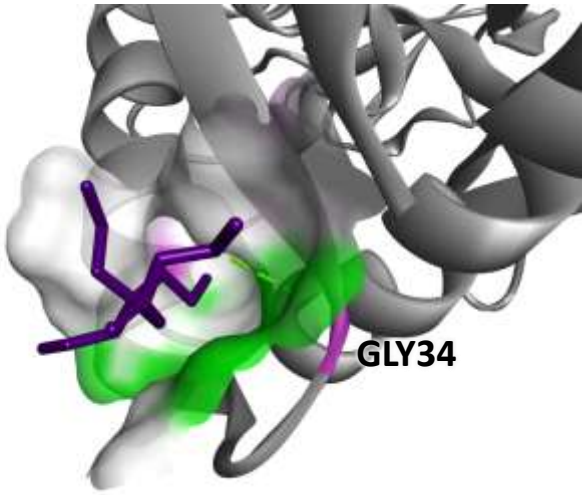

Figure E20. Docking pose with the lowest absolute value of affinity (kcal/mol) for Transferrin with $[Pr_3NC_2]^+$.

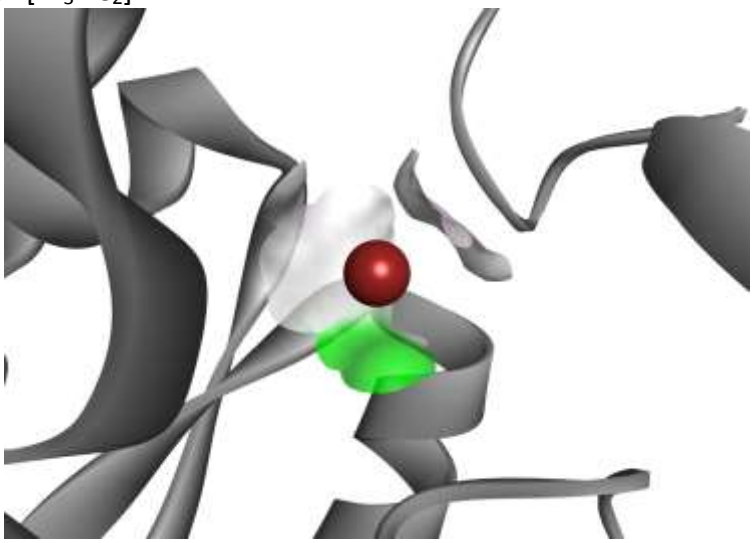

Figure E21. Docking pose with the lowest absolute value of affinity (kcal/mol) for Transferrin with Br^-.

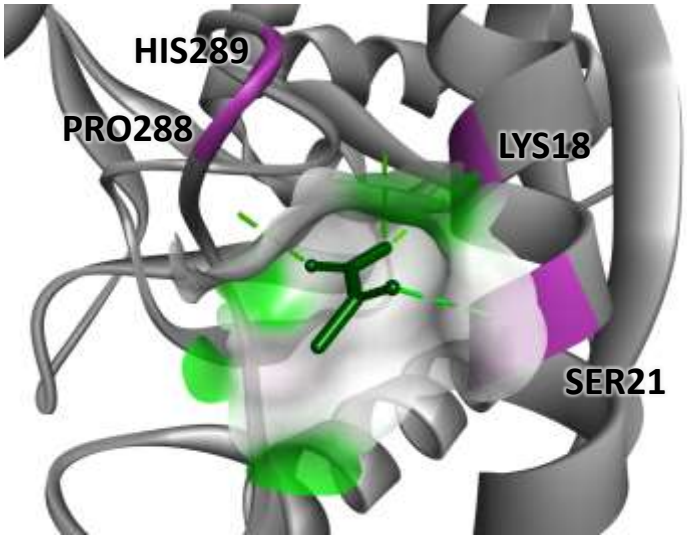

Figure E22. Docking pose with the lowest absolute value of affinity (kcal/mol) for Transferrin with $[Pyr]^-$.

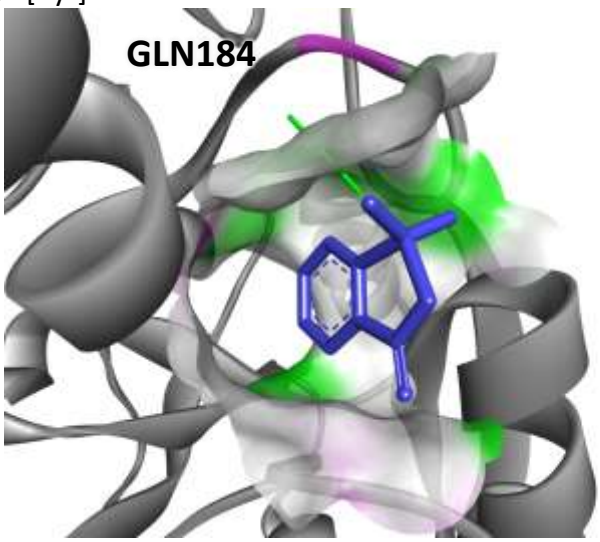

Figure E23. Docking pose with the lowest absolute value of affinity (kcal/mol) for Transferrin with $[Sac]^-$.

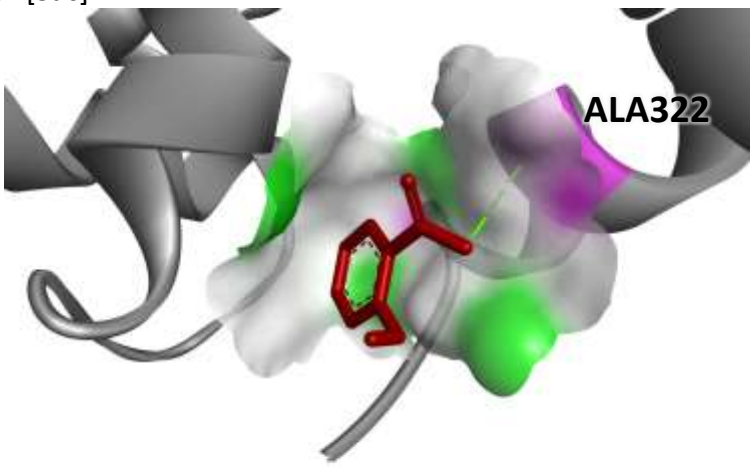

Figure E24. Docking pose with the lowest absolute value of affinity (kcal/mol) for Transferrin with $[Sal]^-$.

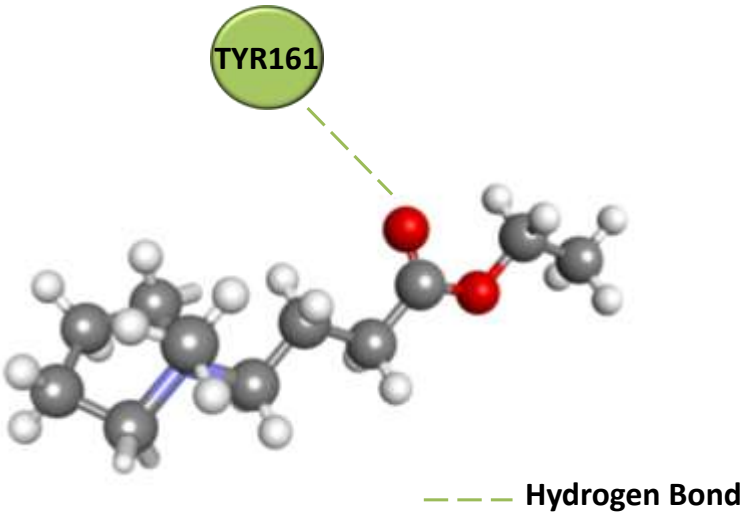

Figure E25. Molecular interaction diagrams of $[MepyrNC_4]^+$ and amino acids residues of HSA.

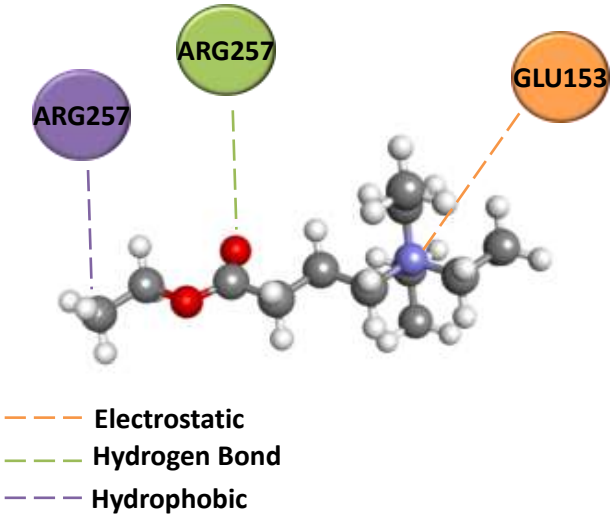

Figure E26. Molecular interaction diagrams of $[EtNC_4]^+$ and amino acids residues of HSA.

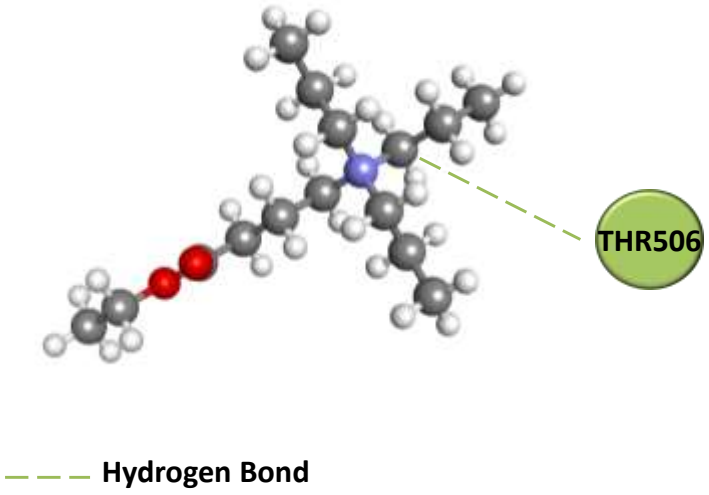

Figure E27. Molecular interaction diagrams of $[PrNC_4]^+$ and amino acids residues of HSA.

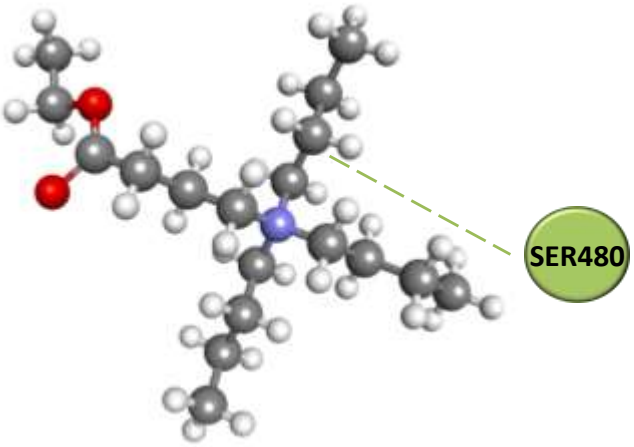

Figure E28. Molecular interaction diagrams of $[BuNC_4]^+$ and amino acids residues of HSA.

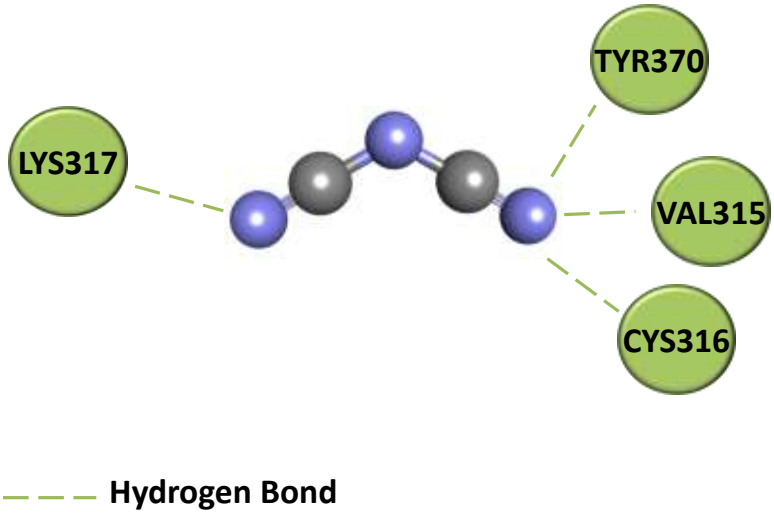

Figure E29. Molecular interaction diagrams of $[Dca]^-$ and amino acids residues of HSA.

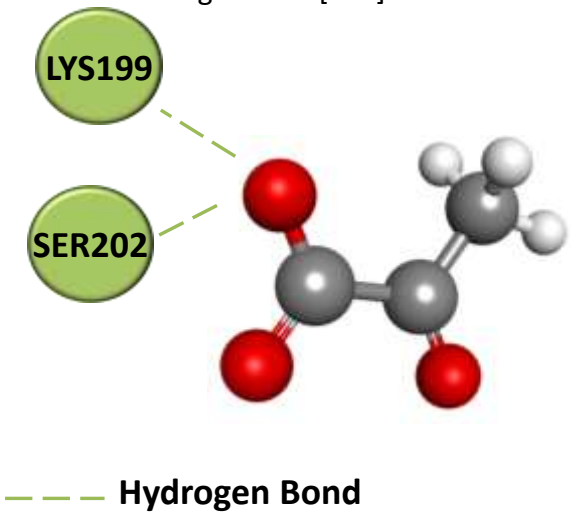

Figure E30. Molecular interaction diagrams of $[Pyr]^-$ and amino acids residues of HSA.

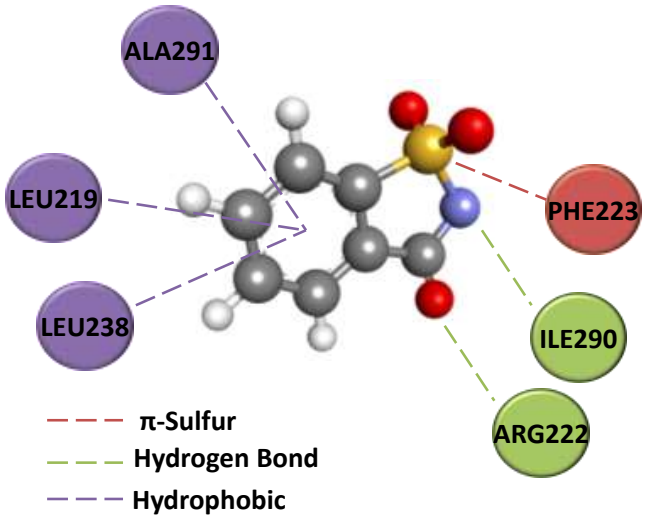

Figure E31. Molecular interaction diagrams of $[Sac]^-$ and amino acids residues of HSA.

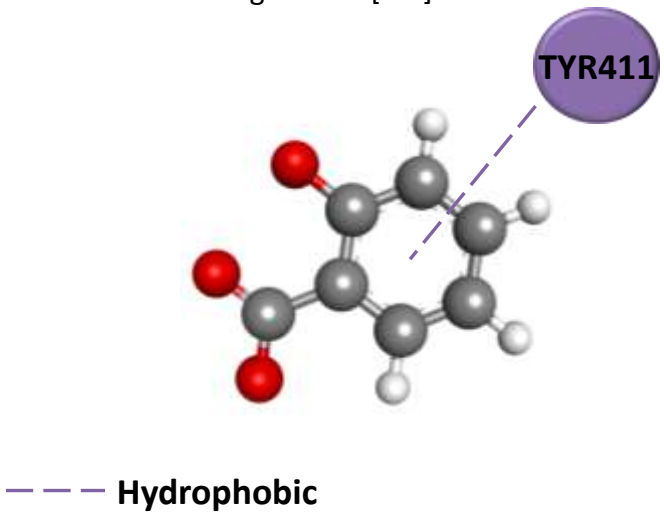

Figure E32. Molecular interaction diagrams of $[Sal]^-$ and amino acids residues of HSA.

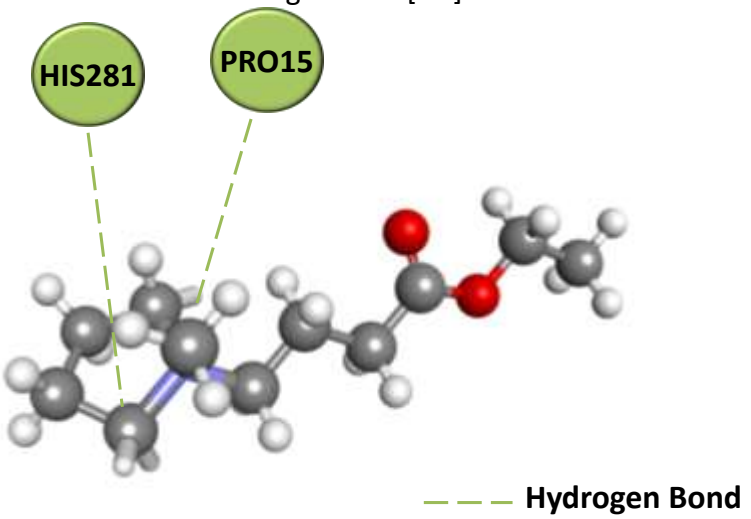

Figure E33. Molecular interaction diagrams of $[MepyrNC_4]^+$ and amino acids residues of IgG.

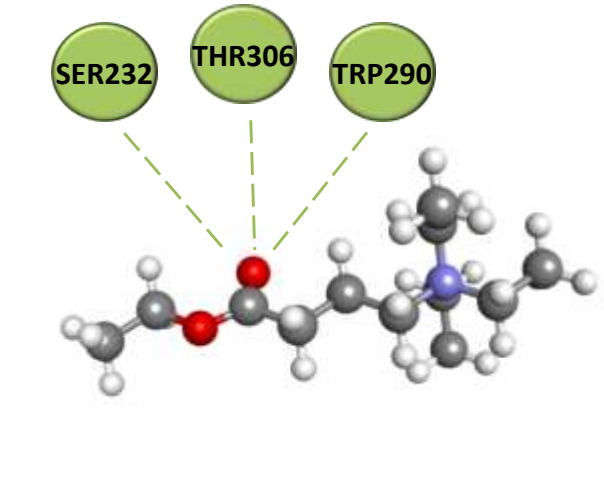

Figure E34. Molecular interaction diagrams of $[EtNC_4]^+$ and amino acids residues of IgG.

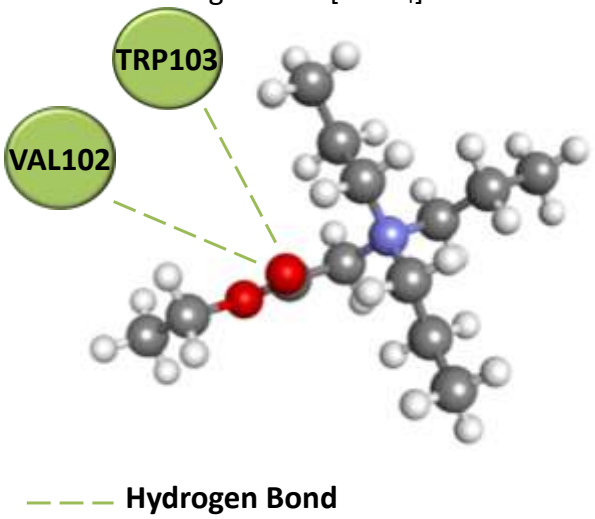

Figure E35. Molecular interaction diagrams of $[PrNC_2]^+$ and amino acids residues of IgG.

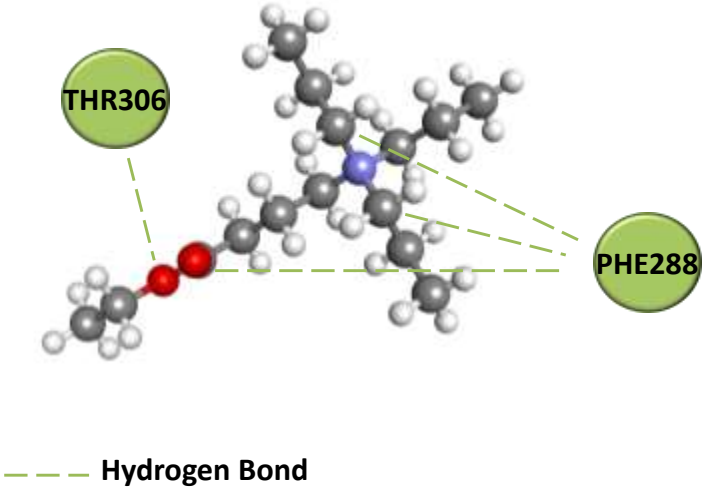

Figure E36. Molecular interaction diagrams of $[PrNC_4]^+$ and amino acids residues of IgG.

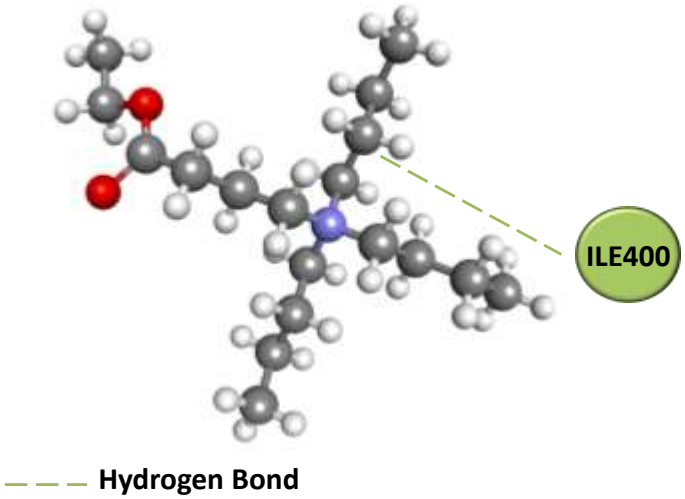

Figure E37. Molecular interaction diagrams of $[BuNC_4]^+$ and amino acids residues of IgG.

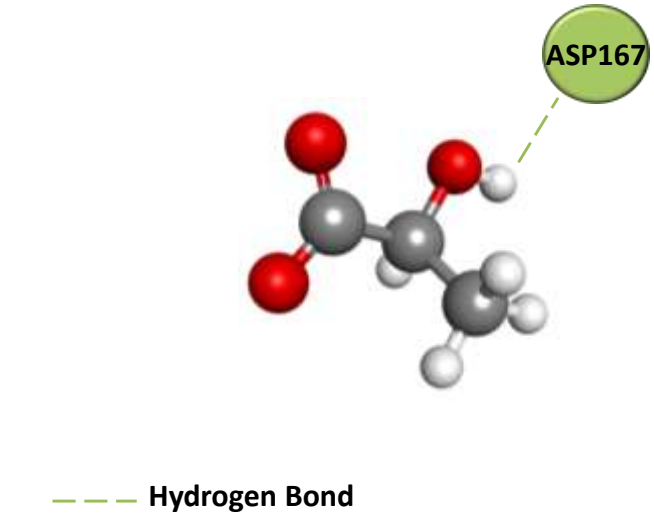

Figure E38. Molecular interaction diagrams of $[Lac]^-$ and amino acids residues of IgG.

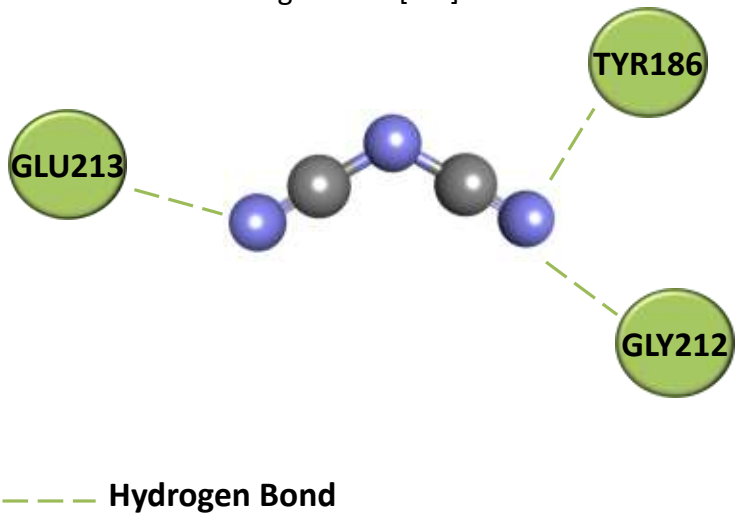

Figure E39. Molecular interaction diagrams of $[Dca]^-$ and amino acids residues of IgG.

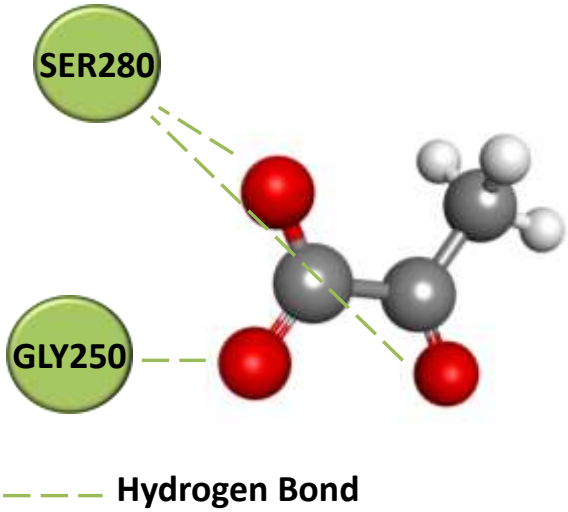

Figure E40. Molecular interaction diagrams of $[Pyr]^-$ and amino acids residues of IgG.

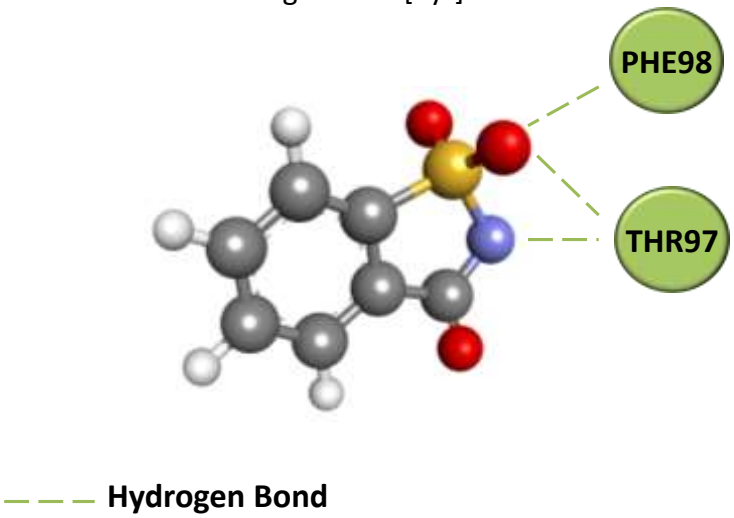

Figure E41. Molecular interaction diagrams of $[Sac]^-$ and amino acids residues of IgG.

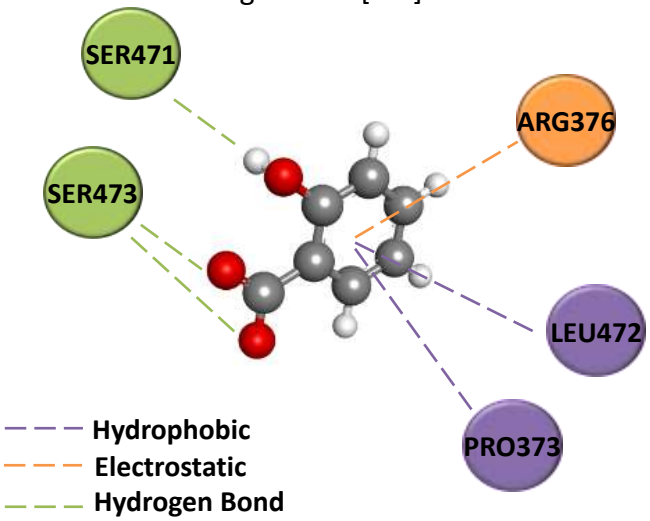

Figure E42. Molecular interaction diagrams of $[Sal]^-$ and amino acids residues of IgG.

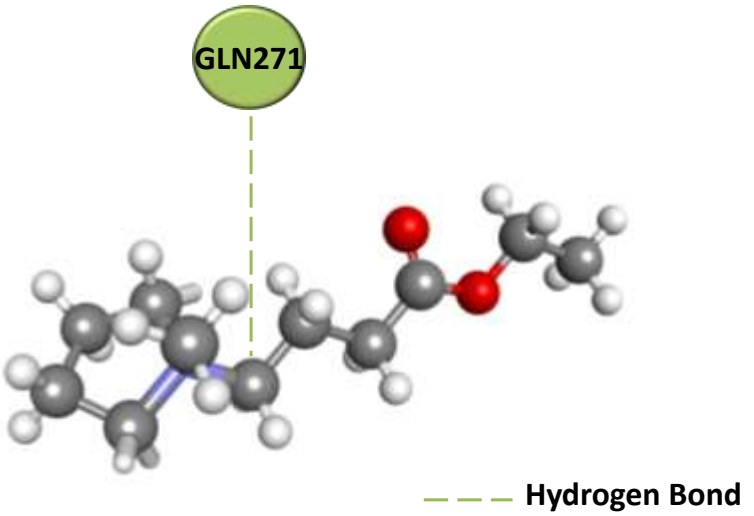

Figure E43. Molecular interaction diagrams of $[MepyrNC_4]^+$ and amino acids residues of Transferrin.

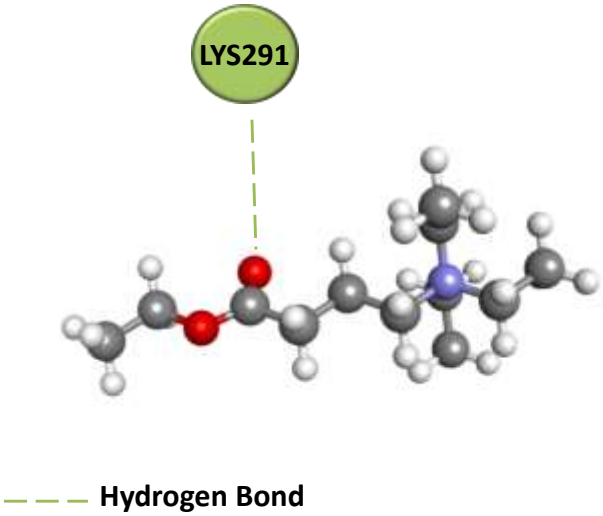

Figure E44. Molecular interaction diagrams of $[EtNC_4]^+$ and amino acids residues of Transferrin.

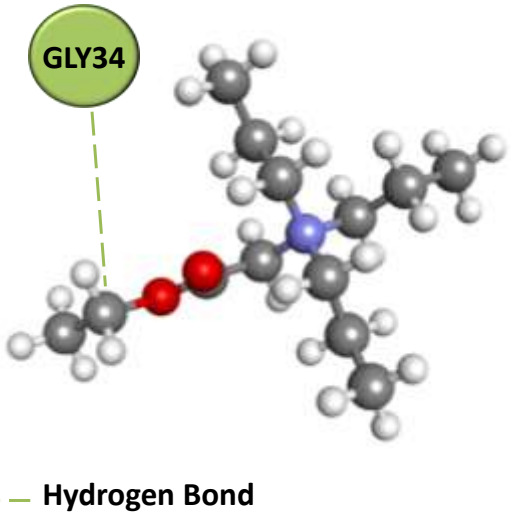

Figure E45. Molecular interaction diagrams of $[PrNC_2]^+$ and amino acids residues of Transferrin.

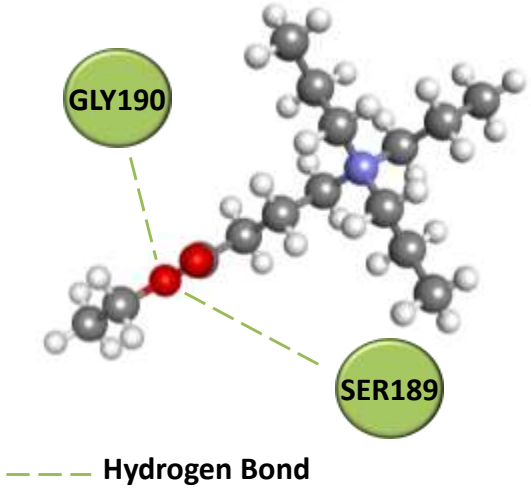

Figure E46. Molecular interaction diagrams of $[PrNC_4]^+$ and amino acids residues of Transferrin.

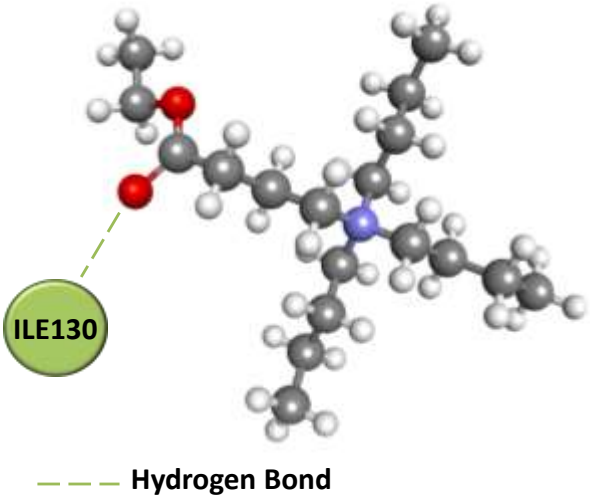

Figure E47. Molecular interaction diagrams of $[BuNC_4]^+$ and amino acids residues of Transferrin.

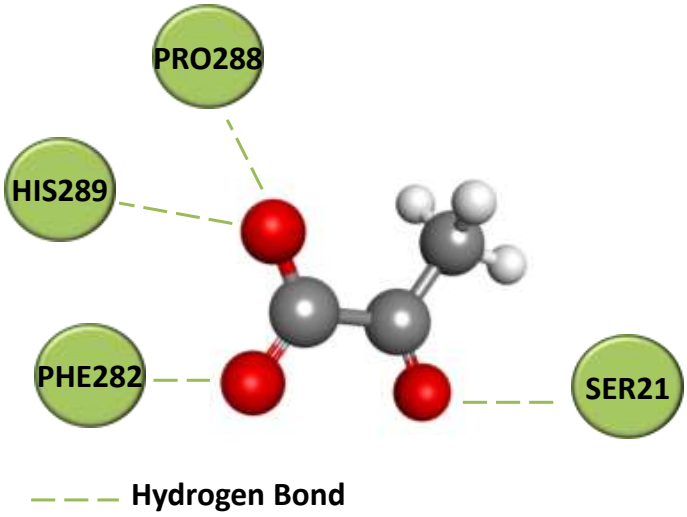

Figure E48. Molecular interaction diagrams of $[Lac]^-$ and amino acids residues of Transferrin.

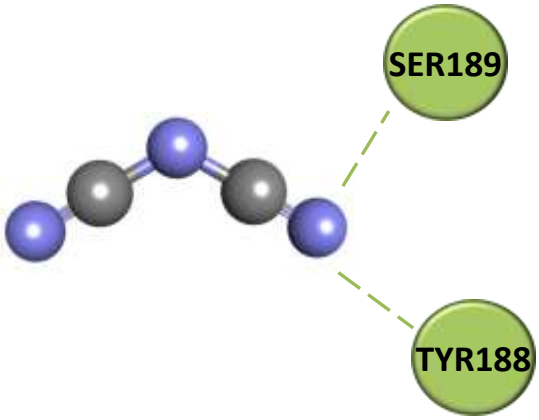

Figure E49. Molecular interaction diagrams of $[Dca]^-$ and amino acids residues of Transferrin.

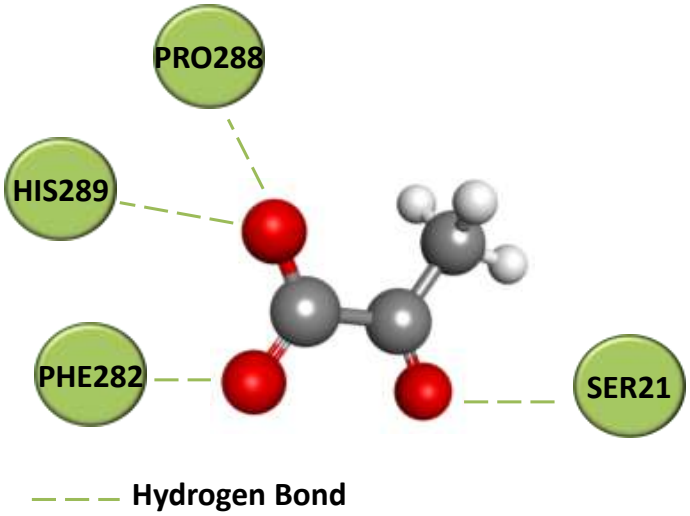

Figure E50. Molecular interaction diagrams of $[Pyr]^-$ and amino acids residues of Transferrin.

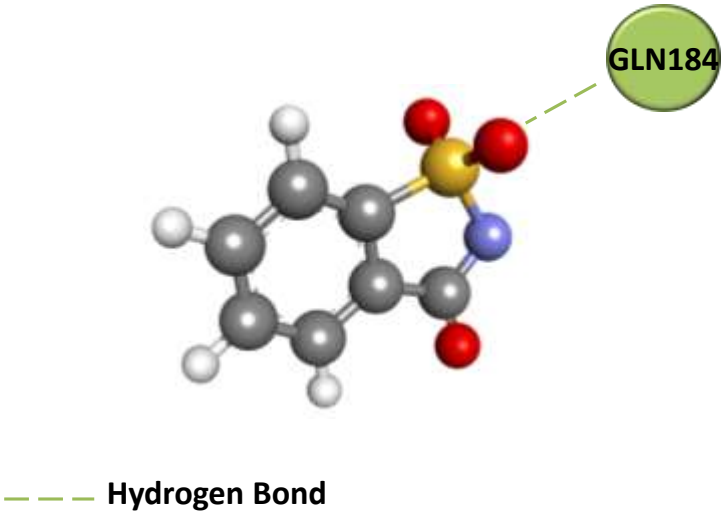

Figure E51. Molecular interaction diagrams of $[Sac]^-$ and amino acids residues of Transferrin.

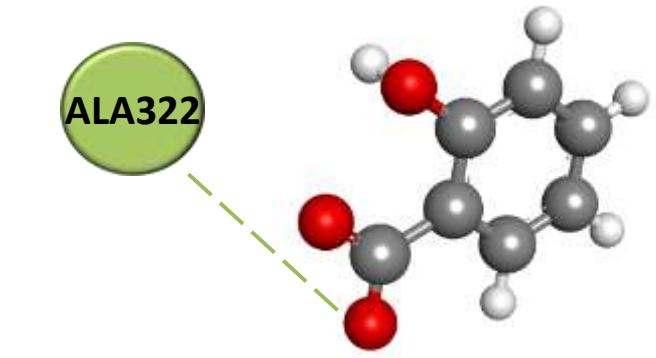

Figure E52. Molecular interaction diagrams of $[Sal]^-$ and amino acids residues of Transferrin.

Table E7. Docking affinity energy and interacting amino acid residues predicted by AutoDock vinna for HSA-ILs.

Compound	Affinity (kcal/mol)	Interacting nucleic acids	Type of interaction	From	To	Distance (Å)
$[MepyrNC_4]^+$	-4.7	TYR161	Hydrogen Bond	Tyrosine - OH	$[MepyrNC_4]^+$- O	3.16
$[Et_3NC_4]^+$	-4.1	GLU153	Electrostatic	$[Et_3NC_4]^+$ - N	GlutamicAcid - O	4.40
		ARG257	Hydrogen Bond	Arginine - N	$[Et_3NC_4]^+$ - O	2.92
				Arginine - NH_2	$[Et_3NC_4]^+$ - O	2.80
		HIS242	Hydrophobic	$[Et_3NC_4]^+$ - C	Histidine - H	3.61
$[Pr_3NC_2]^+$	-3.8	-	-	-	-	-
$[Pr_3NC_4]^+$	-4.1	THR506	Hydrogen Bond	$[Pr_3NC_4]^+$ - C	Threonine - O	3.39
$[Bu_3NC_4]^+$	-3.9	SER480	Hydrogen Bond	$[Bu_3NC_4]^+$ - C	Serine - O	3.55
		LEU347	Hydrophobic		Leucine - C	4.84
		LYS351			Lysine - C	3.65
Br^-	-1.0	-	-	-	-	-
$[Pyr]^-$	-3.5	SER202	Hydrogen Bond	Serine - O	$[Pyr]^-$ - O	2.99
		LYS199		Lysine - C	$[Pyr]^-$ - O	3.74
$[Sal]^-$	-5.7	TYR411	Hydrophobic	Tyrosine - C	$[Sal]^-$ - C	3.78
$[Sac]^-$	-5.8	ARG222	Hydrogen Bond	Arginine - N	$[Sac]^-$ - O	2.80
		ILE290		$[Sac]^-$ - N	Isoleucine- C	3.04
		PHE223	π-Sulfur	$[Sac]^-$ - S	Phenylalanine- C	5.75
		LEU219	Hydrophobic	$[Sac]^-$ - C	Leucine - C	4.94
		LEU238		$[Sac]^-$ - C	Leucine - C	5.20
		ALA291		$[Sac]^-$ - C	Alanine - C	4.68
$[Lac]^-$	-3.5	-	-	-	-	-

$[Dca]^-$	-3.1	VAL315	Hydrogen Bond	Cysteine - N	$[Dca]^-$ - N	3.06
		CYS316		Valine - N		3.20
		LYS317		Lysine - N		3.29
		TYR370		Tyrosine - OH		2.97

Table E8. Docking affinity energy and interacting amino acid residues predicted by AutoDock vinna for IgG-ILs.

Compound	Affinity (kcal/mol)	Interacting nucleic acids	Type of interaction	From	To	Distance (Å)
$[MepyrNC_4]^+$	-3.6	HIS281	Hydrogen Bond	$[MepyrNC_4]^+$- C	Histidine - O	3.37
		PRO15			Proline - O	3.71
$[Et_3NC_4]^+$	-3.2	TRP290	Hydrogen Bond	Tryptophan - N	$[Et_3NC_4]^+$ - O	3.25
		THR306		Threonine - O		3.23
		SER323		Serine - O		2.92
$[Pr_3NC_2]^+$	-3.3	TRP103	Hydrogen Bond	Tryptophan - N	$[Pr_3NC_2]^+$ - O	3.14
		VAL102		Valine - C		3.27
$[Pr_3NC_4]^+$	-3.5	PHE288	Hydrogen Bond	Phenylalanine- N	$[Pr_3NC_4]^+$ - O	2.90
		THR306		Threonine - O		2.89
		PHE288		$[Pr_3NC_4]^+$ - C	Phenylalanine- O	3.54
						3.36
$[Bu_3NC_4]^+$	-3.7	ILE400	Hydrogen Bond	$[Bu_3NC_4]^+$ - C	Isoleucine - O	3.41
		LYS261	Hydrophobic		Lysine - C	4.68
Br^-	-0.9	-	-	-	-	
$[Pyr]^-$	-3.2	SER280	Hydrogen Bond	Serine - O	$[Pyr]^-$ - O	3.07

		GLY250		Glycine - C		3.51
		SER280		Serine - C		3.22
$[Sal]^-$	-4.4	SER473	Hydrogen Bond	Serine - O	$[Sal]^-$ - O	3.19
						3.14
		SER471		$[Sal]^-$ - H	Serine - O	2.46
		ARG376	Electrostatic	Arginine - NH	$[Sal]^-$ - C	3.45
		LEU472	Hydrophobic	Leucine - C		3.62
		PRO373		$[Sal]^-$ - C	Proline - O	5.10
$[Sac]^-$	-5.1	THR97	Hydrogen Bond	Threonine - O	$[Sac]^-$ - O	2.87
		PHE98		Phenylalanine- N		3.02
		THR97		$[Sac]^-$ - N	Threonine - O	3.15
$[Lac]^-$	-3.3	ASP167	Hydrogen Bond	$[Lac]^-$ - H	AsparticAcid - O	2.03
$[Dca]^-$	-2.9	TYR186	Hydrogen Bond	Tyrosine - OH	$[Dca]^-$ - N	3.02
		GLY212		Glycine - N		3.16
		GLU213		GlutamicAcid - N		3.17

Table E9. Docking affinity energy and interacting amino acid residues predicted by AutoDock vinna for Tranferrin-ILs.

Compound	Affinity (kcal/mol)	Interacting nucleic acids	Type of interaction	From	To	Distance (Å)
$[MepyrNC_4]^+$	-3.9	GLN271	Hydrogen Bond	$[MepyrNC_4]^+$- C	Glutamine - O	3.78
$[Et_3NC_4]^+$	-3.1	LYS291	Hydrogen Bond	Lysine - N	$[Et_3NC_4]^+$ - O	3.05
$[Pr_3NC_2]^+$	-3.1	GLY34	Hydrogen Bond	$[Pr_3NC_2]^+$ - C	Glycine - O	3.77
$[Pr_3NC_4]^+$	-3.4	GLY190	Hydrogen Bond	Glycine - N	$[Pr_3NC_4]^+$ - O	3.10

		SER189		Serine - C		3.32
$[Bu_3NC_4]^+$	-3.3	ALA322	Hydrophobic	Alanine - C	$[Bu_3NC_4]^+$ - C	3.86
		ILE130		$[Bu_3NC_4]^+$ - C	Isoleucine - C	4.45
Br^-	-0.8	-	-	-	-	
$[Pyr]^-$	-3.3	SER21	Hydrogen Bond	Serine - O	$[Pyr]^-$ - O	3.05
		LYS18		Lysine - C		3.35
		PRO288		Proline - C		3.39
		HIS289		Histidine - C		3.32
$[Sal]^-$	-4.2	ALA322	Hydrogen Bond	Alanine - O	$[Sal]^-$ - O	3.48
$[Sac]^-$	-4.5	GLN184	Hydrogen Bond	$[Sac]^-$ - O	Glutamine - O	3.28
$[Lac]^-$	-3.4	ARG124	Electrostatic	Arginine - N	$[Lac]^-$ - O	3.14
		ASP63	Hydrogen Bond	AsparticAcid - N		3.02
		HIS249		Histidine - C		3.42
$[Dca]^-$	-3.0	TYR188	Hydrogen Bond	Tyrosine - N	$[Dca]^-$ - N	3.14
		SER189		Serine - N		3.09

REFERENCES

1. Messadi,. A., Mohamadou, A., Boudesocque, S., Dupont, L., Fricoteaux, P. , Nguyen-Van-Nhien, A.. J. Mol. Liq. 184 (2013) 68–72.

2. Sintra, T.E., Cruz, R., Ventura, S.P.M., Coutinho, J.A.P..J. Chem. Thermodyn. 77 (2014) 206–213.

Appendix F

Section F5. Synthesis and characterization of the Good's buffers ionic liquids

[P_{4444}][MES]: From the MES buffer (48.5 mmol), this compound was obtained as a white solid. Water content < 0.05 wt%. 1H NMR (300 MHz, D2O/TSP): 3.63 (t, 4H), 2.99 (t, 2H), , 2.72 (t, 2H), 2.50 (t, 4H), 2.02 (m, 8H), 1.27-1.42 (m, 16H), 0.78 (t,12H,). 13C NMR (75.47 MHz, D2O/TSP): 68.80, 55.44, 55.11, 50.02, 26.28, 20.80, 20.16, 15.44.

[P_{4444}][TES]: From the TES buffer (45.1 mmol), this compound was obtained as a transparent viscous liquid. Water content < 0.05 wt%. 1H NMR (300 MHz, D2O/TSP): 3.31 (s, 6H), 2.82 (s, 2H), 2.57 (t, 2H), 2.10 (m, 8H), 1.29-1.49 (m,16H), 0.79 (t, 12H). 13C NMR (75.47 MHz, D2O/TSP): 60.65, 57.63, 51.58, 37.69, 26.28, 20.83, 20.17, 15.46.

[P_{4444}][CHES]: From the CHES buffer (47.2 mmol), this compound was obtained as a transparent viscous liquid. Water content <0.05 wt%. 1H NMR (300 MHz, D2O/TSP); 1H NMR (300 MHz, D2O/TSP); 2.95 (m, 2H), 2.38-2.47 (*m*, 1*H*), 2.02 (m, 8H), 1.28-1.45 (m, 16H,), 0.94 (m, 10H), 0.78 (t, 12H). 13C NMR (75.47 MHz, D2O/TSP): 63.37, 63.09, 53.42, 39.56, 26.28, 26.08, 25.60, 20.30, 20.15, 15.43.

[P_{4444}][HEPES]: From the HEPES buffer (44.3 mmol), this compound was obtained as a yellowish white solid. Water content < 0.05 wt%. 1H NMR (300 MHz, D2O/TSP): 3.59 (t,4H), 2.97 (t, 2H), 2.94 (t, 2H), 2.67 (t, 2H), 2.46 (t, 8H), 2.03 (m, 8H), 1.28-1.45 (m, 16H), 0.79 (t, 12H). 13C NMR (75.47 MHz, D2O/TSP): 61.59, 60.87, 55.02, 54.78, 54.19, 50.39, 26.29, 20.80, 20.16, 15.44.

[P_{4444}][Tricine]: From the Tricine buffer (50.3 mmol), this compound was obtained as white solid. Water content < 0.05 wt%. 1H NMR (300 MHz, D2O/TSP): 3.37 (s, 6H), 3.12 (s, 2H), 2.00 (m, 8H), 1.27-1.44 (m, 16H), 0.77 (t. 12H). 13C NMR (75.47 MHz, D2O/TSP): 182.71, 63.12, 62.97, 47.68, 26.28, 20.79, 20.15, 15.42.

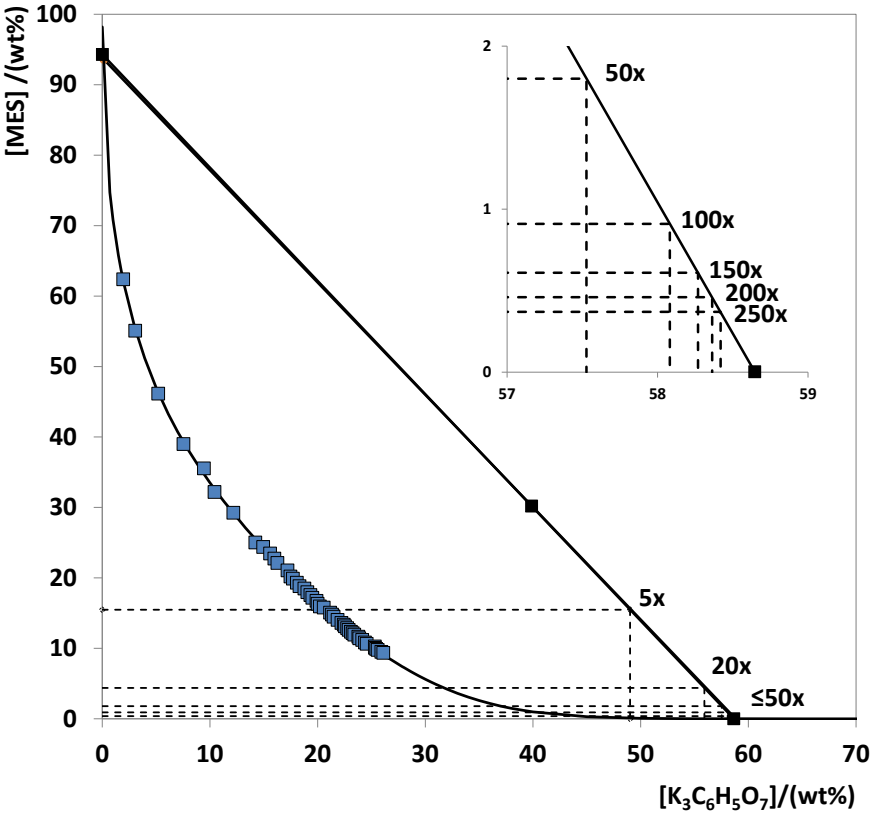

Figure F1. Experimental data for *CF* of the systems composed of $[P_{4444}][MES]$ + $K_3C_6H_5O_7$ + H_2O at (25 ± 1) °C.

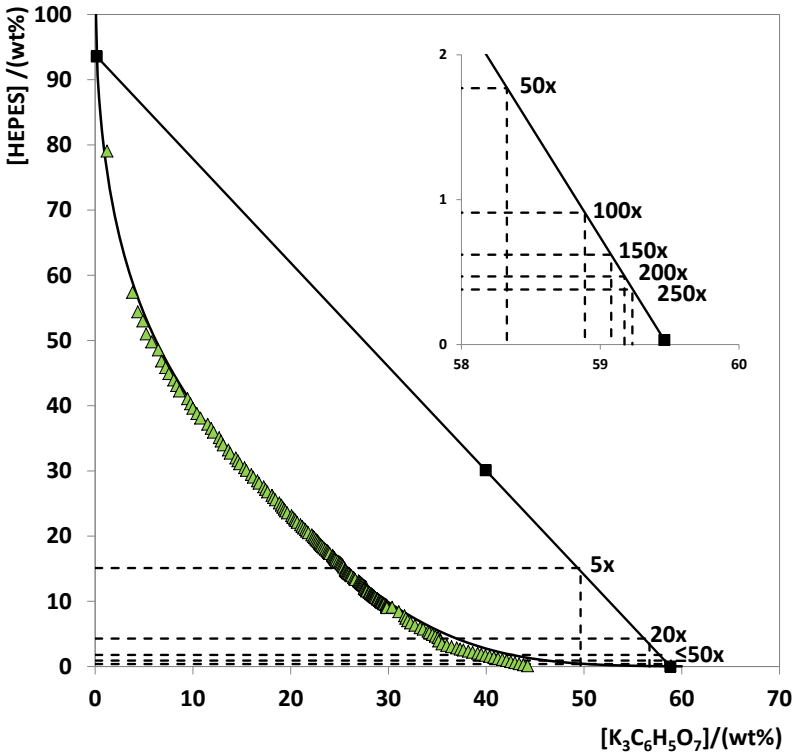

Figure F2. Experimental data for *CF* of the systems composed of $[P_{4444}][HEPES]$ + $K_3C_6H_5O_7$ + H_2O at (25 ± 1) °C.

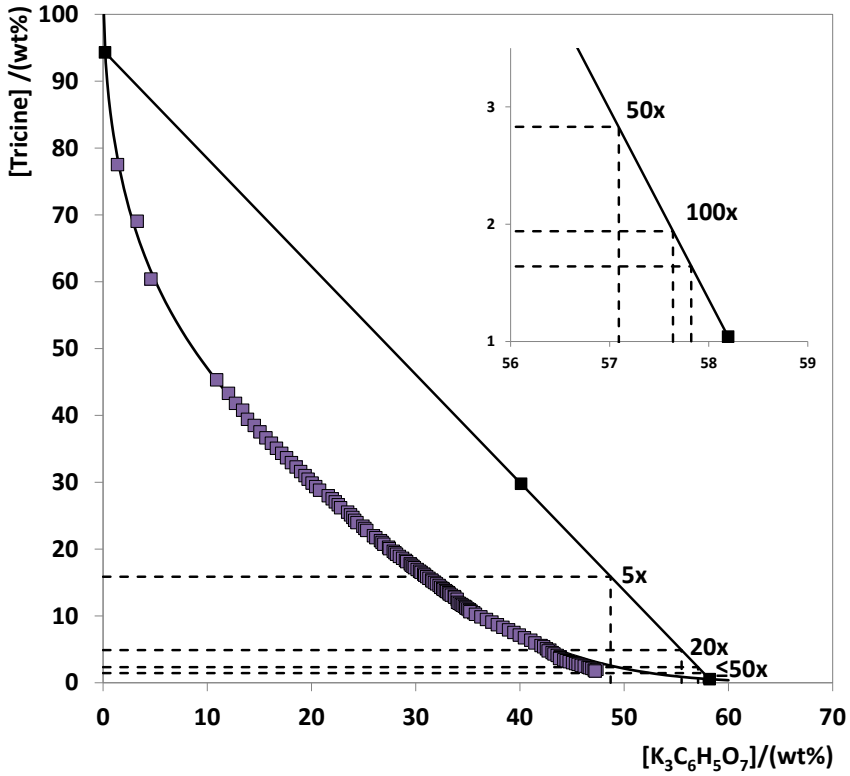

Figure F3. Experimental data for *CF* of the systems composed of $[P_{4444}][Tricine] + K_3C_6H_5O_7 + H_2O$ at (25 ± 1) °C.

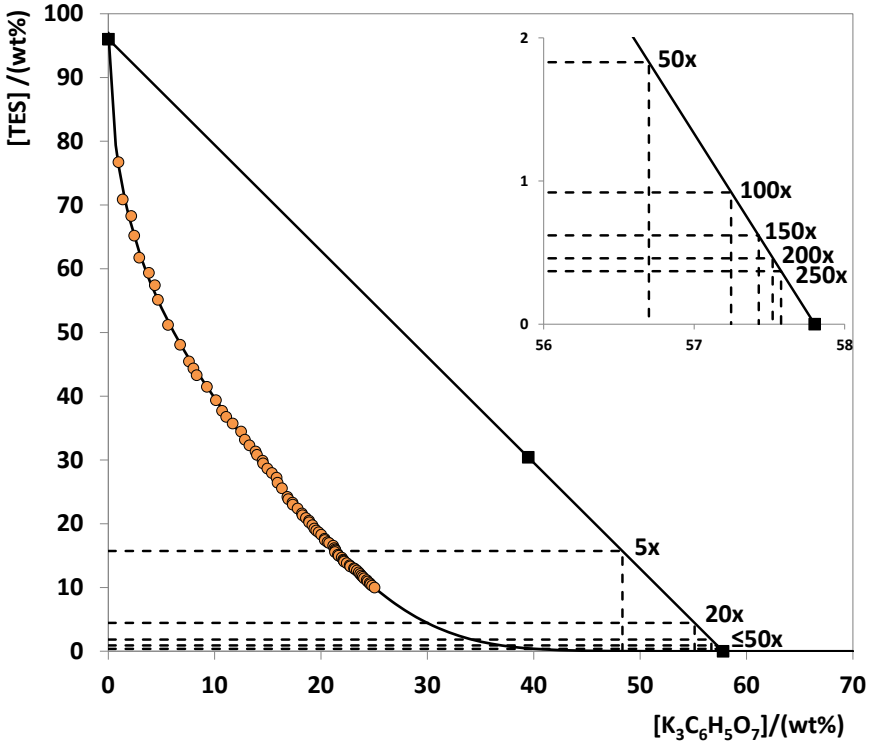

Figure F4. Experimental data for *CF* of the systems composed of $[P_{4444}][TES] + K_3C_6H_5O_7 + H_2O$ at (25 ± 1) °C.

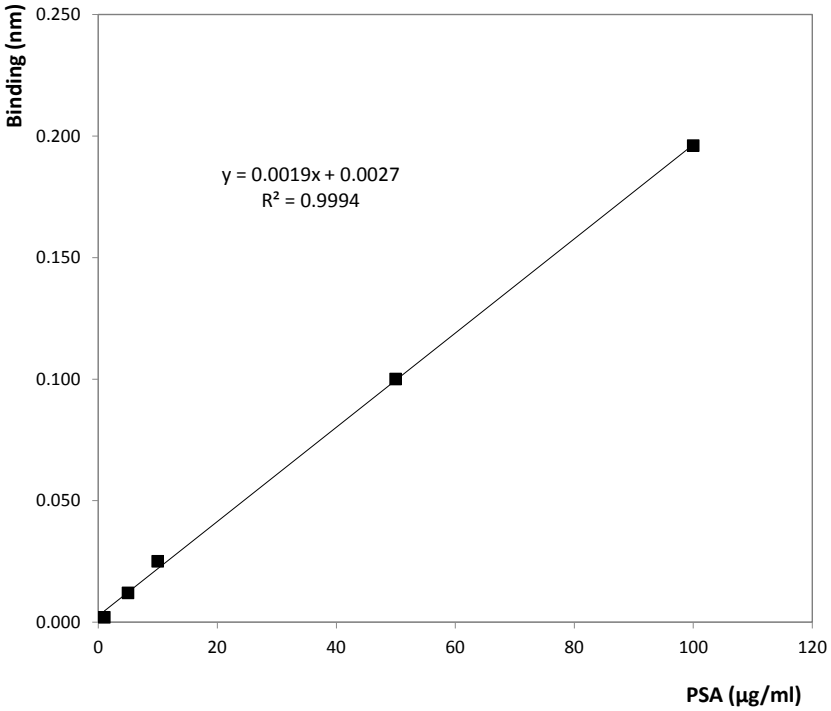

Figure F5. BLItz calibration curve for PSA in aqueous solution.

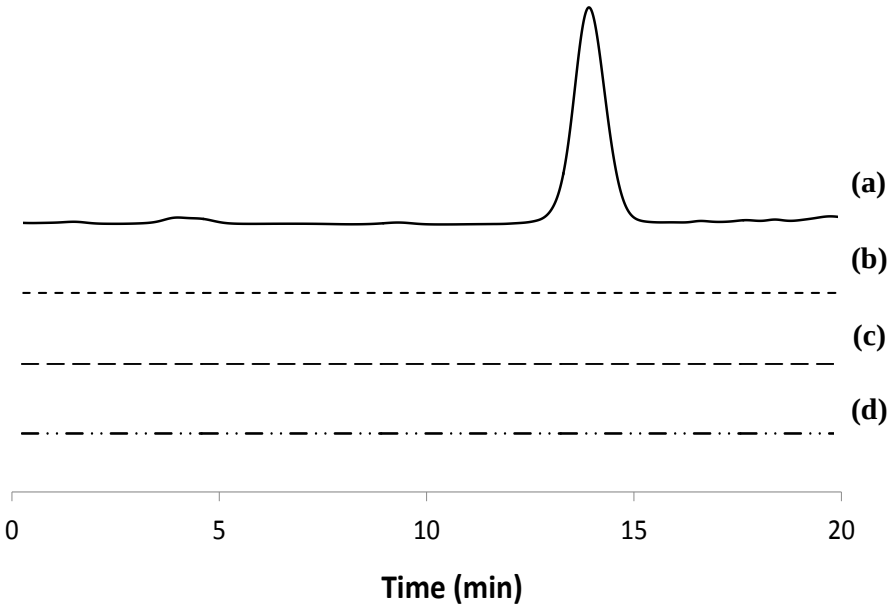

Figure F6. SE-HPLC profile of pure PSA in aqueous solution, human urine (from a female donor and from a healthy male donor) and in the top and bottom phases of an ABS composed of $[P_{4444}][CHES]$ + salt + human urine: (a) PSA in aqueous solution (150 mg/ml); (b) Female urine sample; (c) IL rich-phase (female pure urine); (d) Salt rich-phase (female pure urine).

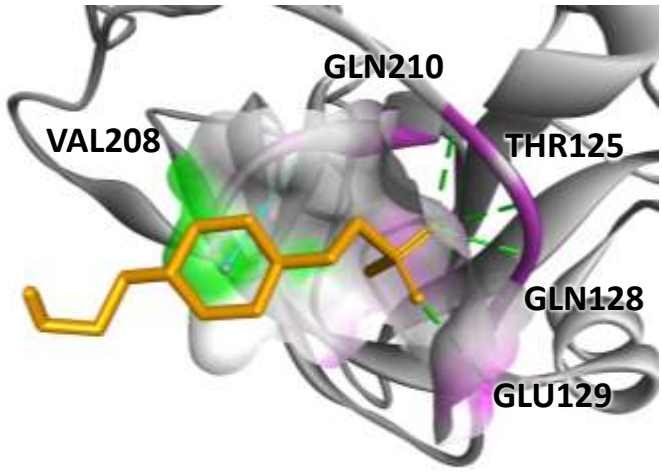

Figure F7. The PSA docking pose with the lowest absolute value of affinity (kcal/mol) for PSA with $[HEPES]^-$.

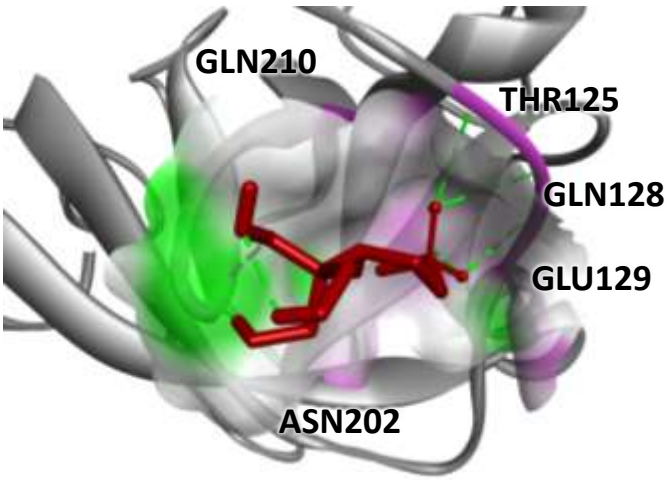

Figure F8. The PSA docking pose with the lowest absolute value of affinity (kcal/mol) for PSA with $[TES]^-$.

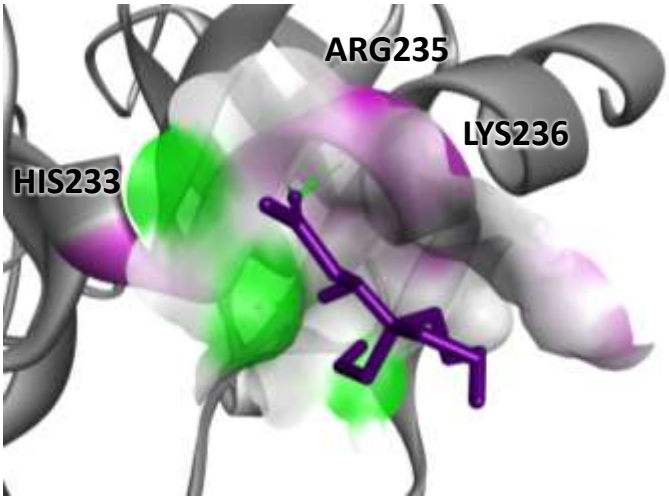

Figure F9. The PSA docking pose with the lowest absolute value of affinity (kcal/mol) for PSA with $[Tricine]^-$.

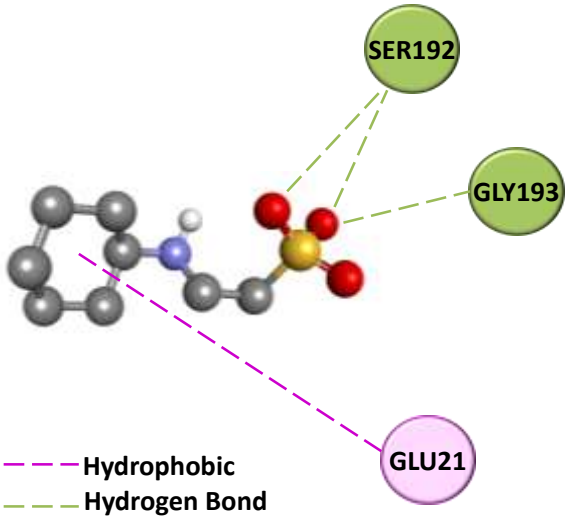

Figure F10: Molecular interaction diagrams of $[CHES]^-$ and amino acids residues of PSA.

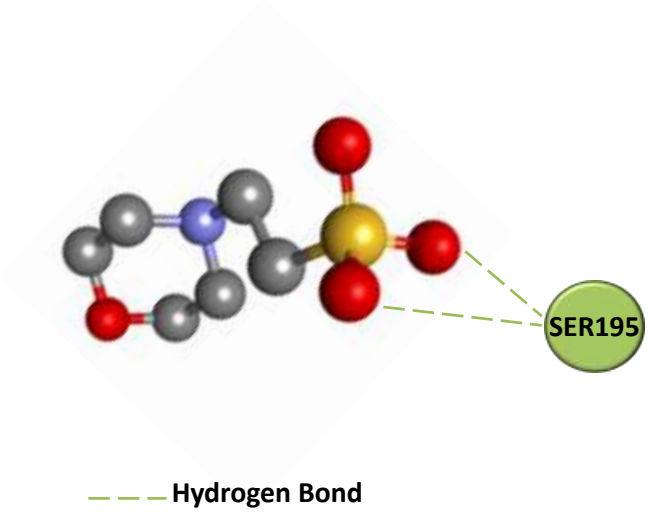

Figure F11: Molecular interaction diagrams of $[MES]^-$ and amino acids residues of PSA.

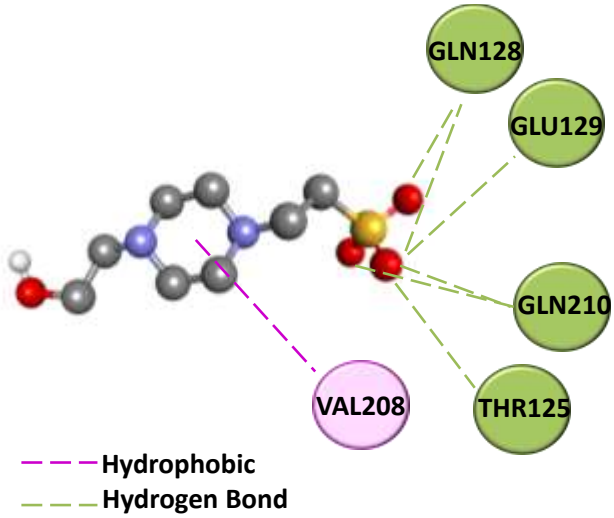

Figure F12: Molecular interaction diagrams of $[HEPES]^-$ and amino acids residues of PSA.

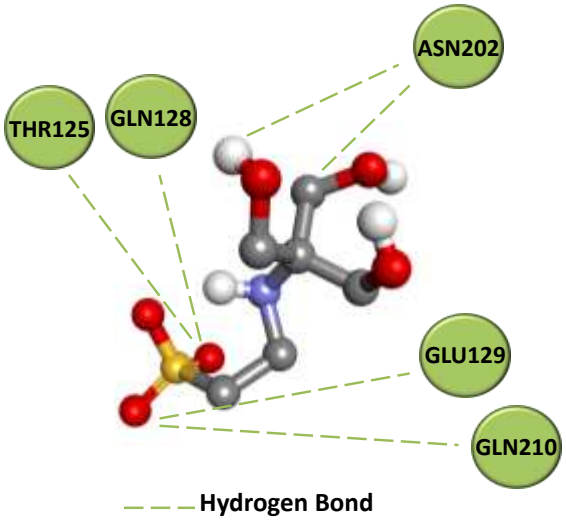

Figure F13: Molecular interaction diagrams of $[TES]^-$ and amino acids residues of PSA.

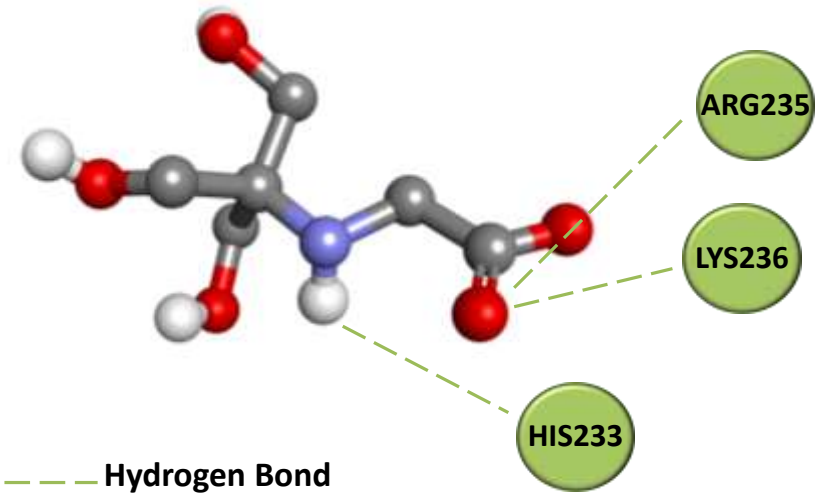

Figure F14: Molecular interaction diagrams of $[Tricine]^-$ and amino acids residues of PSA.

Table F1. Experimental weight fraction data for the system composed of IL (1) + $K_3C_6H_5O_7$ (2) + H_2O (3) at 25 °C and atmospheric pressure.

$[P_{4444}][TES]$		$[P_{4444}][MES]$		$[P_{4444}][HEPES]$	
100 w_1	100 w_2	100 w_1	100 w_2	100 w_1	100 w_2
76.71	0.96	62.37	1.95	79.05	1.21
70.87	1.36	55.07	3.07	57.38	3.82
68.27	2.17	46.15	5.21	54.39	4.36
65.19	2.44	38.99	7.55	52.99	4.88
61.73	2.92	35.53	9.45	51.00	5.21
59.35	3.82	32.17	10.43	49.78	5.79
57.40	4.38	29.24	12.18	48.55	6.45
55.12	4.67	25.01	14.22	46.85	6.80
51.18	5.62	24.37	14.94	45.84	7.21
48.08	6.76	23.45	15.59	44.92	7.54
45.45	7.58	22.73	15.99	43.94	8.03
44.36	8.01	22.10	16.27	43.08	8.33
43.30	8.31	21.05	17.21	42.24	8.63
41.47	9.27	20.19	17.49	41.06	9.46
39.38	10.12	19.88	17.71	40.29	9.76
37.71	10.70	19.30	18.08	39.61	9.99
36.76	11.09	18.82	18.32	38.78	10.41
35.71	11.69	18.48	18.78	38.09	10.79
34.46	12.49	17.96	19.05	37.15	11.51
33.18	12.85	17.56	19.34	36.51	11.87
32.30	13.27	17.16	19.51	35.92	12.10
31.34	13.85	16.73	19.90	35.09	12.68
30.81	13.98	16.30	20.01	34.58	12.88
29.88	14.51	15.93	20.21	33.99	13.09
29.46	14.56	15.77	20.58	33.20	13.63
28.66	14.96	15.05	21.16	32.72	13.81
27.96	15.39	14.78	21.34	31.98	14.39
27.22	15.82	14.47	21.49	31.54	14.60
26.42	15.92	14.02	21.86	31.09	14.79

25.57	16.33	13.60	22.21	30.50	15.29
24.21	16.84	13.35	22.44	30.07	15.47
23.85	16.93	13.12	22.55	29.44	15.97
23.30	17.33	12.86	22.75	29.03	16.18
22.99	17.35	12.62	22.89	28.48	16.60
22.38	17.80	12.33	23.10	28.11	16.77
21.60	18.21	12.13	23.25	27.54	17.25
21.33	18.26	11.94	23.41	27.16	17.43
20.90	18.58	11.64	23.79	26.77	17.63
20.47	18.89	11.41	23.87	26.26	18.10
20.22	18.89	11.19	24.14	25.91	18.23
19.77	19.19	10.81	24.41	25.55	18.44
19.25	19.37	10.64	24.57	25.09	18.84
18.93	19.56	10.26	25.32	24.76	19.04
18.65	19.78	10.05	25.33	24.43	19.19
18.28	20.02	9.90	25.44	24.13	19.35
17.65	20.34	9.76	25.58	23.85	19.47
17.44	20.36	9.49	25.92	23.56	19.66
17.12	20.62	9.35	26.10	23.14	20.09
16.97	20.76			22.88	20.22
16.55	21.14			22.60	20.41
16.16	21.25			22.37	20.51
15.95	21.33			22.09	20.67
15.78	21.37			21.74	21.01
15.56	21.32			21.49	21.16
15.14	21.59			21.23	21.33
14.97	21.66			20.99	21.51
14.68	21.95			20.76	21.65
14.35	22.09			20.50	21.80
14.21	22.12			20.17	22.17
14.06	22.17			19.95	22.32
13.81	22.43			19.74	22.44
13.46	22.70			19.53	22.58

13.30	22.75
13.00	23.11
12.87	23.18
12.66	23.37
12.36	23.56
12.12	23.69
11.86	23.81
11.66	23.92
11.44	24.04
11.15	24.30
10.94	24.38
10.68	24.58
10.50	24.64
10.28	24.80
9.98	25.04

19.33	22.70
19.13	22.81
18.93	22.94
18.74	23.05
18.56	23.13
18.37	23.28
18.18	23.40
17.99	23.56
17.80	23.71
17.64	23.81
17.47	23.90
17.31	23.99
17.06	24.27
16.91	24.34
16.76	24.43
16.62	24.49
16.46	24.55
16.31	24.67
16.16	24.83
16.01	24.98
15.89	25.08
15.75	25.17
15.61	25.27
15.44	25.35
15.25	25.43
14.96	25.57
14.78	25.57
14.66	25.64
14.54	25.73
14.43	25.80
14.33	25.87
14.22	25.96
14.11	26.08

14.01	26.14
13.90	26.24
13.68	26.44
13.44	26.52
13.33	26.61
13.12	26.95
13.02	27.04
12.93	27.10
12.82	27.18
12.73	27.26
12.64	27.31
12.56	27.38
12.45	27.48
12.35	27.56
12.26	27.64
12.18	27.71
12.04	27.55
11.91	27.53
11.83	27.64
11.74	27.74
11.66	27.79
11.57	27.79
11.44	28.00
11.36	28.06
11.21	28.19
11.13	28.24
11.06	28.32
10.98	28.36
10.90	28.43
10.82	28.50
10.75	28.55
10.69	28.59
10.56	28.68

10.45	28.84
10.39	28.88
10.31	28.92
10.17	29.06
10.10	29.11
10.00	29.20
9.93	29.24
9.87	29.29
9.77	29.42
9.71	29.47
9.65	29.52
9.60	29.55
9.51	29.73
9.39	29.79
9.29	29.88
9.13	29.82
9.01	29.84
9.08	30.39
8.39	31.06
7.78	31.65
7.40	31.77
7.01	31.97
6.68	32.26
6.31	32.71
5.94	33.24
5.73	33.55
5.43	34.05
5.19	34.18
4.90	34.49
4.65	34.80
4.42	35.07
4.20	35.30
3.96	35.32

3.90	35.14
3.47	35.48
3.24	35.97
3.03	36.46
2.84	36.98
2.67	37.33
2.53	37.67
2.36	38.17
2.18	38.61
2.03	39.14
1.87	39.49
1.71	39.92
1.55	40.36
1.39	40.79
1.23	41.22
1.07	41.65
0.90	42.08
0.74	42.51
0.58	42.94
0.42	43.38
0.26	43.81
0.10	44.24

Table F2. Experimental weight fraction data for the system composed of IL (1) + $K_3C_6H_5O_7$ (2) + H_2O (3) at 35 °C and atmospheric pressure.

[P_{4444}][CHES]		[P_{4444}][Tricine]	
100 w_1	100 w_2	100 w_1	100 w_2
44.76	3.92	77.51	1.40
41.71	4.74	69.04	3.28
39.33	5.34	60.39	4.60
37.55	5.83	45.31	10.91
36.22	6.34	43.30	12.04
34.48	6.67	41.79	12.71
33.48	7.04	40.77	13.40
32.32	7.47	39.41	13.86
30.98	7.83	38.48	14.52
29.73	8.17	37.52	15.07
28.73	8.39	36.64	15.63
27.94	8.79	35.83	16.16
27.39	9.18	35.08	16.64
26.69	9.53	34.32	17.15
25.86	9.67	33.65	17.61
25.25	10.02	32.93	18.09
24.53	10.24	32.27	18.52
23.96	10.60	31.59	18.97
23.32	10.72	30.98	19.39
22.79	10.83	30.45	19.68
22.46	11.16	29.86	20.06
21.96	11.28	29.33	20.41
21.47	11.46	28.80	20.78
21.06	11.73	27.97	21.61
20.53	11.92	27.50	21.99
20.03	12.05	27.05	22.29
19.69	12.25	26.61	22.58
19.27	12.36	26.18	22.80
18.95	12.57	25.52	23.47

18.58	12.67	25.11	23.75
18.27	12.86	24.71	23.98
17.91	12.90	24.29	24.15
17.61	13.14	23.95	24.37
17.24	13.19	23.41	24.94
16.95	13.38	23.08	25.13
16.60	13.53	22.78	25.31
16.27	13.70	21.98	25.95
15.94	13.83	21.69	26.17
15.64	13.97	21.24	26.63
15.35	14.12	20.99	26.78
15.08	14.19	20.71	26.95
14.87	14.13	20.26	27.41
14.62	14.20	20.04	27.47
14.36	14.23	19.66	27.85
14.17	14.41	19.44	28.02
13.93	14.57	19.21	28.17
13.71	14.61	18.90	28.45
13.49	14.73	18.61	28.74
13.32	14.86	18.30	29.02
13.10	14.96	18.11	29.14
12.89	15.07	17.78	29.48
12.69	15.11	17.58	29.57
12.53	15.23	17.41	29.75
12.36	15.28	17.19	29.88
12.18	15.41	16.93	30.15
11.96	15.35	16.67	30.38
11.87	15.52	16.51	30.52
11.73	15.61	16.25	30.77
11.61	15.71	16.09	30.87
11.47	15.78	15.86	31.06
11.33	15.81	15.61	31.28
11.22	15.89	15.36	31.53

11.11	15.94	15.22	31.58
11.01	16.05	14.99	31.80
10.89	16.07	14.77	32.00
10.78	16.18	14.54	32.24
10.59	16.16	14.27	32.41
10.50	16.22	14.09	32.60
10.40	16.32	13.97	32.64
10.30	16.38	13.78	32.85
10.18	16.43	13.64	32.97
10.05	16.65	13.47	33.15
9.90	16.63	13.27	33.23
9.81	16.70	13.10	33.42
9.73	16.76	12.88	33.71
9.65	16.83	12.77	33.76
9.55	16.88	12.49	33.98
9.46	16.96	12.03	34.02
9.37	16.94	11.87	34.18
9.28	17.00	11.71	34.36
9.17	17.17	11.58	34.49
9.04	17.35	11.43	34.66
8.88	17.45	11.31	34.79
7.88	19.13	11.16	34.83
7.59	19.32	11.03	35.00
7.24	19.86	10.89	35.17
6.97	19.88	10.81	35.17
6.67	20.18	10.70	35.31
6.39	20.24	10.46	35.57
6.16	20.70	10.62	35.21
5.89	20.61	10.23	35.74
5.59	21.35	9.84	36.26
5.27	21.22	9.45	36.79
5.05	21.46	9.06	37.32
4.85	21.89	8.68	37.85

4.64	22.17	8.29	38.37
4.44	22.21	7.90	38.91
4.28	22.48	7.51	39.43
4.15	22.83	7.12	39.95
3.98	23.02	6.72	40.44
3.80	23.28	6.36	41.05
3.67	23.42	5.95	41.44
3.52	23.64	5.55	42.03
3.42	23.80	5.36	42.28
3.30	23.90	5.07	42.55
3.22	24.19	4.87	42.87
3.11	24.21	4.75	42.71
3.00	24.53	4.50	43.09
2.90	25.13	4.30	43.28
2.79	25.33	4.08	43.58
2.71	25.53	3.86	43.86
2.62	25.68	3.73	43.88
2.62	24.71	3.61	43.81
2.45	24.16	3.42	44.21
2.38	24.30	3.28	44.45
2.31	24.53	3.13	44.73
2.25	24.62	2.98	45.05
2.16	24.77	2.86	45.34
2.08	25.04	2.74	45.59
2.00	25.34	2.59	45.88
1.91	25.76	2.48	46.17
1.83	25.92	2.33	46.53
1.75	26.28	2.23	46.67
1.67	26.45	2.13	46.91
1.60	26.74	1.99	47.40
1.52	26.98	1.89	47.13
1.46	27.28	1.74	47.23
1.39	27.59		

1.31	27.82
1.23	28.19
1.17	28.53
1.10	28.85
1.04	29.09
0.99	29.39

Table F3. Experimental data for the CF of the systems composed of $[P_{4444}][GB]$ + $K_3C_6H_5O_7$ + water at (25 ± 1) °C.

$[P_{4444}][MES]$							
Theoretical *CF*	5	20	50	100	150	200	250
w IL / g	0.1538	0.8746	0.9034	0.4669	0.608	0.3206	0.2578
w Salt/ g	0.4907	11.1844	28.8004	29.0330	58.2693	40.8537	40.8927
w H_2O/ g	0.3556	7.9404	20.3765	20.5313	41.1231	28.8267	28.8521
w Top/ g	0.0783	0.4023	0.4108	0.2064	0.2603	0.1476	0.1166
w Bottom/ g	0.8099	18.7884	48.9843	46.2209	98.9366	69.2375	69.1359
Real *CF*	4.54	19.74	49.60	99.47	157.98	195.30	247.45

$[P_{4444}][CHES]$							
Theoretical *CF*	5	20	50	100	150	200	250
w IL / g	0.1546	0.8718	0.896	0.4543	0.3079	0.317	0.2541
w Salt/ g	0.4918	11.2273	28.8647	29.1384	29.2327	40.9848	41.0242
w H_2O/ g	0.3553	7.9012	20.2728	20.4156	20.4793	28.7043	28.7221
w Top/ g	0.0855	0.4322	0.3842	0.2101	0.1319	0.1406	0.1174
w Bottom/ g	0.8246	17.8944	48.8542	49.2884	49.1391	68.4552	69.6864
Real *CF*	4.16	18.28	52.77	97.17	155.26	204.16	244.65

[P_{4444}][HEPES]							
Theoretical *CF*	5	20	50	100	150	200	250
w IL / g	5	20	50	100	150	200	250
w Salt/ g	0.1590	0.8554	0.8861	0.4548	0.6189	0.3307	0.2691
w H_2O/ g	0.4999	11.3395	29.164	29.4442	57.0792	41.4222	41.4620
w Top/ g	0.3530	7.8059	19.95	20.1002	40.3018	28.2491	28.273
w Bottom/ g	0.0730	0.4038	0.3922	0.2042	0.264	0.142	0.1119
Real *CF*	0.7998	18.8912	48.7235	49.3160	98.9670	68.8742	69.4209

[P_{4444}][TES]							
Theoretical *CF*	5	20	50	100	150	200	250
w IL / g	0.1565	0.6673	0.9148	0.4615	0.3091	0.3267	0.2603
w Salt/ g	0.4839	8.2646	28.3289	28.6225	28.7143	40.266	40.3037
w H_2O/ g	0.3588	6.0672	20.7886	20.9159	20.9797	29.413	29.4364
w Top/ g	0.0801	0.3159	0.4201	0.2118	0.1394	0.1438	0.115
w Bottom/ g	0.7982	14.2206	48.4881	49.3160	49.1121	67.8044	69.5518
Real *CF*	4.48	19.21	49.48	98.75	150.50	204.54	255.97

[P_{4444}][Tricine]							
Theoretical *CF*	5	20	50	100	150	200	250
w IL / g	0.1582	0.9758	1.1577	0.7204	0.5731	0.1582	0.9758
w Salt/ g	0.4862	11.1054	28.575	28.8193	28.0000	0.4862	11.1054
w H_2O/ g	0.3542	7.931	20.3498	20.4447	20.5376	0.3542	7.931
w Top/ g	0.0800	0.4147	0.4138	0.2111	0.1426	0.0800	0.4147
w Bottom/ g	0.7948	19.4130	49.1102	49.3373	49.3575	0.7948	19.4130
Real *CF*	4.43	19.12	49.18	96.85	144.02	4.43	19.12

Table F4. Docking affinity energy and interacting amino acid residues predicted by AutoDock vinna for PSA-GB-ILs.

Compound	Affinity (kcal/mol)	Interacting nucleic acids	Type of interaction	From	To	Distance (Å)
$[P_{4444}]^+$	-2.6	-	-	-	-	-
$[CHES]^-$	-3.4	PHE95	Hydrophobic	Phenylalanine - C	$[CHES]^-$ - C	5.46
		SER192	Hydrogen Bond	Serine - O	$[CHES]^-$ - O	2.91
				Serine - O	$[CHES]^-$ - O	2.83
		GLY193		Glycine - N	$[CHES]^-$ - O	3.15
$[MES]^-$.	-3.7	SER195	Hydrogen Bond	Serine - O	$[MES]^-$ - O	2.93
				Serine - O	$[MES]^-$ - O	3.21
$[HEPES]^-$.	-3.2	THR125	Hydrogen Bond	Threonine - N	$[HEPES]^-$. - O	3.14
		GLN128		Glutamine - N	$[HEPES]^-$. - O	2.80
				Glutamine - N	$[HEPES]^-$. - O	3.30
		GLU129		GlutamicAcid - N	$[HEPES]^-$. - O	2.95
		GLN210		Glutamine - N	$[HEPES]^-$. - O	2.97
				Glutamine - N	$[HEPES]^-$. - O	2.96
		VAL208	Hydrophobic	- C	$[HEPES]^-$. - C	5.18
$[TES]^-$.	-3.8	THR125	Hydrogen Bond	Threonine - N	$[TES]^-$.- O	2.94
		GLN128		Glutamine - N	$[TES]^-$.- O	3.14
		GLU129		GlutamicAcid - N	$[TES]^-$.- O	2.97
		GLN210		Glutamine - N	$[TES]^-$.- O	3.21
		ASN202		$[TES]^-$.- H	Asparagine - O	2.06
				$[TES]^-$.- C	Asparagine - O	3.59
$[Tricine]^-$	-3.1	HIS233	Hydrogen Bond	$[Tricine]^-$ -H	Histidine - O	2.13

	ARG235	Arginine - N	$[Tricine]^-$ - O	2.91
	LYS236	Lysine -N	$[Tricine]^-$ - O	2.91

Appendix G

Table G1. Depletion efficiency of IgG and HSA ($DE\%_{PROT}$) and extraction efficiency of LDH ($EE\%_{LDH}$) and weight fraction compositions of the initial mixtures at 25 °C.

IL	Weight fraction composition / (wt %)		$DE\%_{Prot} \pm \sigma$	$EE\%_{LDH} \pm \sigma$
	IL	$K_3C_6H_5O_7/C_6H_8O_7$		
$[P_{4444}]Cl$	30.21 ± 0.03	30.08 ± 0.01	19.31	100
$[P_{4444}]Br$	30.01 ± 0.01	29.97 ± 0.05	100	100
	30.11 ± 0.03	10.28 ± 0.01	100	100
	30.02 ± 0.01	20.31 ± 0.03	100	100
	15.30 ± 0.05	20.16 ± 0.03	100	100
	29.89 ± 0.01	20.09 ± 0.02	100	100
	30.04 ± 0.04	20.05 ± 0.06	100	100

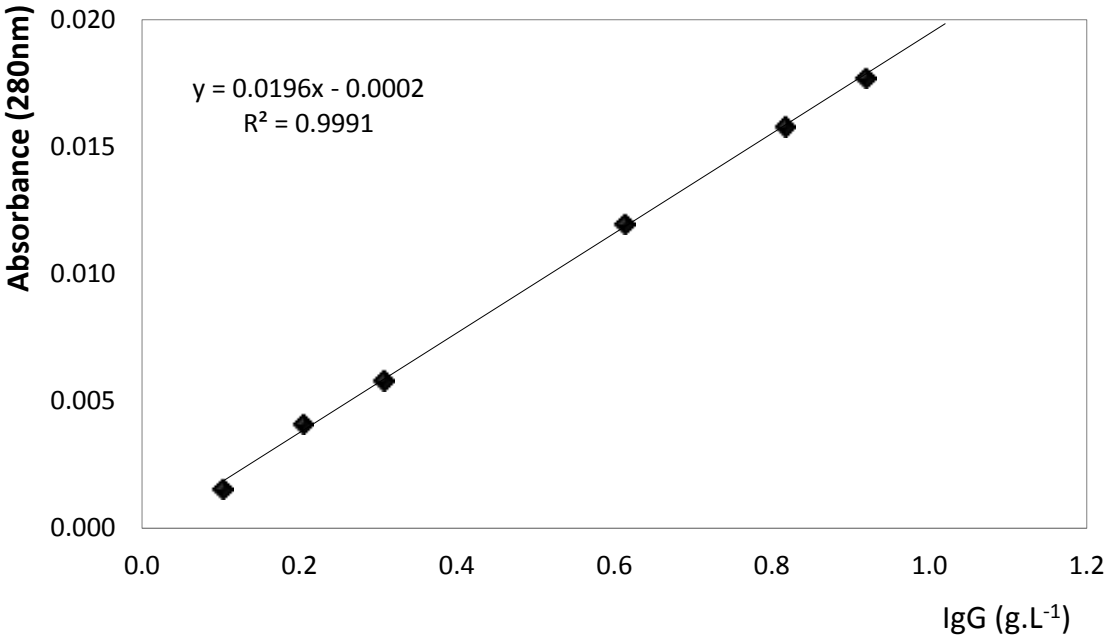

Figure G1. IgG calibration curve by SE-HPLC.

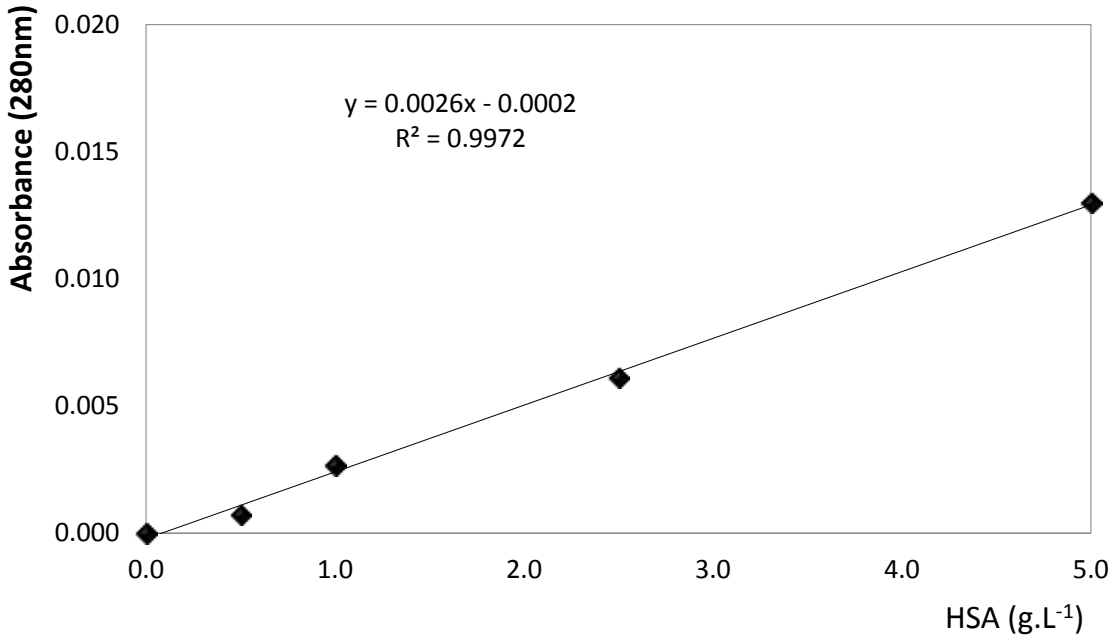

Figure G2. HSA calibration curve by SE-HPLC.

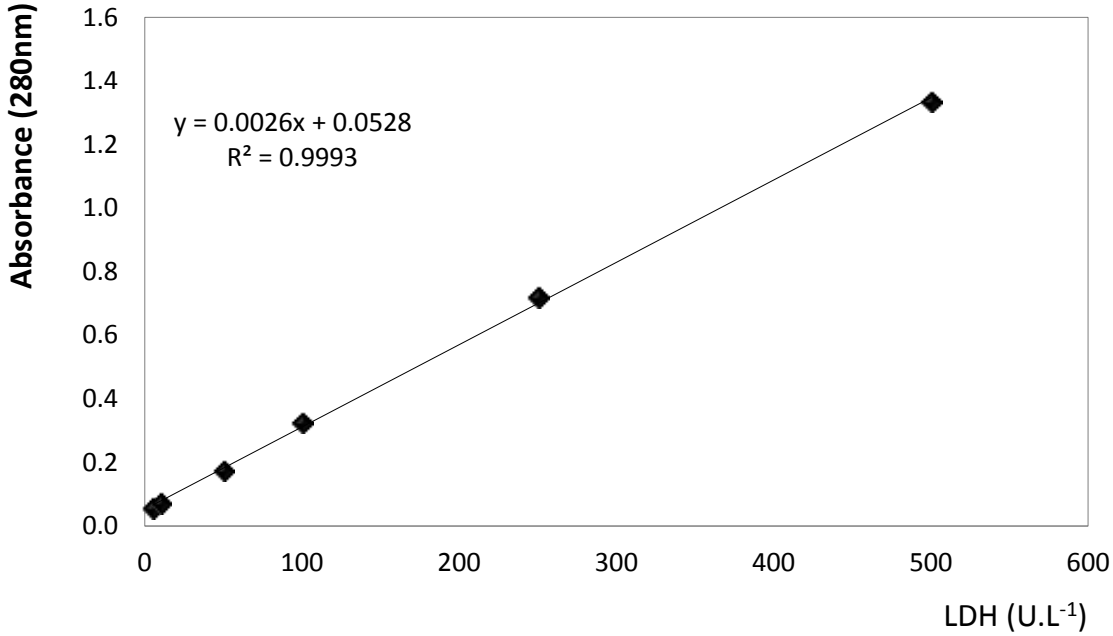

Figure G3. LDH calibration curve by SE-HPLC.

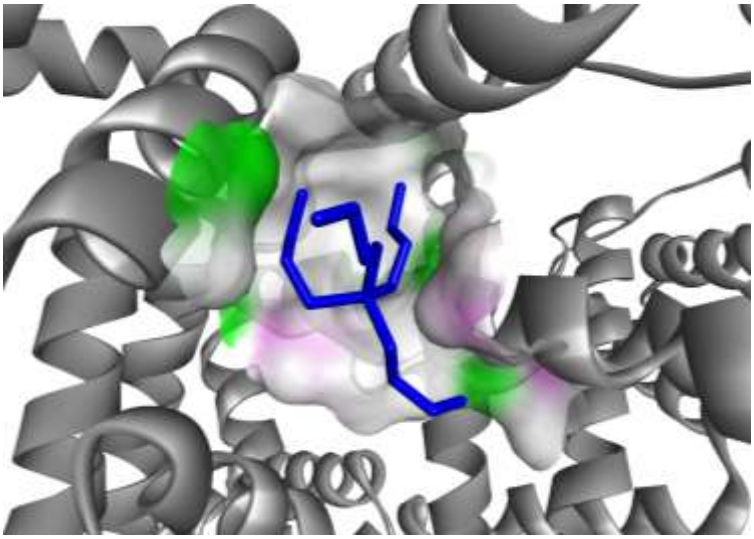

Figure G4. Docking pose with the lowest absolute value of affinity (kcal/mol) for HSA with $[P_{4444}]^+$.

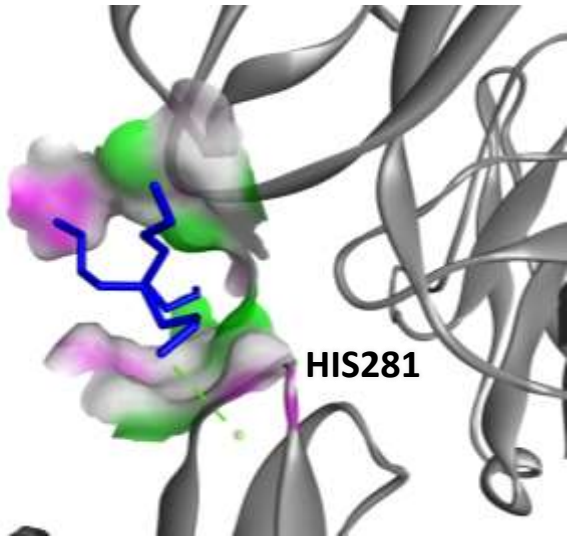

Figure G5. Docking pose with the lowest absolute value of affinity (kcal/mol) for IgG with $[P_{4444}]^+$.

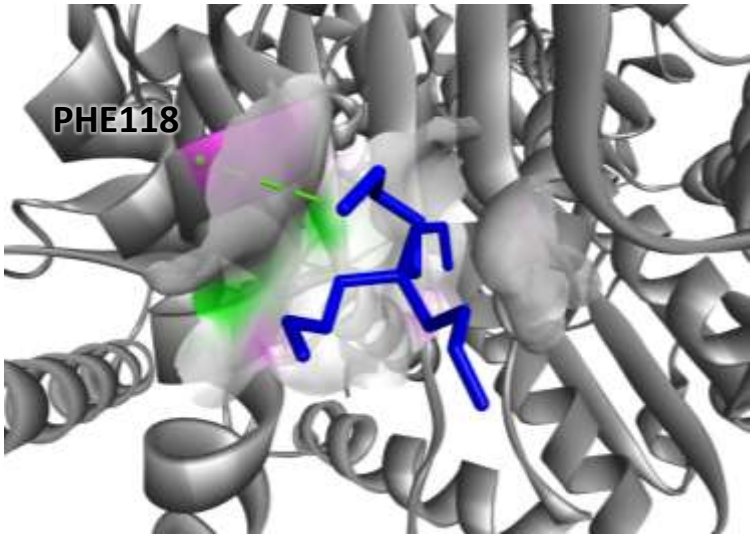

Figure G6. Docking pose with the lowest absolute value of affinity (kcal/mol) for LDH with $[P_{4444}]^+$.

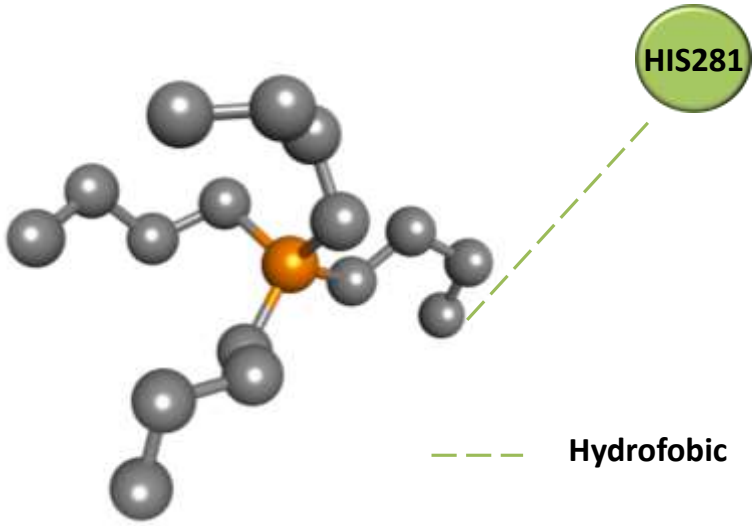

Figure G7. Molecular interaction diagrams of $[P_{4444}]^+$.and amino acids residues of IgG.

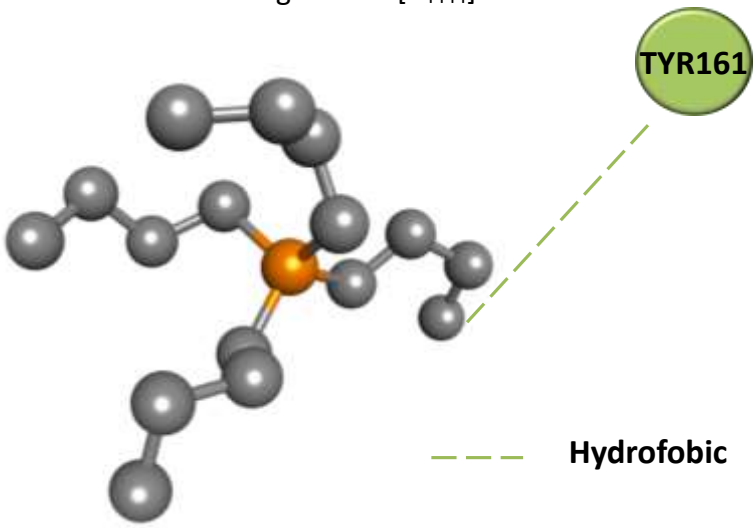

Figure G8. Molecular interaction diagrams of $[P_{4444}]^+$.and amino acids residues of LDH.

Table G2. Docking affinity energy and interacting amino acid residues predicted by AutoDock vinna for HSA-ILs.

Compound	Affinity (kcal/mol)	Interacting nucleic acids	Type of interaction	From	To	Distance (Å)
$[P_{4444}]^+$	-3.6	-	-	-	-	-
Br^-	-1.0	-	-	-	-	-
Cl^-	-1.0	-	-	-	-	-

Table G3. Docking affinity energy and interacting amino acid residues predicted by AutoDock vinna for IgG-ILs.

Compound	Affinity (kcal/mol)	Interacting nucleic acids	Type of interaction	From	To	Distance (Å)
$[P_{4444}]^+$	-2.8	HIS281	Hydrophobic	$[P_{4444}]^+$- C	Histidine - H	3.95
Br^-	-0.8	-	-	-	-	-
Cl^-	-0.9	-	-	-	-	-

Table G4. Docking affinity energy and interacting amino acid residues predicted by AutoDock vinna for LDH-ILs.

Compound	Affinity (kcal/mol)	Interacting nucleic acids	Type of interaction	From	To	Distance (Å)
$[P_{4444}]^+$	-3.2	PHE118	Hydrophobic	$[P_{4444}]^+$- C	Phenylalanine - H	3.96
Br^-	-0.9	-	-	-	-	-
Cl^-	-0.9	-	-	-	-	-